



University  
of Glasgow

Sun, Fang (2010) *Simulation based A-posteriori search for an ICE microwave ignition system*. PhD thesis.

<http://theses.gla.ac.uk/2237/>

Copyright and moral rights for this thesis are retained by the author

A copy can be downloaded for personal non-commercial research or study, without prior permission or charge

This thesis cannot be reproduced or quoted extensively from without first obtaining permission in writing from the Author

The content must not be changed in any way or sold commercially in any format or medium without the formal permission of the Author

When referring to this work, full bibliographic details including the author, title, awarding institution and date of the thesis must be given

# Simulation Based A-Posteriori Search for an ICE Microwave Ignition System

A DISSERTATION SUBMITTED TO  
THE DEPARTMENT OF ELECTRONICS AND ELECTRICAL ENGINEERING  
OF UNIVERSITY OF GLASGOW  
FOR THE DEGREE OF  
DOCTOR OF PHILOSOPHY

By Fang Sun

29/01/2010

©Copyright 2010 by Fang Sun

All Rights Reserved

# Abstract

Petrol internal combustion engines (ICEs) in automobiles use a high-voltage spark ignition system, which currently offers an energy efficiency of 25%-35% only and also produces excessive exhaust emissions. Recent political, economic, social, technical, legal and environmental drive has accelerated the worldwide research in 'greener' engines, such as the homogenous charge compression ignition (HCCI) engines, which focuses on total resource conservation and emission reduction per mile. However, its ignition timing needs real-time control of cylinder pressure and temperature in a closed loop, which is practically intractable to date.

Leapfrogging HCCI and requiring no closed-loop control or modification to the engine, this thesis develops homogenous charge microwave ignition (HCMI) directly to replace the point-based spark ignition. Like HCCI, HCMI is volume based and is also applicable to diesel fuel. Through computer simulations, the thesis verifies the feasibility of the ICE radio frequency ignition concept first proposed by Ward in 1974. Building on the simulation-based design methodology of Boeing 777 aircraft, which required no hardware casting or prototyping at the design stage, this thesis employs intelligent search to evolve 'designs of experiments' by simulation means for vehicle-borne HCMI with potential to offer a step change in fuel efficiency and emission reduction.

Investigation of this thesis into the effect of piston position confirms with graphical visualisation that the resonant frequency of the engine cylinder is very sensitive to the piston motion, because it can easily cause off-resonance and hence degraded field strength. It is revealed that this is the major factor that encumbers practical realisation of an HCMI system. This thesis shows that the natural frequency changes 0.015 GHz per 0.5 mm in average when the piston moves from 5 mm to 0.5 mm TDC and 0.0021 GHz per 0.05 mm when the piston moves from 0.5 mm to 0.05 mm to TDC. For the geometry of the given ICE cylinder, if the input microwave frequency is fixed, the resonance lasts for 7  $\mu$ s.

Investigation on various diameters of cylinders that reveals the results on the effects of piston motion of a certain cylinder can be extended to other cylinders with different diameters. It is also shown that for different types of cylinders the frequency of input

microwave can be very different. Therefore, the different microwave source of the HCMI systems has to be designed for different types of vehicles.

Simulations reported in the thesis also reveal that a microwave based ignition takes 30 ns to 100 ns to break down the median of a permittivity and permeability that are the same as the chemically optimal 14.7:1 air-fuel mixture. This is much shorter than the duration of the microwave resonance and hence makes HCMI feasible in terms of duration. For a running engine, the variations of AFR can also cause off-resonance. It is found that the AFR does not affect the resonant frequency as much as piston motion does. The frequency only changes 38MHz when the AFR varies from 10:1 to 16:1.

Properties and effects of microwave emitter and couplers are also studied and the results confirm with graphical visualisation that, for an emitter in the form of a probe antenna, the electric field intensity is dependant on the antenna length. For the given geometry of the Chrysler-Dodge ICE studied, a probe antenna of a length around 30% of wavelength shorter than the end of transmission line offers the best coupling efficiency in an HCMI system.

To search for globally optimal designs, the Nelder-Mead simplex method and the 'intelligent' evolutionary algorithm (EA) are coupled with CAD simulations. These machine learning methods are shown efficient and reliable in dealing with multiple parameters. Under practical constraints, the best ignition timing and AFR combination is found, which for a 100 W input offers an electric field intensity of up to  $9.8 \times 10^6 \text{ V m}^{-1}$ , almost doubling the minimum requirement of  $5.5 \times 10^6 \text{ V m}^{-1}$  for a plasma breakdown of the air-fuel mixture.

In this work, six different geometric shapes of antennae are studied. Through the EA based global search, it is confirmed that the length and screen radius of the probe antenna do not affect the resonant frequency significantly. For the given ICE geometry, an antenna length of 14.3 mm offers the best efficiency and the least reflection regardless of the screen radius. The radius affects resonance the least among all the parameters searched, although it can contribute to enhancing electric field and reducing reflection of the coupling. For maximal electric field strength in the cylinder, the best combination of the antenna length and the screen radius is also searched and results are fully tabulated in this thesis.

## List of Publication

Li, Y., Sun, F., and Capuano, A., EM field enable timing control of HCCI engines, Proc 7<sup>th</sup> Asia-Pacific Conference on Control and Measurement. pp.39-44 Nyingchi, Tibet, China, 11-16 Aug 2006.

Sun, F., Capuano, A., and Li, Y., Simulation of electromagnetic resonance for open-loop control of ICE ignition timing. Chinese Automation and Computing Society Conf, Loughborough, UK, 16 Sep 2006.

Chen, W., Sun, F., and Li, Y., Evolutionary computation enable CAutoD search for practically-oriented multi-objective field ignition system for internal combustion engines. Proc 13<sup>th</sup> Int Conf Automation and Computing pp. 99-104, Stafford, Sept 2007 (ISBN 978-0-9555293-1-3)

# Table of Content

<b>Abstract</b>	<b>i</b>
<b>List of Publications</b>	<b>iii</b>
<b>Table of Content</b>	<b>iv</b>
<b>Acknowledgements</b>	<b>vii</b>
<b>Abbreviations</b>	<b>viii</b>
<b>1. Introduction</b>	<b>1</b>
1.1 Problems Facing SI Systems	1
1.2 Improving Ignition for High Energy Efficiency	2
1.3 Concept of Microwave Ignition	3
1.4 Simulation and Search Methods Adopted	4
1.5 Organisation of Dissertation	5
<b>2. Background</b>	<b>6</b>
2.1 Ignition Principles of the SI System	6
2.2 Current SI Systems	16
2.3 Homogeneous Charge Compression Ignition	17
2.4 Laser Ignition	17
2.5 Concept of the MI System	18
2.6 Microwave Fundamentals	20

2.6.1 Microwave Resonance	21
2.6.2 Coupling Methods	24
2.7 Progress to Date	25
<b>3. Simulation and Search</b>	<b>28</b>
3.1 Finite Element Method for Microwave Simulation	28
3.2 A-Posteriori Search Methods	30
3.3.1 The Nelder-Mead Method	30
3.3.2 Evolutionary Algorithm Based Search Method	30
3.3 Design via Machine Learning and Search	33
<b>4. Simulation and Analysis of Microwave Volume Distribution and Strength</b>	<b>37</b>
4.1 Geometry Models of Cylinder for Simulation	37
4.1.1 2D Geometry Model for Simulations	39
4.1.2 3-D Geometry Model for Simulations	40
4.1.3 Model Established in Script	41
4.1.4 Electromagnetic Field and Ignition Modelling	42
4.2 Validation of the Simulation	44
4.3 Influence of Piston Motion	50
4.4 Influence of Air/Fuel Ratio	67
4.4.1 The Relation between Air/Fuel Ratios and Relative Permittivity	67
4.4.2 Effects of Air/Fuel Ratios	68

4.5 Microwave Coupling Methods	77
4.5.1 Effects of the Coupling Antenna Length	77
4.5.2 Improvements on the Coupling Antenna	87
4.6 Effects of Plasma Induced by Microwave Resonance	97
<b>5. Simulations Based Design of Experiments Using A-Posteriori Search</b>	<b>102</b>
5.1 Combinations of the Transmission Line Radius and Antenna Length	102
5.1.1 Search Using the NM Simplex Method	102
5.1.2 Search Using the EA Method	121
5.2 Search of Relative Permittivity of the Air-Fuel Mixture	141
5.2.1 Search Using the NM Simplex method	141
5.2.2 Search Using the EA Method	164
<b>6. Conclusions and Further Work</b>	<b>189</b>
6.1. Discussion and Conclusions	189
6.2 Further Work	192
<b>References</b>	<b>193</b>
<b>Appendix A</b>	<b>199</b>

# Acknowledgement

I would like to express my sincere gratitude to my supervisor, Dr. Yun Li, for his patient guidance, sincere encouragement and thoughtful support during my doctoral studies. I am also grateful to the member of the Centre for Systems and Control for their support and advice, in particular Mr. Tom O'Hara, who offered superb technical assistance, and Ms Vi Romanes, who helps with daily caring administrative work.

I am also grateful to University of Glasgow and CVCP for their financial support in the form of a Postgraduate Scholarship and an Overseas Research Scheme Award, respectively.

To my parents, I express my deepest thanks for their unending encouragement, support and love. And thanks to everyone for their help in past four years.

# Abbreviations

AFR	Air/fuel Ratio	2
BTDC	Before Top Dead Centre	8
EA	Evaluation Algorithm	5
EM	Electromagnetic	3
FEM	Finite Element Method	4
HCCI	Homogeneous Charge Compression Ignition	2
HCFI	Homogeneous Charge Microwave Ignition	4
ICE	Internal Combustion Engine	1
IMEP	Indicated Mean Effective Pressure	27
MI	Microwave Ignition	3
MTBE	Methyl Tertiary-Butyl Ether	13
NM	Nelder-Mead	30
PDE	Partial Differential Equation	28
QWCCR	Quarter Wave Coaxial Cavity Resonator	26
SI	Spark Ignition	1
TDC	Top Dead Centre	6
TPI	Transient Plasma Ignition	26

# 1. Introduction

Recent political, economic, social, technical, legal and environmental factors have accelerated the worldwide research and development in more energy efficient and more environmentally friendly vehicles, i.e., pure electric, fuel-cell based and fossil-fuel electric hybrid vehicles (Chan, 2002; Frenken, 2004). The race in research also includes new types of internal combustion engines (ICEs) and new ignition systems to improve over the existing spark ignition (SI) system for petrol ICEs.

## 1.1 Problems Facing SI Systems

The spark ignition system for the Otto engine has been widely used for over a century (Otto, 1888; Taylor, 1985; Starikovskaia, 2006). While the Otto engine itself has been improved continuously since its invention, the spark ignition system has changed little. It ignites a homogenous air-fuel mixture in engine cylinders through applying high voltage pulses to the spark plugs. The voltage ranges between 10 kV and 25 kV for most engines (Dorf, 1998). The ignition occurs between the spark plug electrodes about 2 mm apart. Thus, the air-fuel mixtures in the cylinder are not completely ignited when combustion initiates. It takes about less than 0.6 milliseconds from the time when the ignition first occurs until flame ball grows to 25.4 mm (Jacobs, 1996).

Despite substantial improvements in the modern SI system, it offers only 25%-35% energy efficiency (Jacobs, 1996, Heywood, 1988), although it provides relatively reliable ignition performance with misfire now reduced to 3%-7% (Kutlar, et. al. 2005). The delay and incompleteness in the combustion is one of the reasons for the poor fuel efficiency (Taylor, 1985; Maher, 2004). Partly as a consequence of the low energy efficiency, the SI system also results in excessive pollutant emissions and CO<sub>2</sub> emissions per mile covered (Kutlar, et. al., 2005). Furthermore, to gain high power the SI engine needs to run at a rich air/fuel ratio (AFR), which also causes poor combustion efficiency and high emissions (Taylor, 1985; Maher, 2004).

Statistic data have shown that the automobile industry has developed different technology to improve fuel efficiency of the SI system over past decades since 1970s (Kwon, 2006). During the 17 years from 1973 to 1990 the fuel efficiency of petrol ICEs was improved 16.87% (Kwon, 2006). However, only 1% improvement of fuel efficiency was achieved over 10 year period from 1990 to 2001 (Kwon, 2006). The fuel efficiency of new cars has improved much more slowly since 1990 than earlier period (Kwon, 2006). These facts indicate that there is not much room left for the improvement of fuel efficiency if no revolutionary change is made to the ICE configuration or the SI system.

## **1.2 Improving Ignition for High Energy Efficiency**

During past decades engine research organisations and manufacturers worldwide have developed several techniques to improve ICE ignition, including multi-point ignition, to improve the SI system (Davis, 1987; Schaus, 2001). Multi-point ignition is developed based on the traditional SI system by simply increasing the number of ignition points for each cylinder. However, data show that it does not improve fuel efficiency significantly (Schaus, 2001).

Combining the advantages of both petrol and diesel engines, the concept of homogenous charge compression ignition (HCCI) was proposed and the substantial efforts have been made since 1983 (Najt, 1983). HCCI refers to a form of internal combustion, in which well mixed air and fuel are compressed to the point of auto-ignition. Focusing on total resource conservation, HCCI has been shown to offer an innovative replacement of the traditional SI and has been researched into by many engine research institutions and manufacturers (Zhao, et.al., 2003).

With pre-mixed compression ignition, HCCI forms the ideal volume ignition. However, the control of the HCCI system is more complicated than a traditional SI system because there is no well-defined combustion initiator of HCCI that can be well controlled open-loop or closed-loop. Therefore, HCCI has not been implemented on vehicles on the road yet.

### **1.3 Concept of Microwave Ignition**

Similar to HCCI, Microwave ignition (MI) would provide improved energy efficiency because of volume ignition and fast combustion (Gundersen, 2004; Theiss, et. al. 2005). Microwave ignition is a type of plasma ignition. Theoretically, an MI system can reduce fuel consumption and exhaust emissions by increasing the combustion efficiency (Theiss, et. al. 2005, Gundersen, 2004) with its faster and volume ignition. An MI system uses high electric field intensity generated by the microwave to ignite most of the air-fuel mixture at once. Research has shown feasibility and advantages in the reduction of fuel consumption and pollutant emissions (Gundersen, 2004; Theiss, et. al. 2005; Bellenoue, et. al. 2005).

Since the MI system was first proposed in 1974 (Ward, 1974) it has been studied for decades (Kimura, et. al. 1981; Ward, 1991; Schleupen, 2000; Schmidt & Ruoss, 2003; Schmidt, et. al. 2003). Many types of MI systems have been presented, but none of them has been applied practically to vehicles on the road. Nonetheless, it has been shown that an MI system requires less energy than an SI system to ignite the air-fuel mixture and MI can accommodate a leaner air-fuel mixture than SI can (Manning, 1995; Bokulich, 2001).

This thesis aims to simulate the electromagnetic (EM) properties systematically for the MI concept, so as to investigate design factors that affect resonance in the cylinder such as the piston motion, air/fuel ratio, and coupling means etc.

The piston motion in the cylinder is the major factor that affects the microwave cavity and hence its resonance. Therefore the analysis of effects of the piston position on the resonance is essential. Another factor affecting the resonance is plasma generation before and after ignition, which is also investigated in this thesis. Successfully providing a resonant condition and hence a dramatically enhanced electric field strength for a viable design of the HCMI system is the main goal of this research.

## 1.4 Simulation and Search Methods Adopted

This thesis aims at developing a homogenous charge microwave ignition (HCMI) system to replace the spark plug ignition system used in petrol ICEs with a microwave coupling apparatus. To investigate microwave resonance and field distribution in depth, the finite element method (FEM) is adopted. In particular, a MATLAB based simulation software package is hired to model the electric field and to investigate factors affecting resonance.

With FEM simulations, costly and tedious hardware prototyping and experiments can be avoided, similar to the design process of the Boeing 777 aircraft. Data gathered from simulations in this thesis can be used to guide further research, experiments, and design.

To progress from such a 'simulated prototype' to another, 'design of experiments' by means of simulations should be devised. In order to make the best use of the simulation results, machine learning is employed in this thesis. As machine learning explores unknowns without possessing prior knowledge, it is often by means of a trial-and-error based search with a-posteriori guidance. This process can thus systematically assist researchers to investigate complex problems that are hard to estimate.

The design of an HCMI system involves geometric structures, multiple parameters and performance objectives. Due to an irregular geometric shape of the engine cylinder, some parameters cannot be calculated precisely. However, a-posteriori search can help investigate possibly optimal combinations at the conceptual design stage.

In particular, the evolutionary algorithm (EA) method is adopted for the search for optimal HCMI parameters such as the input microwave frequency and coupling antenna dimensions, etc., because an EA has advantages of solving problems with multiple peaks of the objectives corresponding to different parameters. The EA also helps analyse factors that affect cavity resonance, e.g., the air/fuel ratios and the piston position, etc. The EA search can overcome traps of local optimal and search for the global optimum and for

multiple objectives systematically and automatically, reducing the development cost and time to market.

## **1.5 Organisation of Dissertation**

The next chapter sets the background of ignitions and microwave resonance. Present ignition systems and existing research on MI systems are reviewed. Chapter 3 presents the methods in detail and lays down the foundation of solving the challenging problems that this research faces. Through the simulation methodology, Chapter 4 fully investigates microwave resonance properties and factors that affect the resonance. The simulation methodology is then coupled with an automated search methodology in Chapter 5 to lead to design of experiments and optimal design prototypes, followed by in-depth analysis of the search results. Conclusions are then drawn in Chapter 6, together with future work is suggested.

## **2. Background**

In this chapter, the ignition principles of the SI system and the MI system are studied. The modern SI system and the existing research of MI systems are reviewed.

### **2.1 Ignition Principles of the SI System**

Modern petrol vehicles are commonly fitted with Otto Cycle engines named after Dr. N. A. Otto who invented the stationary petrol engine in 1876 (Otto, 1888; Starikovskaia, 2006). The construct of an Otto Cycle engine cylinder is shown in Figure 2-1 (Britannica, 2007). Its power cycle consists of adiabatic compression, heat addition at constant volume, adiabatic expansion and rejection of heat at constant volume and characterized by four strokes, or reciprocating motion of a piston in a cylinder. These four strokes are intake stroke, compression stroke, power stroke, and exhaust stroke (Taylor, 1985). In this thesis, the intake stroke and cycle start from the top dead centre (TDC) where the piston is furthest away from the crankshaft.

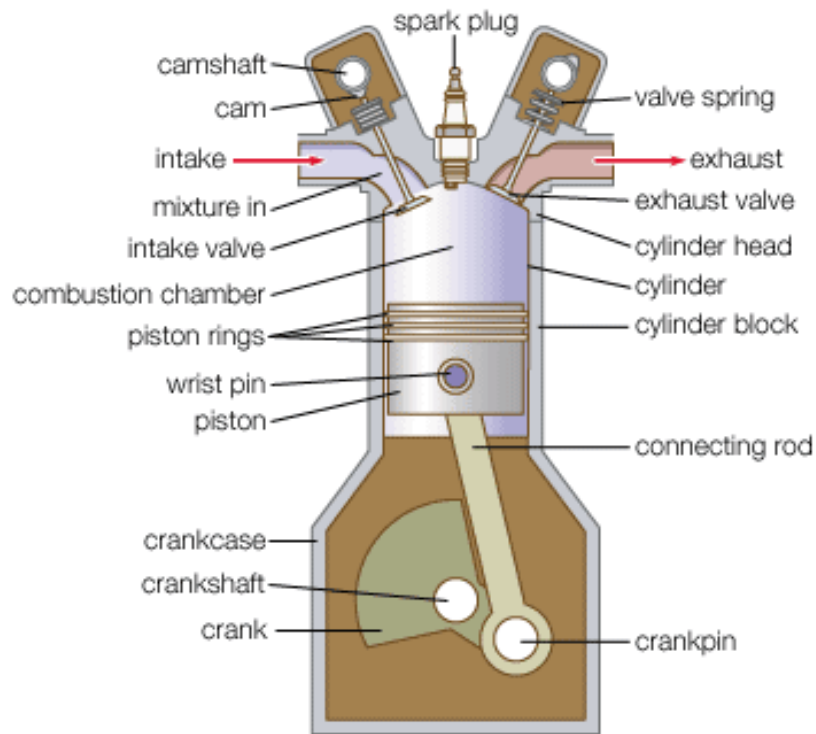


Figure 2-1 Construct of an Otto Cycle engine cylinder (Britannica, 2007)

An Otto cycle includes two revolutions. The crankshaft in Figure 2-1 rotating a round is one revolution. The distance between the piston and TDC is usually measured by degrees that the crankshaft rotates away from the TDC, which is explained in Figure 2-2.

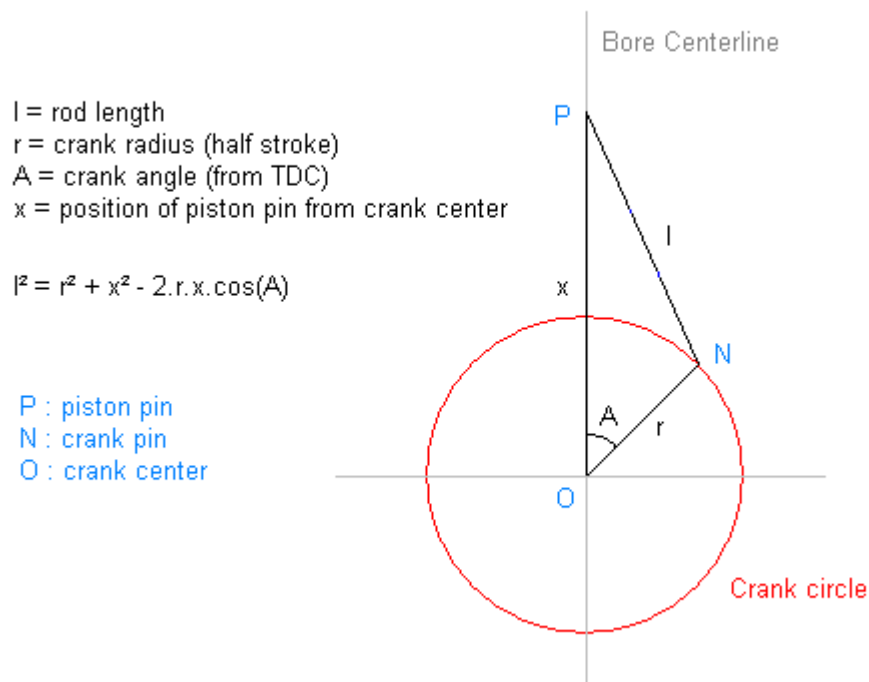


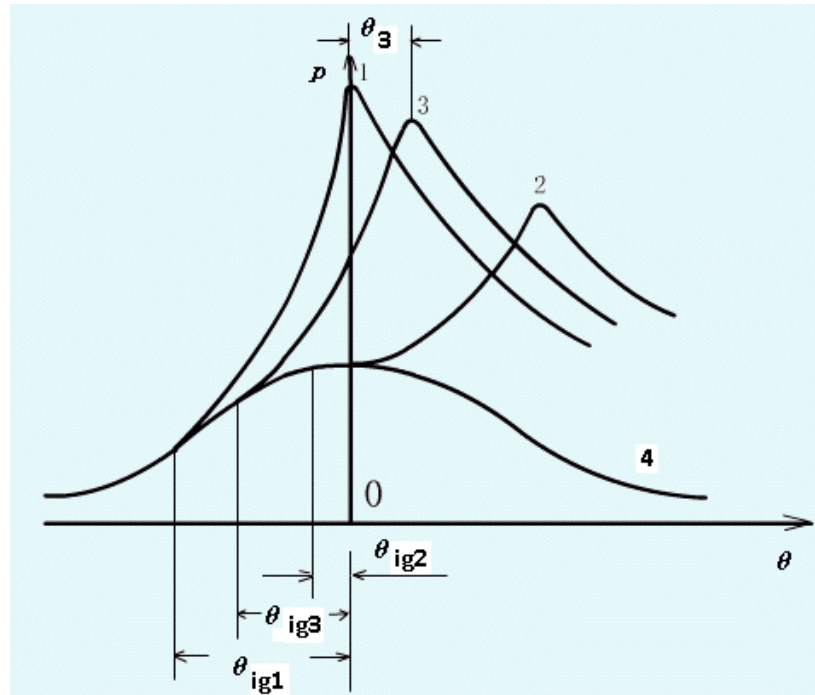
Figure 2-2 Piston motion equations (Wikipedia, 2006)

The ignition of an SI system is usually initiated at 5 to 40 degrees prior to TDC in the compression stroke, depending on the engine speed, i.e., between  $A=360^\circ - 5^\circ$  and  $A=360^\circ - 40^\circ$  (Dorf, 1998). The unit of the engine speed is rpm, or revolutions per minute. These degrees before top dead centre (BTDC) are termed timing advance.

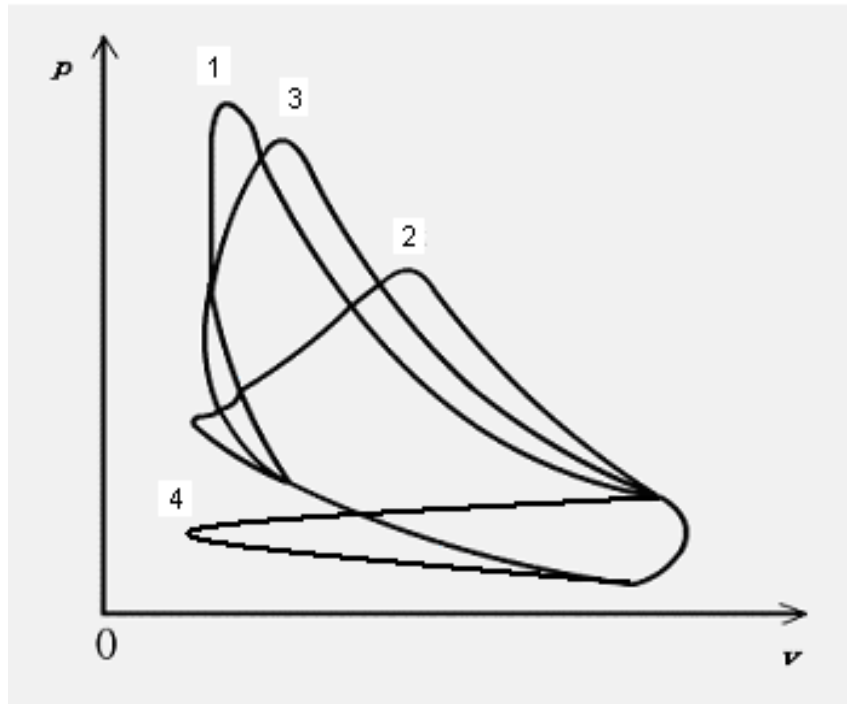
The ignition occurs during the compression stroke. It includes 3 lags, which are voltage rise-time lag, transport lag, and growth lag (Jacob, 1996). The voltage rise-time lag is the time lapse from the spark voltage first starts till spark current begins. The transport lag is the time lapse from the spark current starts till a ball flame is initiated. The growth lag is the diameter of a flame ball grows from the spark plug gap to approximately 25.4 mm (Jacob, 1996). Since then the flame propagates rapidly, which is regarded as combustion stage.

The timing advance is required since the generation and propagation of flame take time. Thus, ignition has to start before the piston reaches TDC. Ideally, the time at which the

air-fuel mixture should be fully burnt is about 20 degrees after TDC according to Hartman's paper (Hartman, 2004). Figure 2-3 illustrates the best ignition timing for a certain engine speed (Xu, 2004).



(a) Highest pressure occurs at the right  $\theta_{ig}$



(b) The relation between pressure and cylinder volume

Figure 2-3 The ignition timing for a petrol engine (Xu, 2004)

In Figure 2-3,  $\vartheta$  refers to the distance between the piston and TDC.  $\vartheta_{ig}$  refers to the timing advance,  $p$  refers to the pressure in the cylinder, and  $v$  refers to the volume of the cylinder. In Figure 2-3 (a), curve 4 shows the pressure changes in cylinder without ignition occurrence. If  $\vartheta_{ig}$  is too large, e.g.  $\vartheta_{ig1}$ , the rapidly expanding air-fuel mixture can actually push against the piston moving towards TDC and cause detonation and power lost. If  $\vartheta_{ig}$  is too small, e.g.  $\vartheta_{ig2}$ , the maximum cylinder pressure reaches when piston has moved too far away from TDC, which results in power lost, high emissions, and unburned fuel. When  $\vartheta_{ig}$  is properly set, e.g.  $\vartheta_{ig3}$ , the force generated to push the piston reaches maximum. Figure 2-3 (b) is a pressure-volume diagram, in which curves 3 has largest area. This implies that the ignition provides greatest force to push the piston towards crankshaft when timing advance is  $\vartheta_{ig3}$ .

During the ignition process, the energy of combustion is transferred to mechanic energy. However, not all combustion energy is used for pushing piston. The energy diagram is

drawn in Figure 2-4 according to Kutlar's paper and Capuano's dissertation (Kutlar, et. al., 2005; Capuano, 2006). From this figure it can be seen that only 25% combustion energy is transferred to the energy used for engine running. There are 40% energy lost in heat transfer of exhaust gas and 35% energy lost in other thermal transfer process.

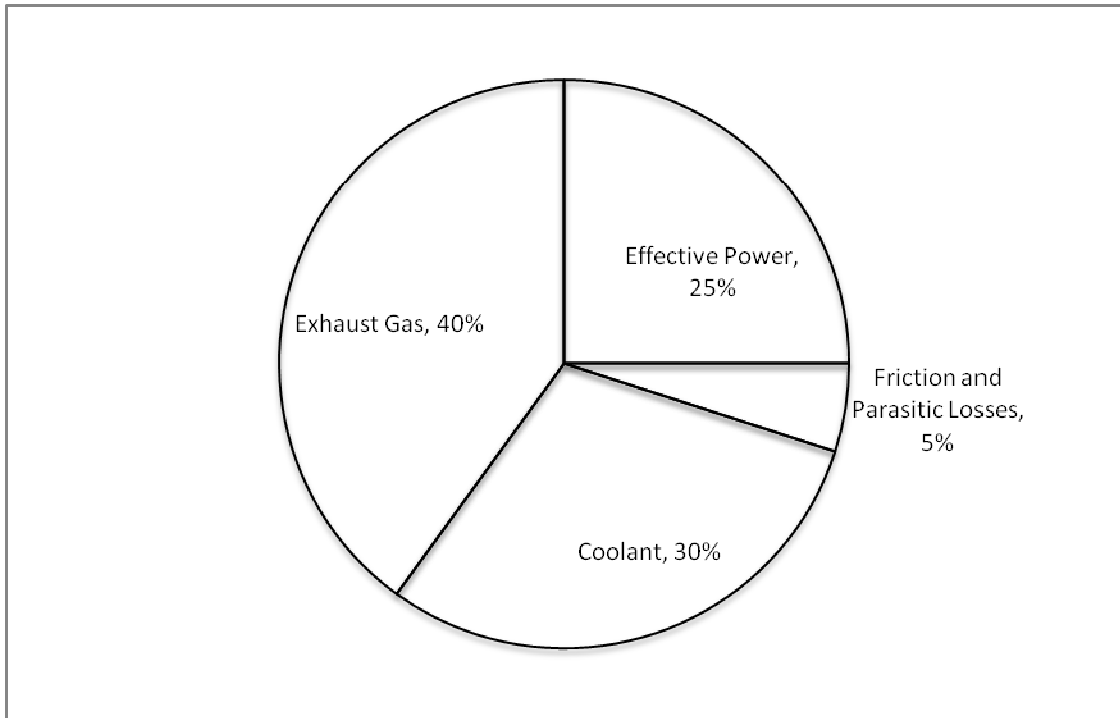


Figure 2-4 Energy split in ICE

Before suggesting a means to improve energy efficiency, the chemistry and physics process of ignitions are studied here. The process of an ignition in an ICE is actually a breakdown process of the air-fuel mixture. The breakdown of a kind of gas is a result of a substantial increase in the concentration of mobile charge carriers in the medium considered. This increase is usually caused by the effect of an electric field on the already existing carriers (Jonassen, 1999). For instance, in air, these charge carriers are ions and some free electrons. Air ions are molecular clusters, which generally consist of water molecules around single charge oxygen or nitrogen molecule. In positive air ions, the charged molecule can be oxygen or nitrogen with from 12 to 15 water molecules

attached. However in negative air ions, the charged molecule is oxygen, with from 8 to 12 attached water molecules (Jonassen, 1999).

Both ions and free electrons participate in the random thermal movement of molecules. If an electric field exists in gas, the charged particles will accelerate in the field and gain extra kinetic energy. As a result of this additional energy electrons would bounce off a gas molecule: the gas is ionized. The process is shown in Figure 2-5 (Oldnall, 2001). This phenomenon is termed *breakdown*. If many molecules are ionized in one region, the ionized gas is called plasma.

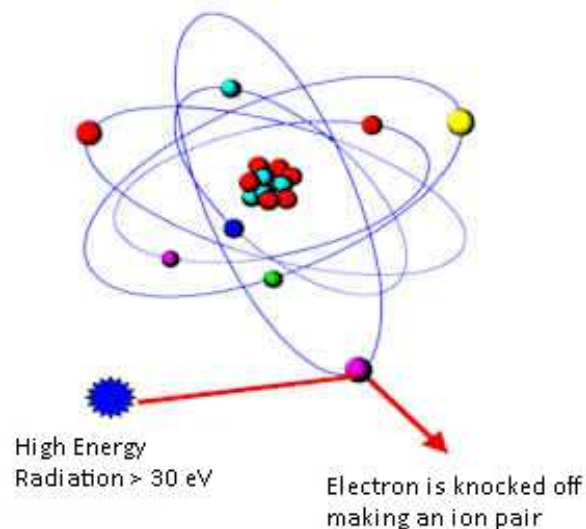


Figure 2-5 Ionization process (Oldnall, 2001)

The gas ignited in petrol engine cylinders is the air-fuel mixture. The air-fuel mixture is a combination of air and fuel at a certain ratio. The ratio is called air/fuel ratio (AFR), which is a mole ratio of air to fuel present during combustion.

When all fuel is combined with all free oxygen in air, the mixture is chemically balanced and the AFR of this combination is called the stoichiometric mixture (often abbreviated to stoich). For petrol, the stoich AFR is approximately 14.7. Any mixture at a ratio less than

14.7 is considered as rich mixture, any at more than 14.7 is lean mixture. For the spark ignition, the required voltages for igniting air-fuel mixture of different mix ratios are different. Likewise, the electric field intensities required to breakdown the air-fuel mixture of different mix ratios are different.

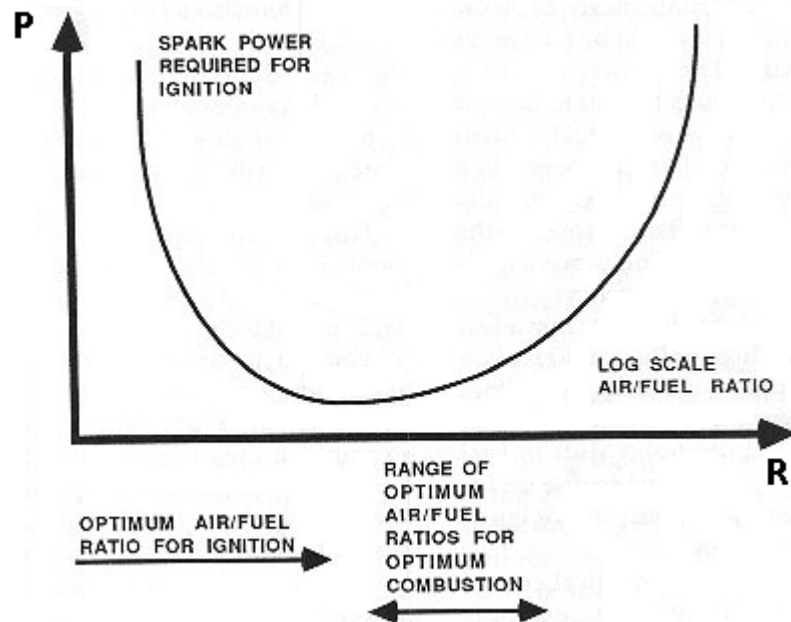


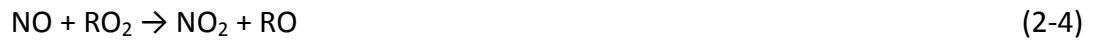
Figure 2-6 Power requirements for ignition vs. AFR (Jacobs, 1996)

Figure 2-6 shows the spark power requirement for ignition against the air/fuel ratio. In Figure 2-6,  $P$  refers to the power required for ignition and  $R$  refers to the AFR in the cylinder. The AFR and spark power depend on type and refinement of fuel used, temperature and compression. For the type of hydrocarbon-type fuels, like petrol, the spark power generally looks like an upside down bell curve against AFR. This figure shows that the optimum ratio for minimum spark power is richer than for optimum combustion efficiency. Thus, at stoich ratio the voltage required to ignite air-fuel mixture is the lowest (Jacobs, 1996).

However, the petrol usually contain the various materials such as heptanes, octane, other alkanes, and additives including detergents, and oxygenators i.e. methyl tertiary-butyl ether (MTBE) or ethanol/methanol. These compounds alter the stoich ratio, with most of

the additives pushing the ratio downward. Lean mixture produces less power than stoich mixture does while rich mixture returns poorer combustion efficiency than stoich mixture does.

According to above analysis, air-fuel mixture primarily consists of  $\text{NO}_2$ ,  $\text{O}_2$ ,  $\text{C}_2\text{H}_6$ , and  $\text{CO}_2$ . The most important chemistry of forming plasma is that of radicals which are formed by molecular dissociation due to high energy electron impact. Such a chemical process is presented below (Qiao, et al., 2003; Hoard, 2001, Starikovskaia, 2006).



where  $R$  is an organic species and  $\bullet$  denotes radical species

Along with generation of plasma O-zone is formed as well. The reaction of forming O-zone is shown in following scheme:



Following the breakdown the air-fuel mixture is combusted. The chemical process of the combustion of air-fuel mixture is expressed below.



(2-1) – (2-6) shown above describe the entire ignition process of a petrol ICE.

The pressure in cylinders also affects the breakdown voltage threshold. The relation between pressure in the cylinder and the breakdown voltage follows Paschen's Law (Paschen, 1889). Paschen's law essentially states that at higher pressures the breakdown characteristics of a gap are a function of the product of the gas pressure and the gap length. It is usually written as (Paschen, 1889):

$$V_{\text{breakdown}} = \frac{B \cdot p \cdot d}{C + \ln(p \cdot d)} \quad (2-7)$$

It can also be expressed for electric field intensity as:

$$E_{\text{breakdown}} = \frac{B \cdot p}{C + \ln(p \cdot d)} \quad (2-8)$$

where  $C = \ln\left(\frac{A}{\ln\left(1 + \frac{1}{\gamma}\right)}\right)$ ,  $\gamma$  is the secondary ionization coefficient,  $p$  is the pressure,  $d$  is the

gap distance,  $A$  and  $B$  are constants that depend on the composition of the petrol. For purely air, Paschen's law is drawn in Figure 2-7 (Duniway, 1998).

## Breakdown Voltage vs. Pressure x Gap (Air)

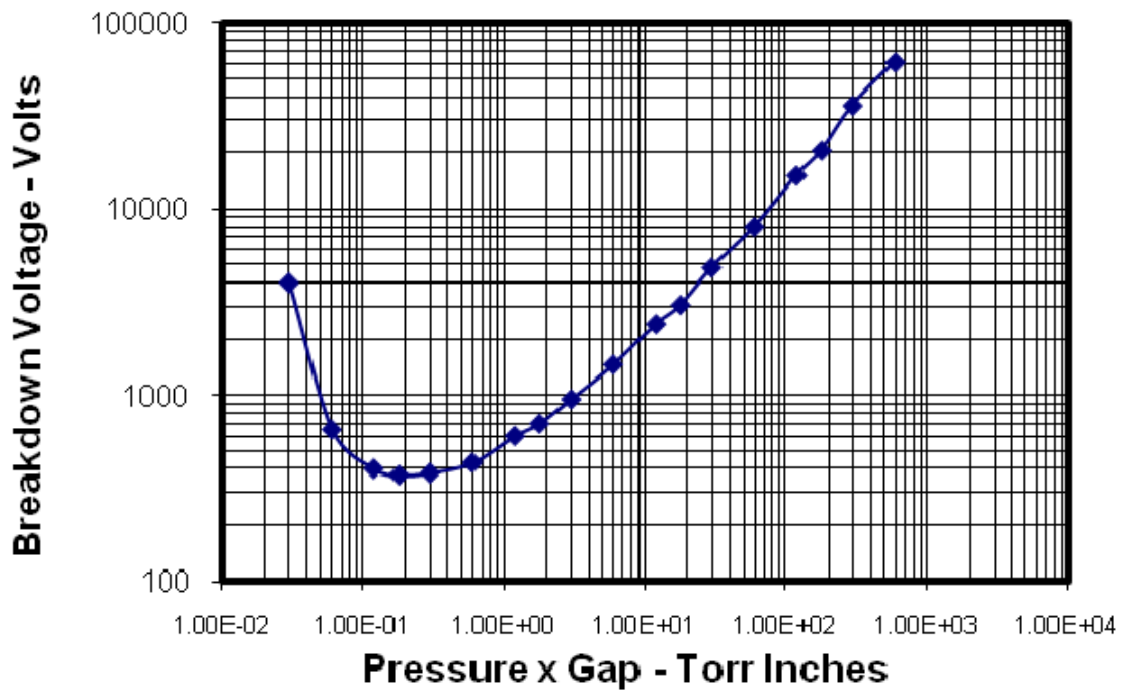


Figure 2-7 Paschen's Curve for Air (Duniway, 1998)

## 2.2. Current SI Systems

In a modern automotive engine based on SI system, typically 25%-35% of the chemical energy stored in the fuel is so transformed (Jacobs, 1996; Kutlar, et.al., 2005; Capuano, 2006). This percentage is referred to as the fuel efficiency or ignition efficiency in this thesis. Hereby, the efficiency means only 25%-35% energy from combustion of fuel contributes to pushing piston. 5% energy from combustion of fuel is used to overcome engine friction and pumping the air and fuel. 30%-40% energy is exhausted on heat through the cylinder wall and cylinder head. This ignition efficiency is so poor that a loss or gain of just three percentage point could make a 20% difference in fuel consumption (Jacobs, 1996). Meanwhile, the low combustion efficiency causes more pollutant emissions.

Researchers have tried to develop the conventional spark ignition so as to improve the ignition efficiency. Multi-point spark ignition technology was invented to enhance the ignition of single point spark plug and to improve the efficiency of the SI system. A multi-point spark ignition system fitted with at least 3 spark plugs in a removable cylinder head is invented to realise a multi-point ignition (Davis, 1987; Schaus, 2001). The spark plug with a multi-point firing cap includes a central electrode having a proximal end, a distal end and a cap having a central portion and plural projections extending radially from the central portion (Davis, 1987; Schaus, 2001). Although the multi-point ignition system enhances the combustion and prevent possible misfire by increasing ignition points it does not raise the ignition efficiency significantly.

### **2.3. Homogeneous Charge Compression Ignition**

To achieve more efficient ignition, homogeneous charge compression ignition (HCCI) is developed to replace the traditional SI system. Due to its volume ignition, HCCI is more efficient than SI.

HCCI refers to a form of internal combustion, in which well mixed air and fuel are compressed to the point of auto-ignition. HCCI has characteristics of two most popular forms of combustion used in ICEs: homogeneous charge spark ignition (petrol spark ignition engine) and stratified charge compression ignition (diesel engine). HCCI is a volume ignition. It aims to ignite all air-fuel mixture in the cylinder at once which makes air-fuel mixture in a cylinder to burn nearly simultaneously. In SI engines fuel must be burned hot to ensure that the flame spreads rapidly enough through the combustion chamber before new mixture enters. However, in an HCCI engine there is no need for a quick spreading flame because combustion occurs throughout the combustion chamber. As a result, combustion temperatures in HCCI engines can be lower than in SI engines so that emissions of nitrogen pollutants are negligible (Warnatz, 2006). HCCI is also designed to burn lean air-fuel mixture so as to reduce incomplete combustion. Although there are several enabling technologies to control the combustion of the HCCI, no well-defined combustion initiator can be directly controlled. Therefore, timing control of the initial

combustion of an HCCI system is a major hurdle for it to achieve more widespread commercialization (Zhao, 2003).

## **2.4 Laser Ignition**

Laser Ignition system is another kind of spark ignition system. It uses laser induced spark ignition technique, in which a laser beam induces gas breakdown at its focal point (Morsy, et al., 2001). Like SI, laser ignition is still a type of ignition that ignites at point(s) though it can ignite leaner air-fuel mixture than traditional SI system (Phuoc, 2006). It does not have much improvement on ignition efficiency with respect to the conventional spark ignition system.

## **2.5 Concept of the MI system**

The MI system concept was first proposed in 1974 (Ward, 1974) to replace the SI system. It was suggested to improve the ignition performance and achieve the complete combustion with its volume ignition so as to reduce pollutant emissions.

The MI system uses microwave resonance to create a strong electric field to break down air-fuel mixture in a cylinder within 30-150 ns (MaierII, et al., 1993; Eways, et al., 1989; Liu, 2003; Starikovskaia, 2006). Due to the resonance in the cylinder an electric field is enhanced to break down the air-fuel mixture. As a result of the breakdown of the air-fuel mixture, plasma is generated. The initiation of the ignition is controlled through the timing control of the generation of microwave. When the piston moves to designed ignition position a control signal is sent to the HCMI system to generate the microwave, which is then transferred to the ignition initiator.

In this thesis, an HCMI system is divided to three parts: microwave source, transmission line, and engine cylinder (combustion chamber) as shown in Figure 2-8.



Figure 2-8 Microwave ignitions construct

Once the control signal is sent to the HCMI system, the microwave is generated by the microwave source and then transferred to engine cylinders through microwave transmission lines. Meanwhile, the piston is moving towards to TDC and passing the designed ignition position where the natural frequency of the cylinder corresponds with the frequency of microwave, the resonance therefore occurs. As a result of resonance, strong electric field is created in each cylinder. The air-fuel mixtures in cylinders are broken down in volume by the strong electric field within 30-150 ns (MaierII, et al., 1993; Eways, et al., 1989; Liu, 2003; Starikovskaia, 2006).

Air and fuel are well mixed before they are injected into engine cylinders for the HCMI system. For a spark plug the gap between the electrodes is 1-2 mm and voltage applied on electrodes is about 15-25 kilovolts (Dorf, 1998, Hartman, 2004). Thus, the equivalent electric field intensity between two electrodes is approximately  $10^7$  V/m.

According to existing experiments this equivalent electric field intensity is higher than the critical electric field intensity for the microwave breakdown of air-fuel mixture. The process of microwave breakdown is different to the process of spark ignition (Hagen, et al., 2001, Dawson, et al., 1973).

The MI has advantages over the SI because it employs a volume ignition, which can ignite 60% air-fuel mixture in the cylinder (Capuano, 2006) and the ignition timing of an MI system is easier to control than of an HCCI system by controlling the timing of the generation of the microwave. However, after decades researching the HCMI system has not yet been successfully implemented on any automotive vehicle on the road. The

previous research is reviewed in the next section and the problem will be addressed in this thesis.

## 2.6. Microwave Fundamentals

The electromagnetic (EM) field can be considered as a combination of electric field and magnetic field. The electric field is produced by stationary charges and the magnetic field by moving charges. Only the electric field contributes to microwave breakdown and inducing plasma in engine cylinders.

Maxwell equations used to describe the EM field are presented below (Seely & Poularikas, 1979)

$$\nabla \cdot \mathbf{D} = \rho \quad (2-9)$$

$$\nabla \cdot \mathbf{B} = 0 \quad (2-10)$$

$$\nabla \times \mathbf{E} = -\frac{\partial \mathbf{B}}{\partial t} \quad (2-11)$$

$$\nabla \times \mathbf{H} = \mathbf{J} + \frac{\partial \mathbf{D}}{\partial t} \quad (2-12)$$

where  $\mathbf{E}$  is electric field intensity (V/m),  $\mathbf{H}$  is magnetic field intensity (A/m),  $\mathbf{B}$  is magnetic flux density (T),  $\mathbf{D}$  is electric displacement field (C/m<sup>2</sup>),  $\mathbf{J}$  is current density (A/m<sup>2</sup>), and  $\rho$  is electric charge density (C/m<sup>3</sup>).

The electric field distribution in a cylinder can be considered as a solution of equations (2-9) – (2-12) under practical boundary conditions. For most engine cylinders, the electric field distribution is hardly calculated manually because of the complicated boundary conditions and irregular geometric shape of the cylinder. Therefore, computer simulations are the most efficient way to resolve this problem.

### 2.6.1. Microwave Resonance

The principle of microwave resonance is studied in this section. Resonance is a phenomenon that occurs frequently in a variety of systems under certain circumstances. The microwave resonance is the resonance at the frequency greater than 1 GHz. It normally occurs in metallic enclosures. The energy in the resonator is generated from the standing-wave electric and magnetic fields. The currents flowing through the wall of the resonator causes the power loss. The resonance can be excited by applied microwave via small openings on the walls or by a coupling coaxial cable with a probe shape antenna or a loop antenna (Seely and Poularikas, 1979).

Cylindrical cavities have features of the high quality factor (Q factor) value and wide frequency range. For the resonance in a cylindrical cavity there are two types of resonance mode, i.e. TM mode and TE mode.  $TM_{010}$  mode is the dominant mode in a  $d/a < 2$  cylindrical cavity where  $d$  is the depth of the cylinder and  $a$  is the radius of the cylinder. The field distribution at points of minimum transverse electric field is shown in Figure 2-9 (Seely and Poularikas, 1979, Capuano, 2006).

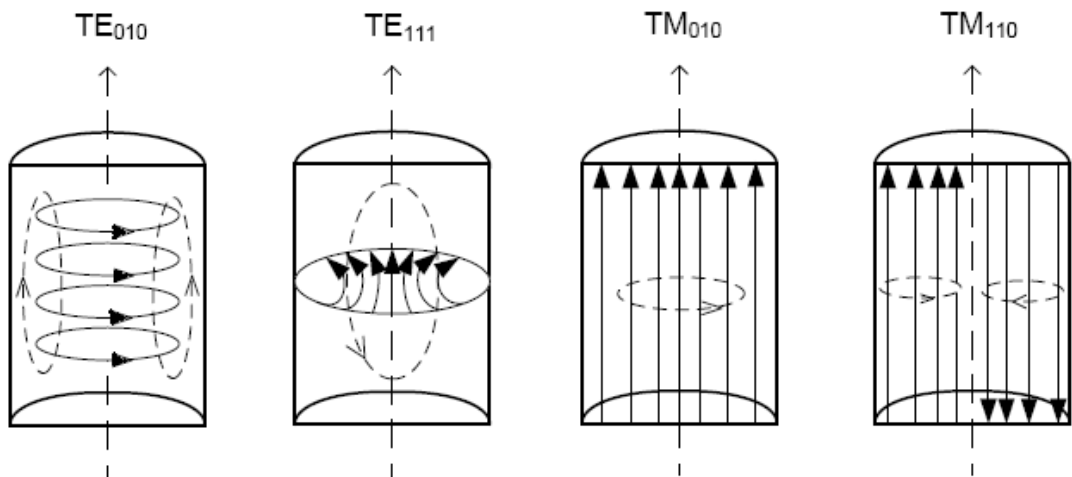


Figure 2-9 Electric field distributions in cylinder cavity (Seely and Poularikas, 1979, Capuano, 2006)

In Figure 2-9 the solid lines represent electric field and the dashed lines represent magnetic field. The solution of  $TM_{010}$  mode of Maxwell equations is presented in equations (2-13) – (2-15):

$$\mathbf{E}_{oz} = A_1 2jJ_0\left(\frac{P_{01}r}{a}\right) \cos k_z z \quad (2-13)$$

$$\mathbf{E}_{or} = 2k_z A_1 J_1\left(\frac{P_{01}r}{a}\right) \sin k_z z \quad (2-14)$$

$$\mathbf{H}_{o\phi} = 2j\omega\epsilon A_1 J_1\left(\frac{P_{01}r}{a}\right) \cos k_z z \quad (2-15)$$

where  $\mathbf{E}$  is electric field intensity (V/m),  $\mathbf{H}$  is magnetic field intensity (A/m),  $J_1$  is first order Bessel function,  $P_{01}$  is 2.405;  $k_z$  is  $\frac{2\pi}{\lambda_z}$ ,  $r$  is the radius of cylinder,  $a$  is the length of cylinder,  $\omega$  is the angle frequency,  $A_1$  is a constant,  $z$  is coordinates of  $z$ .  $TM_{010}$  mode does not have  $\mathbf{E}_{o\phi}$ ,  $\mathbf{H}_{oz}$ ,  $\mathbf{H}_{or}$  opponents.

The engine cylinder is not a regular cylindrical cavity. However, the geometry of a cylinder is similar to a cylindrical cavity except the cylinder head. During the compression stage, valves are all closed. The cylinder becomes a metal closure. The distribution of the electric field in an engine cylinder is similar to the one shown in Figure 2-9.  $TM_{010}$  mode in a cylindrical cavity is analysed here to assist understanding and investigating the resonance in an engine cylinder.

The essential requirement of resonance is the input microwave frequency equals the natural frequency of a resonator, which is called frequencies match. Either the natural frequency of the resonator changes away from the frequency of input microwave or the input microwave frequency changes away from the natural frequency of the resonator the resonance will gradually disappear, which is called off-resonance. For the purpose of

frequency match, the frequency of the input microwave is obtained by calculating the frequencies of the resonant cavity.

The natural frequency of a cylindrical resonator is defined as in (2-16) (Seely and Poularikas, 1979)

$$f_i = \frac{c}{2\pi} k_i \quad (i = 1, 2, 3, \dots) \quad (2-16)$$

where  $k_i$  is eigenvalue of resonance,  $c$  is the speed of light in vacuum, and  $f$  is natural frequencies, which is discrete.

According to equation (2-16) there is more than one natural frequency for a certain resonant cavity. The natural frequency of the dominant mode or resonance is the  $f$  at  $i = 1$  which is the lowest frequency of natural frequencies. When the resonance occurs, the field strength in the cylinder is amplified. Q factor is a parameter to evaluate the amplitude of energy in a cylinder. The Q factor is defined as in (2-17)

$$Q = \omega_0 \frac{\text{Energy Stored}}{\text{Power Loss}} = \omega_0 \frac{W}{P} \quad (2-17)$$

where  $\omega_0$  is resonant frequency.

The Q factor can be derived as (Seely & Poularikas, 1979):

$$Q = \frac{1}{\sigma} \frac{V}{S} \quad (2-18)$$

where  $\sigma$  is skin depth,  $V$  is the volume of resonator and  $S$  is the surface area of resonator walls. From this equation it can be seen that the Q factor is relative to the skin depth of resonance walls.

## 2.6.2. Coupling Methods

The microwave energy is normally coupled into a resonant cavity via small openings on the walls or by a coaxial cable with a probe shape antenna or a loop antenna. Three coupling means for a cylindrical cavity are shown in Figure 2-10.

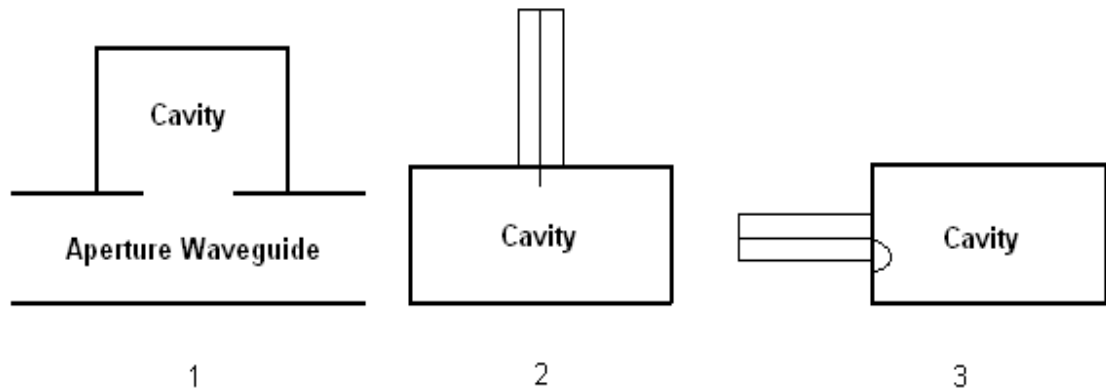


Figure 2-10 Coupling methods for cylinder cavity

To apply an MI system on existing engine with the least modification to the engine, it requires that the coupling apparatus are fitted in the engine cylinder with no modification to the cylinder body. For this goal Figure 2-10 (2) is obviously the most suitable coupling method for the HCM system with the consideration of the geometry of the engine cylinder. The coupling method (2) uses a coaxial cable as the transmission line, which is connected to the resonant cavity through the opening for spark plug at the cylinder head. The impedance match is an important factor that affects the microwave coupling efficiency. The output impedance of coaxial-line is calculated using (2-19) (Seely and Poularikas, 1979).

$$Z = \frac{60}{\sqrt{\epsilon_r}} \ln \frac{b}{a} \quad (2-19)$$

where  $\epsilon_r$  is relative permittivity,  $b$  is outer radius of the coaxial cable and  $a$  is the radius of the centre core of the coaxial cable. Ideally when output impedance of coaxial-line equals input impedance of cavity the microwave energy can be transmitted into cavity without reflection.

## 2.7 Progress to Date

An MI system for ICEs was first proposed and patented in 1974 by Ward (Ward, 1974). In principal, through a microwave transmission line and a microwave emitter, microwave energy is coupled into the engine cylinder specially designed for this purpose. A strong electric field is then created by microwave resonance in the cylinder and breaks down air-fuel mixture injected into the cylinder.

Several more patents with respect to MI systems have been filed since then. Some research papers have also been published on the developments of MI systems and on some experiment results.

These can be classified to two approaches. One is to use the engine cylinder as a resonator as described in the initial concept (Kimura, et al., 1981; Ward, 1991; Schleupen, 2000; Schmidt & Ruoss, 2003; Schmidt, et al., 2003); the other is to build an independent resonator to ignite the air-fuel mixture in the cylinder (Manning, 1995; Bokulich, 2001, Pertl & Smith, Jun. 2009).

When the engine is running the cylinder forms a cavity varying with the motion of the piston. Several patents have therefore tried to fit an apparatus on the piston so as to retain the natural frequency of the cavity and to ensure the occurrence of resonance (Kimura, et al., 1981; Ward, 1991; Schleupen, 2000; Schmidt & Ruoss, 2003; Schmidt, et al., 2003).

However, there is no detail provided in these patents, as to whether the apparatus can cover a reasonable range of frequency or how much the natural frequency of the cavity

changes when the piston moves. It is challenging for this method to work for all types of engines due to various geometries of the cylinders because hardware experiments are expensive and time taking.

To address this problem, researchers at West Virginia University developed a quarter wave coaxial cavity resonator (QWCCR) (Pertl and Smith, 2009). The QWCCR works as an independent resonator, in which a strong electric field is generated through the resonance to ignite lean air-fuel mixture for increased fuel efficiency (Manning, 1995; Bokulich, 2001).

Similarly an RF plasma ignition device for ICE was investigated by Smith, et al., (Smith, et al, 1997), using a high  $Q$  factor QWCCR in a special cylinder. The frequency range of this QWCCR is 800-1500MHz (Smith, et al., 1997).

The QWCCR is designed to replace the spark plug easily without any other modification to the engine. The disadvantage of a QWCCR is that it only breakdown the air-fuel mixtures surrounding the centre electrode, hence losing much of the advantage of an MI system.

In addition to automotive MI systems, there exist methods to realise plasma MI system for jet engines, which have been tested in laboratory and have shown to generate a stronger power than ordinary ignition system.

In 2005, Dana Corporation also demonstrated a microwave based plasma ignition technique, AtmoPlas<sup>(TM)</sup>, where a vehicle-borne synchronized microwave source feeds short microwave pulse into the engine through a modified spark plug to ignite air-fuel mixture with a plasma temperature reaching 1200 degrees Celsius (DanaCorporation, 2005). Although, there is no detail published on AtmoPlas<sup>(TM)</sup>, experiments confirm the feasibility of MI for petrol engine (Tran, 2004).

In addition, a non-thermal transient plasma ignition (TPI) technique is investigated as an alternative to the SI for petrol ICEs, offering 3 times shorter ignition and pressure rising times. Test on a 2.5 litre 4-cylinder engine shows typical 15%-20% increases in indicated

mean effective pressure (IMEP), much shorter burn durations at identical operating conditions and reduced NO<sub>x</sub> emissions (Gundersen, 2004, Theiss, et. al. 2005). Research on corona discharge plasma ignition also shows that the combustion with plasma ignition is at least 25% faster than with SI (Bellenoue, et. al., 2005). It is reported that the necessary electric field strength for microwave to induce plasma and ignition of an air-fuel mixture is around  $7.77 \times 10^5$  V/m (Hagen, et al., 2001, Dawson, et al., 1973).

Furthermore, it is also reported that propane-air mixture can also be ignited by microwave discharge for jet engine (Pancheshnyi, et. al, 2006; Esakov, et. al 2006). Propane is a three carbon alkane and hence has a higher octane rating than petrol, which makes it harder to be ignited. It has been reported that the critical breakdown intensity for the microwave electric field is  $8.4 \times 10^5$  V/m under 100 torr pressure and 150K temperature (Pancheshnyi, et. al, 2006; Esakov, et. al 2006).

All research reviewed above shows the feasibility of the MI system and the advantages of an HCMI system over the SI system. However no one has successfully realised a practical MI system on the road. The thesis will address the problem of realising it through computer simulations and automated search.

## **3. Simulation and Search**

### **3.1 Finite Element Method for Microwave Simulation**

The finite element method (FEM) is a 'divide and conquer' numerical technique for finding approximate solutions to partial differential equations (PDE). It has been commonly used for complicated domains, if a domain changes, if the desired precision varies over the entire domain, or if the solution lacks of smoothness.

The FEM has been widely used in design and development of production of mechanical engineering discipline, such as aeronautical, biomechanical, and automotive industries. The FEM is used in the research and design of engine systems in this thesis owing to the irregular shape of engine cylinders and various conditions inside the cylinders when the engine is running. These factors affect the design of an HCMI system more than an SI system.

In practical environment, the problems usually involve boundary conditions. To solve a boundary value problem using FEM, two essential steps are taken (Pepper, 1992):

1. Rephrase the original boundary value problem in its weak, or variation form.
2. Discrete the weak form in a finite dimensional space.

The simulation of electric field in a cylinder of an engine is actually to find a solution to the Maxwell equations in a continual region with certain boundary conditions. FEM is a common way to simulate electromagnetic field. However, when engines' conditions change it is hard to find the right solution for the problem. Thus, an automated search method coupled with FEM based simulations is hired to search for a solution for this problem.

For FEM analysis purpose Maxwell equations need to be expressed in form of the hyperbolic system of partial differential equations. This gives the access to powerful

mathematical theories for the numerical solutions to hyperbolic partial differential equations’.

In this thesis an FEM based simulation software Multiphysics from COMSOL is used to simulate the EM field in an engine cylinder. The user interface of COMSOL Multiphysics is shown in Figure 3-1.

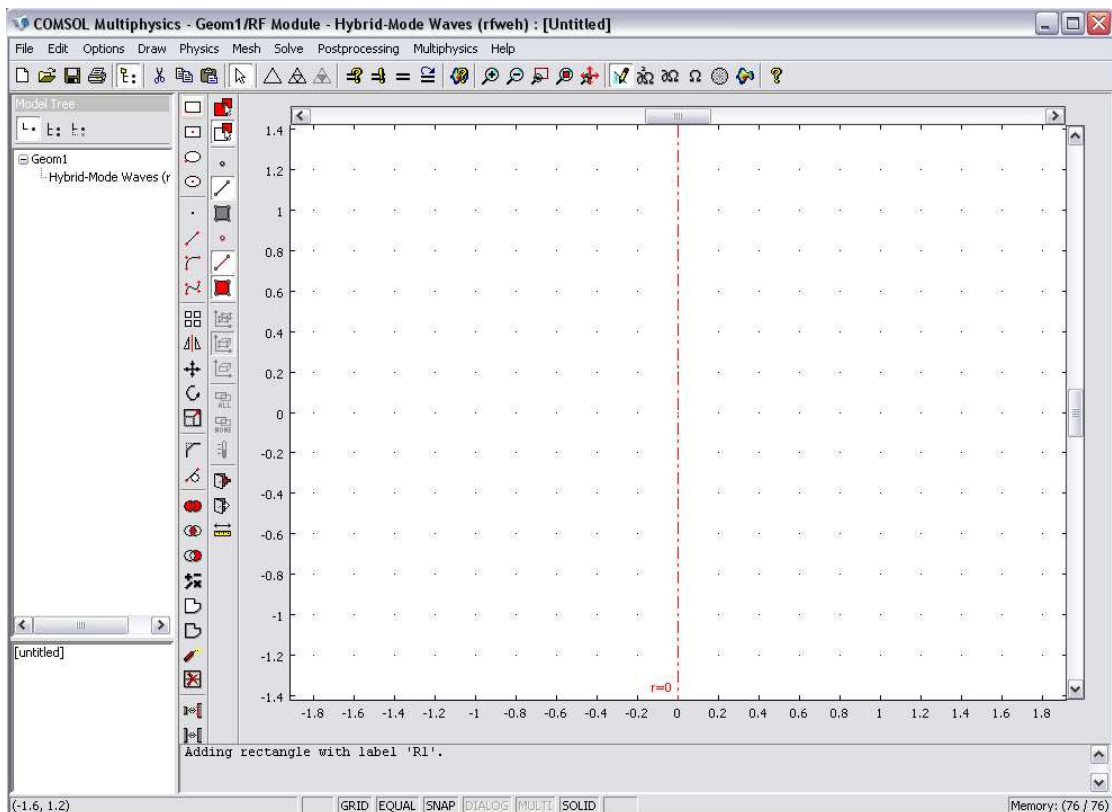


Figure 3-1 User interface of COMSOL Multiphysics

The simulation of the EM field generated by microwave resonance is the essential part of this research. To design an HCM system and find suitable and practical design parameters for an HCM system, massive simulations have to be carried out. However, this huge amount of work causes long research period and huge expenses. Using an automated search method the amount of simulations can be reduced significantly.

## **3.2 A-Posteriori Search Methods**

The search methods used in this thesis have been widely used for many years in various fields. In this thesis, two search methods are employed to the automate simulation based design of experiments. One is the Nelder-Mead (NM) simplex search method and the other is the EA based search method.

### **3.2.1 The Nelder-Mead Method**

The Nelder-Mead simplex method, also called the downhill simplex method, is a nonlinear optimization algorithm (Nelder and Mead, 1965) for a multi-dimensional space. A simplex is a poly-tope of  $(N+1)$  vertices in  $N$  dimensions. The method finds a locally optimal solution to a problem with  $N$  variables if the objective function varies smoothly (Haupt, 1998).

Although NM simplex method is a local search method, it still has some advantages over other search methods. NM simplex method can give significant improvements in early stage. It only requires a few function evaluations per iteration. Compare NM simplex method to EA search method, the NM search method needs much less function evaluations to reach satisfied search results, which saves much time.

In this thesis a state-machine simplex minimiser that implements NM simplex method embedded in MATLAB is employed.

### **3.2.2 Evolutionary Algorithm Based Search Method**

The EA based search method is a kind of a-posteriori search method. The idea of the EA is first proposed in 1960s by several computer scientists for solving practical problems (Mitchell, 1996). It adopts Darwin's evolution theory and includes 3 processes, selection, crossover, and mutation to perform so called nature choice. It simulates the nature evaluations of the human being. The evolutionary algorithm was first invented in 1960s

by computer scientists to solve complicated practical problems. It has been widely used in many areas.

An EA initializes its population randomly. Evolution measures the fitness of each individual in a population based on its worth in certain environment. Fitness evaluation may be as simple as computing a mathematical function or as complex as running an elaborate simulation. In this thesis the FEM based simulation is employed as a fitness function for the EA search method. Selection is usually performed in two steps, parent selection and survival. Parent selection decides who becomes parent and how many children the parents have; higher-fitness individuals are more likely to be parents and have more children. Children are created via crossover which exchanges information between the parents. Mutation further perturbs the children. The children are then evaluated. Finally, the survival step decides who survives in the population (Haupt, 1998).

In this thesis an EA search tool of FT3PAK is employed to work and compare with the NM simplex method. FT3PAK is a toolbox used under the MATLAB environment. The interface of FT3PAK is shown in Figure 3-2 below.



Figure 3-2 The Ft3pak interface

To achieve an efficient and effective search performance the EA parameters has to be set properly. The main EA parameters include crossover rate, mutation rate, population, and generation. The EA tool supports multiple parameters and multiple objectives. During the search the progress is shown in a pop up window, which is shown in Figure 3-3. In this window the search progress can be monitored.

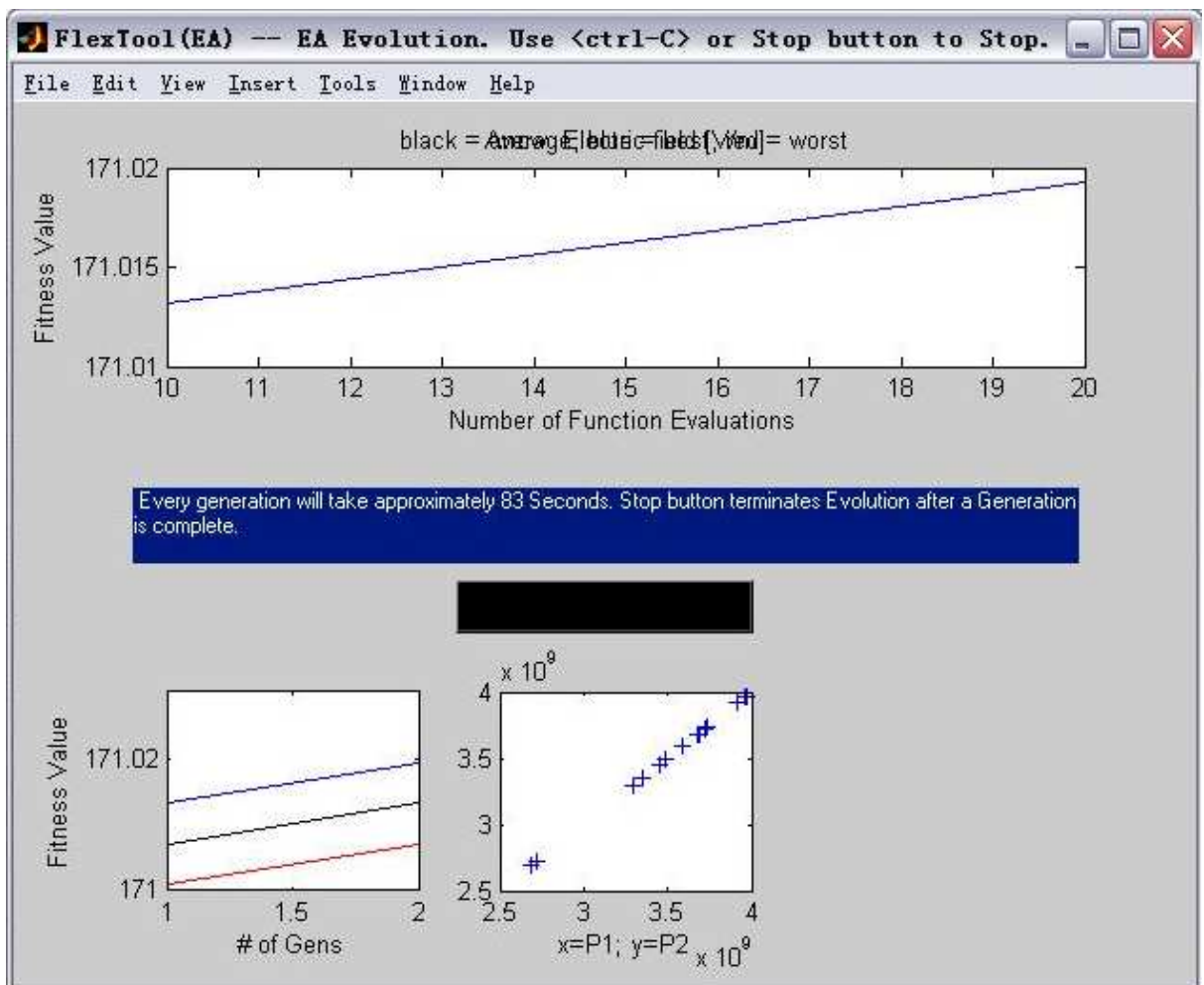


Figure 3-3 The search progress monitor window

The EA search method has its advantage of searching for global optimal solutions over the NM simplex search method. This allows EA to be used to search or optimise the complicated practical problems.

### 3.3 Design via Machine Learning and Search

This thesis adopts the a-posteriori search method to assist research and design so as to avoid the huge amount of simulations and calculations and reduce the research time. The machine learning employs an a-posteriori search method coupled with FEM simulation for fitness evaluations.

The a-posteriori search tool works in a loop as shown in Figure 3-4. The search tool searches parameters for the problem. These parameters are transferred to the FEM based simulation software. Then the FEM based simulation software simulates the parameters and returns the results to the search tools for objectives evaluation.

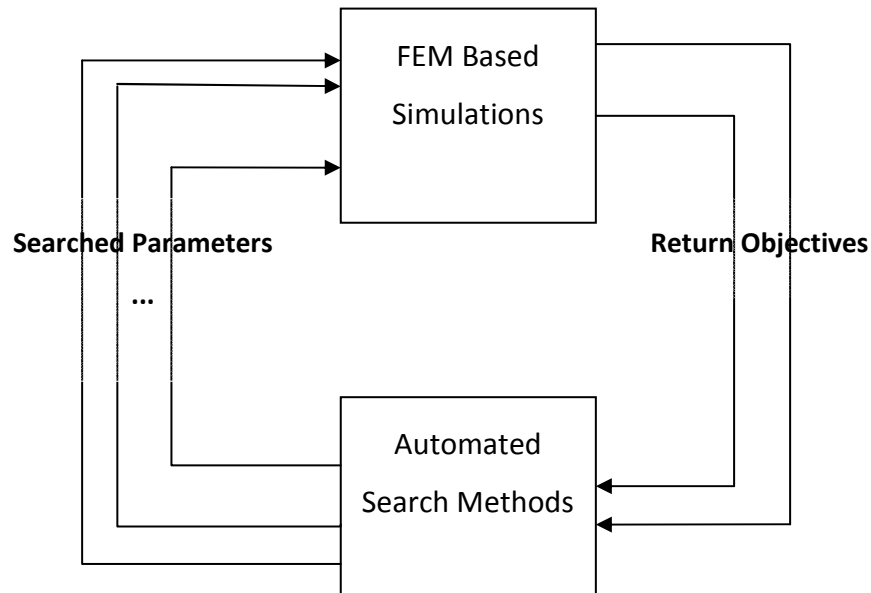


Figure 3-4 The relation between EA program and simulation program

In Figure 3-4, the values of parameters are searched by automated search method through evaluating the results which are returned from simulation software. Then the searched parameters are sent to simulation software. NM simplex method needs to have the initial values of parameters pre-set before the search starts. Differently, the EA tool generates an initial population of parameters randomly. The flow chart of the search procedure is shown in Figure 3-5.

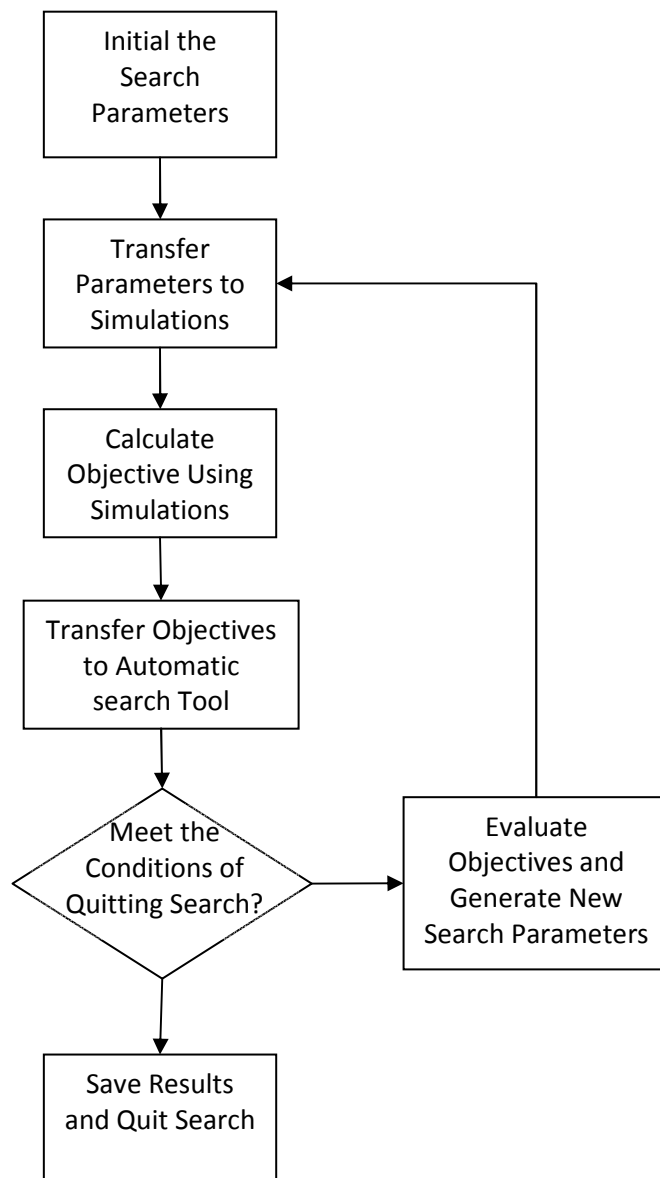


Figure 3-5 Automated search process

Figure 3-5 shows a flow chart of search process of NM search method and the EA search method employed in this thesis. Both the NM simplex method and the EA search method are connected with FEM based simulation software through a MATLAB program.

In Figure 3-5, for EA search method, the EA program randomly generates an initial population which includes a certain number of chromosomes for each parameter of the

simulation model. The simulation program then applies these parameters to a simulation model. Once receives these parameters the simulation program calculates objectives for the EA program. These objectives are then transferred back to the EA program. The EA program performs a role of fitness evaluation and new generation of parameters using evolutionary algorithm. The EA program keeps generating new sets of parameters and transfers them to the simulation program for calculation of the values of objectives until a certain number of search generations are reached. When the final generation is reached the EA program will terminate the search process and return search results.

The differences between the NM method and the EA method are mainly on the 1st and 5th steps. In the first step initial values of search parameters have to be preset for the NM search method and in the fifth step, the NM simplex method evaluates the convergence of the search and decides whether the search completes.

## **4. Simulation and Analysis of Microwave Volume Distribution and Strength**

To design an HCMI system with the least modification to the engine cylinder the simulation models of the engine cylinder are created. The microwave resonance in the cylinder and the coupling methods are investigated in this chapter. The coupling apparatus is fitted in the spark plug hole of the cylinder head. Thus, it does not require any physical modification to the engine cylinder body.

### **4.1 Geometry Models of Cylinder for Simulation**

In this section the geometry models of the cylinder and the microwave coupling apparatus are created for FEM based simulation and analysis of the HCMI system. The analysis in this thesis is focused on the influence of the running of the engine. The model is created based on a four stroke Otto cycle engine. It is created in both 2D and 3D for different research purposes.

A four stroke Otto cycle engine cylinder includes a cylinder head, a cylinder body, inlet and outlet valves, a spark plug, and a piston. An example of the cylinder head is shown in Figure 4-1 (Widmer, 2004).



Figure 4-1 The cylinder head (Widmer, 2004)

Figure 4-1 shows a Honda H22 cylinder head. It has two inlet valves, two outlet valves, and a spark plug opening. The diameters of the cylinders are usually between 80 mm and 100 mm. The diameters of cylinder heads are between 80 mm and 90 mm. It can be seen that the cylinder head has an irregular geometric shape in Figure 4-1. For an SI, both inlet and outlet valves are completely closed during the compression stroke.

In this thesis, a microwave coupling apparatus is designed to fit in the opening for spark plug at cylinder head. According to the dimensions of a 2.4 litres Chrysler-Dodge engine (Allpar, 2004), an illustration picture of an engine cylinder geometry model is shown in Figure 4-2. The geometric models of the cylinder are created for the purpose of FEM based simulations. Therefore, it is required to present all electric features of the engine cylinder. Electromagnetic characteristics of the engine cylinder should be monitored in simulations. Some parts of an engine cylinder that do not affect the resonance are neglected in these models.

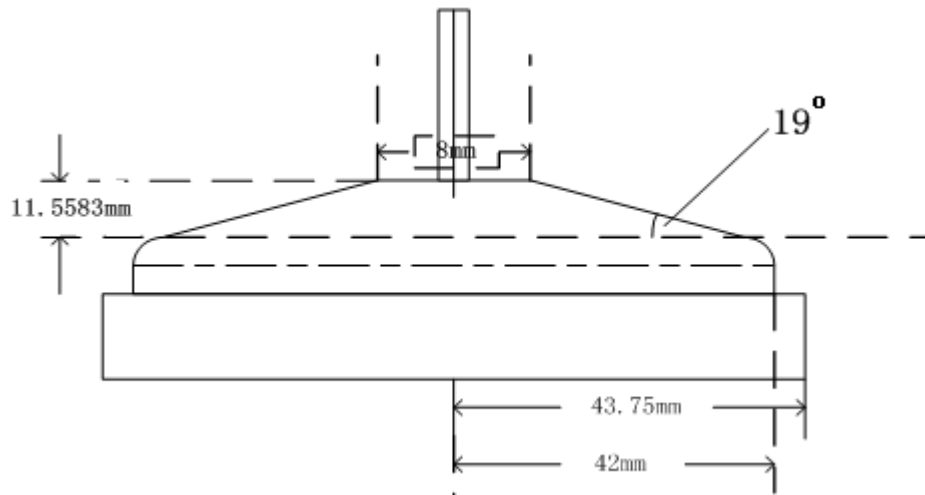


Figure 4-2 Dimension of cylinder model

As discussed in Chapter 2, for TM mode resonance the natural frequency of the cylinder changes when the piston is moving up and down. Once the natural frequency of the cavity changes away from the frequency of input microwave the resonance will be weakened or even disappear. This phenomenon is called off-resonance. To address the problems of existing MI system and propose an effective solution, the factors affecting microwave resonance and ignition are investigated comprehensively. These factors are piston position, air-fuel mixture, dimension of cylinders and coupling means. These factors affect the natural frequency and the  $Q$  factor of the resonant cavity.

#### 4.1.1. 2D Geometry Model for Simulations

An engine cylinder is considered as an axial symmetric cavity during the compression stroke. The cylinder body is regarded as a cylindrical cavity with a moving bottom. The cylinder head is fitted with a coaxial cable and antenna as shown in Figure 4-2.

Figure 4-3 shows a 2D model created for simulations. In Figure 4-3, part 1 is the cylinder head; part 2 is the cylinder body; part 3 is an antenna; and part 4 is the coaxial cable. The piston position and top dead centre (TDC) are also indicated in this figure. Units of both vertical and horizontal axes in this figure are m.

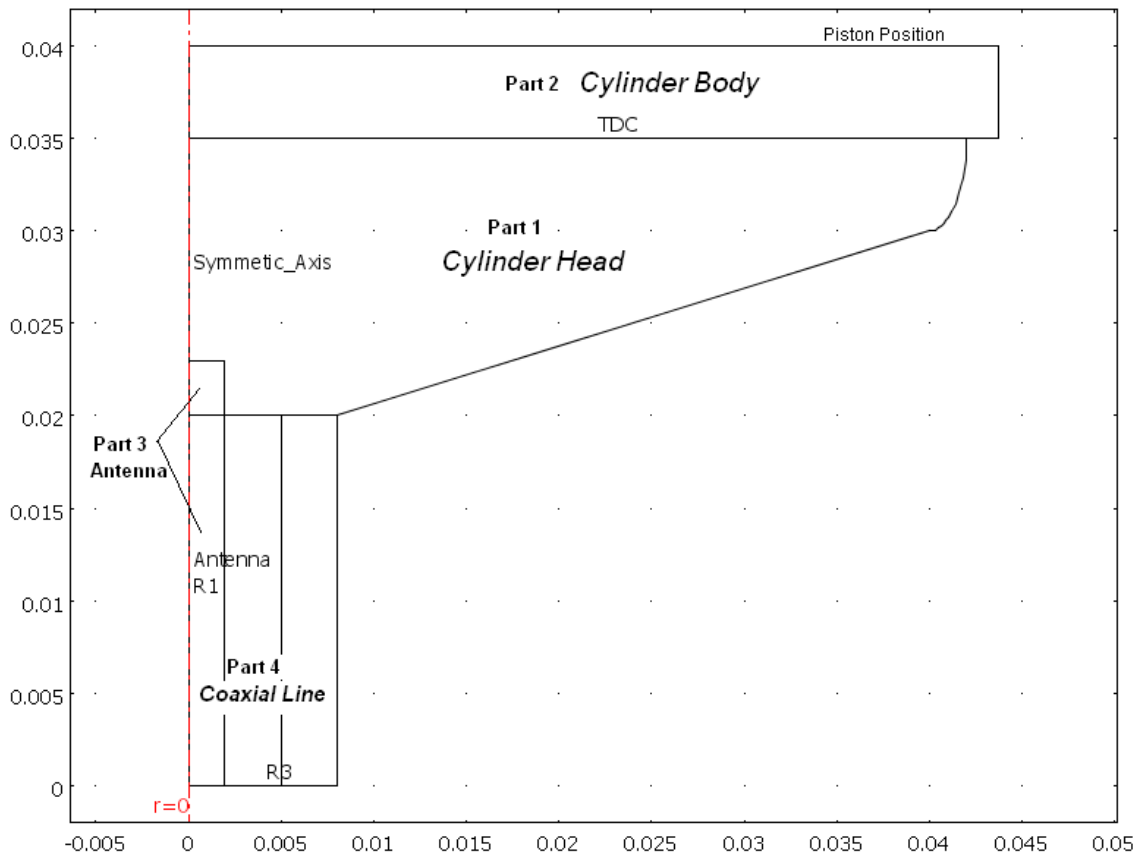


Figure 4-3 A 2D model established for simulations

#### 4.1.2. 3-D Geometry Model for Simulations

For the investigation of non-symmetric geometries, a 3D geometric model of an engine cylinder is created as well. In this thesis the 3D geometric model is used to investigate non-symmetric antenna system for microwave ignition system. Figure 4-4 shows a 3D geometric model of an engine cylinder.

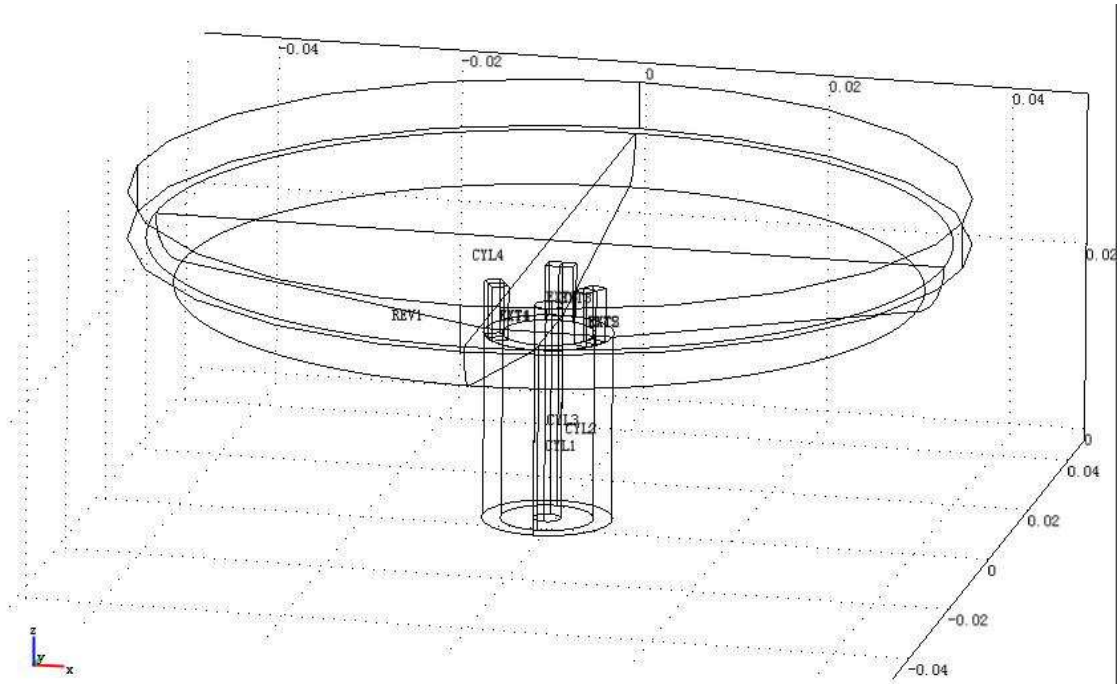


Figure 4-4 The 3-D model for simulations

Spark plug shape antenna shown in Figure 4-4 is just one of possible antenna shapes. There are a few more possible shapes of antenna that are investigated in this thesis.

#### 4.1.3. Model Established in Script

Other than the models created in graphic above, they can also be created by programming with MATLAB so as to use in or with other programs in this thesis. The script model is shown in appendix A and partially shown below.

```
% Geometry
g7=rect2('0.0070','0.02','base','corner','pos',{'0','0'},'rot','0');
carr={curve2([0.045,0.045,0.043],[0.03,0.025,0.025],[1,0.707106781186548,1]), ...
curve2([0.043,0.0070],[0.025,0.02],[1,0.707106781186548]), ...
curve2([0.0070,0],[0.02,0.02],[1,1]), ...
curve2([0,0],[0.02,0.03],[1,1]), ...
curve2([0,0.045],[0.03,0.03],[1,1])};
g12=geomcoerce('solid',carr);
g14=rect2('0.05','0.0050','base','corner','pos',{'0','0.03'},'rot','0');
g15=rect2('0.00197','lenstr','base','corner','pos',{'0','0'},'rot','0');
```

```

carr={curve2([0.0050,0.0050],[0.0175,0.02],[1,1]), ...
      curve2([0.0050,coaxial],[0.02,0.02],[1,1]), ...
      curve2([coaxial,0.0050],[0.02,0.0175],[1,1])};
g20=geomcoerce('solid',carr);
g21=rect2('0.0050','0.02','base','corner','pos',{0,0},'rot','0');
clear s
s.objs={g7,g12,g14,g15,g20,g21};
s.name={'R3','CO1','R1','R4','CO2','R5'};
s.tags={'g7','g12','g14','g15','g20','g21'};

fem.draw=struct('s',s);
fem.geom=geomcsg(fem);

```

#### 4.1.4. Electromagnetic Field and Ignition Modelling

The numerical models of simulation are set in this section. In this thesis there are 3 FEM based simulation module involved, electromagnetic module, heat transfer module, and Diffusion module.

1. Electromagnetic module:

$$\nabla \times (\mu_r^{-1} \cdot \nabla \times \mathbf{E}) - k_0^2 \left( \epsilon_r - j \frac{\sigma}{\omega} \epsilon_0 \right) \cdot \mathbf{E} = 0 \quad (4-1)$$

2. Heat transfer module:

$$\frac{\partial \mathbf{T}}{\partial t} - \nabla \cdot (k \nabla \mathbf{T}) = \mathbf{Q} \quad (4-2)$$

3. Diffusion module:

$$\frac{\partial c}{\partial t} + \nabla \cdot (-\mathbf{D} \nabla c) = \mathbf{R} - \nu \nabla c \quad (4-3)$$

where,  $\mathbf{T}$  is the electron temperature,  $\mu_r$  is the relative permeability of material in the cavity,  $\epsilon_r$  is the relative permittivity of the material in the cavity,  $\sigma$  is the relative conductivity of material in the cavity,  $\omega$  is the angle frequency of the resonance,  $k_0$  is

the wave number of free space,  $\epsilon_0$  is the absolute permittivity,  $\mathbf{R}$  is the recombination rate,  $\nu$  is the scattering rate,  $\mathbf{E}$  is the electric field intensity,  $\mathbf{Q}$  is the energy source,  $c$  is the electron density,  $k$  is the thermal conductivity,  $\mathbf{D}$  is the diffusion coefficient, and  $t$  is time.

For each module the coefficients are set according to constraint conditions in a cylinder. There are a few coefficients here to be set (Porteanu & Gesche, 2008, Porteanu, et. al., 2009),

### 1. Permittivity

Before plasma is formed: between 1.02 and 1.07

When plasma is formed: 
$$\epsilon_r = 1 - \frac{\omega_p^2}{\omega^2} + j \frac{\omega_p^2 \cdot \nu}{\omega^3}$$

### 2. Conductivity

Before plasma is formed: 0

When plasma is formed: 
$$\sigma = \frac{\epsilon_0 \cdot \omega_p^2 \cdot \nu}{\omega^2} + \frac{\epsilon_0 \cdot \omega_p^2}{\omega}$$

### 3. Frequency of plasma

$$\omega_p = \frac{c \cdot e^2}{m \cdot \epsilon_0}$$

### 4. Scattering rate

$$\nu = \mathbf{T}^{\frac{3}{2}} \cdot N$$

where,  $\omega_p$  is the plasma frequency and  $N$  is the density of neutral molecules.

Coefficients 1 and 2 are set for the simulation of electric field distribution before and when plasma forms. Coefficients 3 and 4 are for the simulation of electric field distribution when plasma forms. Once the ignition occurs the plasma is generated in the cylinder. Consequently, the resonant conditions will change. The natural frequency of the cavity will change as well.

## **4.2 Validation of the Simulation**

Before any investigation using COMSOL Multiphysics is carried out, a test simulation is run to validate the simulation method. The test simulation simulates the electric field in a regular shape of cylindrical cavity and the results are compared with the theoretic calculations.

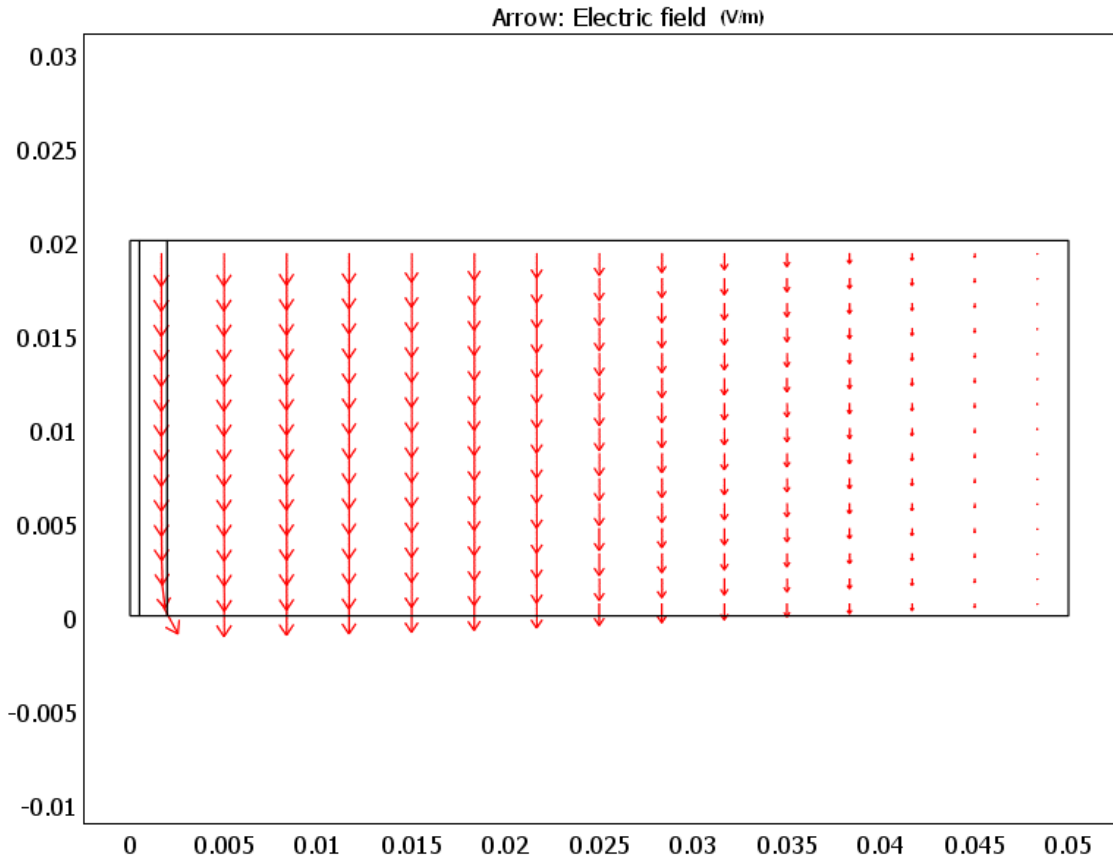


Figure 4-5 The electric field in a regular shape cylindrical cavity

In Figure 4-5 the resonance in a regular shape cylindrical cavity is simulated. It is easy to calculate the electric field strength in this cavity and the resonance frequency of this cavity. Therefore, the results of the simulation are compared to the calculations based on electromagnetic theory (Seely and Doularikas, 1979).

The resonant frequency of  $TM_{010}$  mode for this cavity is 2.2951527GHz according to the result from the simulation using COMSOL Multiphysics, which is an FEM based simulation software. The resonant frequency of  $TM_{010}$  mode for this cylinder can be calculated by (4-4) in theory (Seely and Doularikas, 1979).

$$f = \frac{p_{01} \cdot c}{2 \cdot \pi \cdot r} \tag{4-4}$$

where  $r$  is the radius of cylinder,  $p_{01}=2.405$  is the first root of zero order Bessel function, and  $c$  is the speed of light. The resonant frequency hence equals 2.295GHz, which is very close to the simulation results.

Then the propagation analysis is carried out to show the distribution of the electric field in the cylinder. The result is shown in Figure 4-6.

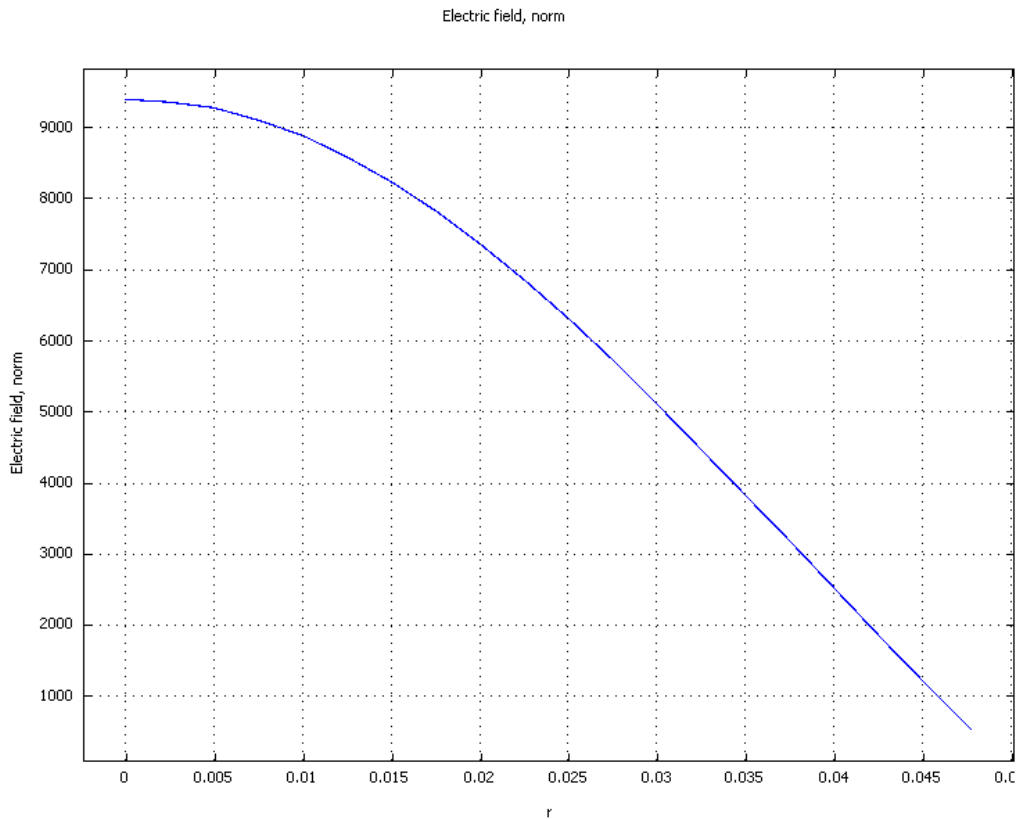


Figure 4-6 Electric field distributions in a cylinder

To compare with simulation result, the electric field in a cylindrical cavity is calculated by (4-5).

$$\mathbf{E}_z(r) = E_0 \cdot \mathbf{J}_0\left(\frac{p_{01} \cdot r}{a}\right) \quad (4-5)$$

where  $E_0$  is the initial electric field intensity and  $r$  is a variable in  $r$  direction. The  $E_z(r)$  is drawn in Figure 4-7 using MATLAB.

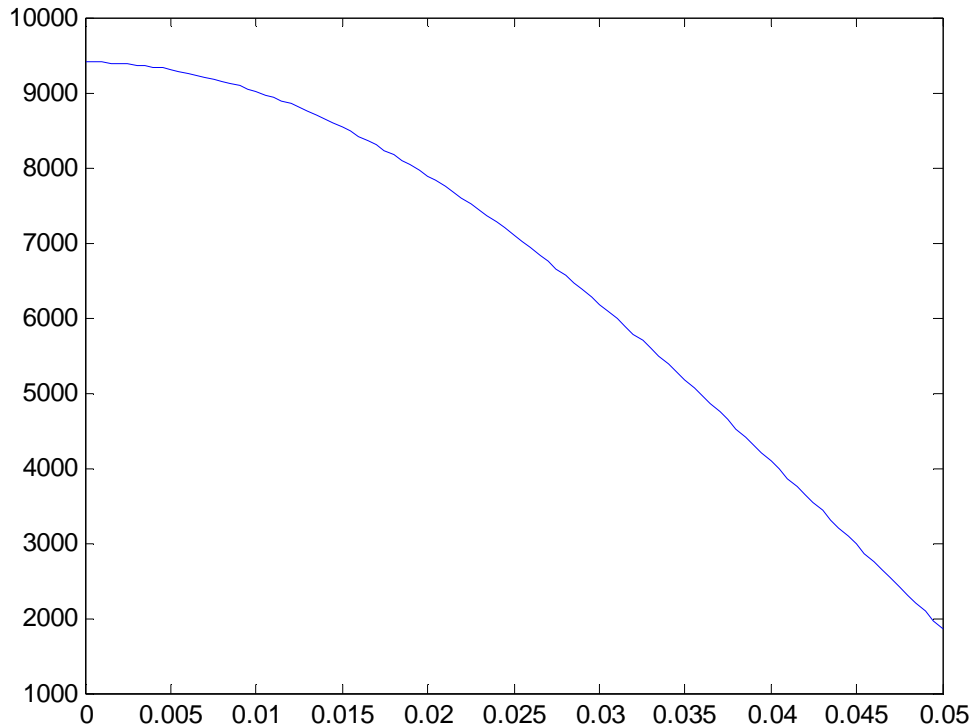


Figure 4-7  $E_z(r)$  calculated from (4-5)

Compare Figure 4-7 with Figure 4-6 it can be found that the simulation result of the distribution of the electric field in a cylindrical cavity does not completely agree with the calculated results because an excitation of microwave has to be assigned in the cylinder, which slightly affects the distribution of electric field in the cylinder.

Furthermore, the resonances in the regular shape cylinders with different radius and different piston position are simulated. The radiuses of cylinders simulated are 0.035 m and 0.05 m. The simulation results are drawn in Figures 4-8 and 4-9.

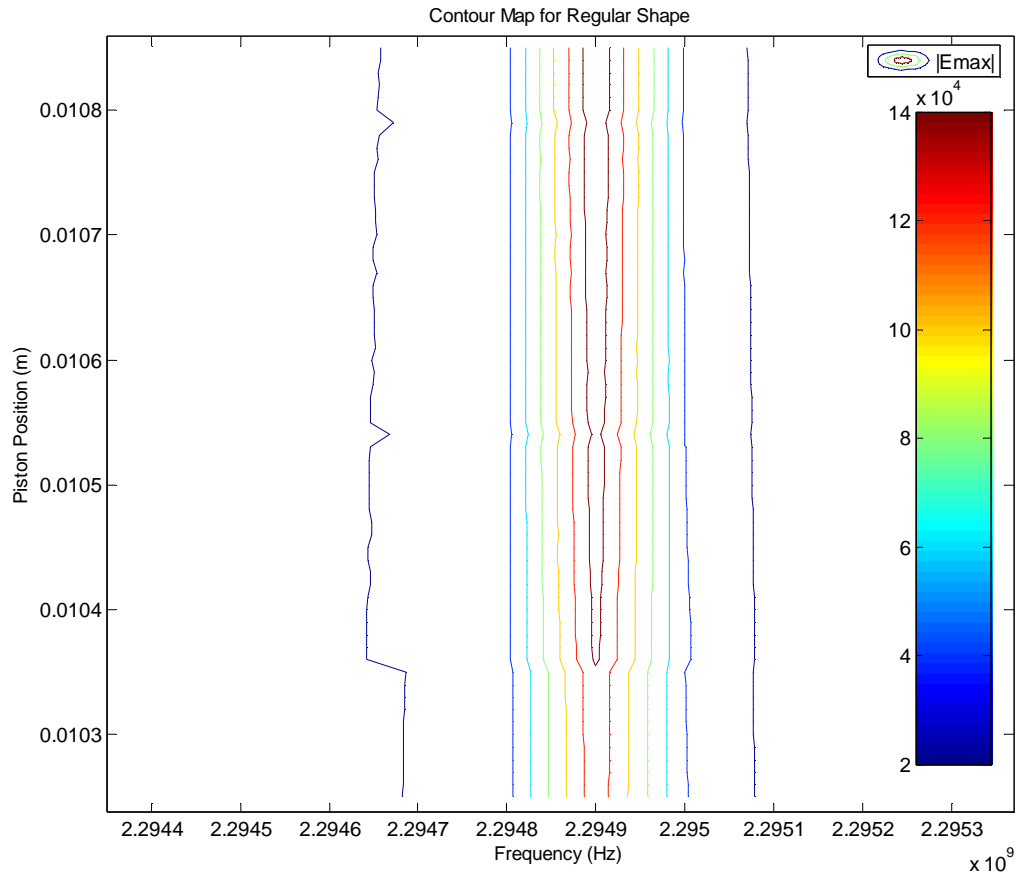


Figure 4-8 Piston position against frequency of a regular shape cylinder with radius at 0.035m ( $TM_{010}$ )

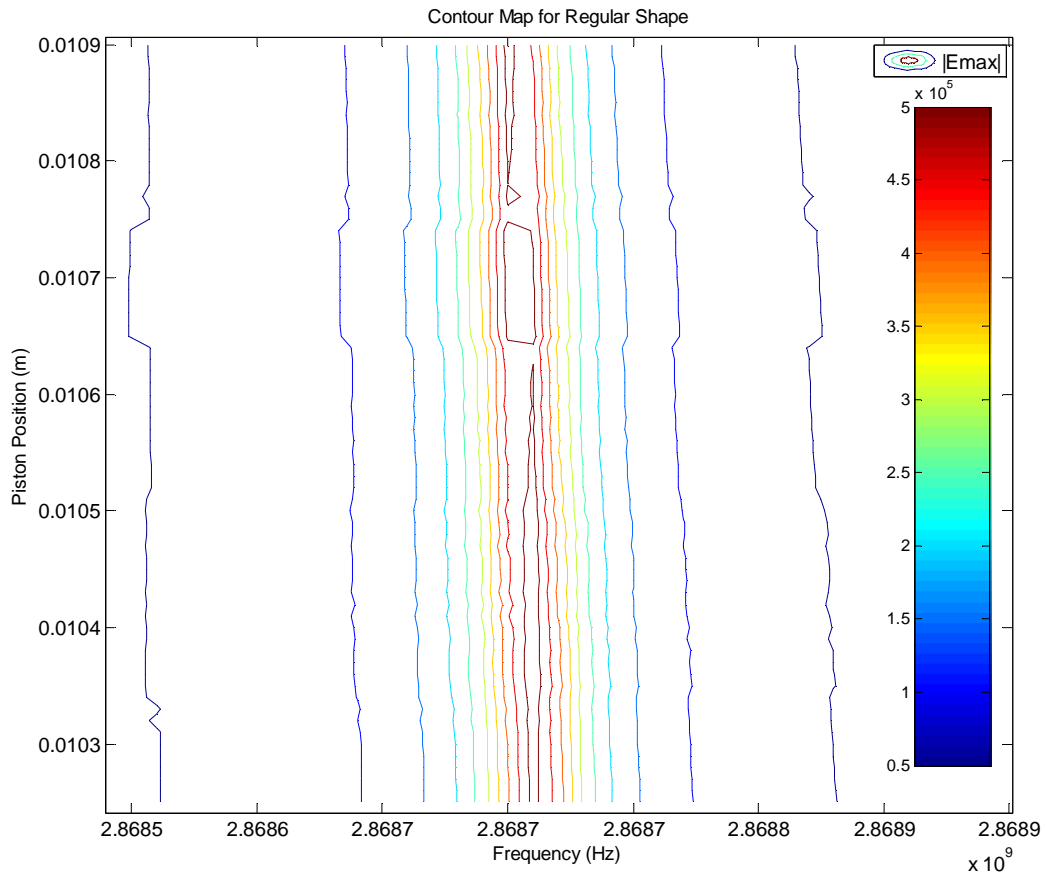


Figure 4-9 Piston position against frequency of a regular shape cylinder with radius at 0.05m ( $TM_{010}$ )

Figure 4-8 and 4-9 are the contour map of maximum electric field intensity in cylinders with frequency and piston position as its (x, y) coordinates. In Figure 4-8 and 4-9, it can be seen that the frequency for different electric field strength nearly remains the same value. However it has small changes when piston position changes. In theory the frequency is not affected by piston position for  $TM_{010}$  mode. This slight disagreement is due to the microwave excitation opening in the simulation geometry model in Figure 4-5, which can not be avoided when using this simulation software. However, this implies the accuracy of the simulation, which can reflect the slight changes from the simulated geometry. The slight changes are also possibly caused by the coarse resolution of piston

position and frequency. From the simulation it can be seen that the resonant frequencies at different cylinder radius agree with the theoretical calculations.

### **4.3 Influence of Piston Motion**

To address the problems of the application of an HCMI system and analyse them, a series of simulations are carried out based on the geometry model in Figure 4-3. The piston motion is a major factor that affects the natural frequency of a cylinder cavity of  $TM_{010}$  mode as it changes the shape and electric characteristics of a cylinder cavity. It is also a major problem of encumbering the application of an HCMI system. Once the engine starts, the piston is moving continuously. The speed of piston does not remain unchanged but changes with engine speed. The engine usually works at a certain speed between 650 rpm and 7200 rpm, which means that the speed of a piston can be up to 43.2 m/s. Because the combustion takes time and the piston moves at a high speed the timing advance is required, which has been specified in Chapter 2.

The ignition time for an MI system is much shorter than for an SI system. The microwave based ignition occurs in 30 ns to 100 ns (Gundersen, 2004; Gundersen, 2007). The combustion with an MI is 25% faster than with SI (Bellenoue, et. al., 2005). Therefore, the timing advance for an HCMI system is much less than an SI system. Consequently the power used to push the piston down of an HCMI system is more than of an SI system.

In this thesis the piston motion measured by the distance to TDC instead of degrees to TDC. The piston positions from 10 mm to 0.5 mm to TDC, which is approximately from 20 degrees to 1 degree to TDC for a 90 mm cylinder, are first simulated to investigate of the effects of the piston motion based on the geometry in Figure 4-3. The simulation results are shown in Figure 4-10.

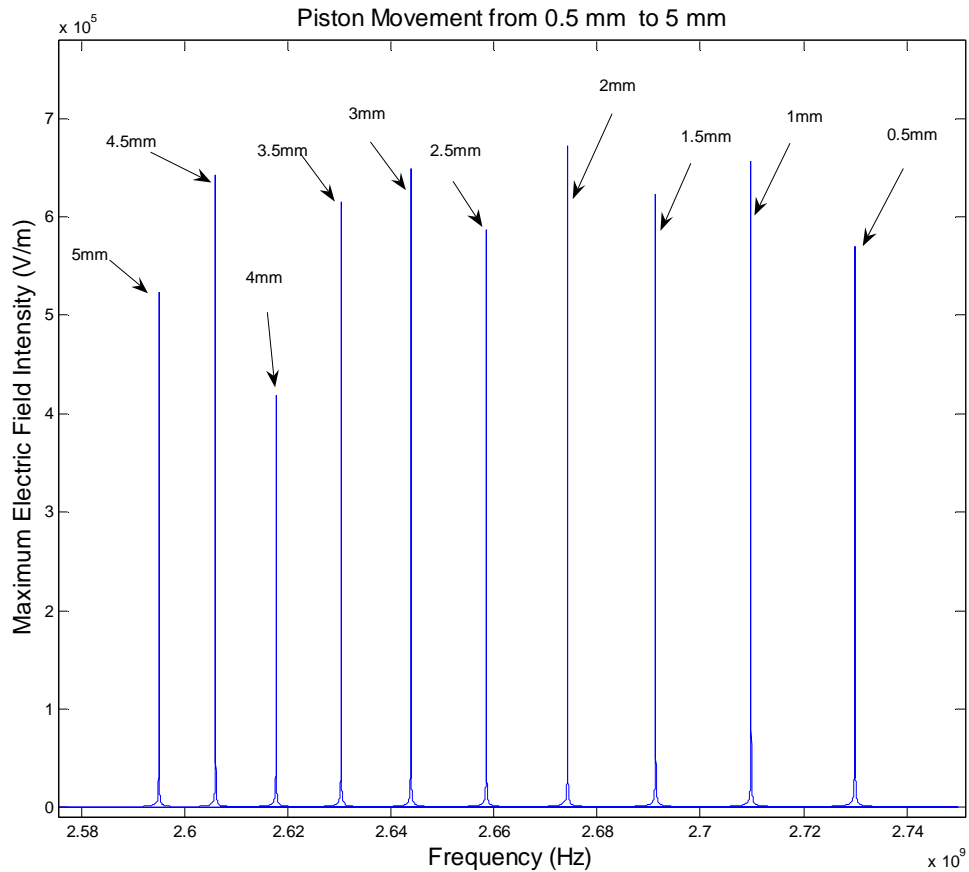


Figure 4-10 Piston position moves from 5 mm to 0.5 mm to TDC

Figure 4-10 shows the maximum electric field intensity in the cylinder against the frequency when piston position moves from the 5 mm to TDC to 0.5 mm to TDC with 0.5 mm step. This figure shows the consistency of maximum electric field strength in the cylinder, regardless of piston position or resonance frequency. From this figure it can be seen that the maximum electric field strength varies from  $4.2 \times 10^5$  V/m to  $6.72 \times 10^5$  V/m in the cylinder, which does not change significantly along with the change of piston position. This also means the piston position does not affect the Q factor significantly. It has to be noticed that the change of electric field strength is likely caused by coarse resolution of search parameters. The search resolution of frequency in this search is chosen for exhaustive search to compromise between accuracy and runtime. Because the electric

field intensity drops fast as frequency changes, the electric field intensity in this figure for some piston positions may not be the ones at resonance.

The lowest electric field strength is  $4 \times 10^5$  V/m roughly when piston position is 4 mm to TDC and the input power is 1 watt. When the input power is 100 watts the electric field can reach  $4 \times 10^6$  V/m, which is still strong enough to ignite the air-fuel mixture. This implies the piston motion in a certain range does not change the Q factor of the cylinder cavity significantly.

However, this figure indicates that for a fixed frequency electric field intensity drops fast when piston position moves. Therefore, there is very little overlap area between each peak. This shows resonant frequency is sensitive to the position of the piston. To investigate the sensitivity of the frequency to the piston motion the piston position at 0.5 mm is focused in figure 4-11.

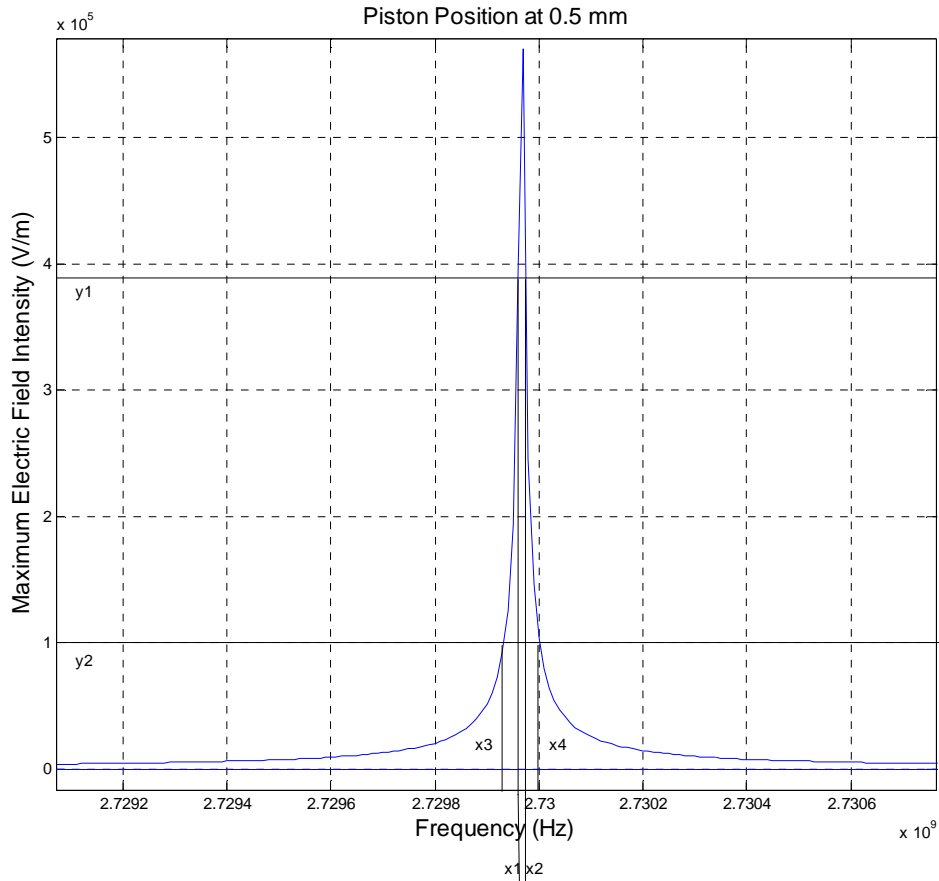


Figure 4-11 The electric field intensity against frequency at 0.5mm timing advance

In Figure 4-11  $y_1=3.9 \times 10^5$  V/m indicates the 30% dropping of electric field strength from the maximum strength. From the crossover points two vertical line are drawn. It can be read from Figure 4-9 that these two vertical line cross the x axis at  $x_1=2.72996$  GHz and  $x_2=2.72998$  GHz. The width between  $x_1$  and  $x_2$  is considered as bandwidth usually. However, in the case of the design of an HCMI system the bandwidth can be extended to  $x_3=2.72993$  GHz and  $x_4=2.73$  GHz, which are the crossover points of the horizontal line at  $y_2=1 \times 10^5$  V/m as  $y_2$  is the minimum requirement of the electric field intensity for ignition of the air-fuel mixture, which has been discussed in chapter 2. Thus, the bandwidth for timing advance of 0.5 mm equals  $(x_4-x_3)$ , which is 0.0007 GHz. Likewise, the bandwidth of other timing advances in Figure 4-10 are calculated. The results obtained from simulations and the data calculated from these results are then summarised in Table 4-1.

Table 4-1 Simulation results of piston position moving from 5 mm to 0.5 mm to TDC

Distance to TDC (mm)	Resonant Frequency (GHz)	Band Width (GHz)	Max Elec. Field Intensity (V/m)
0.5	2.72997	0.00007	$5.7 \times 10^5$
1	2.70984	0.00007	$6.6 \times 10^5$
1.5	2.69133	0.00008	$6.35 \times 10^5$
2	2.67426	0.00006	$6.72 \times 10^5$
2.5	2.6585	0.00006	$5.9 \times 10^5$
3	2.64392	0.00005	$6.5 \times 10^5$
3.5	2.63036	0.00006	$6.2 \times 10^5$
4	2.61778	0.00005	$4.2 \times 10^5$
4.5	2.60605	0.00005	$6.4 \times 10^5$
5	2.5951	0.00005	$5.2 \times 10^5$

From Table 4-1 it can be seen that the resonant frequency gradually increases when the piston moves from 5 mm to 0.5 mm to TDC while the bandwidth increases slowly.

Results in Table 4-1, are depicted in Figures 4-12 and 4-13.

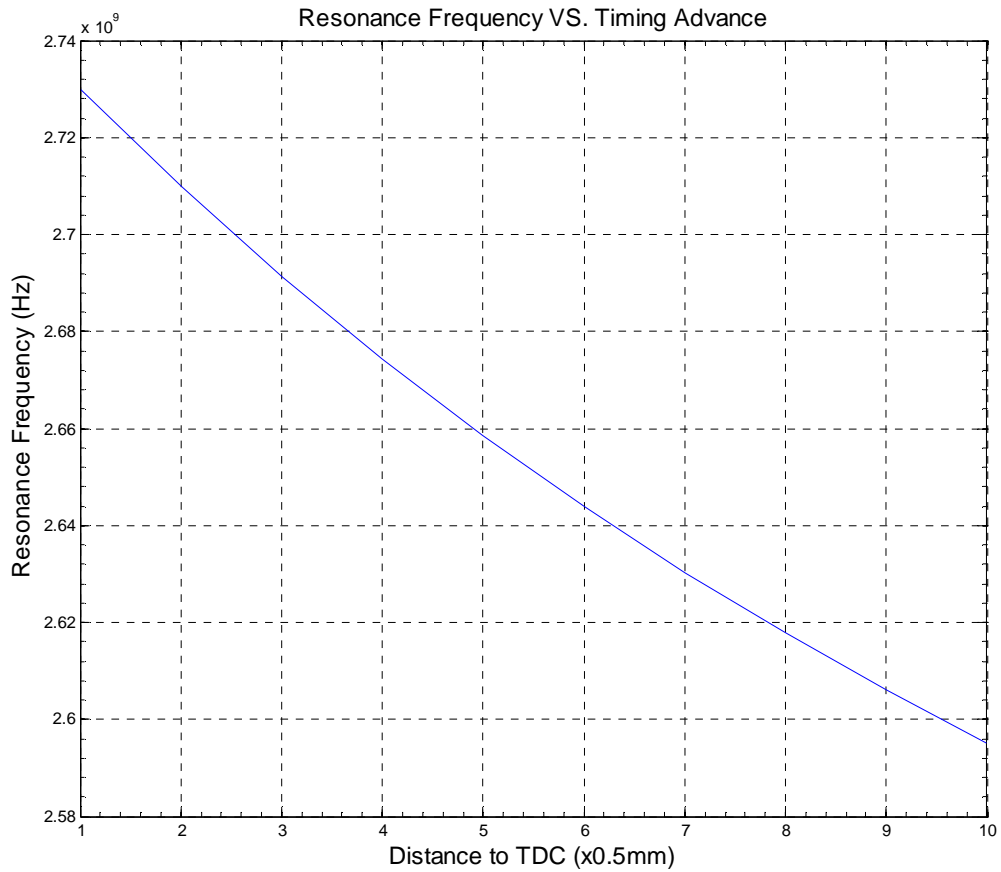


Figure 4-12 Resonant frequency when piston at different positions

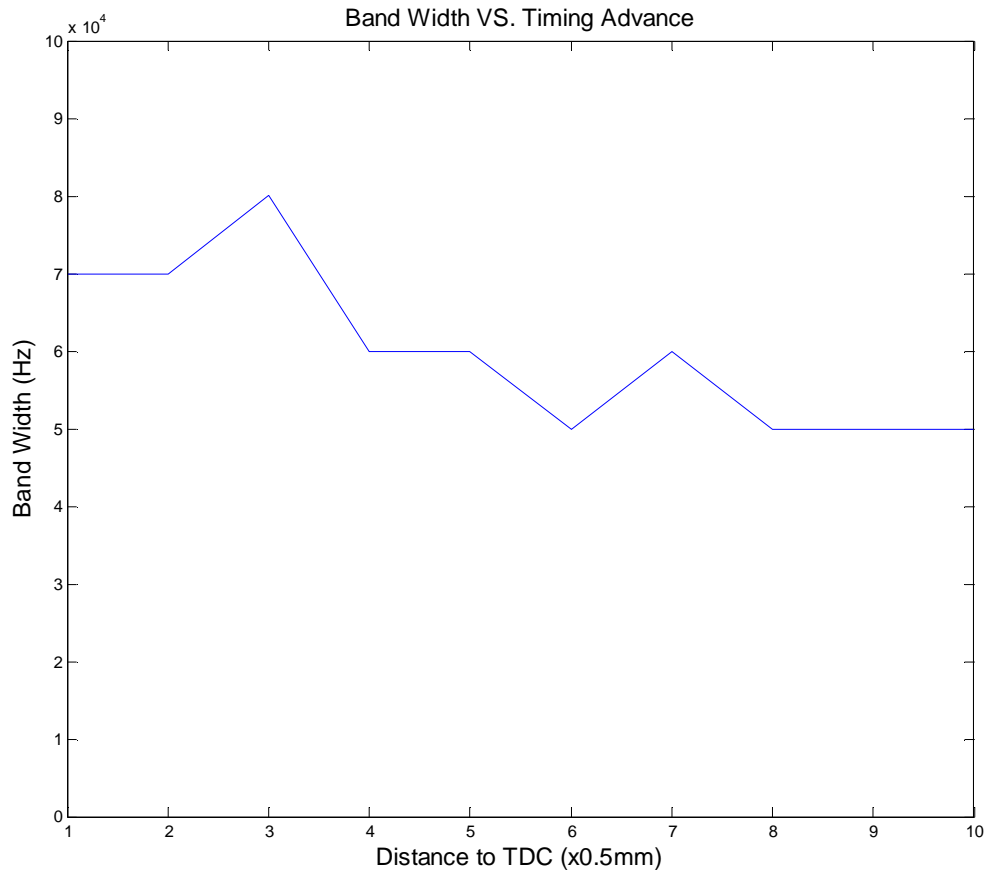


Figure 4-13 Bandwidth when piston moves every 0.5 mm

Figure 4-12 shows the natural frequencies of the cylinder against various timing advances, which represent the positions of the piston. Figure 4-13 shows the bandwidth of resonances at various timing advances.

From Figure 4-12 the magnitude of the natural frequency that changes every 0.5 mm can be calculated. It can be seen that the natural frequency in Figure 4-12 changes nearly linearly. From the data calculated based on Figure 4-10 it can be found that when piston moves from 5 mm to 3 mm the resonant frequency increases 0.012 GHz each degree. When piston moves from 3 mm to 1.5 mm the resonant frequency increases 0.015 GHz. When piston moves from 1.5 mm to 0.5 mm the resonant frequency increases around

0.02 GHz. These changes indicate that the closer the piston moves towards TDC the more sensitive the resonant frequency is to the piston position. This means the resonance lasts less time when piston moves closer to the TDC

As stated before that ignition process of an HCMI system only takes less than 100 ns, of which the ignition volume is more than  $4 \text{ cm}^3$ . According to calculation in Chapter 2, approximately, the piston takes 0.11 ms to move 0.5 mm at 7200 rpm and 0.23 ms at 1500 rpm. Thus the timing advance required by an HCMI system can be less than by an SI system. The simulations of piston position moving every 0.05 mm from 0.5 mm to 0.05 mm to TDC are hence carried out to analyse the sensitivity of the resonant frequency to the piston motion further. The simulation results are shown in Figure 4-14.

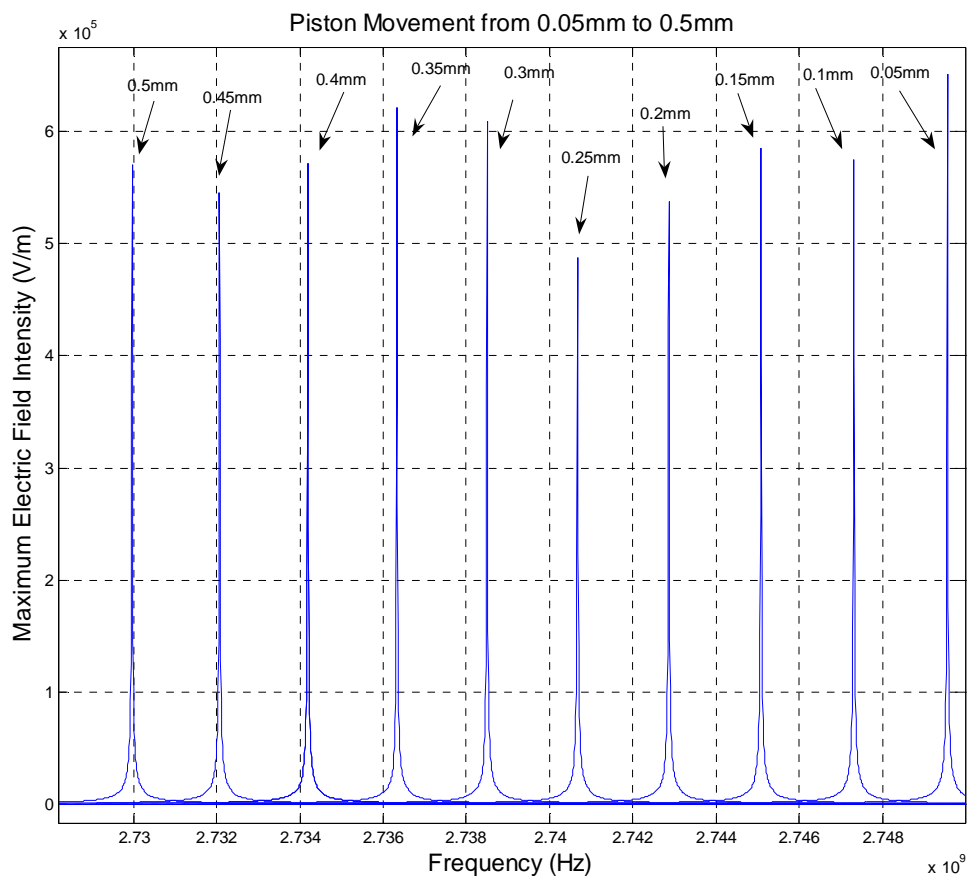


Figure 4-14 Piston position moves from 0.5 mm to 0.05 mm to TDC

Figure 4-14 shows the natural frequency of the cylinder changes from 2.73 GHz to 2.75 GHz while piston position moves from 0.5 mm to 0.05 mm to TDC. The peaks in the figure are very sharp as well, which means the bandwidth of the resonance frequency is narrow and the resonant frequency is sensitive to piston position even if the piston moving distance is as short as 0.05 mm. This figure also shows that the electric field intensities are greater than  $4 \times 10^5$  V/m at all simulated piston position.

The same as in Figure 4-10 it is noticed that the change of electric field strength is also likely caused by coarse resolution of search parameters. The search resolution of frequency in this search is chosen for exhaustive search to compromise between accuracy and runtime. Because the electric field intensity drops fast as frequency changes, the electric field intensity in this figure for some piston positions may not be the ones at resonance.

The piston position of 0.05 mm is focused and shown in Figure 4-15.

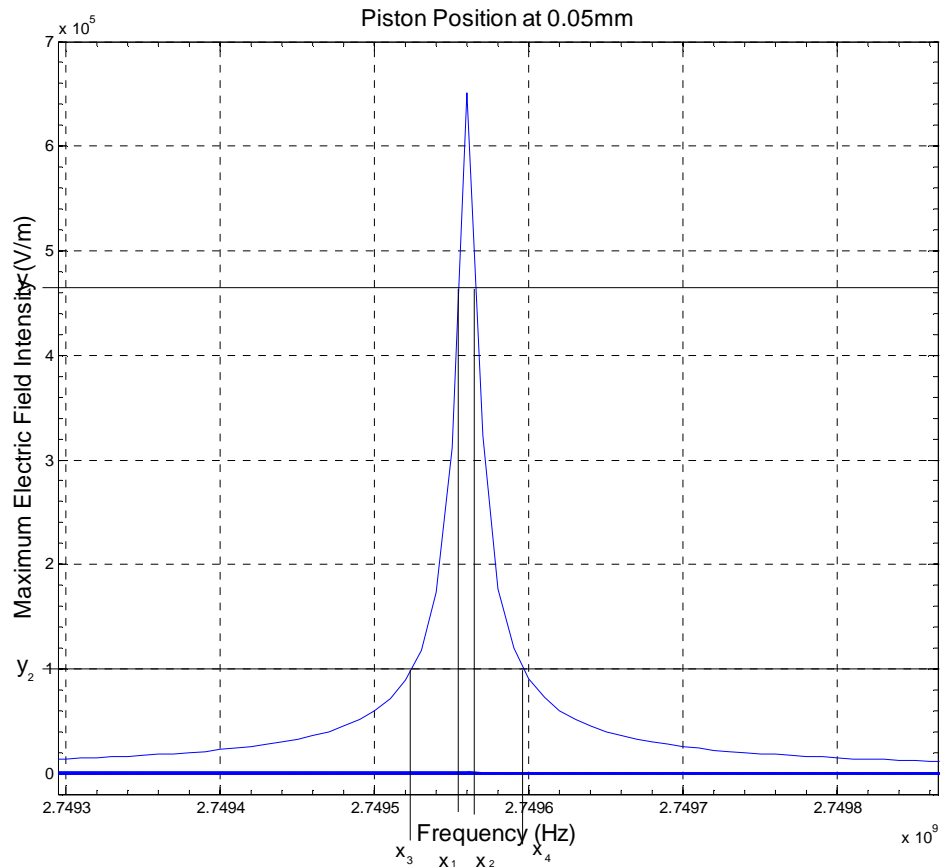


Figure 4-15 The electric field intensity against frequency at timing advance of 0.05 mm

In Figure 4-15 the bandwidth of the timing advance of 0.05 mm can be calculated. It is roughly 0.00005 GHz. Likewise the bandwidths of other timing advances are calculated as well. The results obtained from simulations and calculations are then listed in Table 4-2.

Table 4-2 Simulation results of piston position moving from 0.5 mm to 0.05 mm to TDC

Distance to TDC (mm)	Resonant frequency (GHz)	Band Width (GHz)	Max Elec. Field Intensity (V/m)
0.05	2.74956	0.00008	$6.6 \times 10^5$
0.1	2.74731	0.00007	$5.78 \times 10^5$
0.15	2.74508	0.00007	$5.82 \times 10^5$
0.2	2.74287	0.00007	$5.4 \times 10^5$
0.25	2.74068	0.00007	$4.9 \times 10^5$
0.3	2.7385	0.00007	$6.1 \times 10^5$
0.35	2.73634	0.00007	$6.21 \times 10^5$
0.4	2.7342	0.00007	$5.575 \times 10^5$
0.45	2.73207	0.00007	$5.45 \times 10^5$
0.5	2.72997	0.00007	$5.7 \times 10^5$

In Table 4-2 it can be seen that the frequency increases when the piston position moves from 0.5 mm to 0.05 mm to TDC. The bandwidth nearly remains unchanged. Results in Table 4-2 are depicted in Figures 4-16 and 6-17.

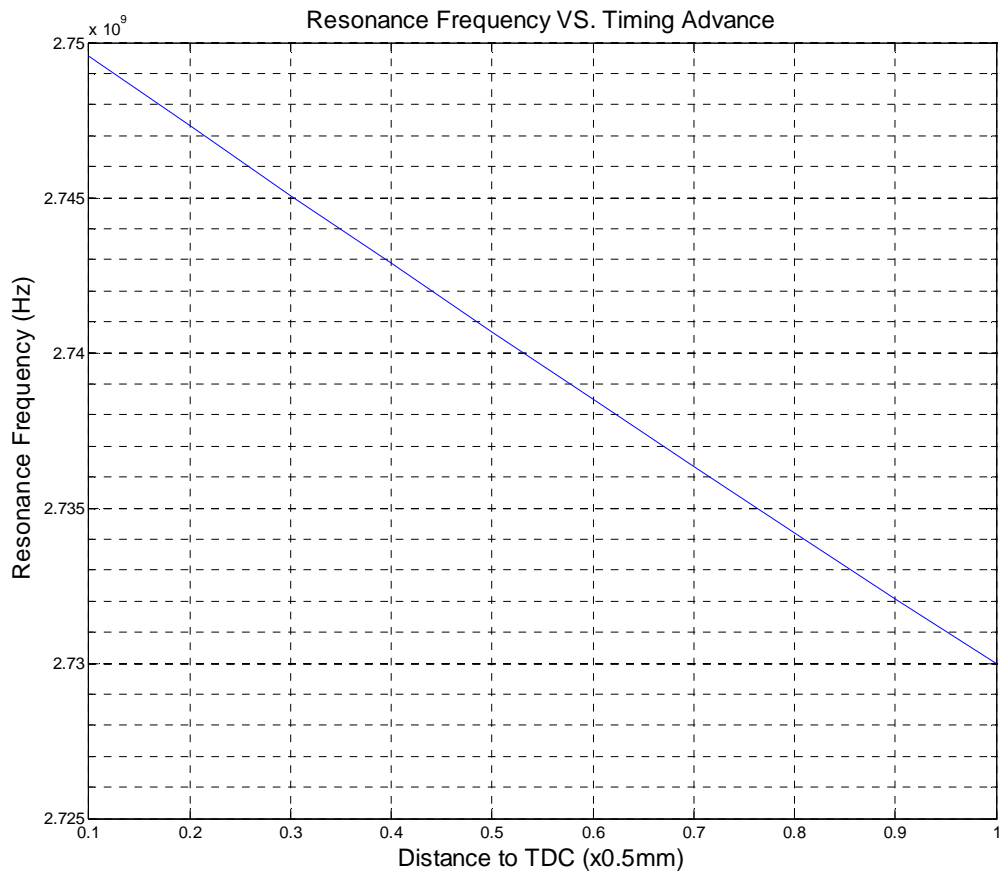


Figure 4-16 Resonant frequency VS piston position

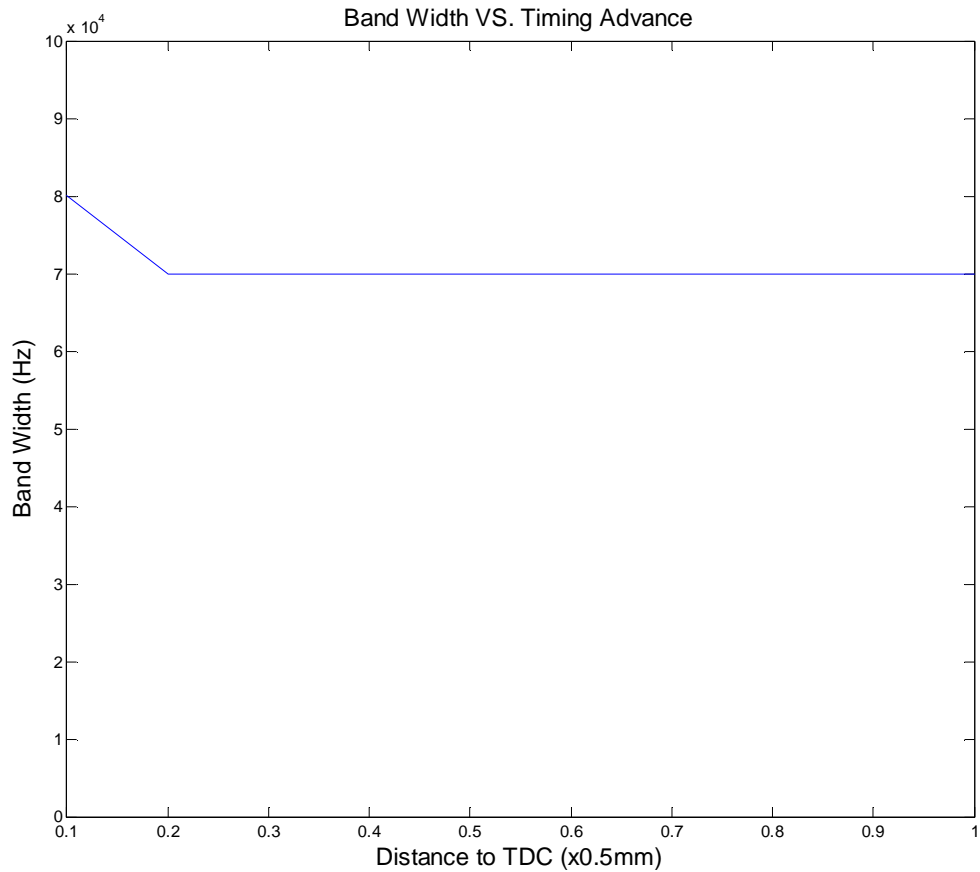


Figure 4-17 Bandwidth VS piston position

It can be read from Figure 4-16 that when piston moves from 0.5 mm to 0.45 mm to TDC the resonant frequency changes 0.002 GHz. When piston moves from 0.45 mm to 0.15 mm to TDC the resonant frequency changes 0.0021 GHz each 0.05 mm. When piston moves from 0.15 mm to 0.05 mm to TDC the resonant frequency changes 0.0023 GHz each 0.05 mm. This implies the resonant frequency changes faster when piston moves closer to TDC, which means the resonant frequency is more sensitive to piston position when piston is closer to TDC. The sensitivity depends on piston position but not the engine speed.

As studied in Chapter 2 the generation of plasma takes only 100 nanoseconds, during which the piston only travel  $2.175 \times 10^{-4}$  mm. The resonant frequency does not change much when piston moves only  $2.175 \times 10^{-4}$  mm. If compare Figure 4-16 with Figure 4-15 it

can be seen that the strong electric field through resonance can last at least 7  $\mu$ s during which the piston can move 0.015 mm. Therefore the time that the resonance lasts is much longer than the time of the formation of the plasma, which is between 30 ns and 100 ns. According to the simulations carried out and analysis above it can be proved that the design of an HCMI system without modification to engine cylinder is feasible. This investigation can guide the design of the resonance timing and timing advance for an HCMI system.

For different types of engine the dimensions of cylinders vary. Diameter of the cylinder is a main parameter of a cylinder and it affects the electromagnetic characters of a cylinder. Therefore, the investigation of the effects of piston motion of cylinders with different diameters is carried out. The investigation aims to analyse the difference of the effects of piston motion in cylinders of different diameters.

The thesis investigates the different diameters of the cylinder in Table 4-3.

Table 4-3 Diameters of cylinder for simulations

Diameters of Cylinders	105 mm	98 mm	90 mm	87 mm	80 mm
------------------------	--------	-------	-------	-------	-------

The results of simulations are drawn in Figure 4-18.

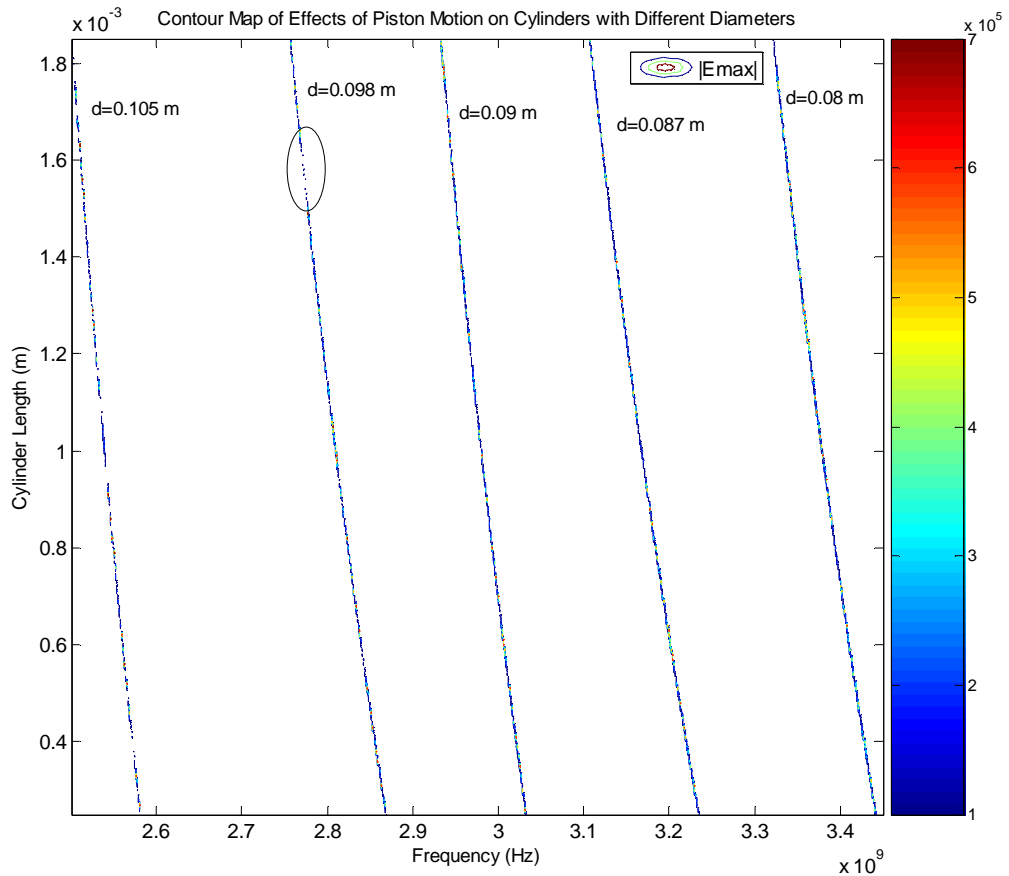


Figure 4-18 Effects of piston motion on cylinders with different diameters

This figure is a contour map of maximum electric field intensity in cylinder with frequency and cylinder length as its (x, y) coordinates. In this figure, cylinder length represents the piston position. This figure shows the resonance frequency range of each cylinder with a certain diameter. It also shows the sensitivity of the resonance frequency for different diameters of cylinders. From this figure it can be seen that for different diameters the cylinders have different resonance frequencies. For each diameter of the cylinder the change of the frequency is similar while the piston moves. This implies that the effects of piston motion to different diameters of cylinders are similar. It also means the sensitivity of the resonance frequency to piston motion is not affected by the diameter of a cylinder. Therefore, the analysis of the effects of piston motion to a cylinder applies to different cylinders. The ellipse area in Figure 4-18 is zoomed in and shown in Figure 4-19.

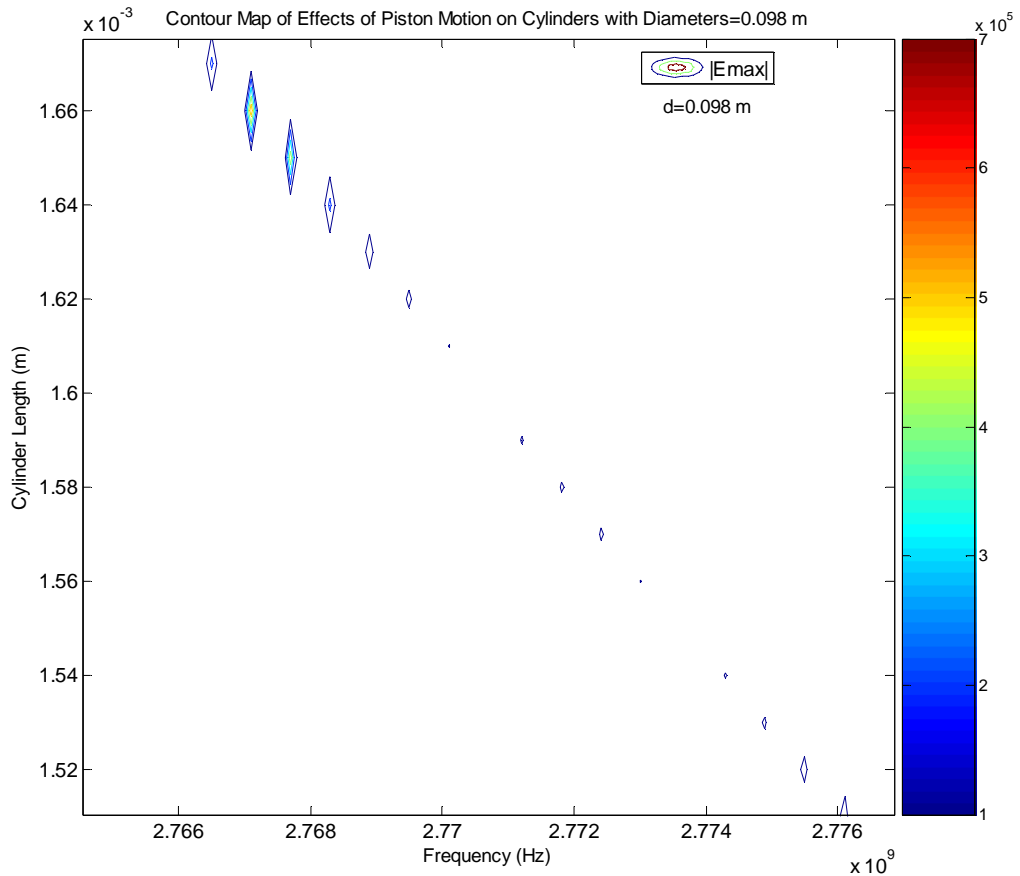


Figure 4-19 (a) A zoomed in view of ellipse area in Figure 4-18

Figure 4-19 (a) is a close up look of the ellipse area in Figure 4-18. Therefore, it is also the contour map of electric field intensity in cylinder with frequency and cylinder length as its (x, y) coordinates. The resolution of frequency in this figure is 100 MHz. From this figure it can be seen that the resonance frequency of a cylinder is very sensitive to the piston motion, which confirms the conclusion drawn before. This figure also shows that at different piston position the sensitivity of the resonance frequency is different. It is noticed that at different cylinder length the maximum electric field strength is different and at an irregular order. This figure, at the same time, displays the effects of resolution chosen for search parameters. The frequency resolution of exhaustive searches here is chosen to compromise between accuracy and runtime of searches. However, this implies the sensitivity of frequency from another angle and also indicates that auto design

methods used in next chapter is essential and the only way to investigate such a problem. To verify this further, the finer search of narrower range of cylinder length (0.001657 m – 0.001663 m) is carried out in Figure 4-19 (b) with the resolution of frequency at 4 MHz.

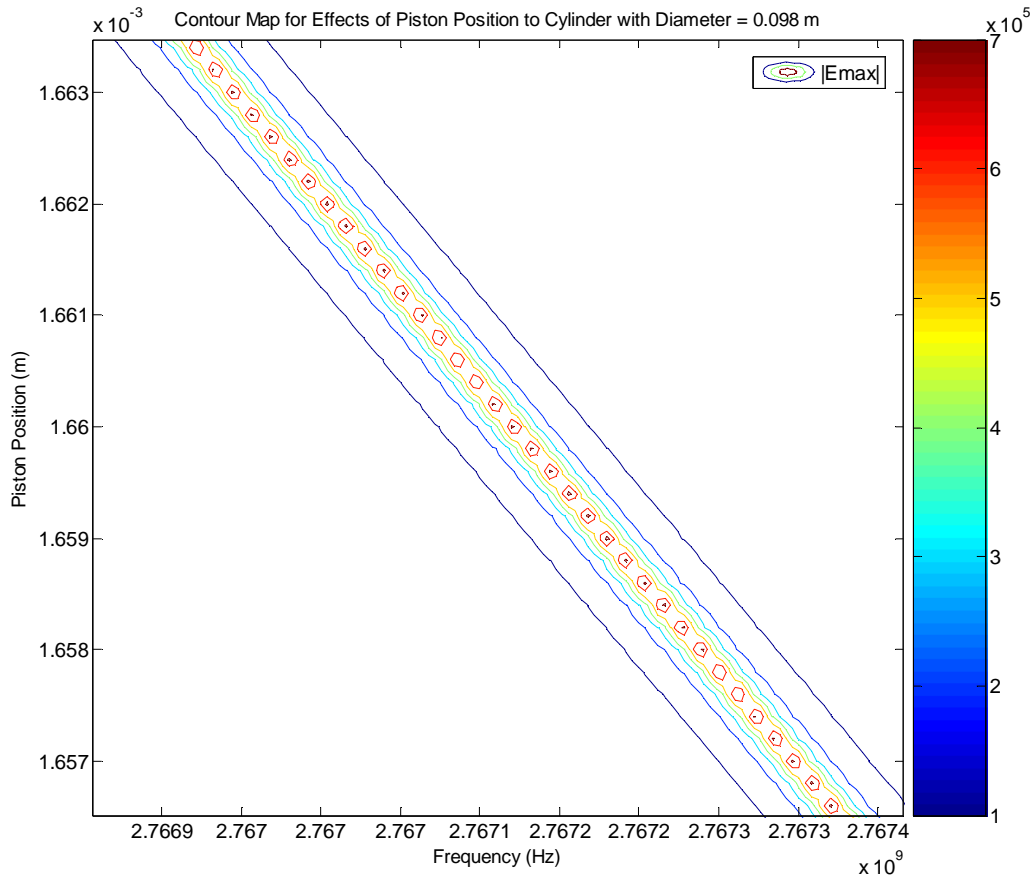


Figure 4-19 (b) Finer Search for Figure 4-19 (a) with cylinder length from 1.657 mm to 1.663 mm

Figure 4-19 (b) is the contour map of electric field intensity with frequency and piston position as its (x, y) coordinates. This figure is a finer search for Figure 4-19 (a). This figure confirms the sensitivity of the frequency to piston position. It also confirms the effects of the search resolution of frequency to the accuracy of simulations.

The results above also imply that for different types of engine the frequency of input microwave of an HCMI system may vary. Therefore, the different microwave source of

HCMI systems has to be designed for different cars. These results will also be helping the design of ignition timing and input power of microwave.

## 4.4 Influence of Air/Fuel Ratio

### 4.4.1 The Relation between Air/Fuel Ratios and Relative Permittivity

The AFR changes when engine is running. Before plasma generated the material in a cylinder is pure air-fuel mixture. The AFR is relevant to the relative permittivity which affects both the  $Q$  factor and the natural frequency of a cylinder. It has been studied that plasma enables ignition of air-fuel mixtures that are significantly richer or leaner than the upper and lower limits ignitable with spark ignition systems (Bokulich, 2001). To design a reliable HCMI system, the influence of a wide range of AFR is studied in this section.

Air and fuel are mixed at different ratio which is determined based on many factors and it is an ever-changing parameter. For a petrol engine the AFR can be tuned from 11:1 to 16.2:1 roughly depending on engine status, load, and power that needs to be achieved (Taylor, 1985).

The AFR is the factor that affects the dielectric of the mixtures in the cylinder cavity. For an HCMI system, air and fuel are well mixed before being injected into a cylinder. The timing of ignition is controlled by injection of microwave. Therefore, the air-fuel mixture remains its state before ignition occurs for an HCMI system. The air-fuel mixture is hence regarded as an equilibrium mixture in this thesis and dielectric is modelled with an equilibrium model.

In order to simulation the electric field in a cylinder at different AFR in this section, the dielectric can be calculated using the power-law model (Karkkainen, et. al., May 2000):

$$\epsilon_{\text{eff}}^{\beta} = f\epsilon_1^{\beta} + (1-f)\epsilon_2^{\beta} \quad (4-6)$$

where  $\epsilon_{\text{eff}}$  is the effective permittivity of the mixture,  $\epsilon_1$  is the host dielectric component of the mixture,  $\epsilon_2$  is the inclusive dielectric component of the mixture,  $f$  is the volume fraction of the host dielectric component, and  $\beta$  is a dimensionless parameter. For air-fuel mixture  $\epsilon_1$  refers to fuel and  $\epsilon_2$  refers to air. Known examples are the Birchak formula ( $\beta=1/2$ ) and Looyenga formula ( $\beta=1/3$ ). (Karkkainen, et.al., May 2000)

The Lichtenecker formula:

$$\ln \epsilon_{\text{eff}} = f \ln \epsilon_1 + (1 - f) \ln \epsilon_2 \quad (4-7)$$

is a special case of power model, for the limit  $\beta \rightarrow 0$  (Karkkainen, et. al., May 2000). where  $f$  is the coefficient to represent AFR. It can be calculated via (4-8).

$$f = \frac{1}{AFR + 1} \quad (4-8)$$

#### 4.4.2 Effects of Air/Fuel Ratios

According to the previous section, each AFR corresponds with an  $\epsilon_{\text{eff}}$ , which is calculated in Table 4-4 using equation (4-7).

The 2D model is used in this section. It is assumed here that air and fuel are well mixed before being injected into cylinder and evenly distributed in cylinder during a compression stroke.

Table 4-4 Effective permittivity of mixtures with various AFR

AFR	$\epsilon_{\text{eff}}$
10:1	1.054890000
11:1	1.050201680
12:1	1.046252109
13:1	1.042878587
14:1	1.039963667
14.7:1	1.038150000
15:1	1.037419797
16:1	1.035180374
17:1	1.033193834
18:1	1.031419635
19:1	1.029830000
20:1	1.028390000

First of all, a wide range relative permittivity values are investigated. The simulations are carried out to cover the relative permittivity from 1 to 5. The results of these simulations help researchers study the effects of changes of the material in cylinder. The simulation results are summarised in Table 4-5.

Table 4-5 Data of simulations under different relative permittivity

Relative Permittivity	Resonant frequency (GHz)	Max Electric Field Intensity (V/m)
1	2.6129	$1.4805 \times 10^5$
1.5	2.1339	$7.9244 \times 10^4$
2	1.8483	$7.2136 \times 10^4$
3	1.5095	$5.9771 \times 10^4$
4	1.3075	$6.0644 \times 10^4$
5	1.1696	$1.3638 \times 10^5$

Results in Table 4-4 are depicted in Figures 4-20 and 4-21, which are drawn below.

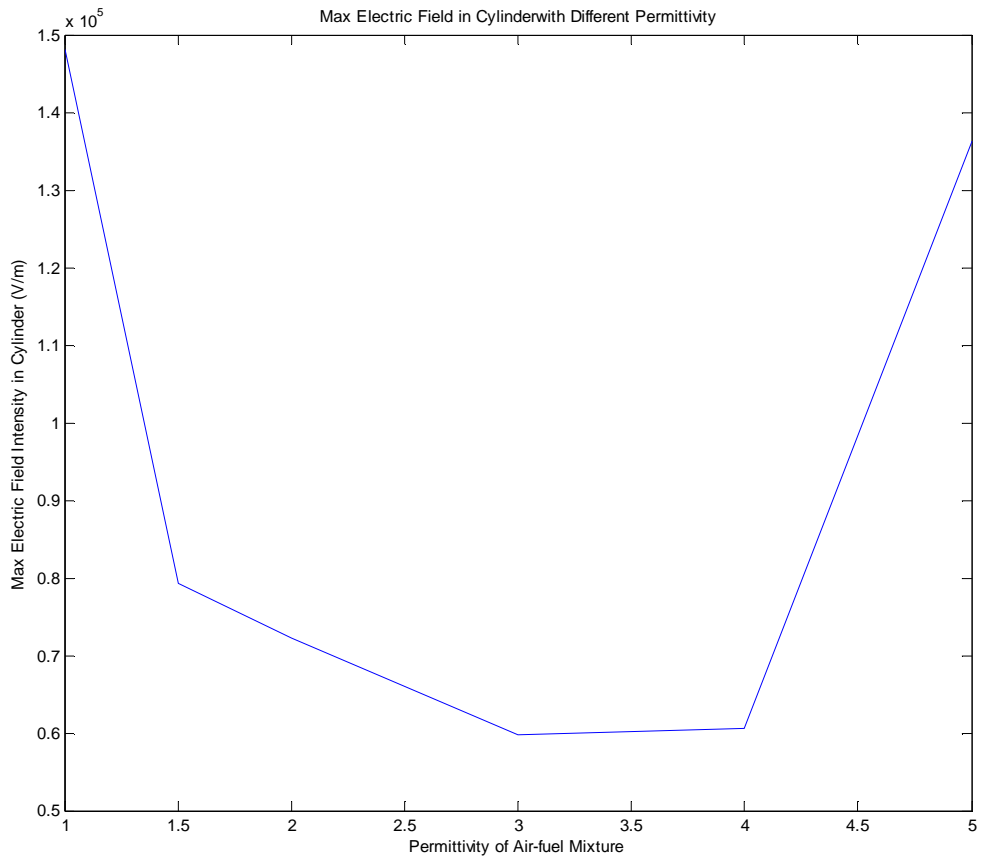


Figure 4-20 Max electric field intensities in cylinder with different relative permittivity

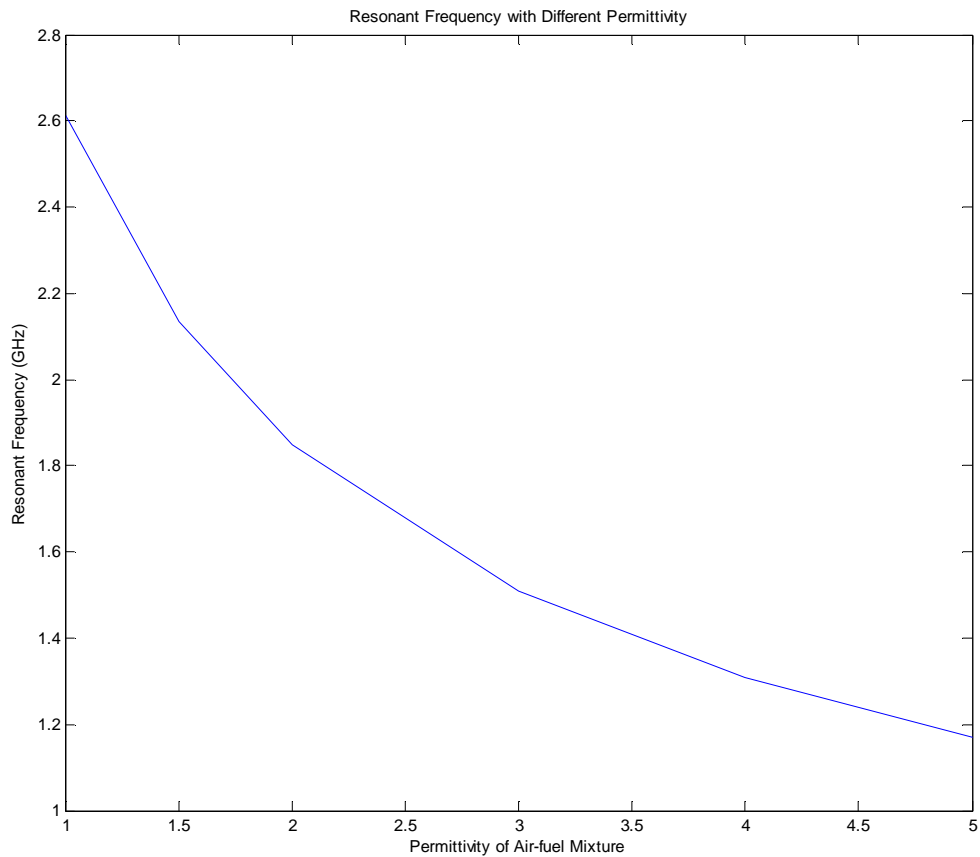


Figure 4-21 Resonant frequencies under different relative permittivity

Figure 4-20 indicates that the electric field intensity does not change much along with the increase of the relative permittivity. Figure 4-21 shows the resonant frequency decreases along with the increase of the relative permittivity. The search resolution of frequency also affects the accuracy of curve in Figure 4-20.

Then, the simulations of a series of relative permittivity values, which covers possible AFRs of petrol engines, are carried out. This is to investigate the effects of the change of AFR. The relative permittivity values investigated here are between 1.01 and 1.07. The simulation results are summarised in Table 4-6 and drawn in Figure 4-22.

Table 4-6 Data of simulations under different relative permittivity

Relative Permittivity	Resonant frequency (GHz)	Max Electric Field Intensity (V/m)
1.01	2.6	$1.9891 \times 10^5$
1.02	2.5882	$3.3046 \times 10^5$
1.03	2.5747	$2.3709 \times 10^5$
1.04	2.5623	$2.6229 \times 10^5$
1.05	2.55	$2.792 \times 10^5$
1.06	2.5379	$2.3944 \times 10^5$
1.07	2.5261	$3.4352 \times 10^5$

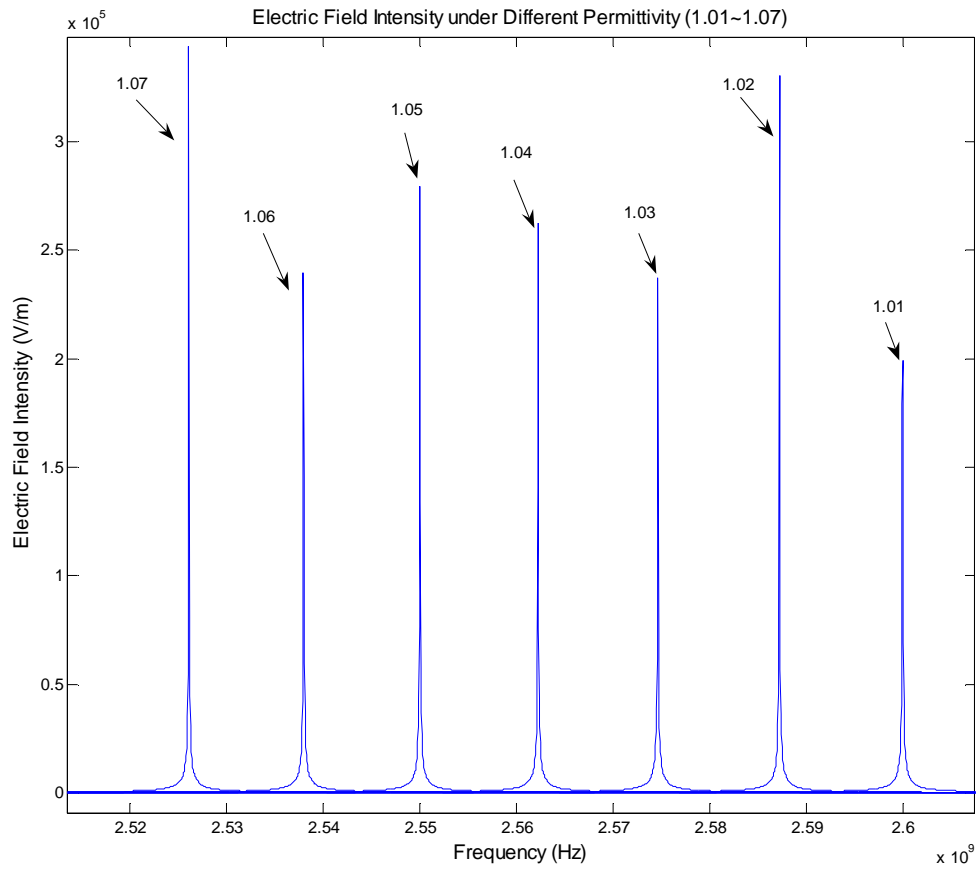


Figure 4-22 Simulations of resonance with relative permittivity from 1.01 to 1.07

Results in Table 4-6 are depicted in Figures 4-23 and 4-24.

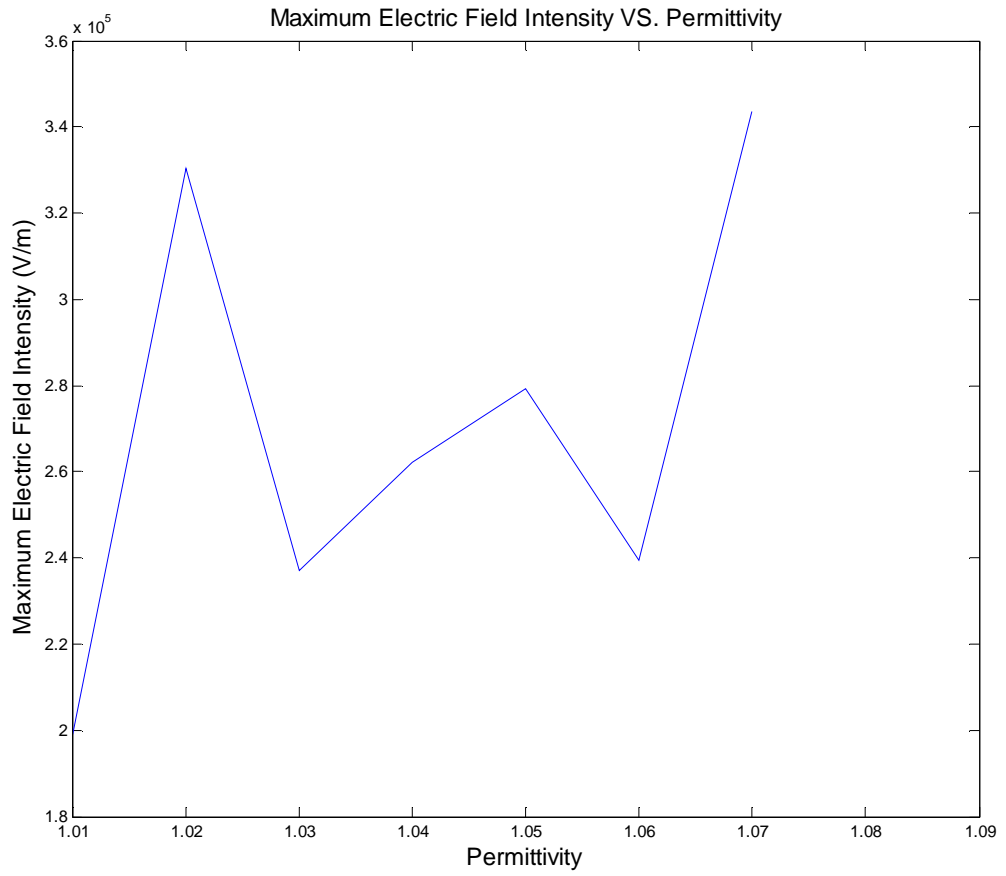


Figure 4-23 Maximum electric field intensities in cylinder under different relative permittivity

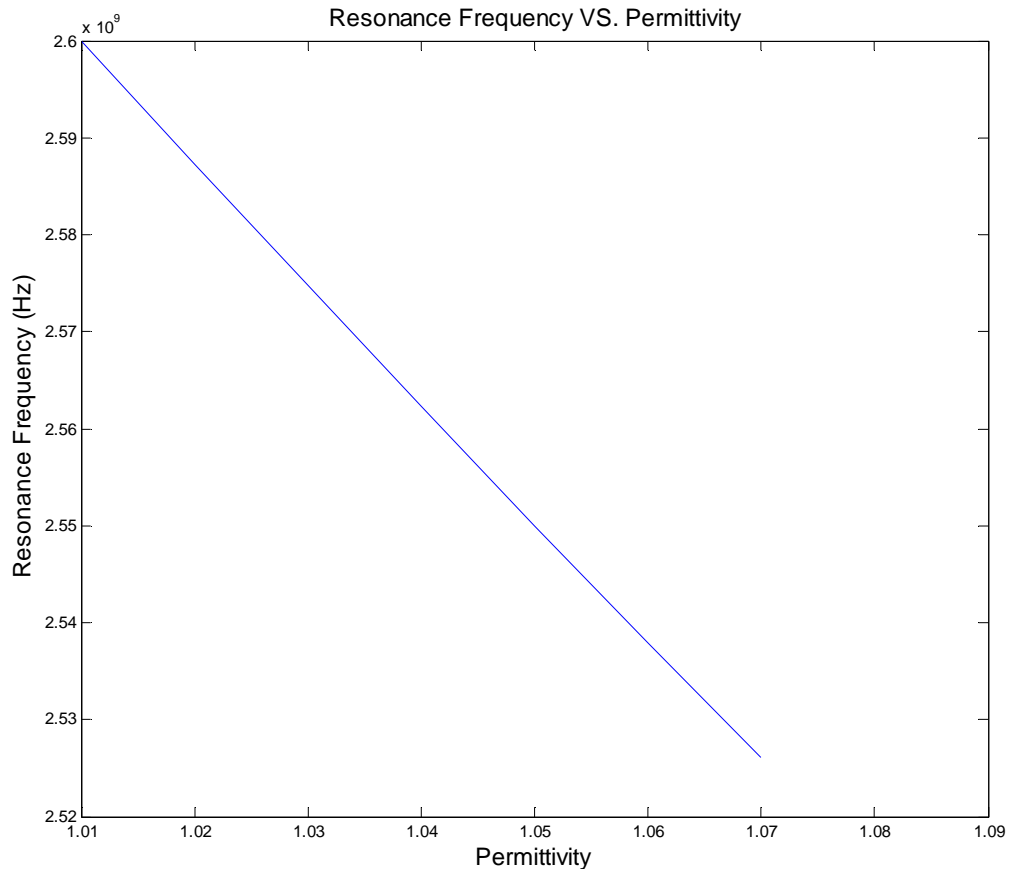


Figure 4-24 Resonant frequencies under different relative permittivity

Figure 4-23 illustrates that the change of the maximum electric field intensity is not significant when relative permittivity increases from 1.01 to 1.07. This implies that the air-fuel mixture ratio does not affect electric field intensity or the Q factor significantly. The maximum electric field does not appear a simple uptrend or downtrend. This is possibly caused by coarse search resolution of frequency. However this influence does not affect the above conclusions.

In Figure 4-24 it can be seen that the resonant frequency decreases nearly linearly when the relative permittivity increases from 1.01 to 1.07. The resonant frequency decreases average 0.0123 GHz while the relative permittivity increases every 0.01. This indicates that the effect of the changes of the relative permittivity is gravely though the tolerance for frequency has yet to be investigated in the future.

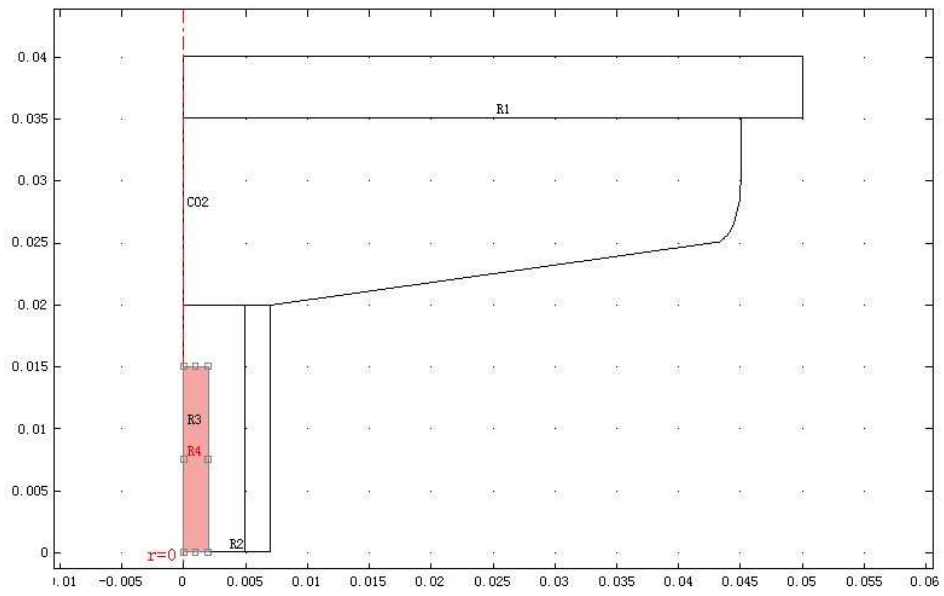
The investigation of the influence of piston position and AFR is to address the problems of application of a practical HCMI system that employs the cylinder as a resonant cavity. It has been found at this stage that the sensitivity of the resonant frequency to the piston position is a major problem to realise a practical HCMI system. The way to overcome this problem is either to increase the electric field strength or to reduce the effect of piston motion to the resonant frequency. The coupling methods are researched in the next section to show the possible means of overcoming this problem.

## **4.5 Microwave Coupling Methods**

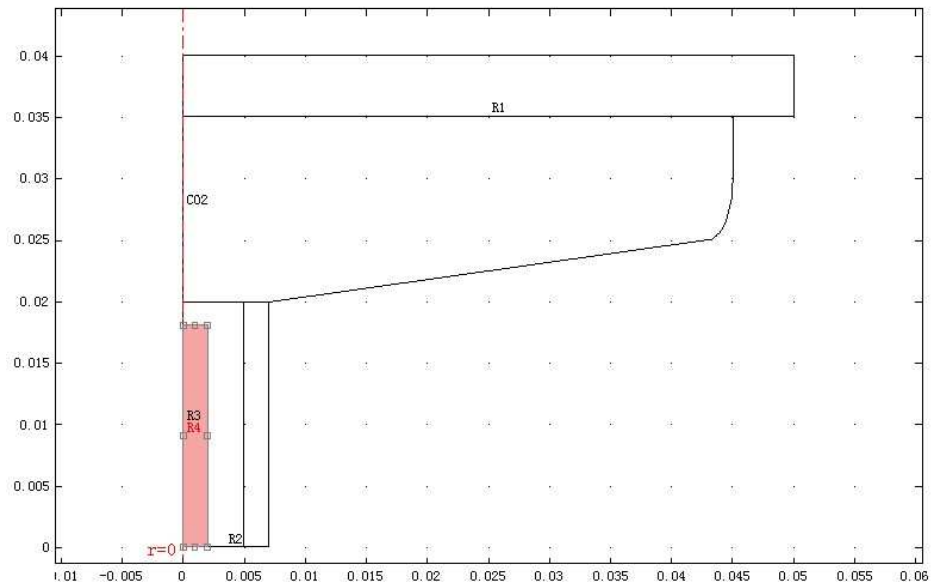
The coupling antennae are investigated in this section. This investigation aims to design an effective coupling apparatus for an ICE HCMI system with the least modification to the engine. When a cavity is fitted with an antenna the geometric shape of cavity actually has been changed slightly. Thus, the  $Q$  factor and the natural frequency of a cavity vary for different antenna dimension or the geometric shape. Besides, the antenna shape and dimensions also affect the coupling efficiency. The probe antenna is the most commonly used for coupling microwave from the coaxial line to a cylindrical cavity.

### **4.5.1 Effects of the Coupling Antenna Length**

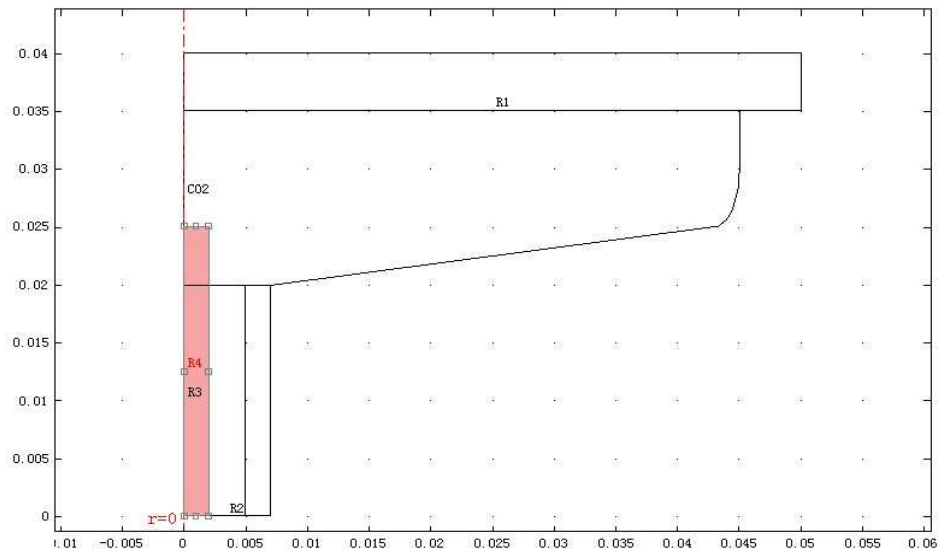
The probe antenna is analysed in depth in this section. A probe antenna has an axial symmetric geometry so that a 2D symmetric model is adopted, which saves numerical calculations during the simulation with the respect to a 3D model. There is one parameter of a probe antenna that is adjusted in this section, i.e. antenna length. The parameter affects the coupling efficiency most for a probe antenna. This section exhaustive search is carried out to scan the probe antenna length from 10mm to 30mm with 1mm step. Figure 4-25 shows a few examples of the probe antenna with various lengths.



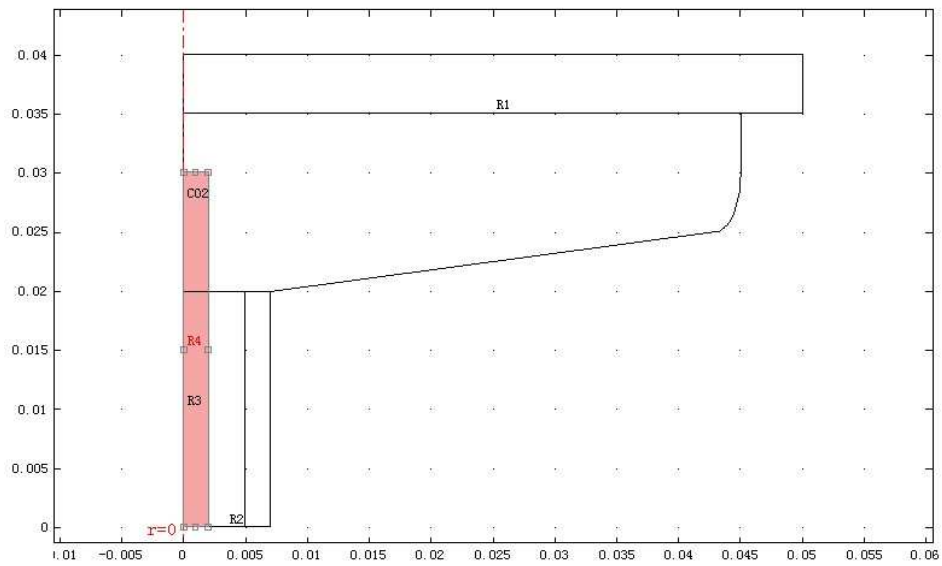
(a) Antenna length: 15 mm



(b) Antenna length: 18 mm



(c) Antenna length: 25 mm

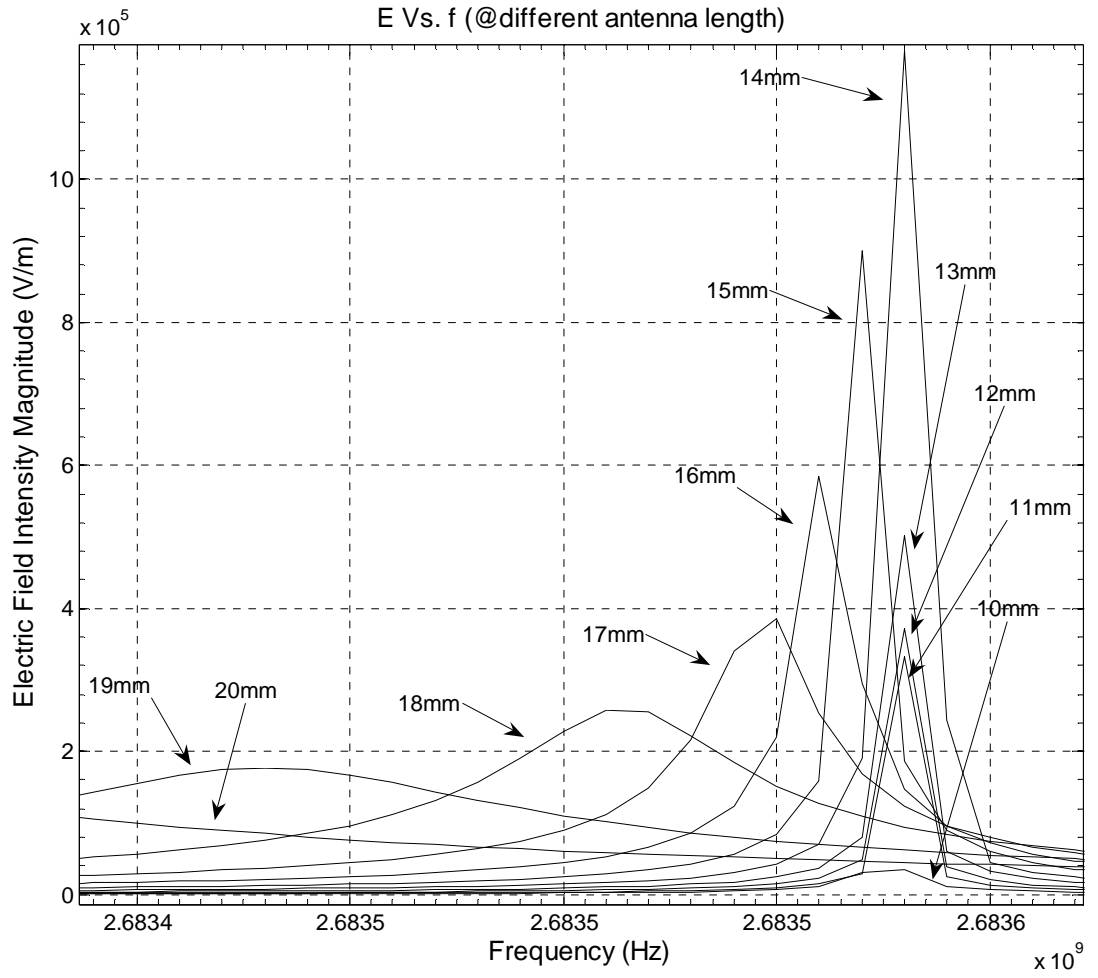


(d) Antenna length: 30 mm

Figure 4-25 Various antenna length

The coupling antenna length is measured from the start of the emitter, which is designed to fit in the opening for spark plug at cylinder head. This makes the adjustment of the parameter in program easier. Figure 4-25 shows that the antenna length actually affects the volume of a cylinder. Thus, it affects the  $Q$  factor and the natural frequency of the cylinder. It also slightly affects the distribution of the electric field as it is extended into the cylinder head.

The impedance of the cylinder is difficult to be calculated because of its irregular geometric shape. Therefore, simulation is carried out to assist the design of antennae for HCMI systems. The data of the EM field obtained from this exhaustive search can help researchers design coupling antennae for HCMI systems. The results of exhaustive searches for various antenna lengths are shown in Figure 4.26 and Table 4-7. The resolution of frequency for this search is 10 MHz.



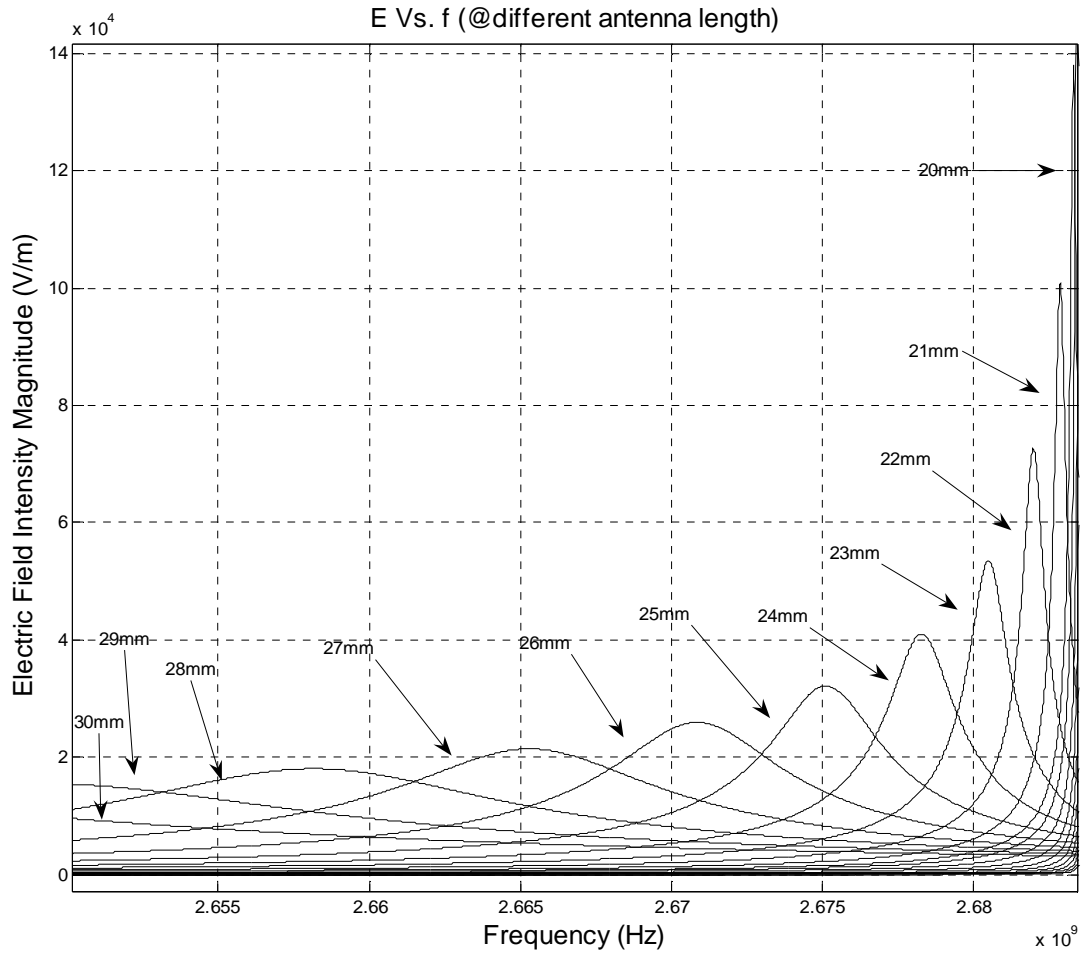


Figure 4-26 Antenna exhaustive search results

Table 4-7 Antenna exhaustive search results

Antenna Length (mm)	Input Microwave Frequency (GHz)	Max Electric Field Intensity (V/m)
10	2.6836	$3.4 \times 10^4$
11	2.6836	$3.31 \times 10^5$
12	2.6836	$3.72 \times 10^5$
13	2.6836	$5.02 \times 10^5$
14	2.6836	$1.18 \times 10^6$
15	2.6836	$9.02 \times 10^5$
16	2.6836	$5.84 \times 10^5$
17	2.6835	$3.86 \times 10^5$
18	2.6835	$2.58 \times 10^5$
19	2.6834	$1.75 \times 10^5$
20	2.6833	$1.38 \times 10^5$
21	2.6829	$1.01 \times 10^5$
22	2.682	$7.26 \times 10^4$

Table 4-7 Antenna exhaustive results (Continues)

Antenna Length (mm)	Input Microwave Frequency (GHz)	Max Electric Field Intensity (V/m)
23	2.6805	$5.37 \times 10^4$
24	2.6783	$4.1 \times 10^4$
25	2.6752	$3.21 \times 10^4$
26	2.6708	$2.6 \times 10^4$
27	2.6655	$2.3 \times 10^4$
28	2.6582	$1.81 \times 10^4$
29	2.65	$1.543 \times 10^4$

The data in Table 4-7 confirm that the length of a coupling antenna affects the natural frequency of a cylinder. The antenna also affects the coupling efficiency. When antenna length is 14 mm the electric field intensity is the strongest.

Results in Table 4-7 are depicted in Figures 4-27 and 4-28.

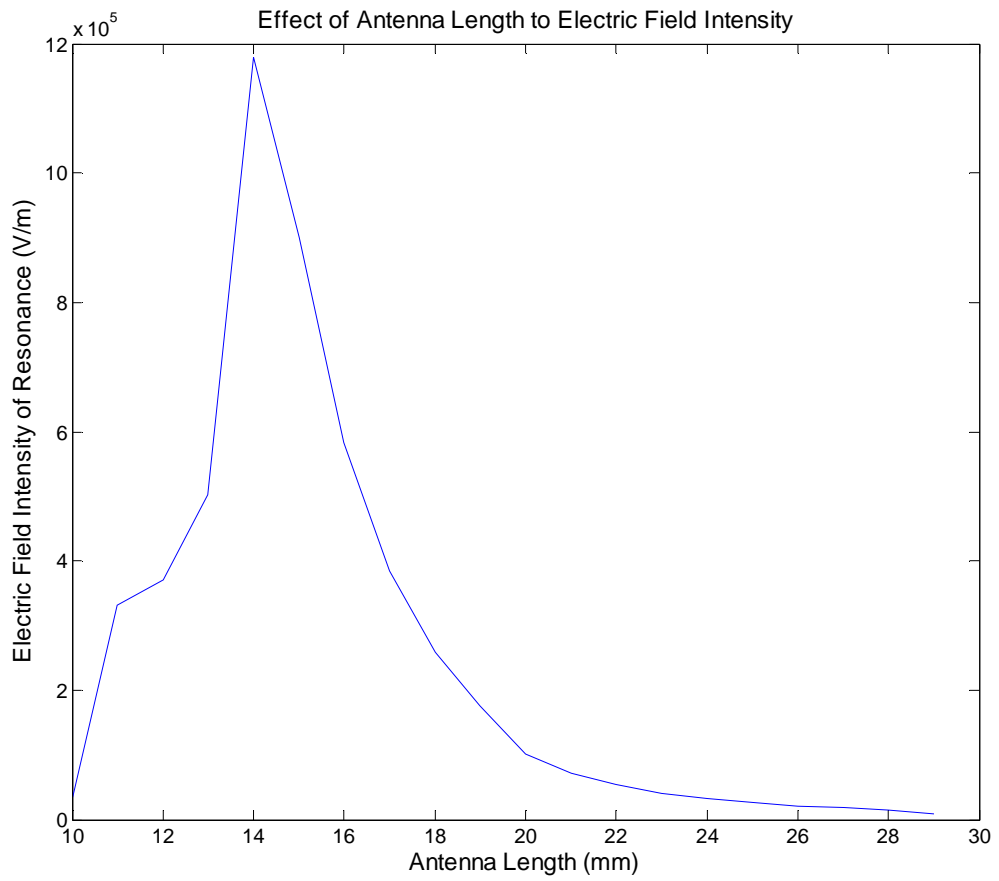


Figure 4-27 Effect of antenna length on electric field intensity of resonance

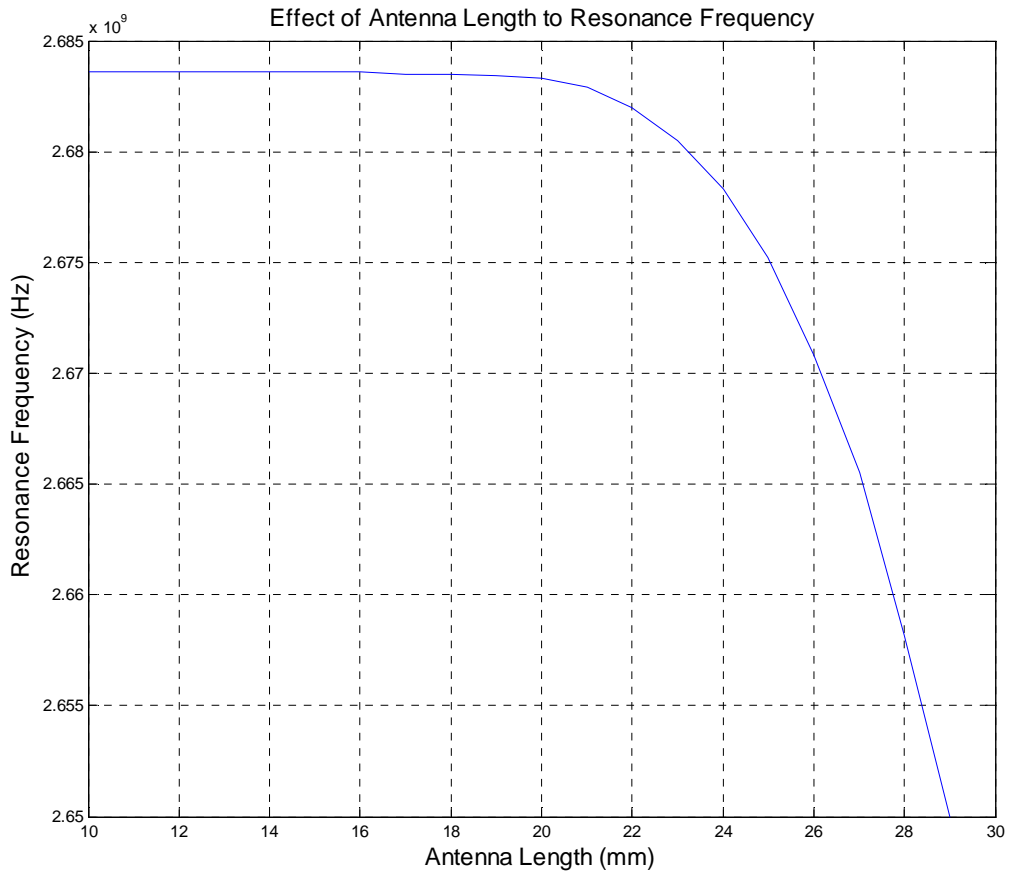


Figure 4-28 Effect of antenna length on resonant frequency

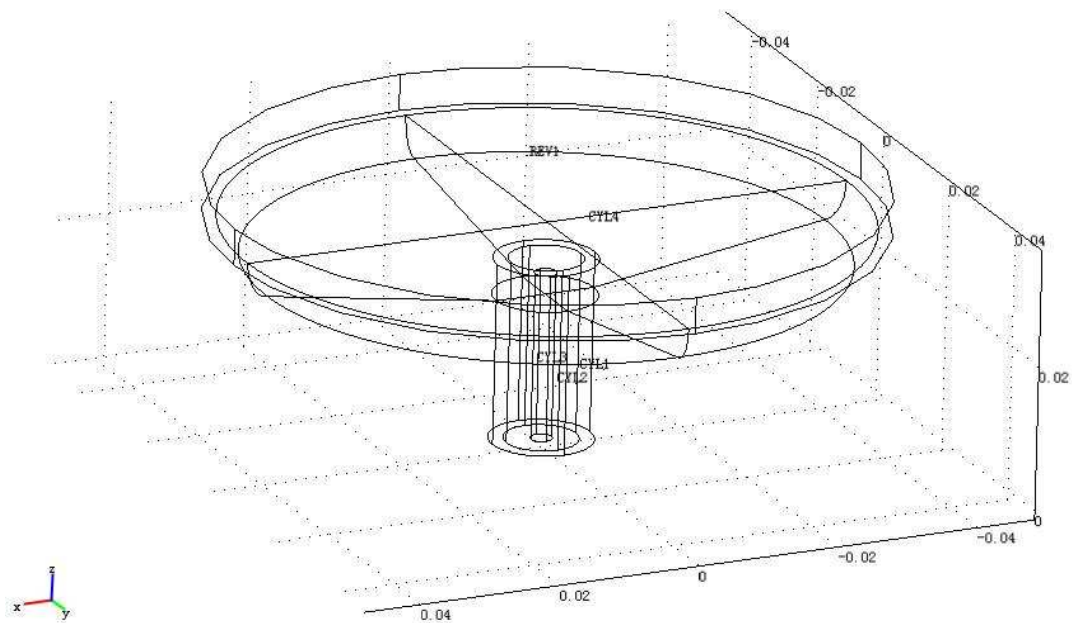
It can be seen in Figure 4-27 that the peak is at 14 mm. In Figure 4-28 it is found that the antenna length has little effect to frequency when it is between 10 mm and 18 mm, i.e., when the antenna is not sticking out. However, when antenna length is greater than 20 mm the resonant frequency changes significantly.

This shows that when the antenna is extended into the cylinder it affects the resonant frequency of a cylinder more than it shrinks into the coaxial cable. These figures also show that when the coupling antenna shrinks into the coaxial cable it brings better coupling efficiency.

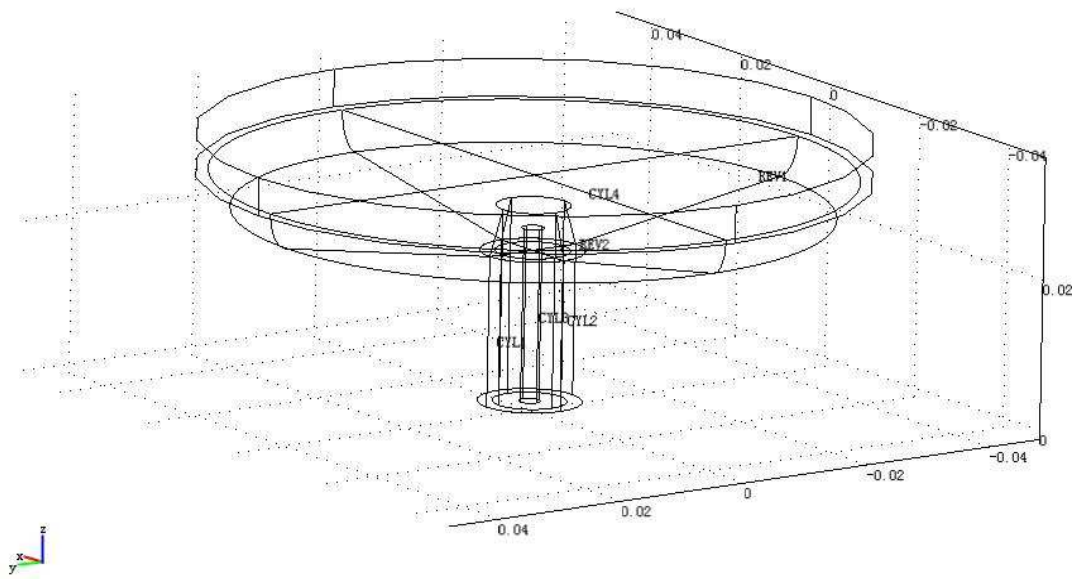
It has to be noticed that the accuracy of this simulation results might be affected by the search resolution of frequency. However, it does not affect the conclusions drawn above.

## 4.5.2 Improvements on the Coupling Antenna

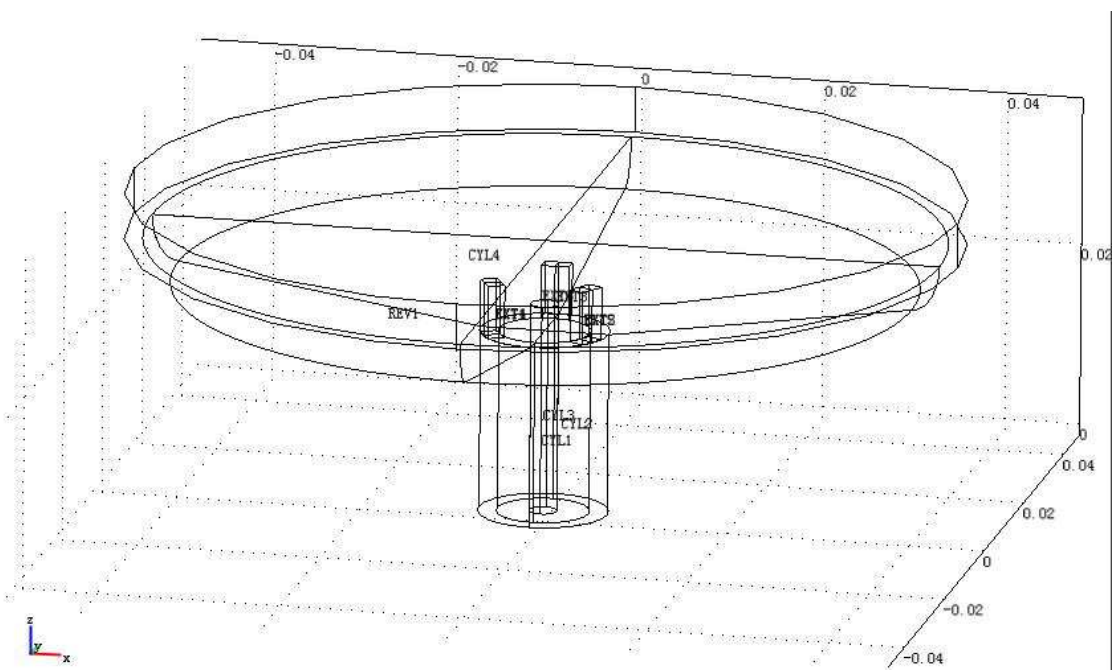
For a cylindrical cavity the probe shape antenna is most commonly used. However, here are six different shape antennae investigated as well to compare with the probe shape antenna. These antennae are derived from the spark plug and the probe shape antenna. The possibility of improvements of the coupling efficiency is investigated. Figure 4-29 illustrates these six types of antennae.



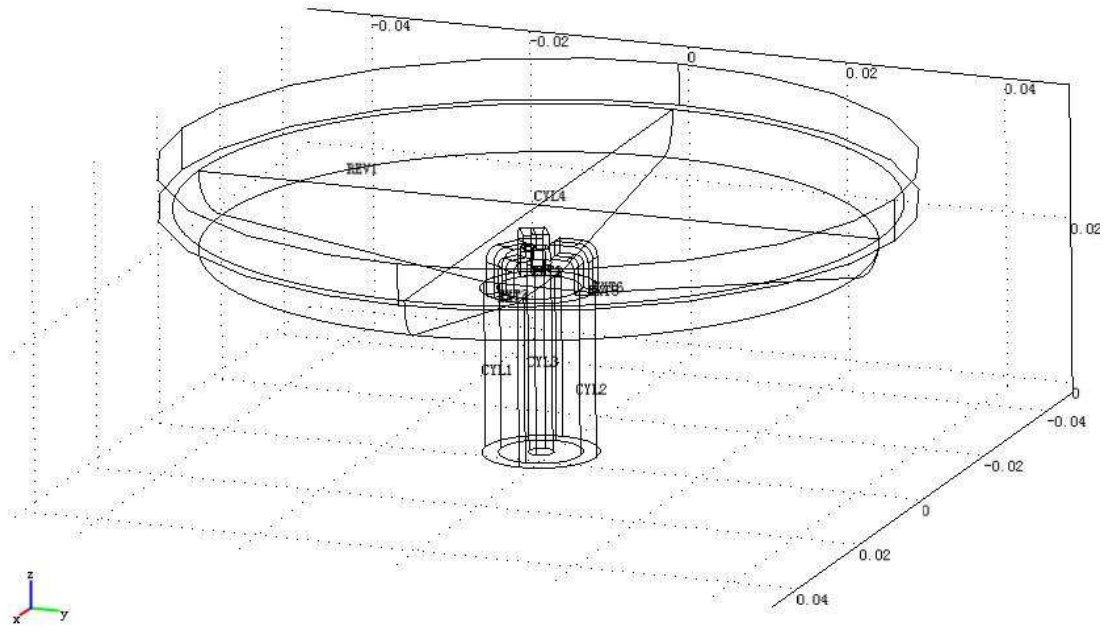
(a) Antenna type 1



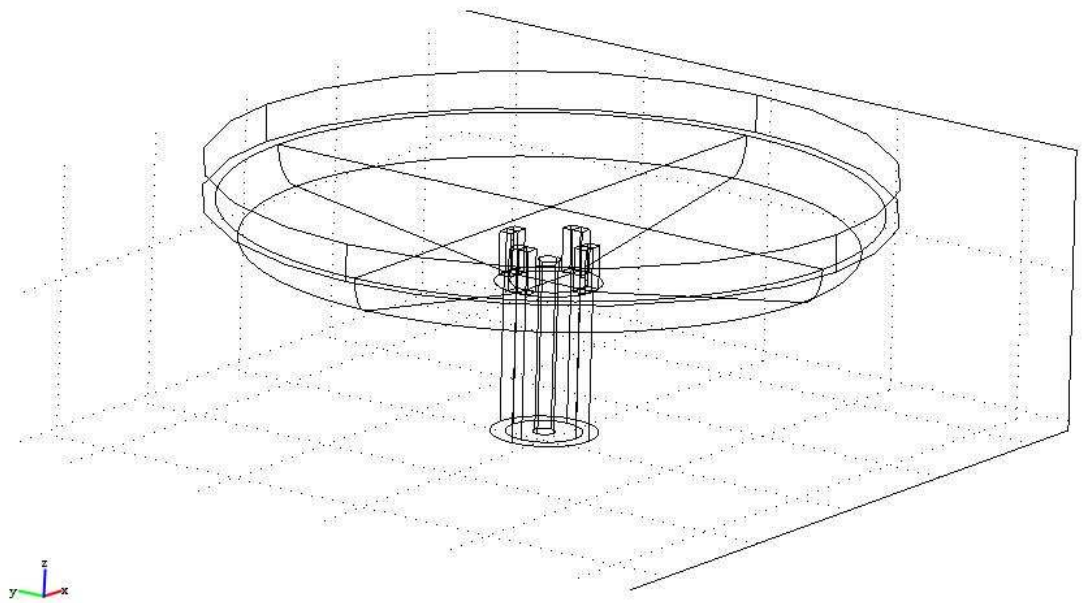
(b) Antenna type 2



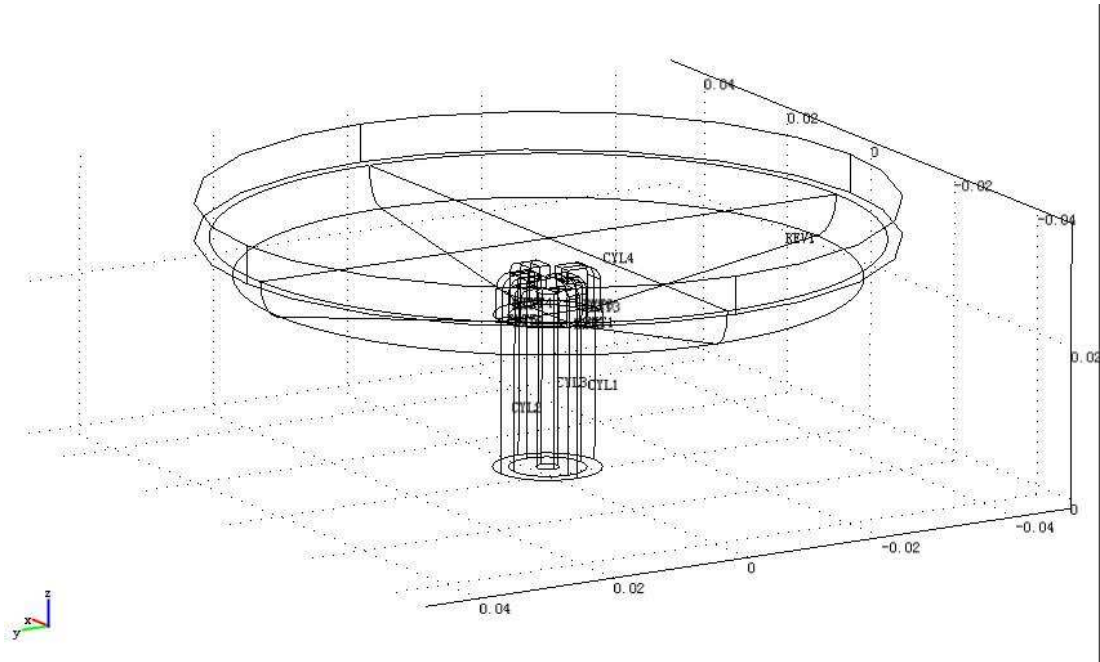
(c) Antenna type 3



(d) Antenna type 4



(e) Antenna type 5

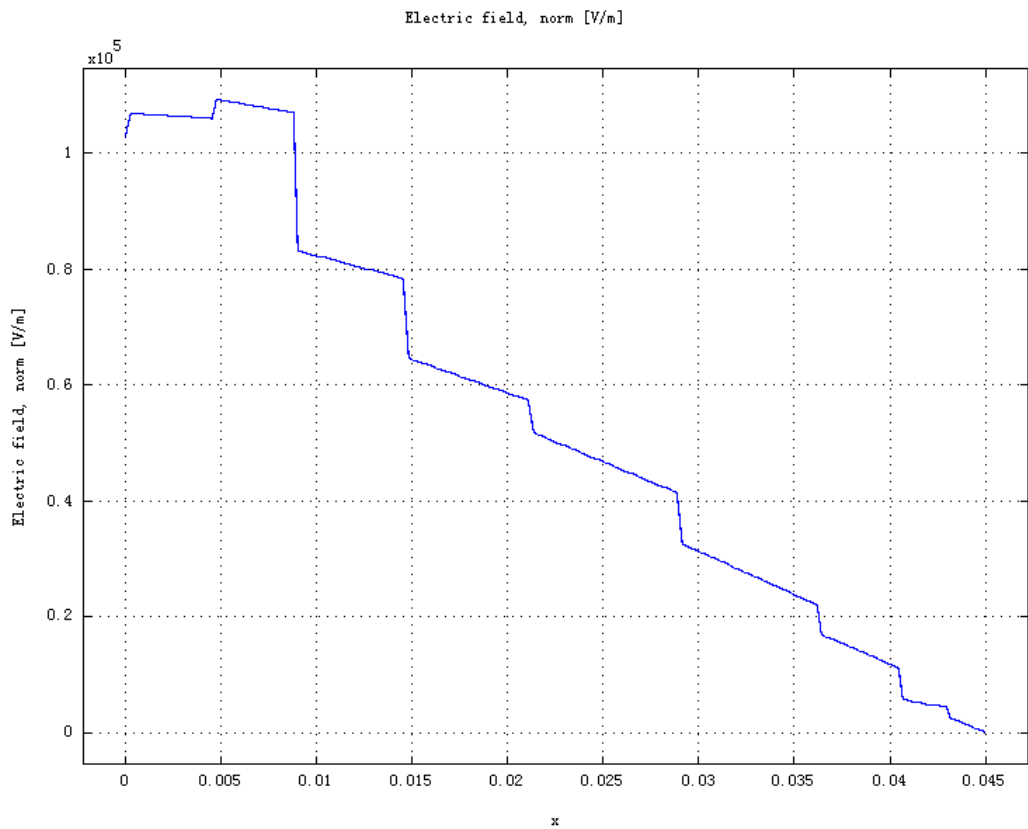
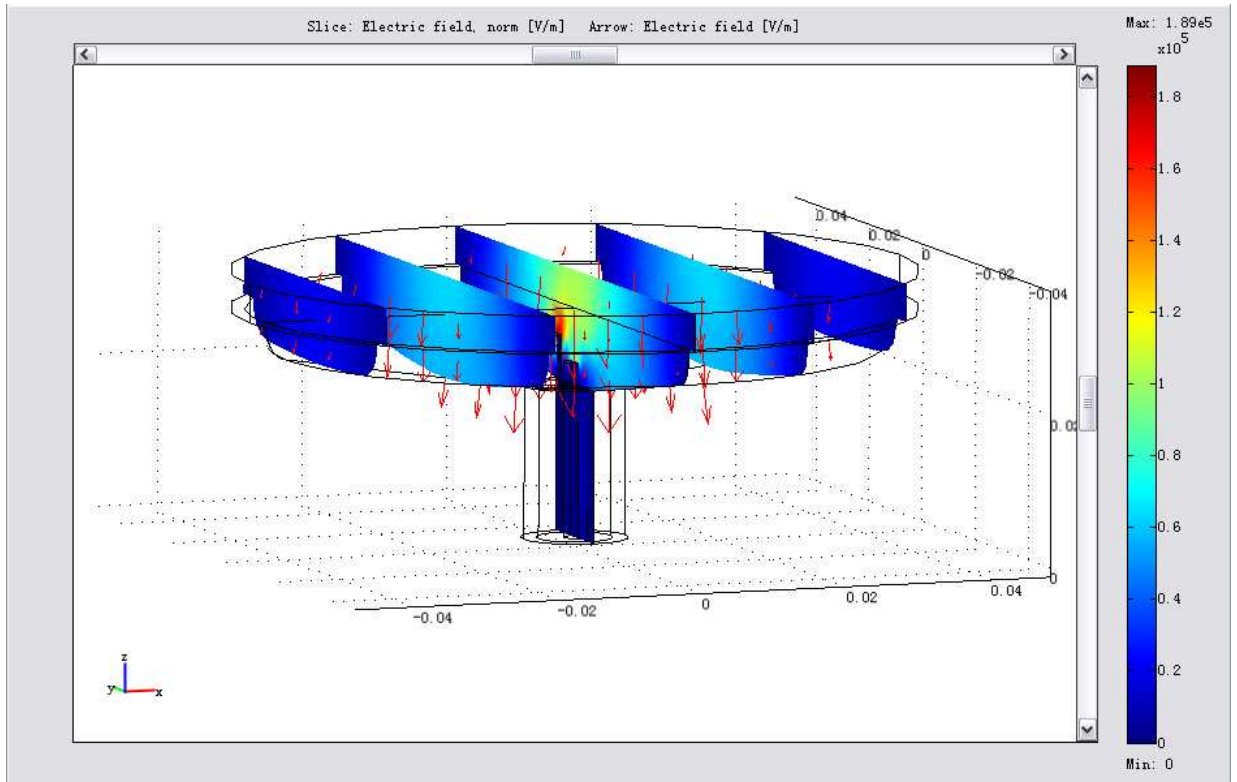


(f) Antenna type 6

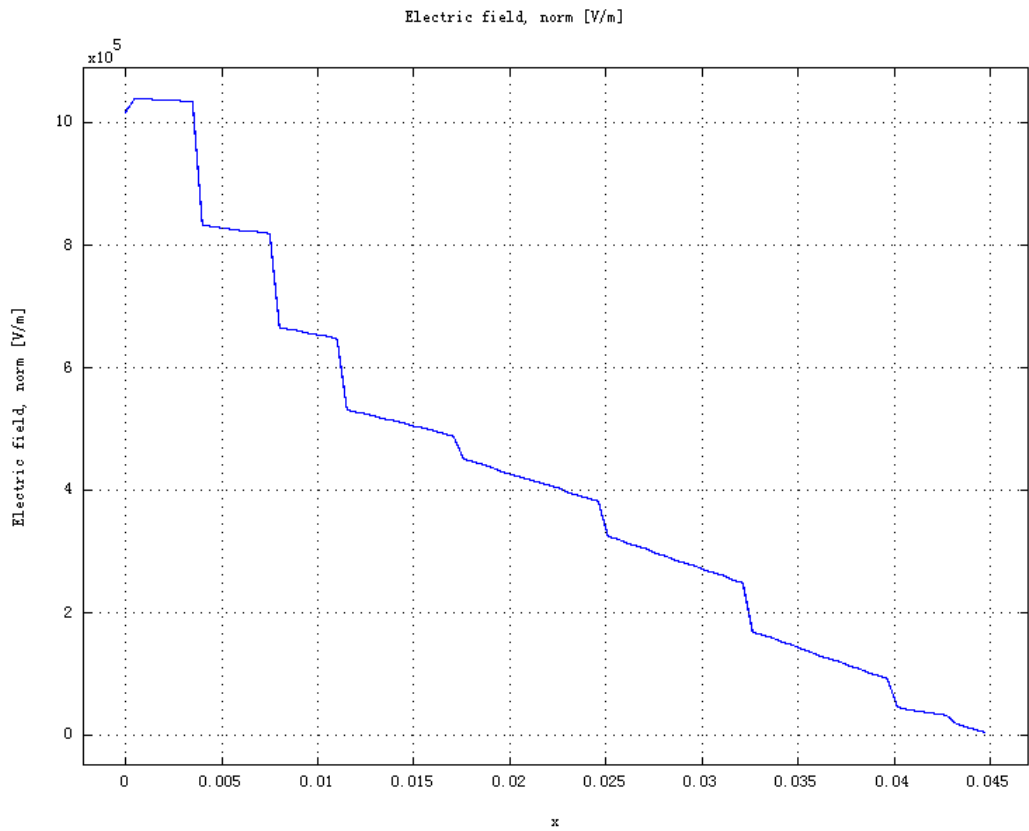
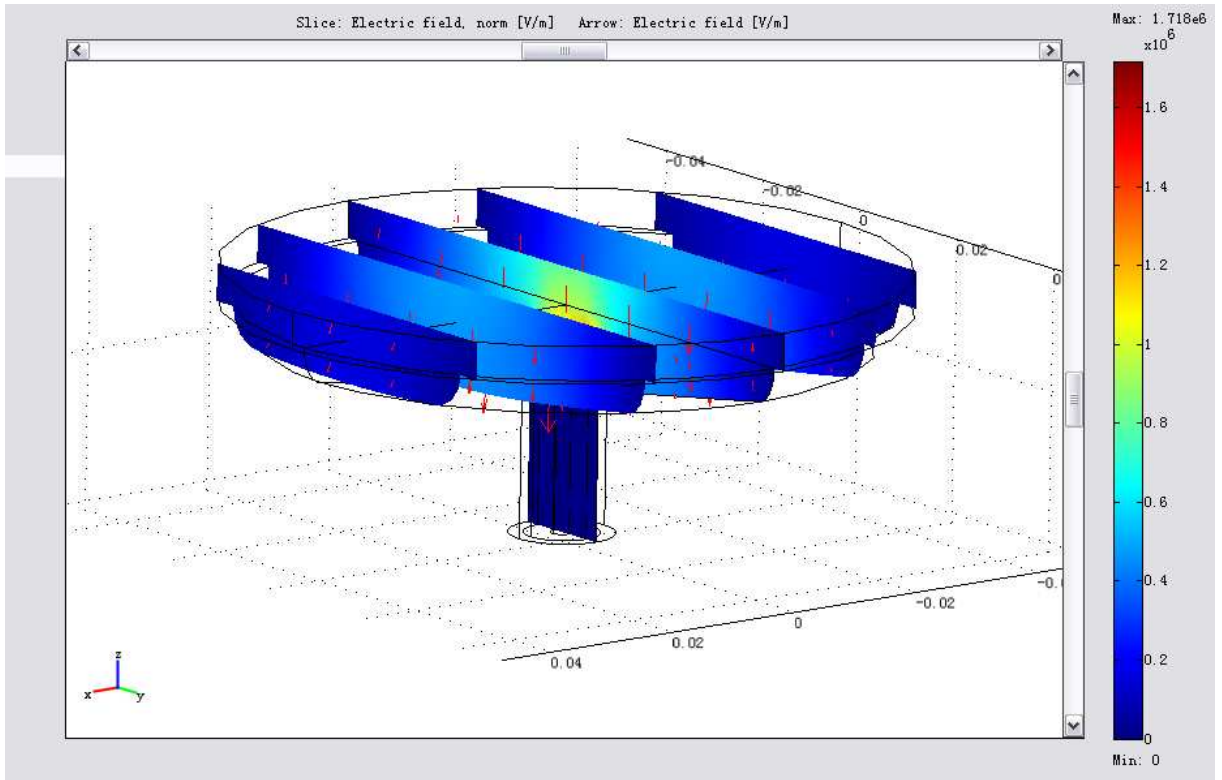
Figure 4-29 Different shapes of antennae

For these simulations 3D models are adopted due to the non-symmetric of antennae. The idea of the shapes of the antennae in above figures comes from spark plugs. The objective of these designs is to achieve the highest maximum electric field intensity as well as strong electric field in big volume. These designs have similar features to the probe shape antenna.

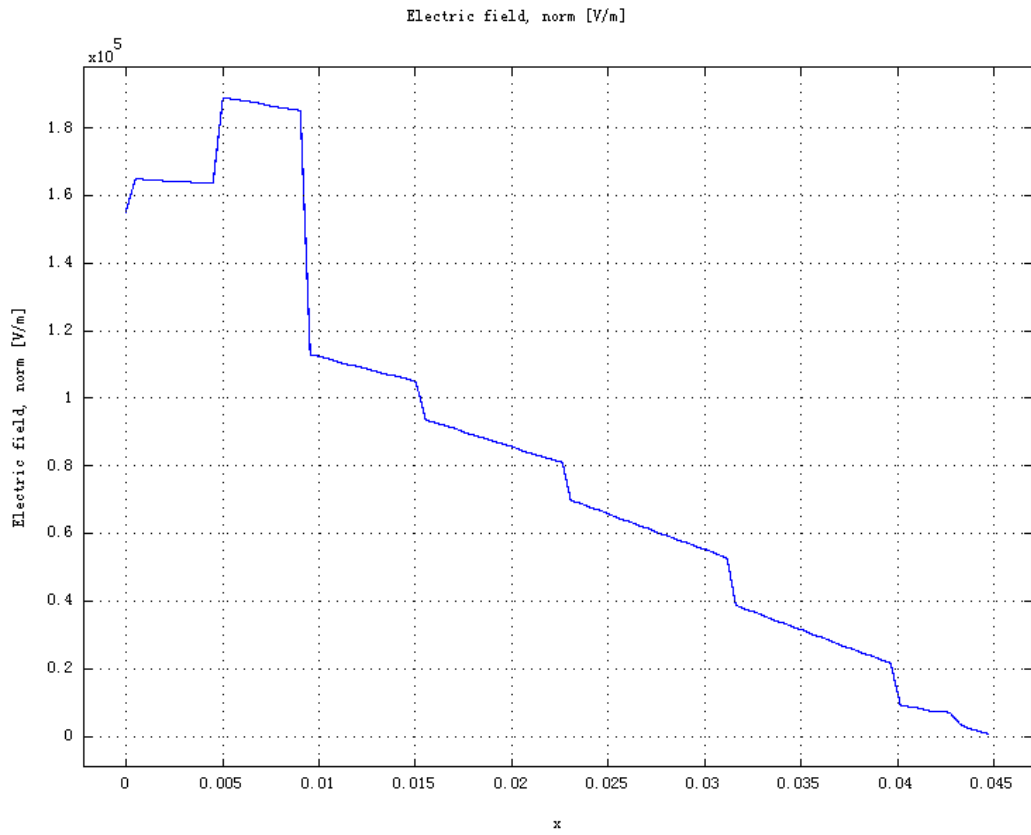
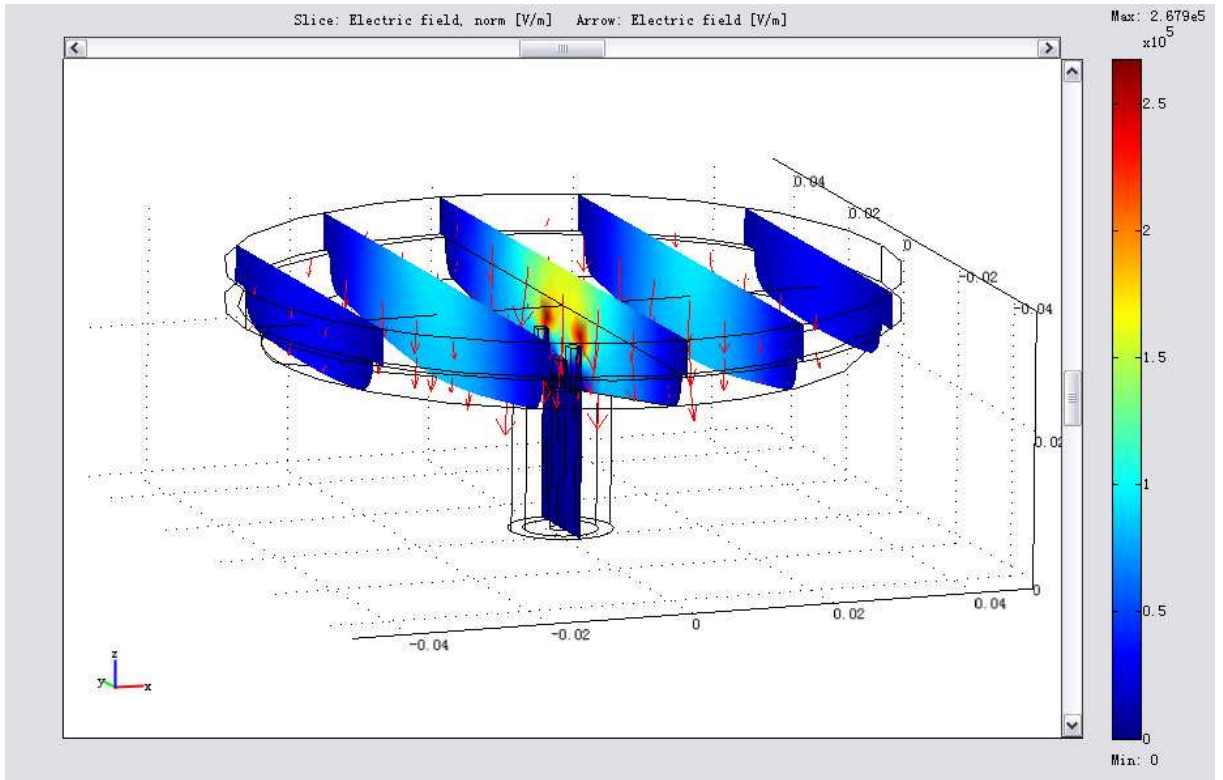
There are two main reasons to investigate these antennae. One is to investigate the differences and improvements of different shapes of antennae other than the probe shape antenna. The other is to study the effects of the antenna shape on EM characteristics of an engine cylinder. The results of these simulations are shown in Figure 4-30 and summarised in Table 4-8.



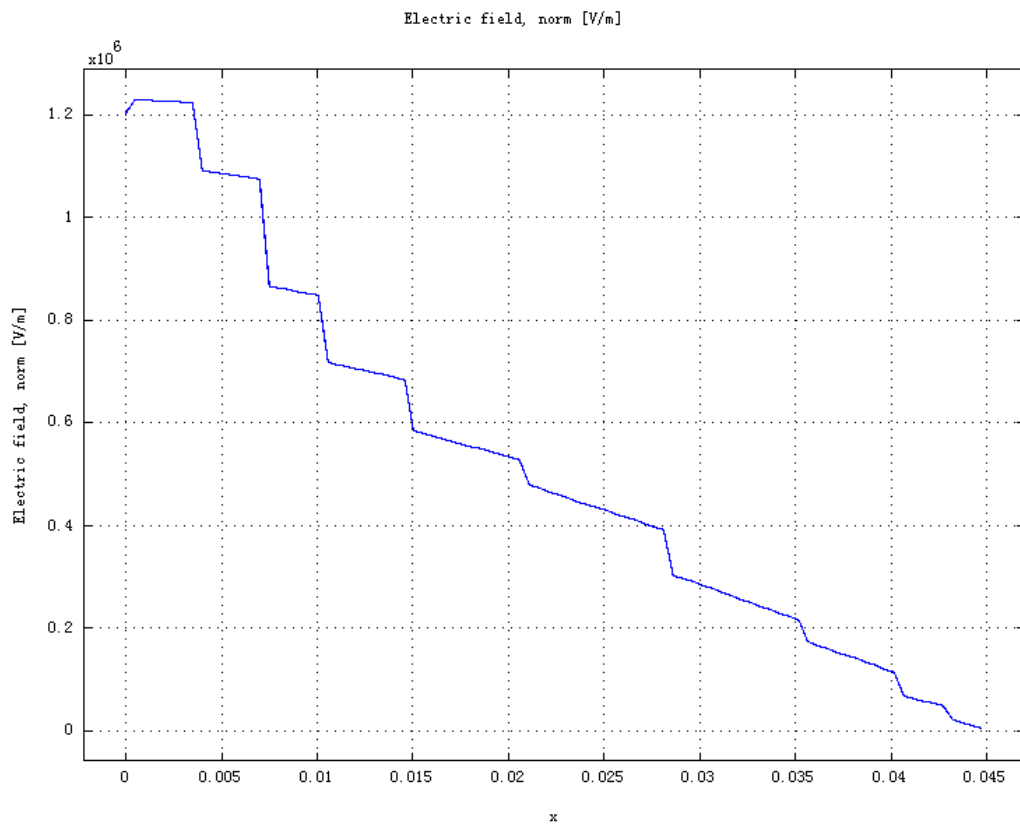
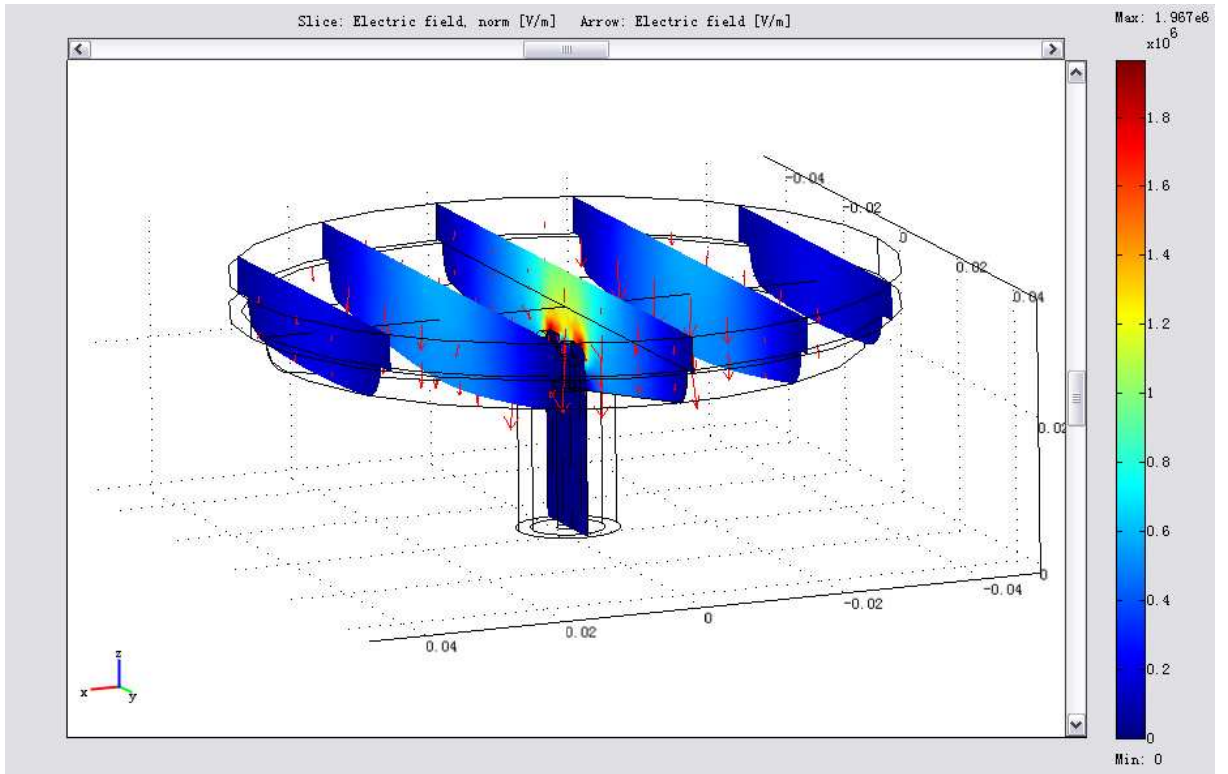
(a) Antenna type 1



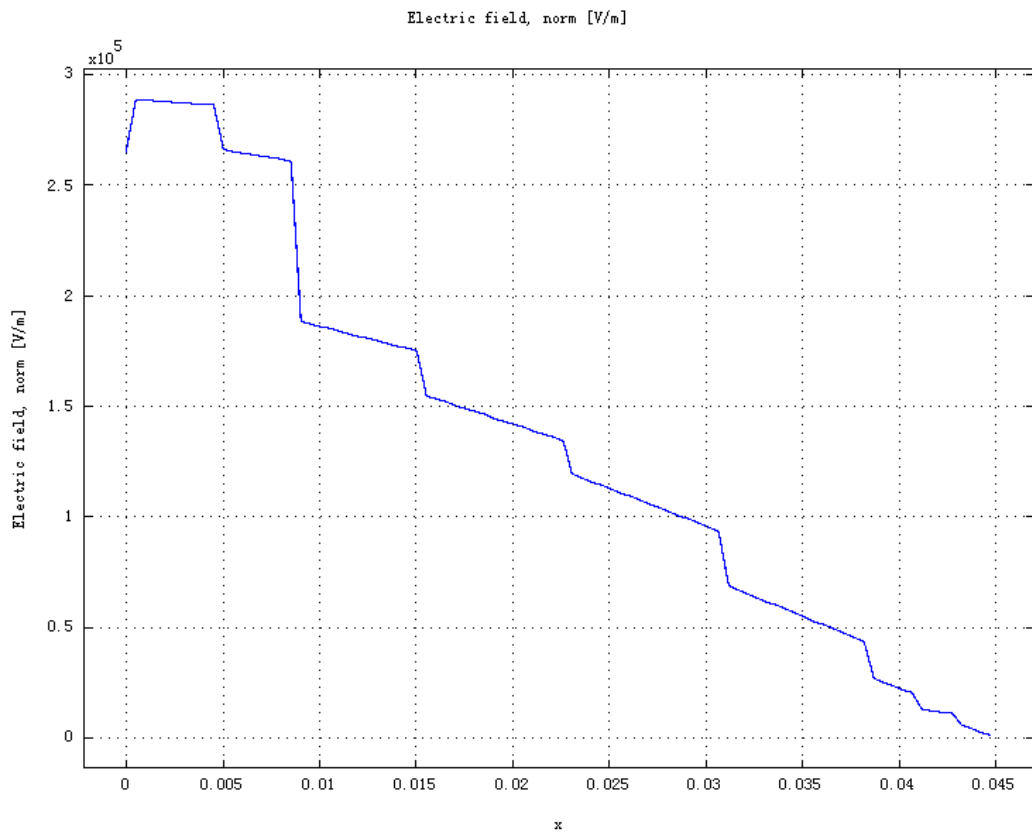
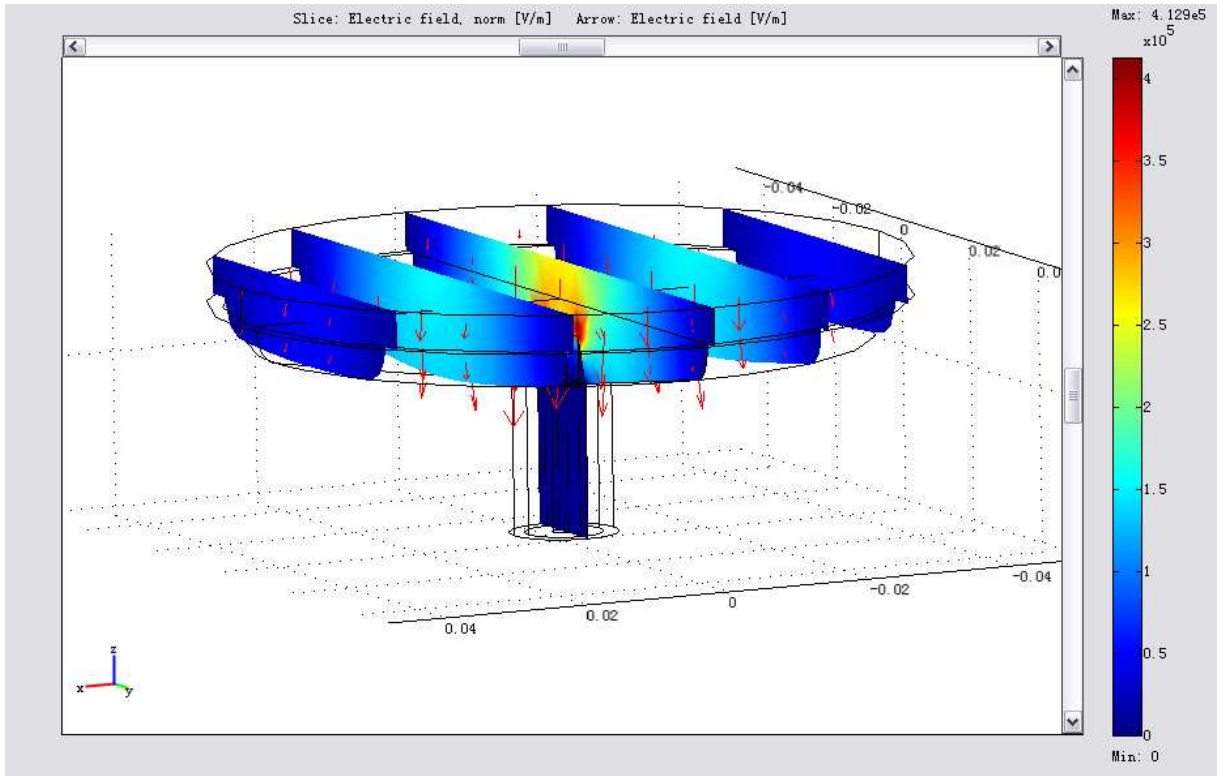
(b) Antenna type 2



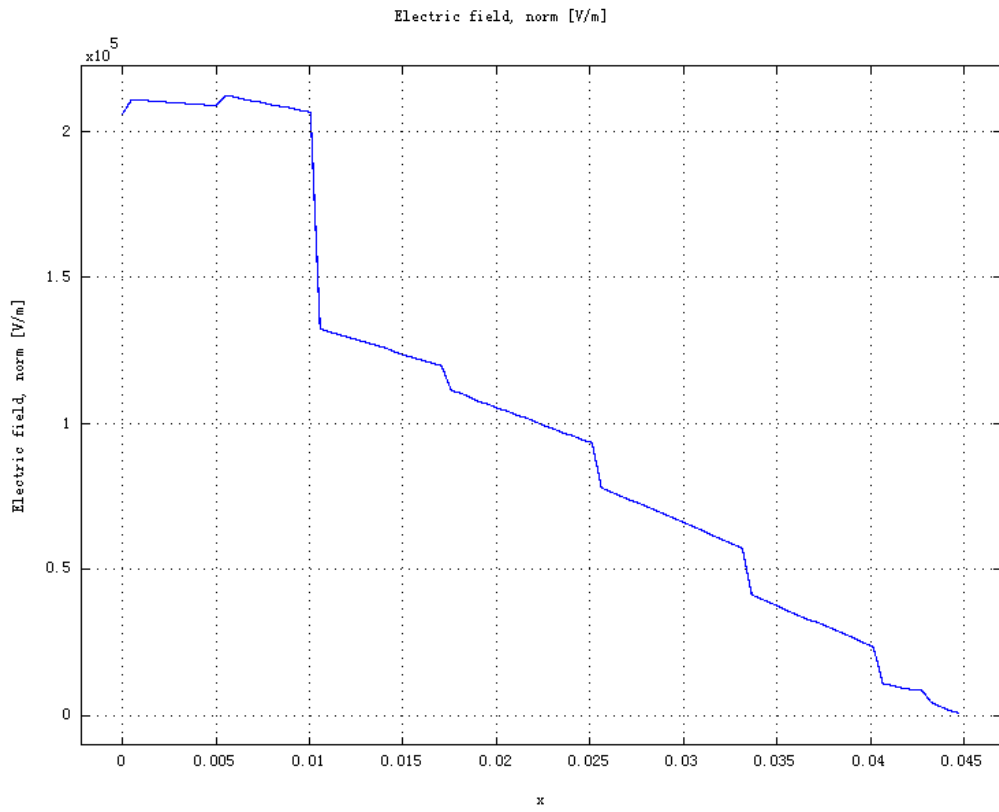
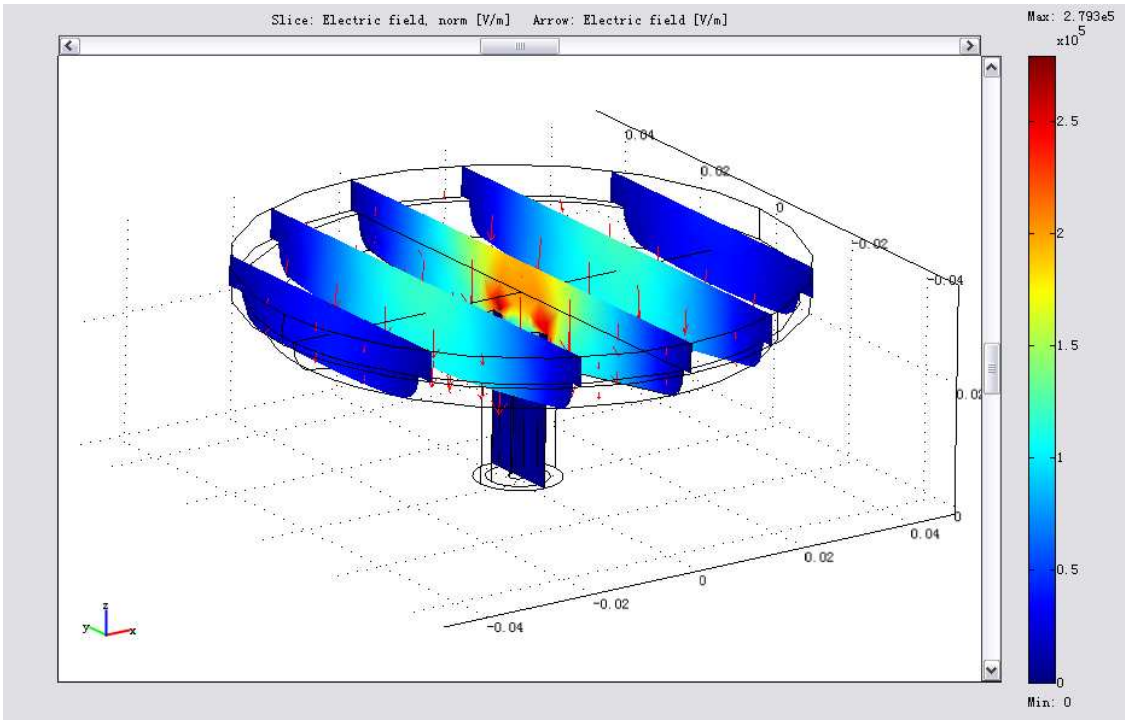
(c) Antenna type 3



(d) Antenna type 4



(e) Antenna type 5



(f) Antenna type 6

Figure 4-30 Simulations of six types of coupling antenna

Table 4-8 Comparison of six types of antenna

Type	1	2	3	4	5	6
Frequency (GHz)	2.732483	2.728356	2.708302	2.716533	2.713997	2.706938
Field Strength (V/mm)	189	1718	267.9	1967	412.9	279.3

From Figure 4-30 it can be seen that antenna type 4 gives the strongest electric field in the cylinder. In Figure 4-30 the distribution of the electric field in the cylinder for those six antenna geometries are almost the same, which means the antenna shape does not alter the distribution of the electric field in a cylinder.

From these data it can be found that some shapes of antenna have better efficiency of coupling than others. However their coupling efficiency is not much higher than a probe antenna's while these antennae have much more complicated structure, because of which they affect the nature frequency of a cylinder and the sensitivity of the resonant frequency more than a probe shape antenna does. This also possibly causes occurrence of off resonance when conditions in the cylinder changes. Therefore, more investigation of the antenna and coupling system has yet to be carried on in the future.

#### **4.6 Effects of Plasma Induced by Microwave Resonance**

As cited in Chapter 2, once the ignition occurs the plasma will be induced. The plasma will not affect the combustion in the cylinder after the air-fuel mixture is broken down.

However, if any unexpected plasma were induced before the air-fuel mixture is broken down it would cause off-resonance and the ignition would not occur. The initial research on the effect of the plasma on resonant frequency and electric field intensity is carried out in this section.

With the model defined in 4.1.4 the resonance in the cylinder where plasma is present is simulated. The results are shown in Figures 4-31 and 4-32.

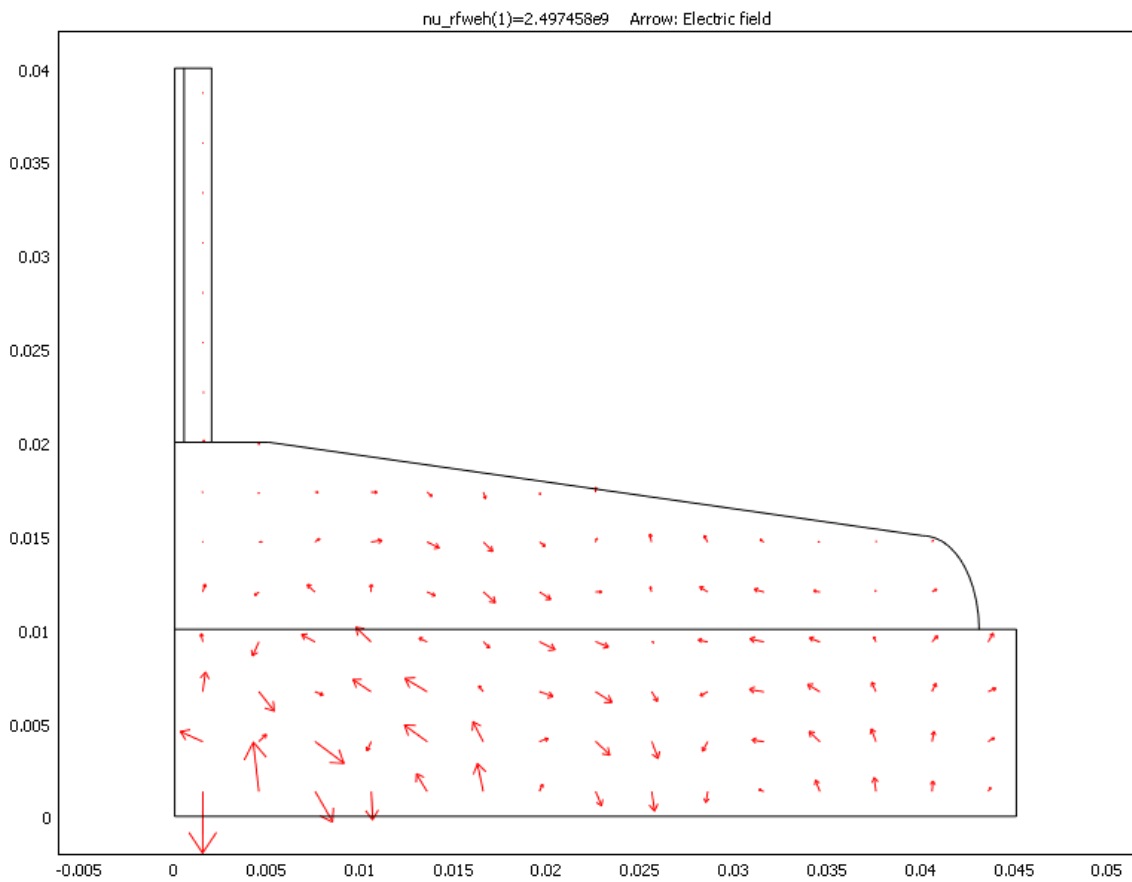


Figure 4-31 Resonance in a cylinder where plasma is present

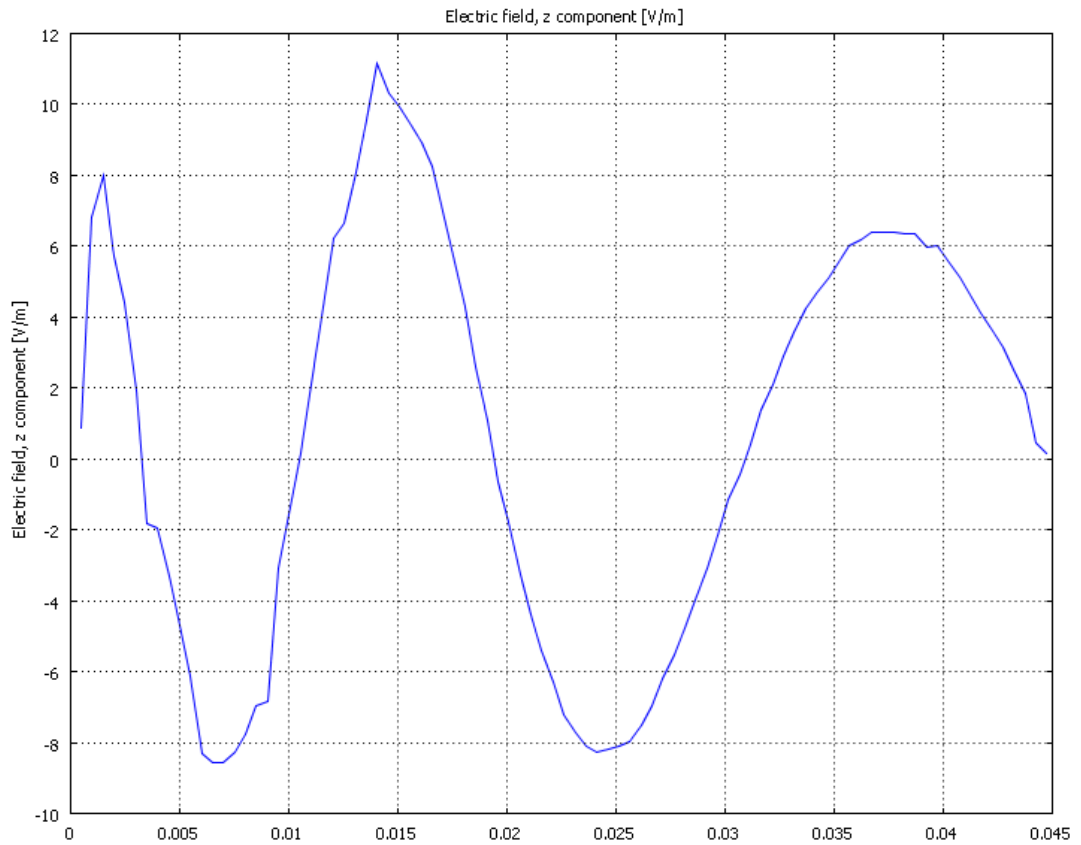


Figure 4-32 Electric field distribution

Through the simulation it can be found that the frequency of the resonance in the cylinder where the plasma is present is 2.497458 GHz. The maximum electric field intensity is only 10 V/m. The electric field intensity is much lower than minimum requirement of the electric field intensity for the ignition.

As a comparison the resonance in the same cylinder where plasma has not been induced is simulated in Figure 4-33.

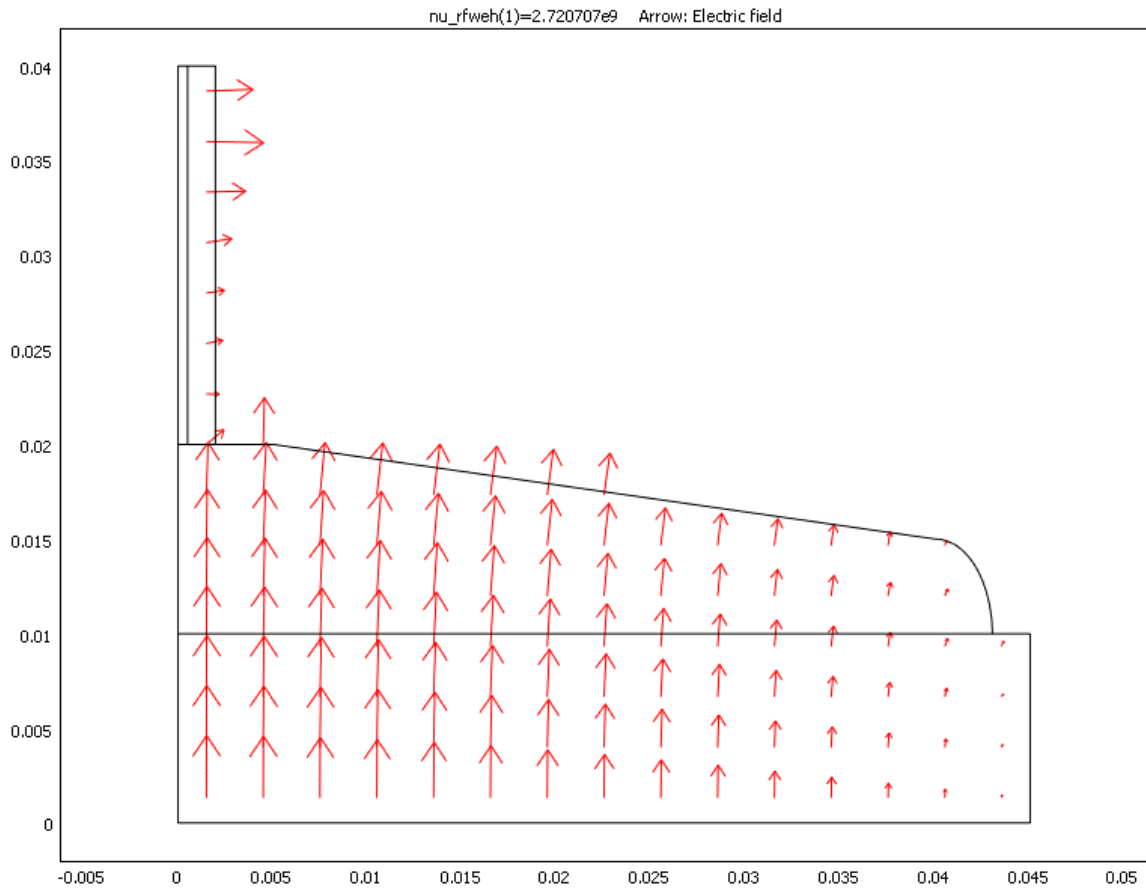


Figure 4-33 Resonance in a cylinder where only air-fuel mixture present

In Figure 4-33 it can be seen that the resonance frequency is 2.720707 GHz. This implies the plasma induced by electric field in the cylinder before the ignition occurs will prevent the occurrence of ignition because of lacking of strong electric field. This could possibly happen when microwave pulse signal is coupled into the cylinder before the piston moves to the ignition position. Therefore the proper ignition timing and proper microwave pulse coupling timing are the important factors of the realisation of an HCMI system.

To avoid this happen, the microwave energy can be applied precisely at or little after the piston moves to resonant point where the electric field intensity reaches max. Although this could reduce at least 50% of the time that the resonance can last, the electric field intensity can still remain stronger than minimum requirement for ignition for 3.5 microseconds as analysed previously. This is much longer than time required for ignition, i.e. 30-150 nanoseconds. Thus, applying microwave energy precisely at the resonant point

can effectively avoid off-resonance caused by the presence of plasma as well as ensure the occurrence of ignition.

## **5. Simulation Based Design of Experiments Using A-Posteriori Search**

In this chapter, the a-posteriori search method is employed to attempt to search and calibrate several design parameters at once. It is extremely hard for engineers to calibrate several parameters in hardware experiments at the same time. However, using automated search method searching several design parameters simultaneously is feasible and efficient.

Four parameters are investigated using automated search methods in this chapter. They are coupling antenna length, the screen of transmission line radius (also called coaxial cable outer radius in figures), relative permittivity of air-fuel mixture, and resonant frequency. The search objective is to maximise the maximal electric field intensity in the cylinder. Two automated search methods are used in this chapter. They are NM Simplex method in MATLAB and EA in FT3PAK.

### **5.1 Combinations of the Transmission Line Radius and Antenna Length**

In this section the screen of the transmission line radius (coaxial cable outer radius), the antenna length, and the resonant frequency are searched using both the NM Simplex method and the EA method. The search results are used for analysis and design of antenna and coupling system.

#### **5.1.1 Search Using the NM Simplex Method**

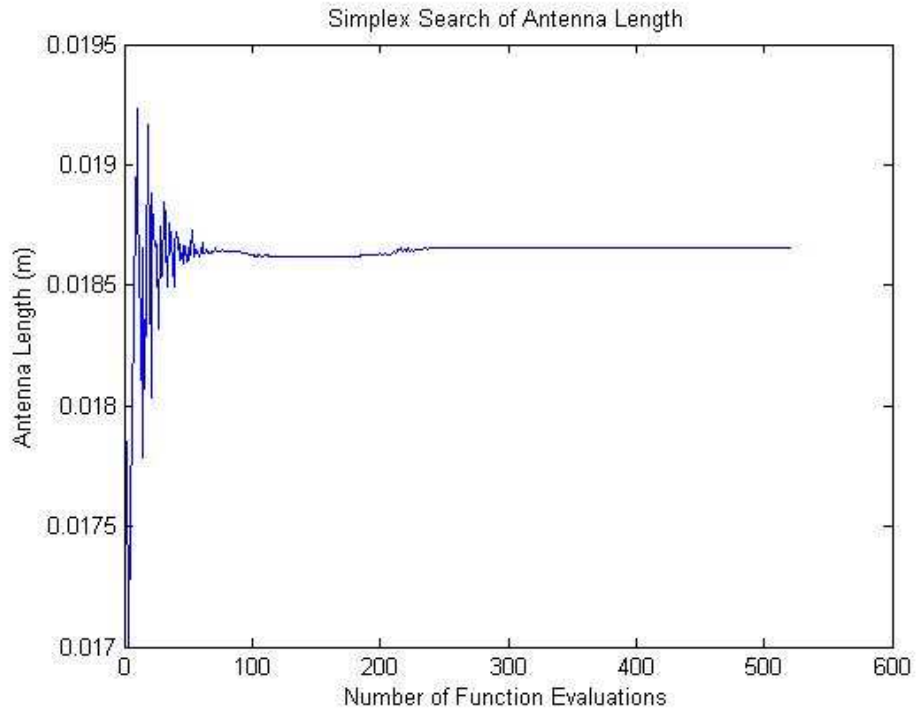
To carry out a search using NM method the initial value of parameters has to be preset. In this thesis, several searches are carried out with various initial values of each parameter. The data for analysis are collected during the search process.

The initial values of each parameter are preset based on the experience gained from exhaustive search in previous chapters and the practical constraints. The initial values set for searches are shown in Table 5-1.

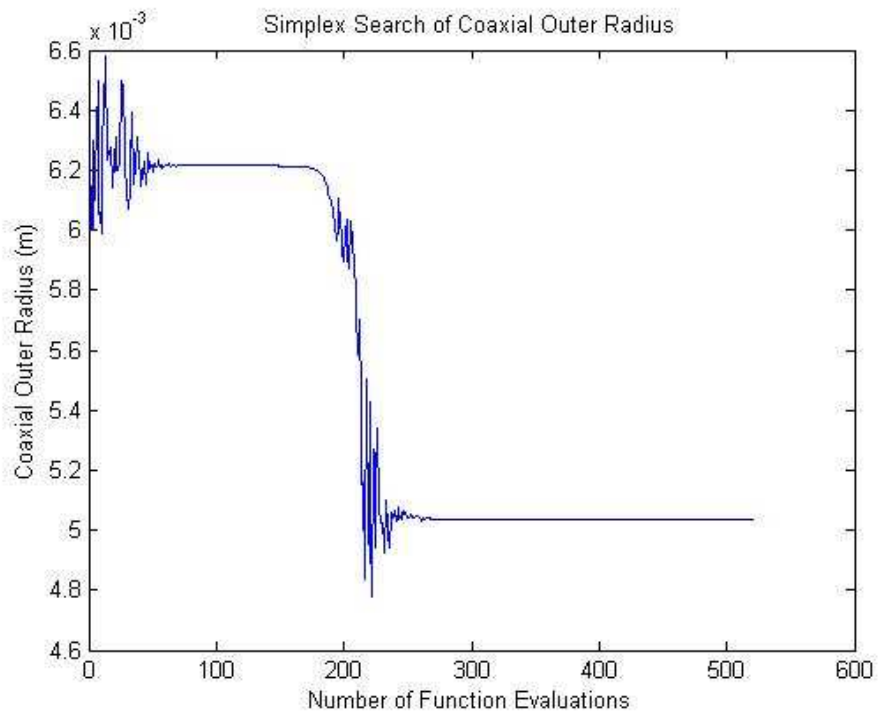
Table 5-1 Initial values of parameters for the NM search

	Antenna Length	Screen Radius	Frequency
1	17mm	6mm	2.65GHz
2	14mm	5.5mm	2.65GHz
3	15mm	5mm	2.6GHz
4	16mm	6.5mm	2.55GHz

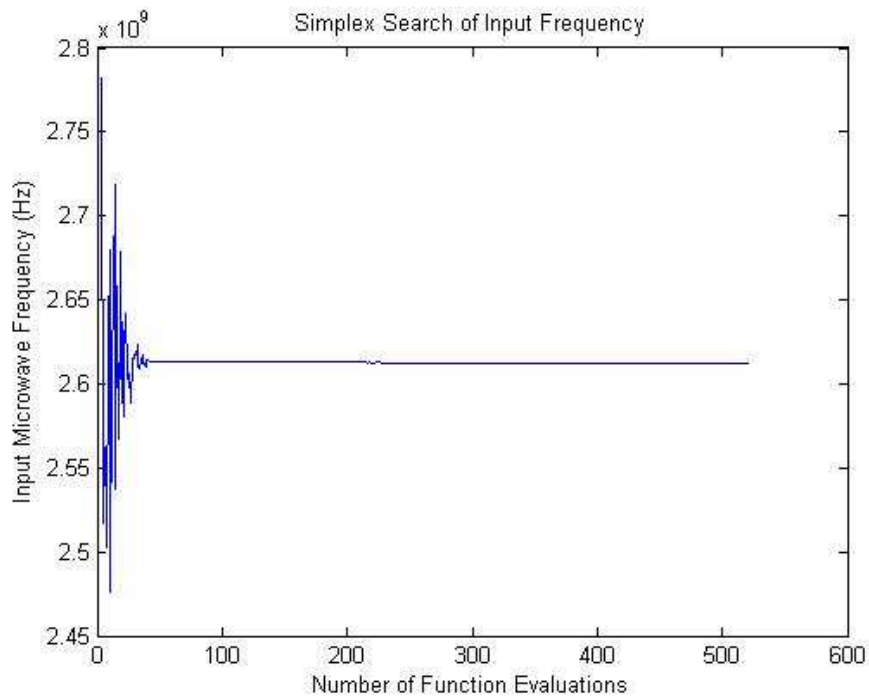
The NM simplex search will start with these initial values and search for the best solution for each parameter. The results of the NM search are shown below. The search processes and results of the NM search are shown in Figures 5-1 – 5-8. The figures show the progress of each parameter and the objective during the search. The data collected from searches are analysed after four searches are accomplished as a single search process can not show an overall view of the problem that it searches for.



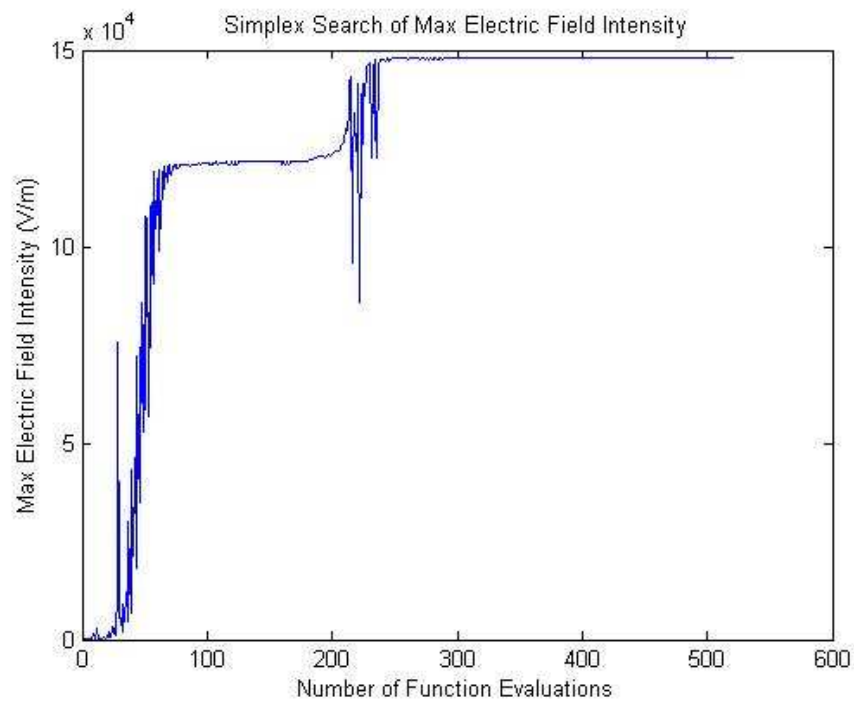
(a) Search trace of searching for antenna length with NM search method



(b) Search trace of searching for screen radius with NM search method



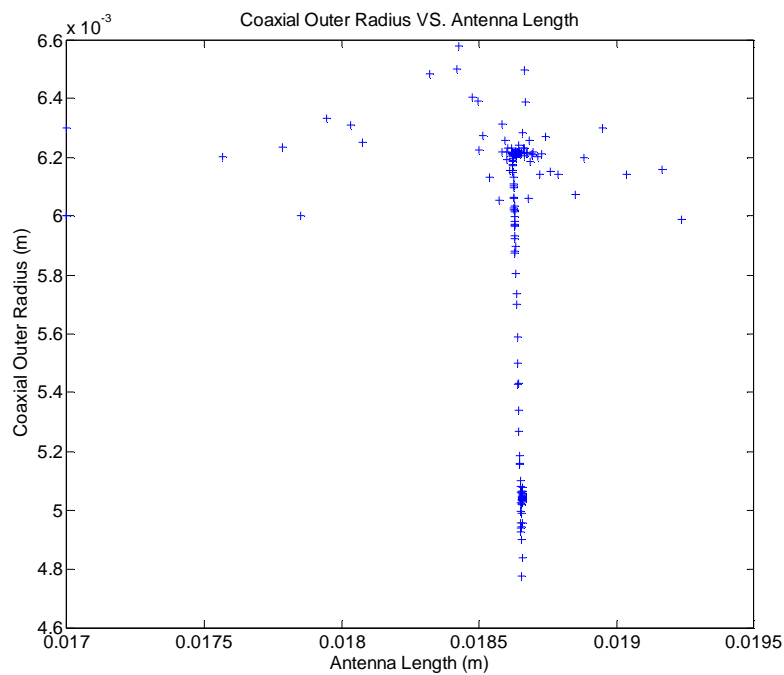
(c) Search trace of searching for resonant frequency with NM search method



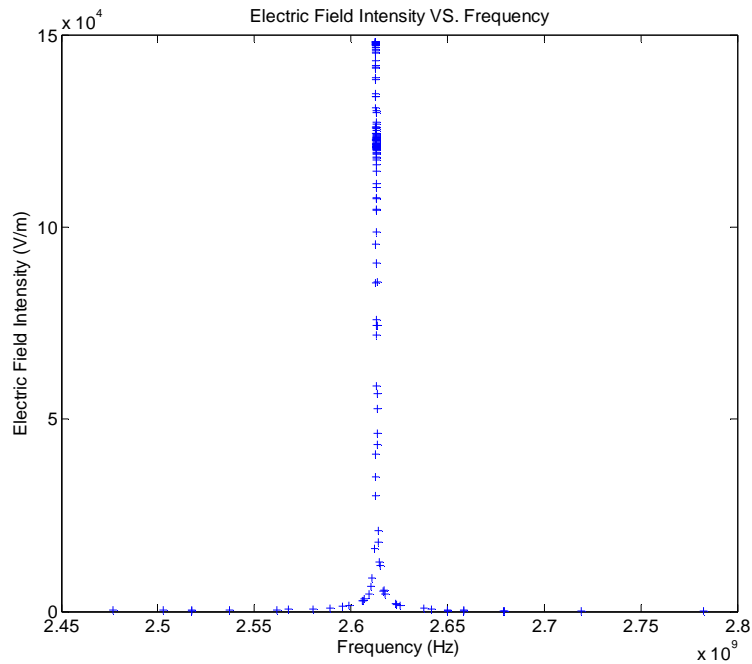
(d) Search trace of the search objective: maximum electric field intensity

Figure 5-1 NM search for 1<sup>st</sup> set of initial values of parameters in Table 5-1

Figure 5-1 shows the NM simplex search process carried out with the 1<sup>st</sup> set of initial values in Table 5-1 by connecting each evaluation points. The figures show the parameters and the objective of each step in the search process. Figure 5-1 (a) shows the values of the antenna length used to simulate resonance for each search step during the search process. Figure 5-1 (b) shows the values of the screen of transmission radius used to simulate resonance for each search step during the search process. Figure 5-1 (c) shows the values selected for the resonant frequency to simulate resonance for each search step during the search process. Figure 5-1 (d) shows the progress of the search objective at each step during the search process. All figures will be analysed after 4 NM simplex searches are accomplished.



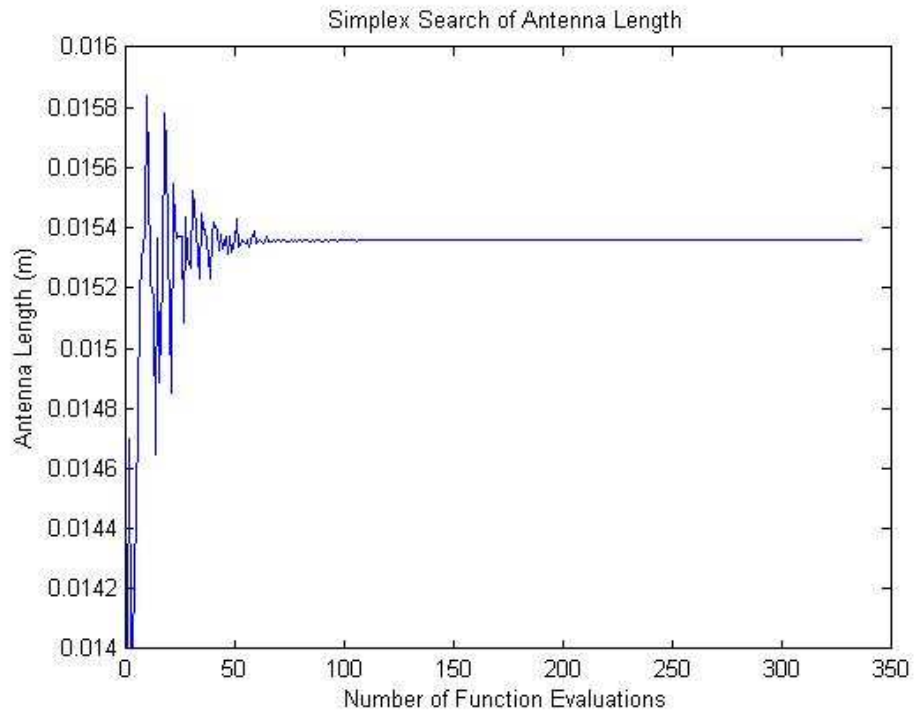
(a) Distribution of search points of antenna length and screen radius



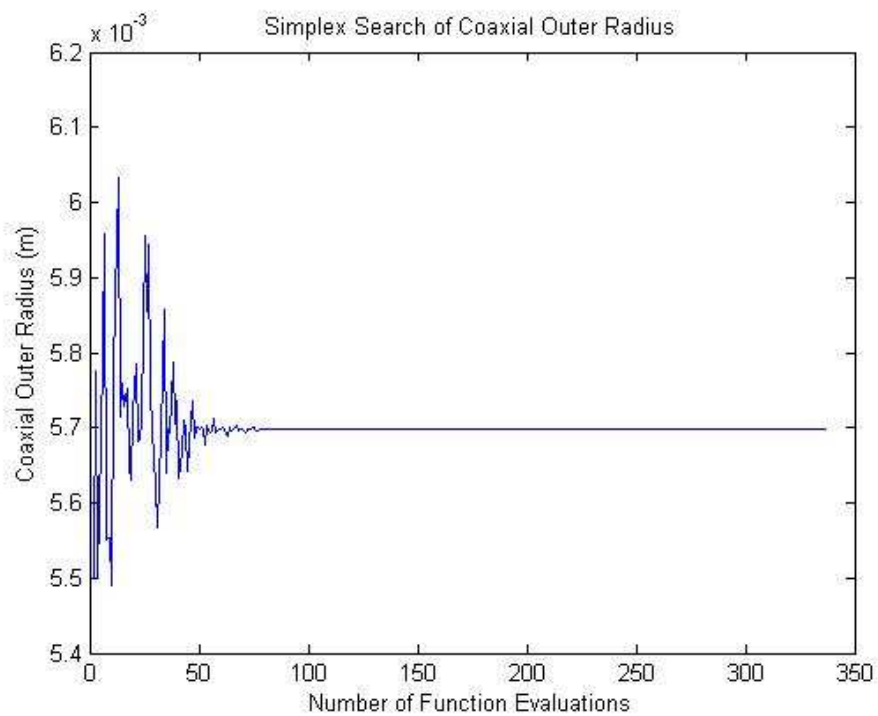
(b) Sensitivity of the resonant frequency

Figure 5-2 Relations between parameters from 1<sup>st</sup> NM search

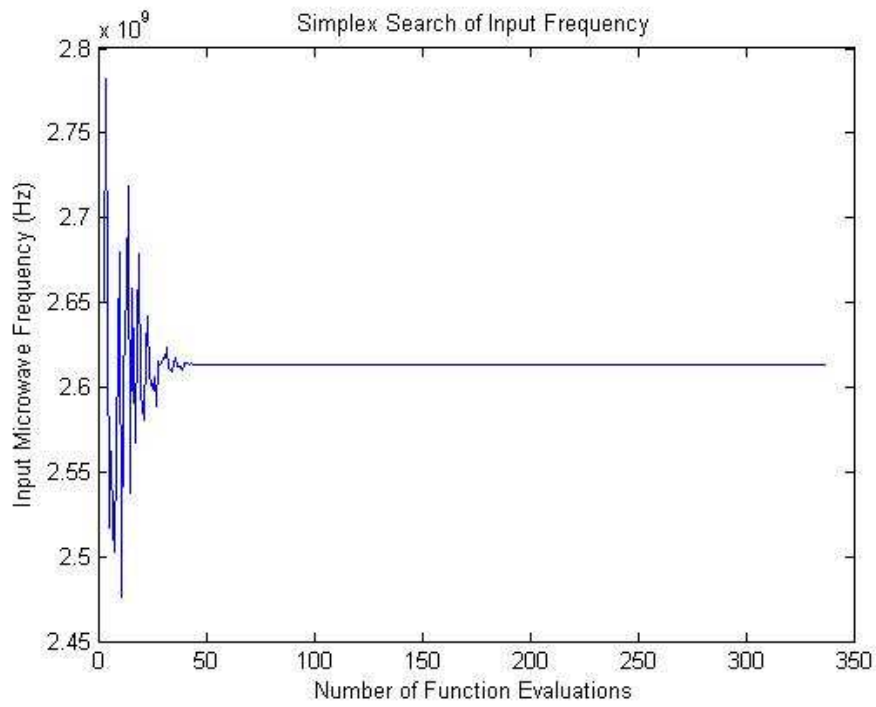
Figure 5-2 shows the relations between parameters and between the objective and parameters in 1<sup>st</sup> NM search. Figure 5-2 (a) draws all search points of the screen of transmission line radius and antenna length in one figure to show the distribution of both parameters in the search range and the search trace of both parameters during the search. From this figure it can be seen that the search managed to jump out of a local optimum at the 210<sup>th</sup> fitness evaluation. Figure 5-2 (b) draws the search objective, maximum electric field intensity against the search points of frequency to analyse the sensitivity of the frequency to screen of transmission line radius and antenna length and to compare with the results from exhaustive search. Figure 5-2 confirms that the resonant frequency is dependent on antenna length and coaxial outer radius as in theory. Further, the jump of coaxial outer radius from 6.2 mm to 5 mm does not affect resonant frequency, but maximum electric field intensity in the cylinder.



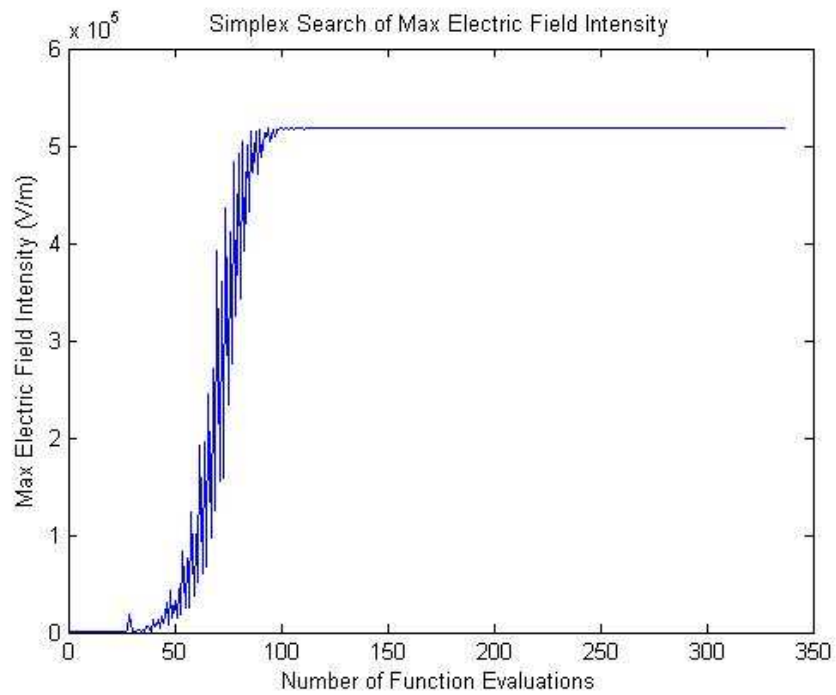
(a) Search trace of searching for antenna length with NM search method



(b) Search trace of searching for screen radius with NM search method



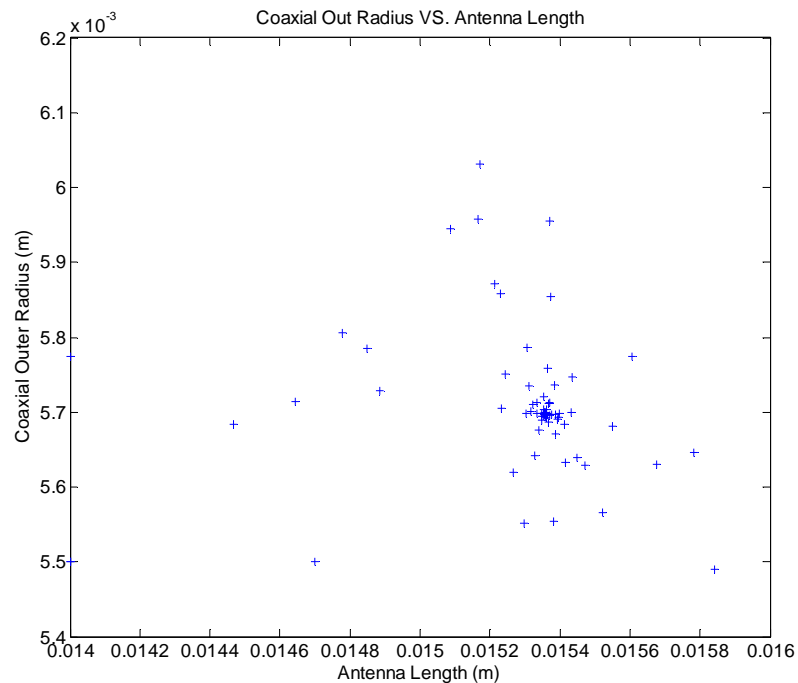
(c) Search trace of searching for resonant frequency with NM search method



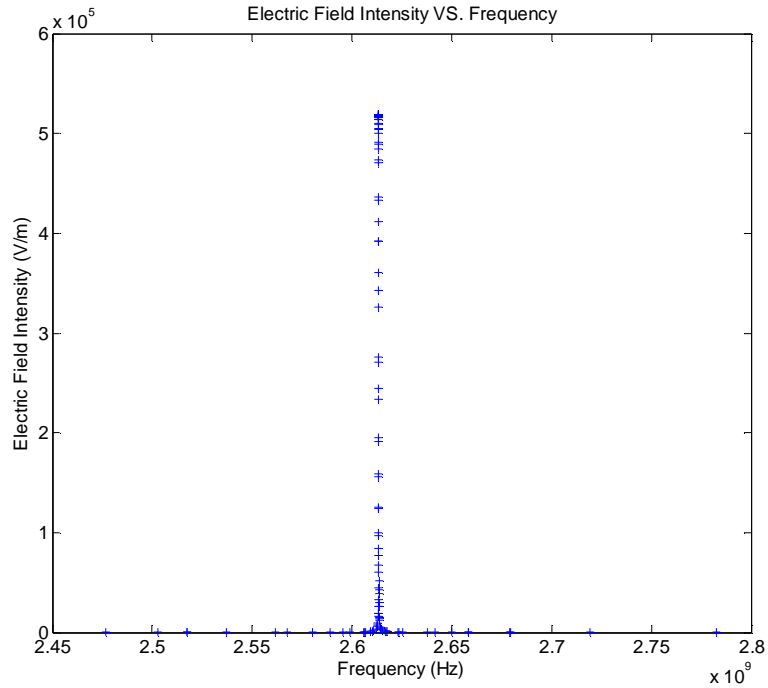
(d) Search trace of search objective: maximum of electric field intensity

Figure 5-3 NM search for 2<sup>nd</sup> set of initial values of parameters in Table 5-1

Figure 5-3 shows the NM simplex search process carried out with the 2<sup>nd</sup> set of initial values by connecting each evaluation points. The figures show the parameters and the objective of each step in the search process. Figure 5-3 (a) shows the values of the antenna length used to simulate resonance for each search step during the search process. Figure 5-3 (b) shows the values of the screen of transmission radius used to simulate resonance for each search step during the search process. Figure 5-3 (c) shows the values selected for the resonant frequency to simulate resonance for each search step during the search process. Figure 5-3 (d) shows the progress of the search objective at each step during the search process.



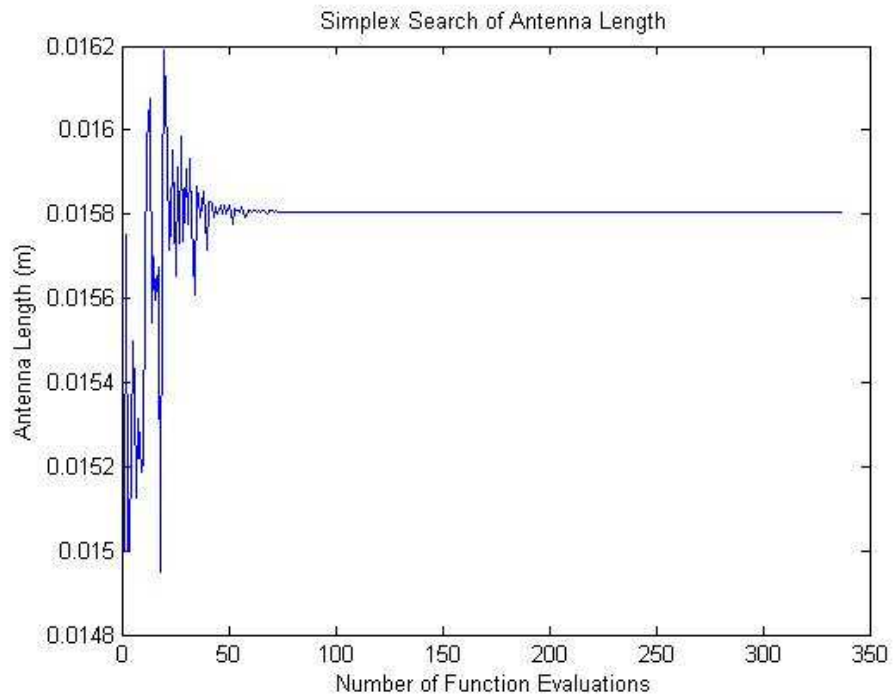
(a) Distribution of search points of antenna length and screen radius



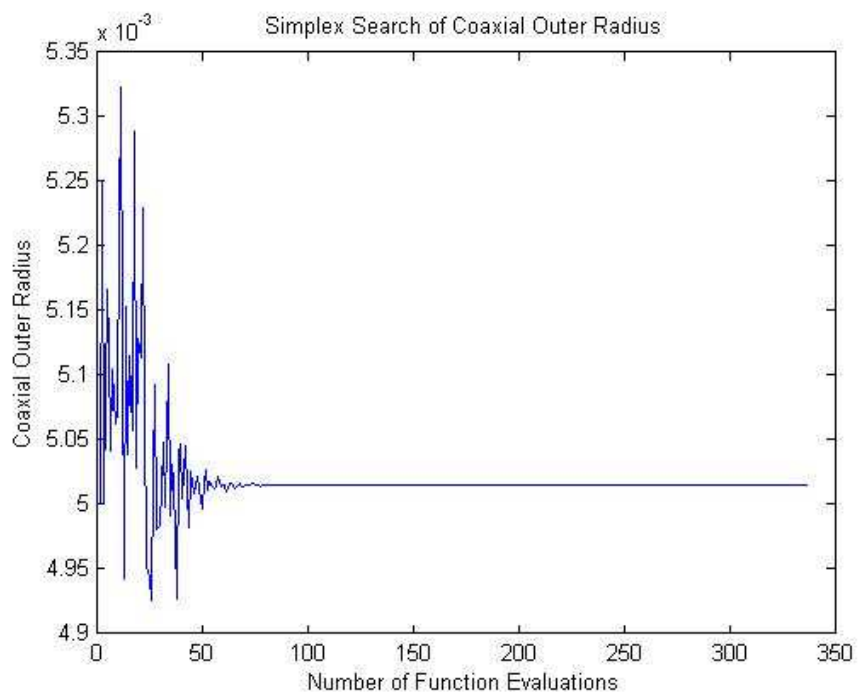
(b) Sensitivity of the resonant frequency

Figure 5-4 Relations between parameters from 2<sup>nd</sup> NM search

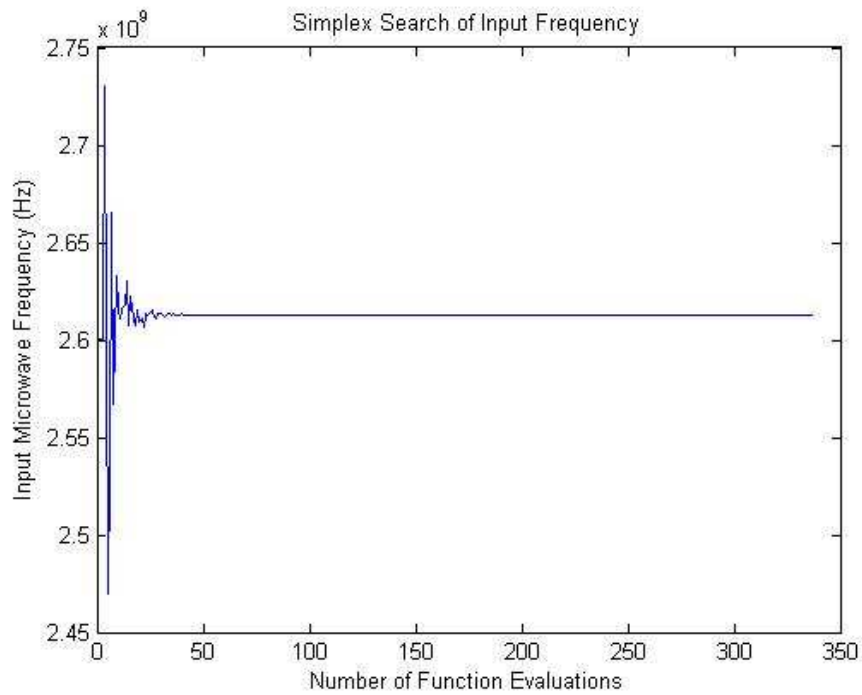
Figure 5-4 shows the relations between parameters and between the objective and parameters in 2<sup>nd</sup> NM search. Figure 5-4 (a) draws all search points of the screen of transmission line radius and antenna length in one figure to show the distribution of both parameters in the search range and the search trace of both parameters during the search. Figure 5-4 (b) draws the search objective, maximum electric field intensity against the search points of frequency to analyse the sensitivity of the frequency to screen of transmission line radius and antenna length and to compare with the results from exhaustive search.



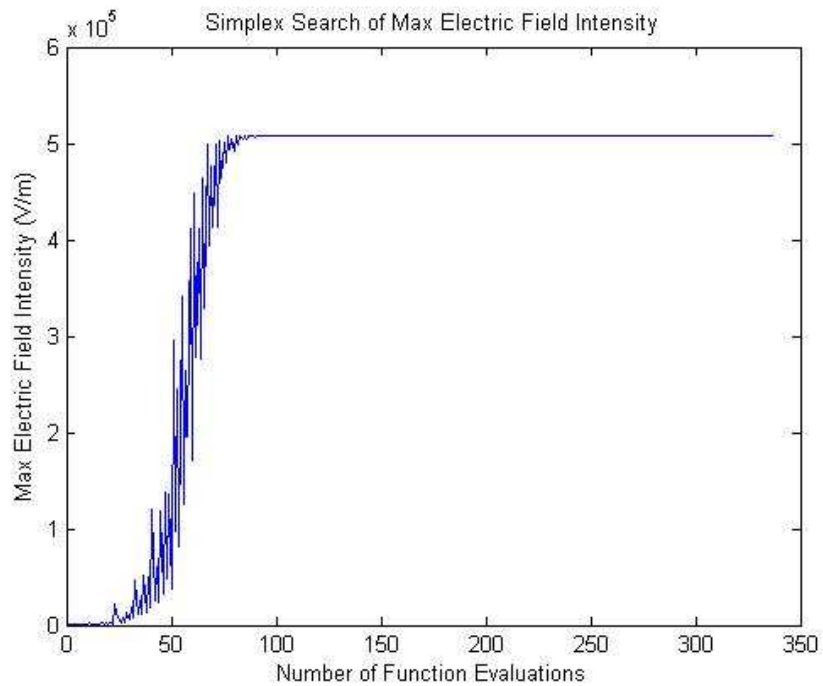
(a) Search trace of searching for antenna length with NM search method



(b) Search trace of searching for screen radius with NM search method



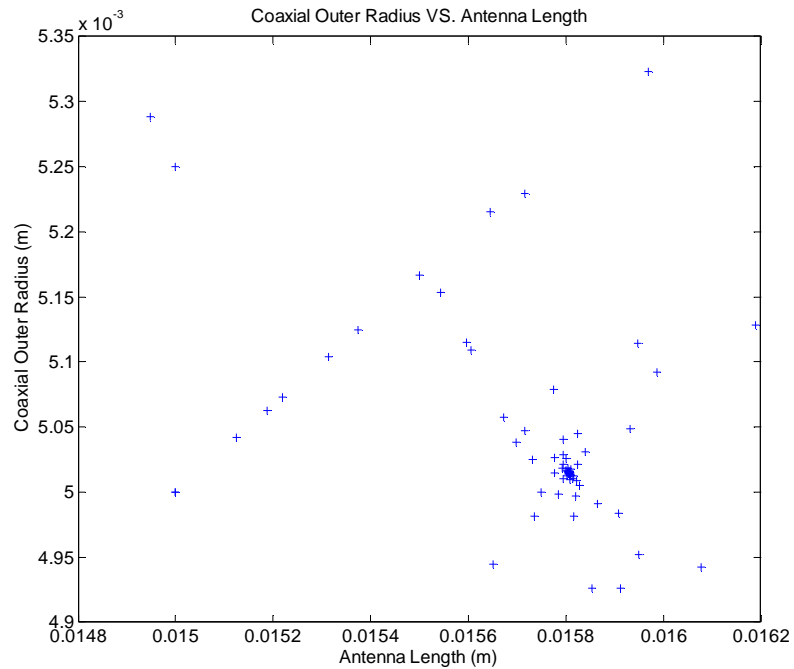
(c) Search trace of searching for resonant frequency with NM search method



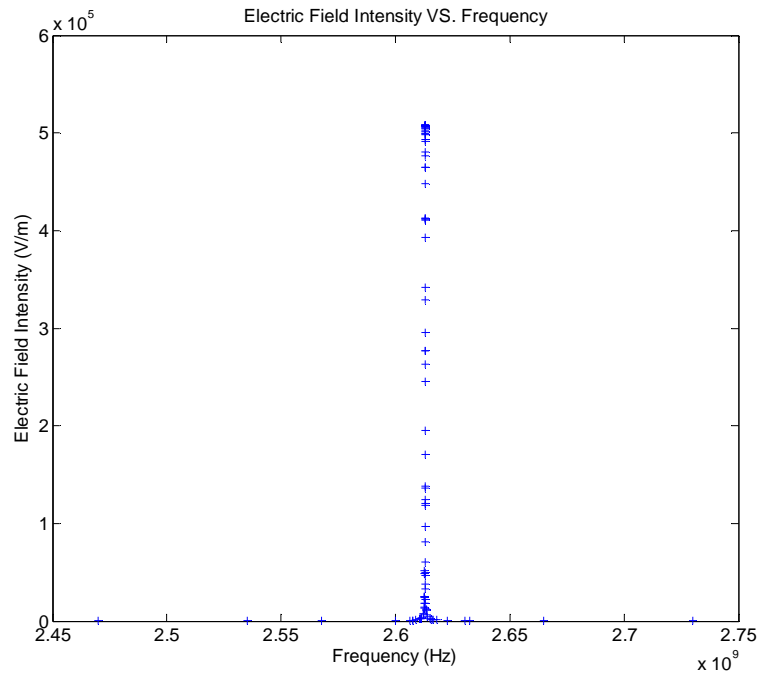
(d) Search trace of search objective: maximum electric field intensity

Figure 5-5 NM search for 3<sup>rd</sup> set of initial values of parameters in Table 5-1

Figure 5-5 shows the NM simplex search process carried out with the 3<sup>rd</sup> set of initial values by connecting each evaluation points. The figures show the parameters and the objective of each step in the search process. Figure 5-5 (a) shows the values of the antenna length used to simulate resonance for each search step during the search process. Figure 5-5 (b) shows the values of the screen of transmission radius used to simulate resonance for each search step during the search process. Figure 5-5 (c) shows the values selected for the resonant frequency to simulate resonance for each search step during the search process. Figure 5-5 (d) shows the progress of the search objective at each step during the search process.



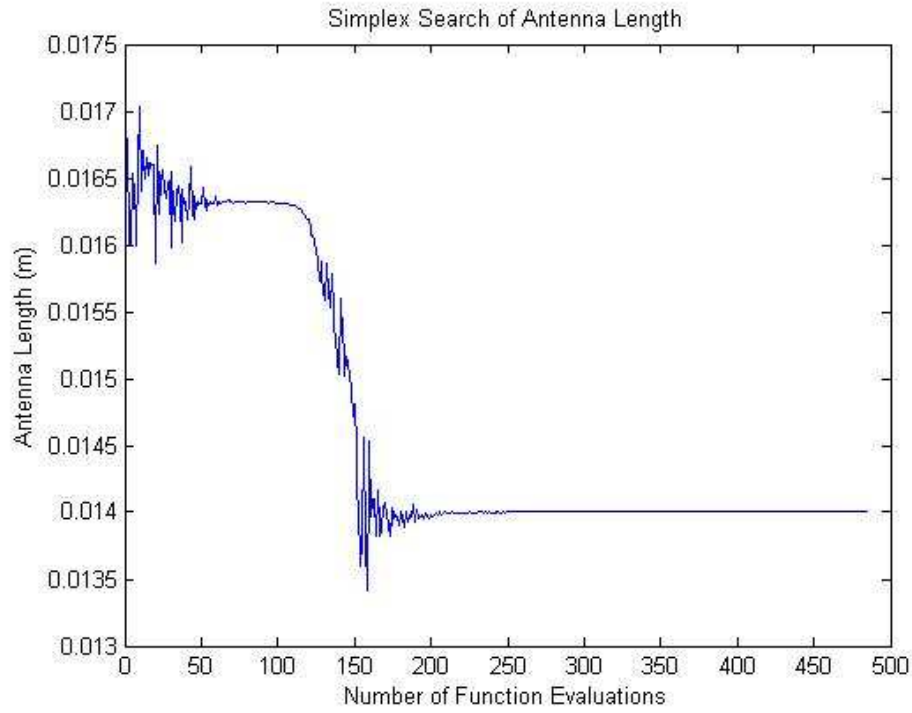
(a) Distribution of search points of antenna length and screen radius



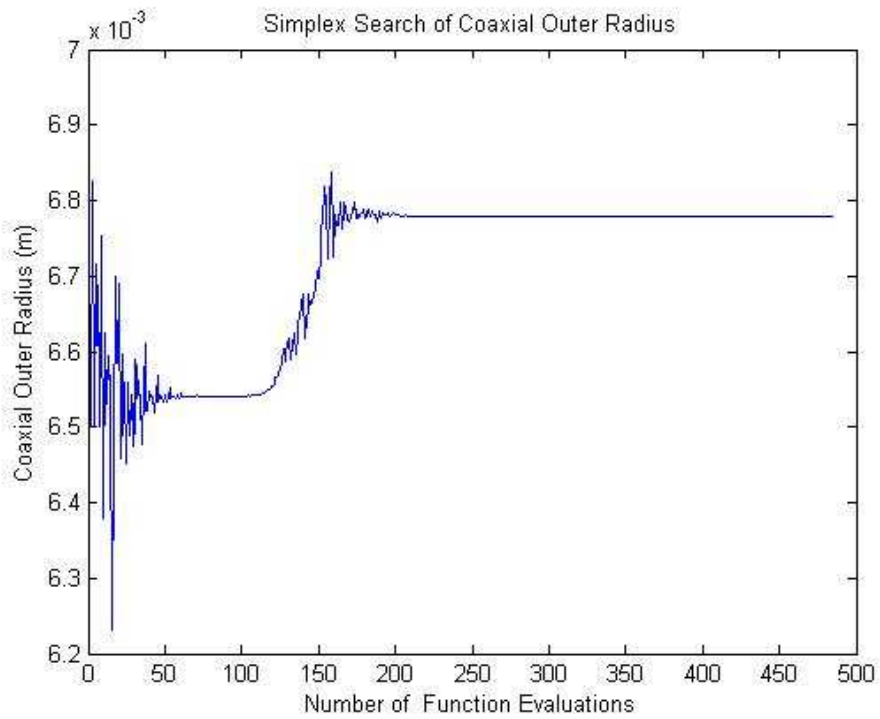
(b) Sensitivity of the resonant frequency

Figure 5-6 Relations between parameters from 3<sup>rd</sup> NM search

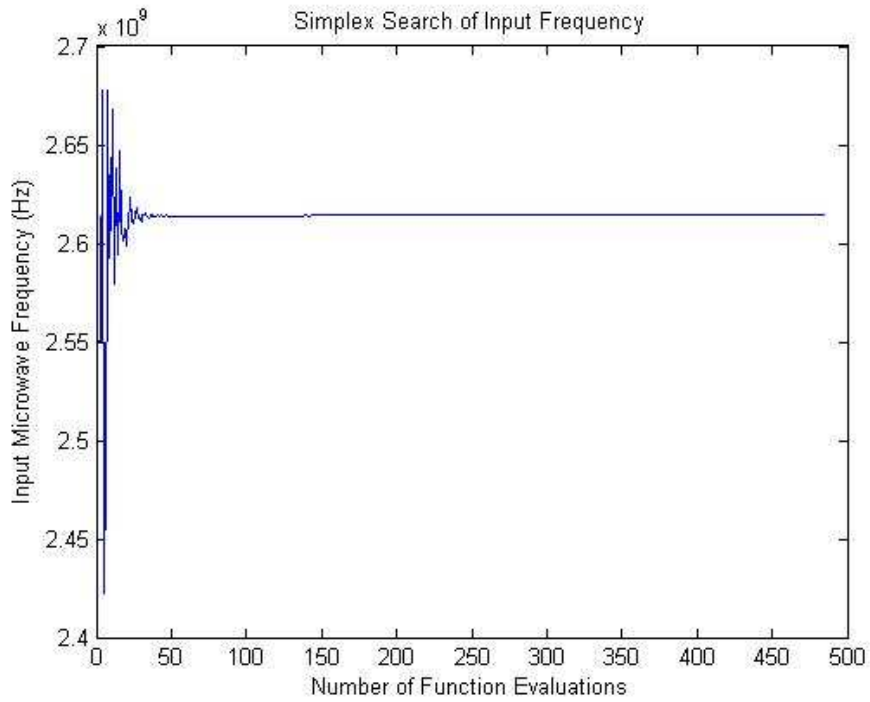
Figure 5-6 shows the relations between parameters and between the objective and parameters in 3<sup>rd</sup> NM search. Figure 5-6 (a) draws all search points of the screen of transmission line radius and antenna length in one figure to show the distribution of both parameters in the search range and the search trace of both parameters during the search. Figure 5-6 (b) draws the search objective, maximum electric field intensity against the search points of frequency to analyse the sensitivity of the frequency to screen of transmission line radius and antenna length and to compare with the results from exhaustive search.



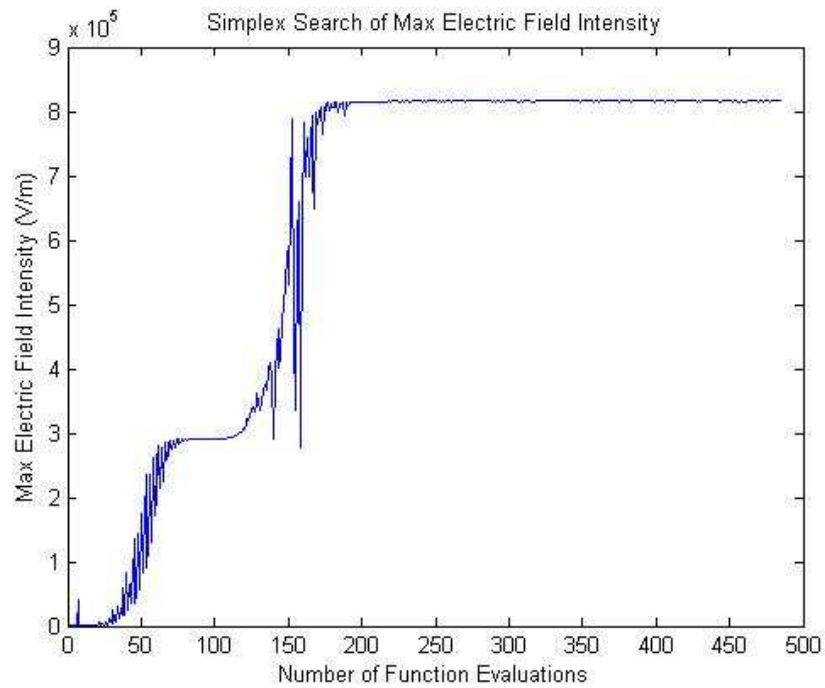
(a) Search trace of searching for antenna length with NM search method



(b) Search trace of searching for screen radius with NM search method



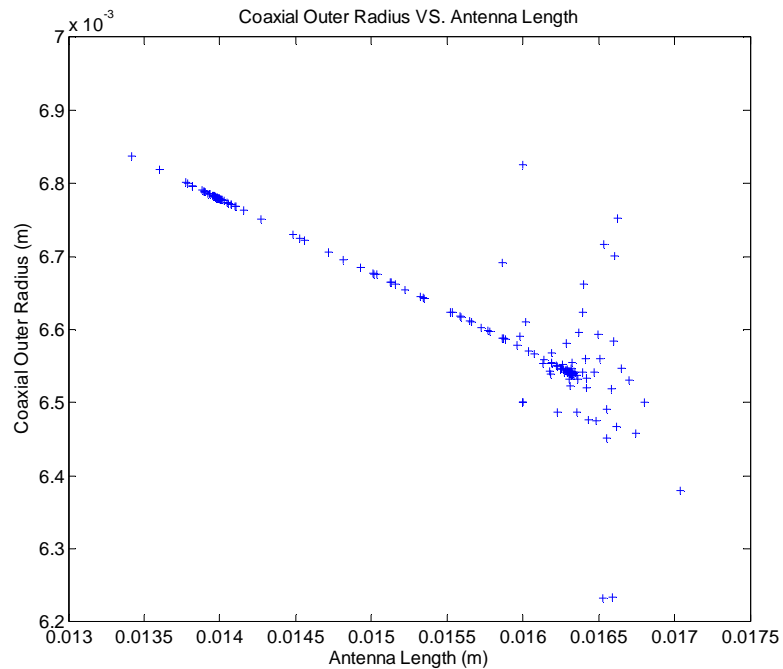
(c) Search trace of searching for resonant frequency with NM search method



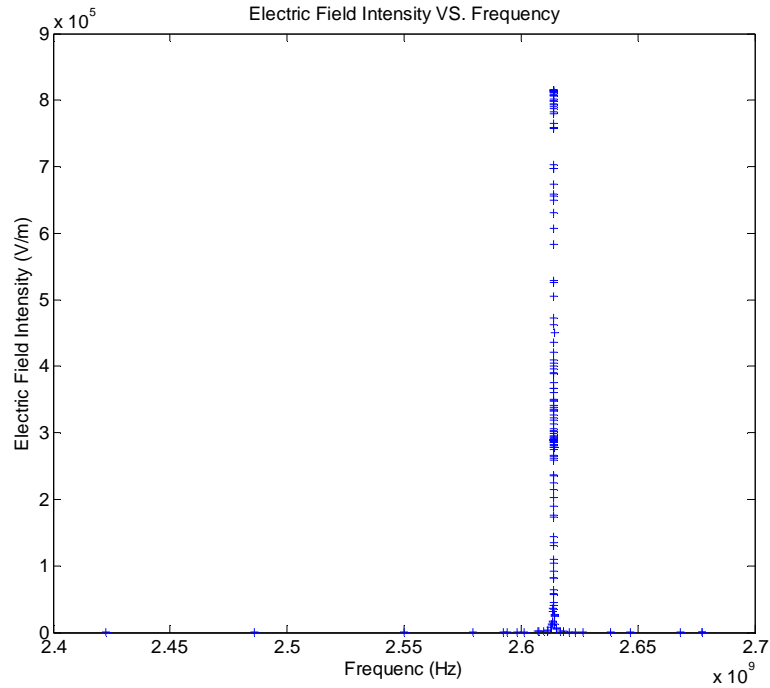
(d) Search trace of search objective: maximum electric field intensity

Figure 5-7 NM search for 4<sup>th</sup> set of initial values of parameters in Table 5-1

Figure 5-7 shows the NM simplex search process carried out with the 4<sup>th</sup> set of initial values by connecting each evaluation points. The figures show the parameters and the objective of each step in the search process. Figure 5-7 (a) shows the values of the antenna length used to simulate resonance for each search step during the search process. Figure 5-7 (b) shows the values of the screen of transmission radius used to simulate resonance for each search step during the search process. Figure 5-7 (c) shows the values selected for the resonant frequency to simulate resonance for each search step during the search process. Figure 5-7 (d) shows the progress of the search objective at each step during the search process.



(a) Distribution of search points of antenna length and screen radius



(b) Sensitivity of the resonant frequency

Figure 5-8 Relations between parameters from 4<sup>th</sup> NM search

Figure 5-8 shows the relations between parameters and between the objective and parameters in 4<sup>th</sup> NM search. Figure 5-8 (a) draws all search points of the screen of transmission line radius and antenna length in one figure to show the distribution of both parameters in the search range and the search trace of both parameters during the search. Figure 5-8 (b) draws the search objective, maximum electric field intensity against the search points of frequency to analyse the sensitivity of the frequency to screen of transmission line radius and antenna length and to compare with the results from exhaustive search.

Although this is a 3d search it is hard to present the results clearly by drawing 3 search parameters together. Furthermore, when search parameters are more than 3 it is impossible to draw all parameters together. For this reason 3 parameters are drawn separately to analyse.

In Figure 5-1, 5-3, 5-5 and 5-7, Figures (a, b, and c) show the values of probe antenna length, screen of transmission line radius, and resonant frequency selected by the NM simplex search tool for each search step respectively and Figures (d) of Figure 5-1, 5-3, 5-5 and 5-7 show the search progress for the search objective, maximum electric field intensity at each step. In these figures, the way of NM search method approaching the optimal results is presented. From Figures (a, b, c, and d) in Figure 5-1, 5-3, 5-5, and 5-7, it can be found that the best value of resonant frequency is always found in early search stage. This indicates the resonant frequency is sensitive to the coupling antenna length and screen radius. For the fixed probe antenna length and screen radius, a small change of the resonant frequency in the search process could affect the electric field intensity significantly. From these figures it can also be found that both the probe antenna length and the screen of transmission radius do not affect the maximum electric field intensity in the cylinder as much as the resonant frequency within their search range. However with the proper design of the probe antenna length and screen transmission line radius the electric field intensity can be improved due to more efficient coupling and less reflection.

In Figure 5-2, 5-4, 5-6, and 5-8, Figures (a) show us the distribution of all search points of the coupling antenna length and the screen of transmission line radius within the search range. From these Figures (a) of Figure 5-2, 5-4, 5-6 and 5-8 it can be seen where the best antenna length and screen radius are located by comparing them to Figures (a) and (b) of Figure 5-1, 5-3, 5-5, and 5-7. For instance, from the last NM simplex search it can be seen the coupling antenna and screen radius are located between 0.0135 m to 0.0145 m and between 0.0067 m and 0.0069 m respectively. Therefore these Figures (a), (b) in Figure 5-1, 5-3, 5-5, and 5-7 and Figures (a) in Figure 5-2, 5-4, 5-6, and 5-8 can help researchers to identify a specific search range for further investigation and to avoid spending time on investigating unimportant area. Figures (b) in Figures 5-2, 5-4, 5-6, and 5-8 confirm the resonant frequency is sensitive to probe antenna length and screen radius. By comparing Figures (b) of Figure 5-2, 5-4, 5-6, and 5-8 with Figure 4-26 it can be found that the results of NM simplex search agree with the results of exhaustive search while it consumes much less time.

The search results are summarised in Table 5-2.

Table 5-2 Search results of NM searches

	Antenna Length (m)	Screen Radius (m)	Frequency (GHz)	Elec. Field Strength (V/m)
1	0.0187	0.005	2.62	$1.48 \times 10^5$
2	0.0154	0.0057	2.62	$5.1 \times 10^5$
3	0.0158	0.005	2.63	$5.1 \times 10^5$
4	0.0141	0.0068	2.62	$8.1 \times 10^5$

From Table 5-2 it can be found that when the dimensions of the antenna and transmission line change in search range the resonant frequency varies from 2.62 GHz to 2.63 GHz. The data in Table 5-2 show the frequency ranges from 2.62 GHz to 2.63 GHz when the probe antenna length and screen of transmission line radius vary from 0.0141 m to 0.0187 m and from 0.005 m to 0.0068 m respectively. The maximum electric field intensity in the cylinder can always reach  $1 \times 10^5$  V/m regardless the change of the probe antenna length and screen of transmission line radius.

### 5.1.2 Search Using the EA Method

Similar searches are carried out using the EA method in this section. The EA is a powerful search algorithm and it has its advantage on global search and multi-objectives search.

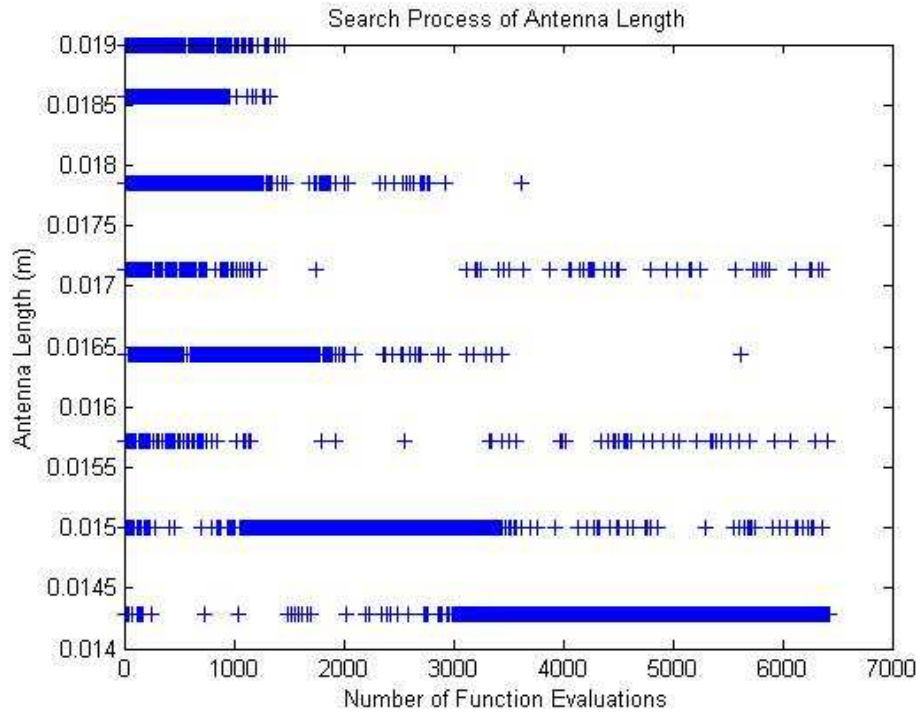
Several EA searches are carried out for investigation of the performance of the EA method and collecting sufficient data for analysis in this section based on 4 sets of EA parameters.

Table 5-3 lists four sets of EA parameters used to carry out the EA searches in this section.

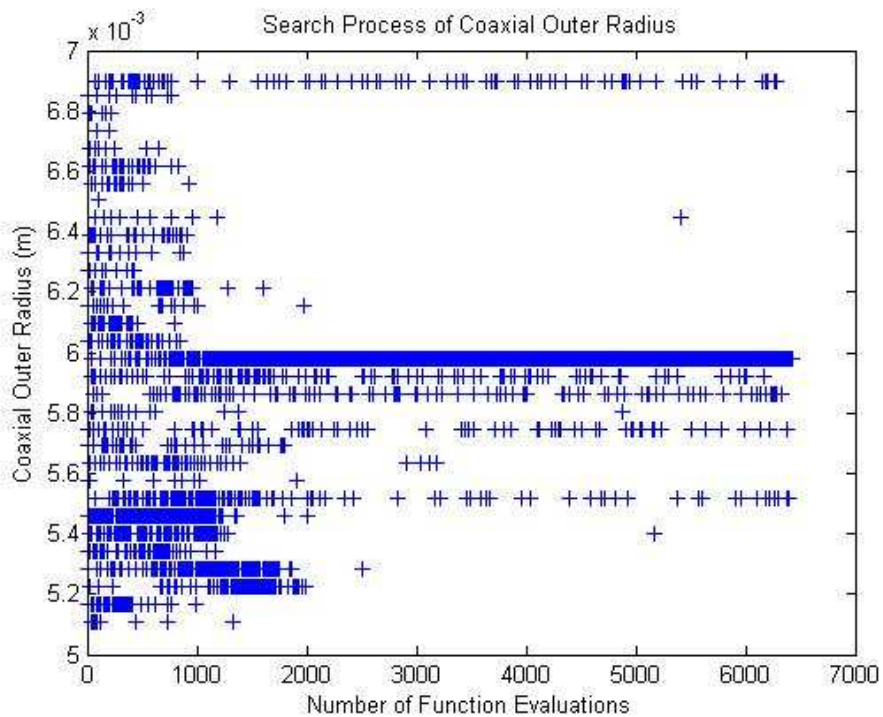
Table 5-3 The EA parameter settings

	Population	Crossover Rate	Mutation Rate	Generations
1	101	50	0.02	100
2	101	50	0.01	80
3	101	70	0.02	80
4	101	70	0.01	80

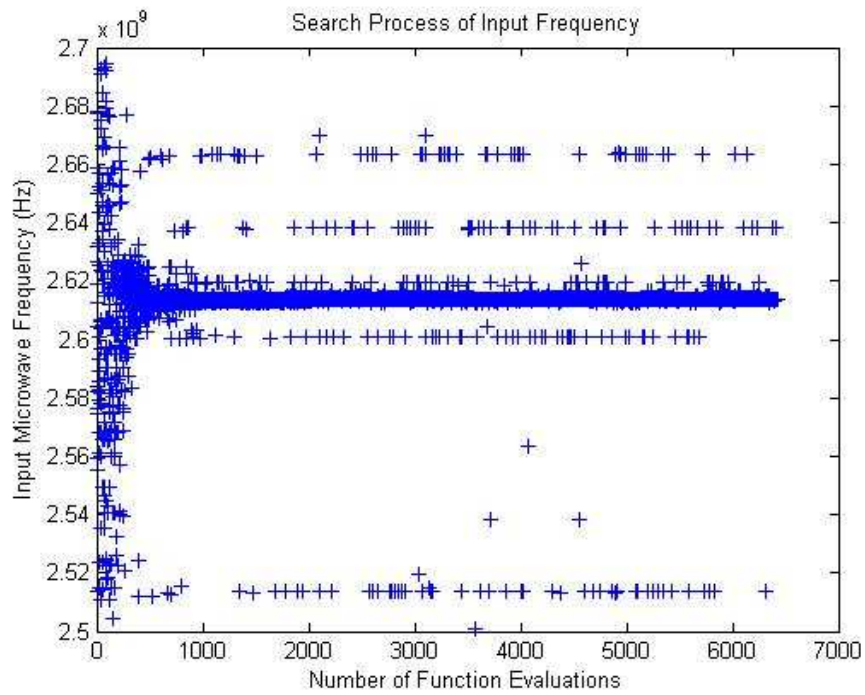
For EA searches, the initial values for search parameters are not needed to be preset. Search program generates a population for each parameter that EA searches for. According to exhaustive search in Chapter 4 and practical conditions the antenna length should not exceed depth of cylinder head and not be 10 mm shorter than the end of the transmission line. The search range of resonant frequency is set between 2.6GHz and 2.8GHz. The EA searches are carried out under these constraints. The search processes and results of the EA search are shown in Figure 5-9 – 5-16.



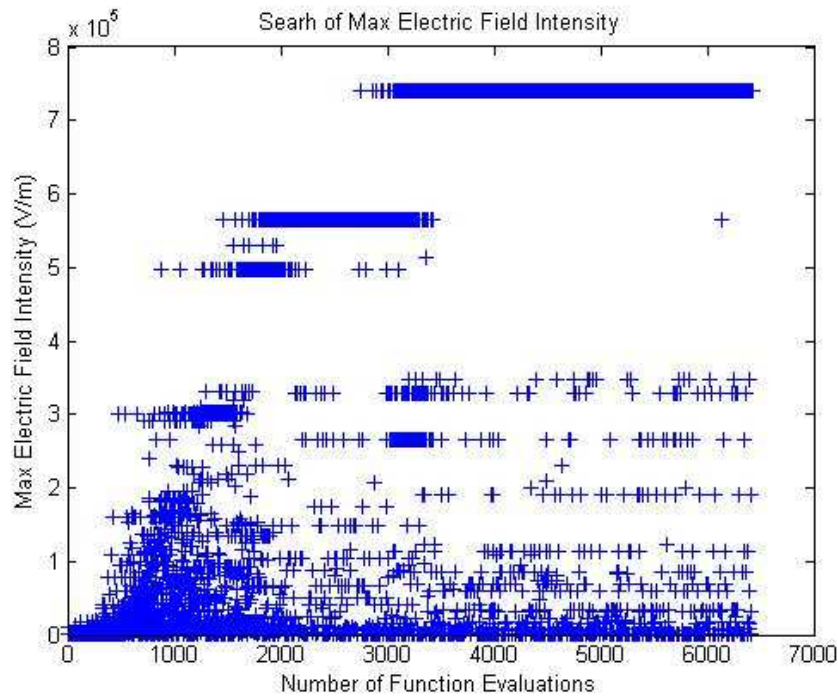
(a) Search trace of searching for antenna length with EA search method



(b) Search trace of searching for screen radius with EA search method



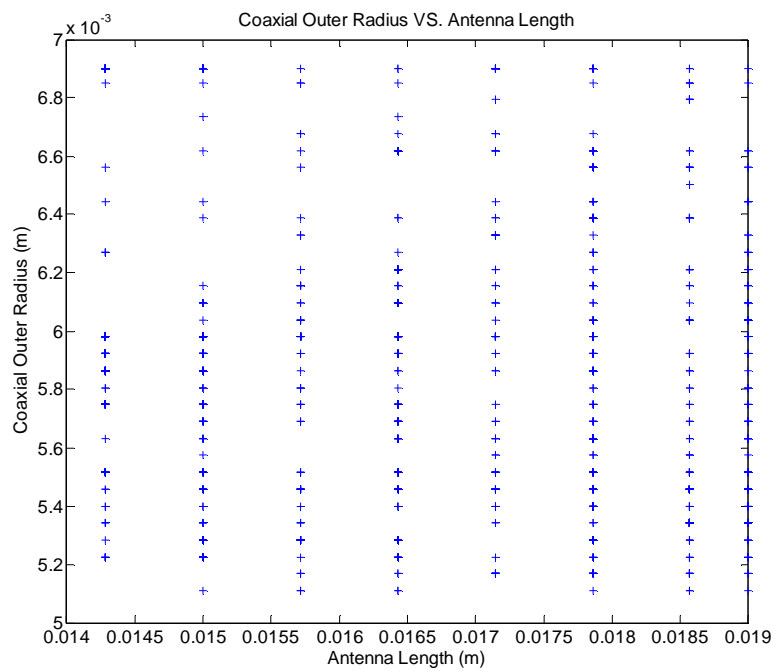
(c) Search trace of searching for resonant frequency with EA search method



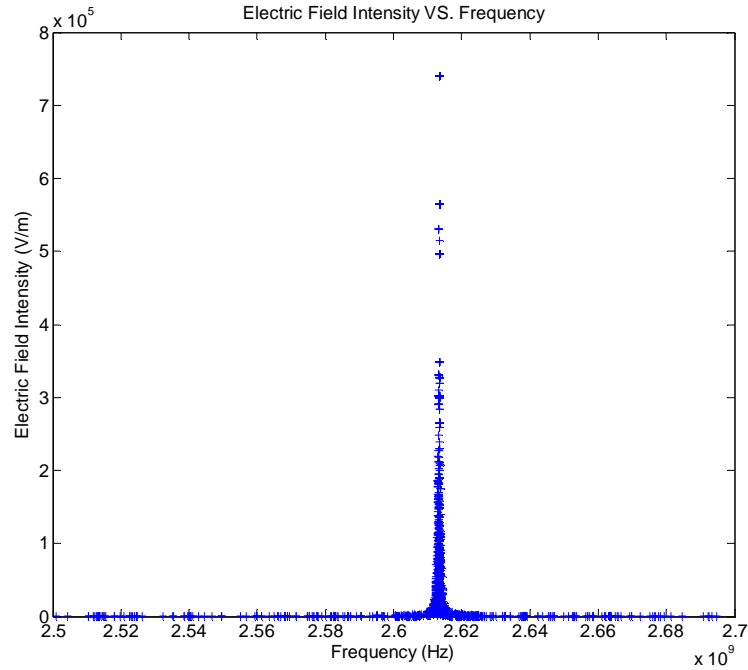
(d) Search trace of search objective: maximum electric field intensity

Figure 5-9 EA search for 1<sup>st</sup> set of EA parameters in Table 5-3

Figure 5-9 shows the EA search process carried out with the 1<sup>st</sup> set of EA parameters by showing all the points of each search step throughout the whole search process. Figure 5-9 (a) shows the values of the antenna length used to simulate resonance for each search step during the search process. Figure 5-9 (b) shows the values of the screen of transmission radius used to simulate resonance for each search step during the search process. Figure 5-9 (c) shows the values selected for the resonant frequency to simulate resonance for each search step during the search process. Figure 5-9 (d) shows the progress of the search objective at each step during the search process.



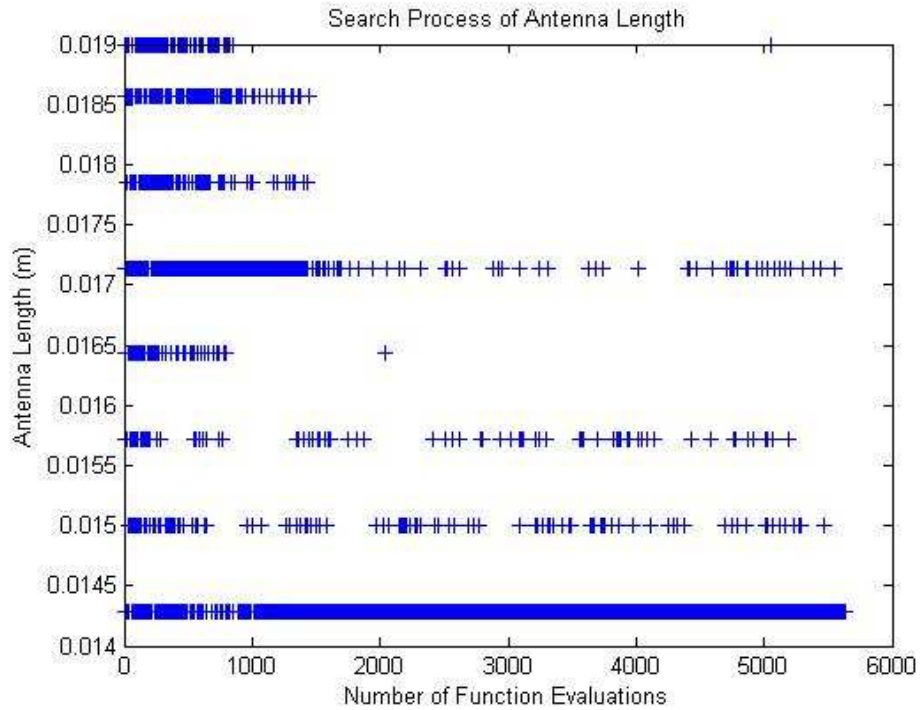
(a) Distribution of search points of antenna length and screen radius



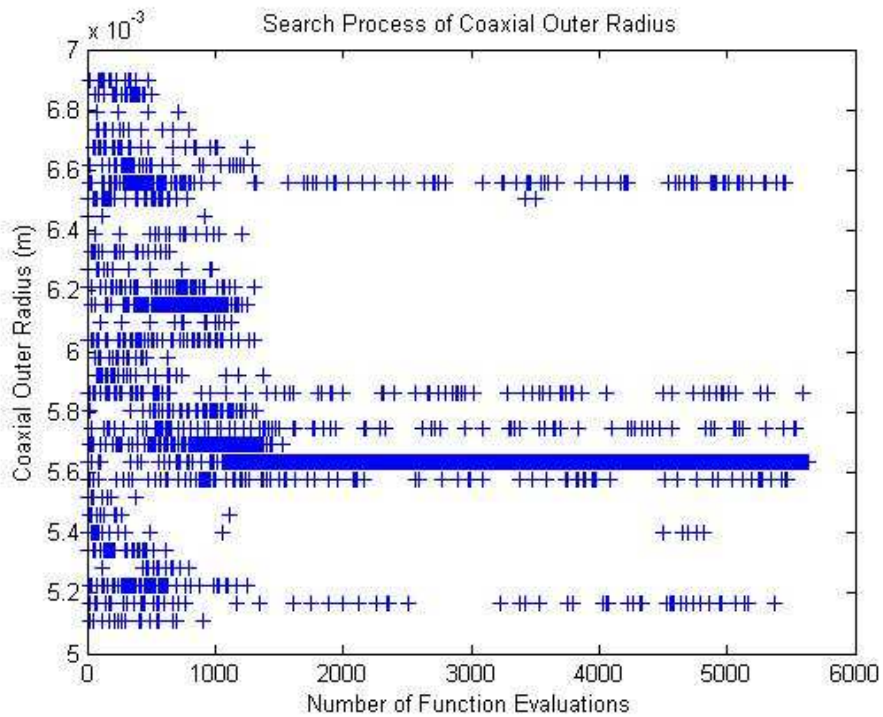
(b) Sensitivity of the resonant frequency

Figure 5-10 Relations between parameters from 1<sup>st</sup> EA search

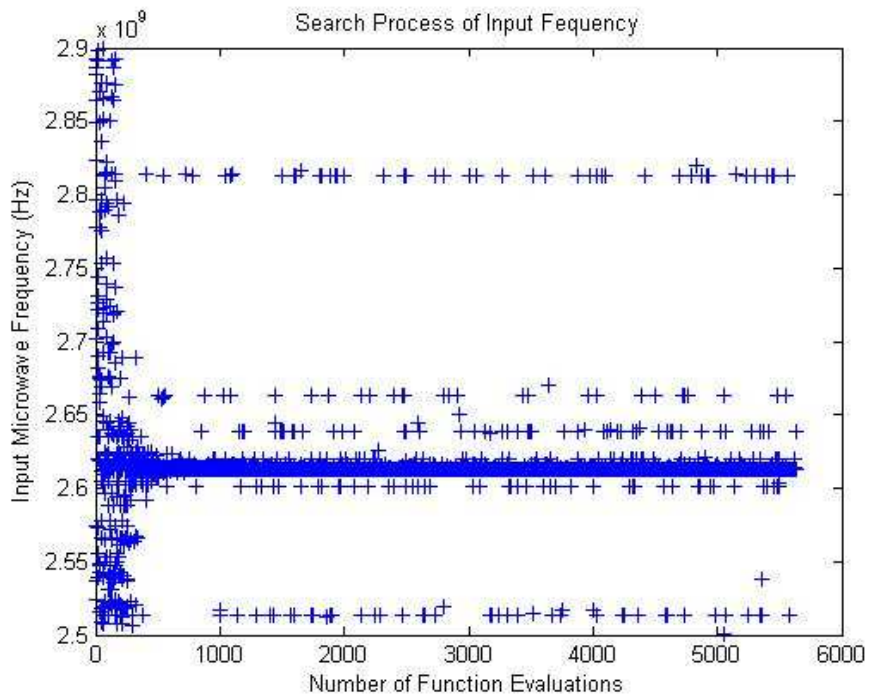
Figure 5-10 shows the relations between parameters and between the objective and parameters in 1<sup>st</sup> EA search. Figure 5-10 (a) draws all search points of the screen of transmission line radius and antenna length in one figure to show the distribution of both parameters in the search range and the search trace of both parameters during the search. Figure 5-10 (b) draws the search objective, maximum electric field intensity against the search points of frequency to analyse the sensitivity of the frequency to screen of transmission line radius and antenna length and to compare with the results from exhaustive search.



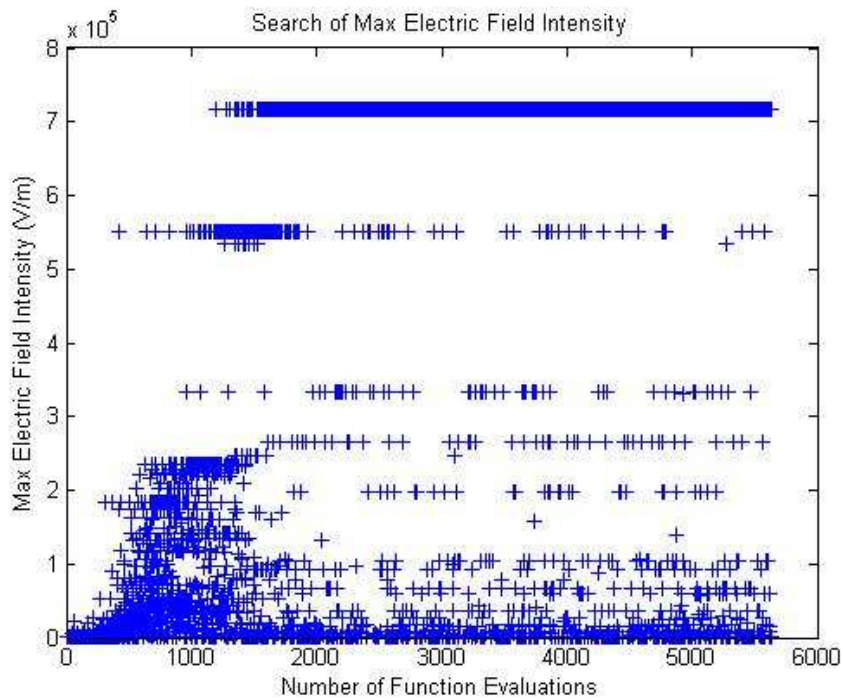
(a) Search trace of searching for antenna length with EA search method



(b) Search trace of searching for screen radius with EA search method



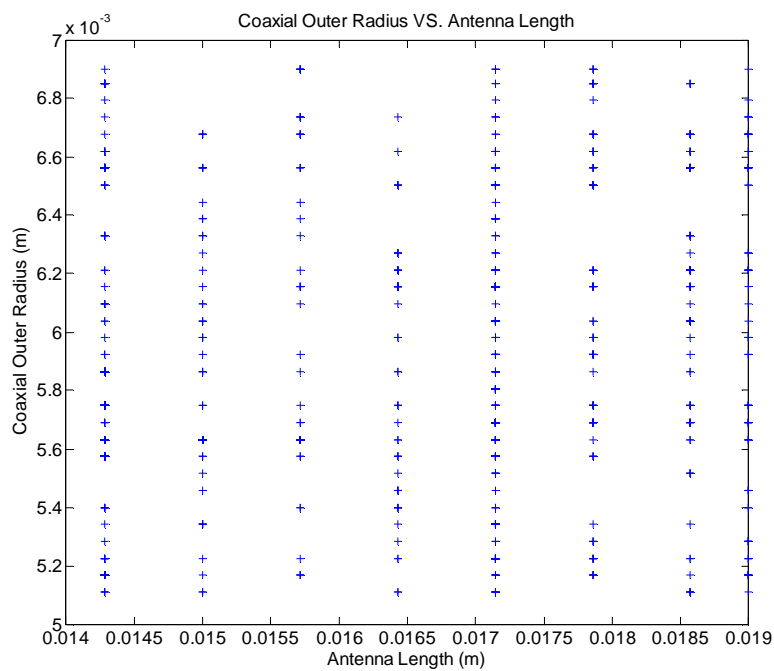
(c) Search trace of searching for resonant frequency with EA search method



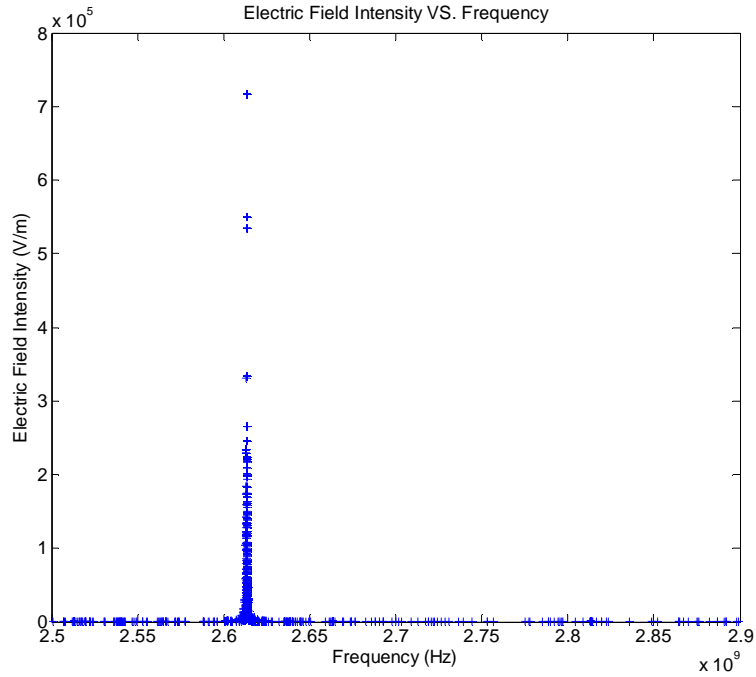
(d) Search trace of search objective: maximum electric field intensity

Figure 5-11 EA search for 2<sup>nd</sup> set of EA parameters in Table 5-3

Figure 5-11 shows the EA search process carried out with the 2<sup>nd</sup> set of EA parameters by showing all the points of each search step throughout the whole search process. Figure 5-11 (a) shows the values of the antenna length used to simulate resonance for each search step during the search process. Figure 5-11 (b) shows the values of the screen of transmission radius used to simulate resonance for each search step during the search process. Figure 5-11 (c) shows the values selected for the resonant frequency to simulate resonance for each search step during the search process. Figure 5-11 (d) shows the progress of the search objective at each step during the search process.



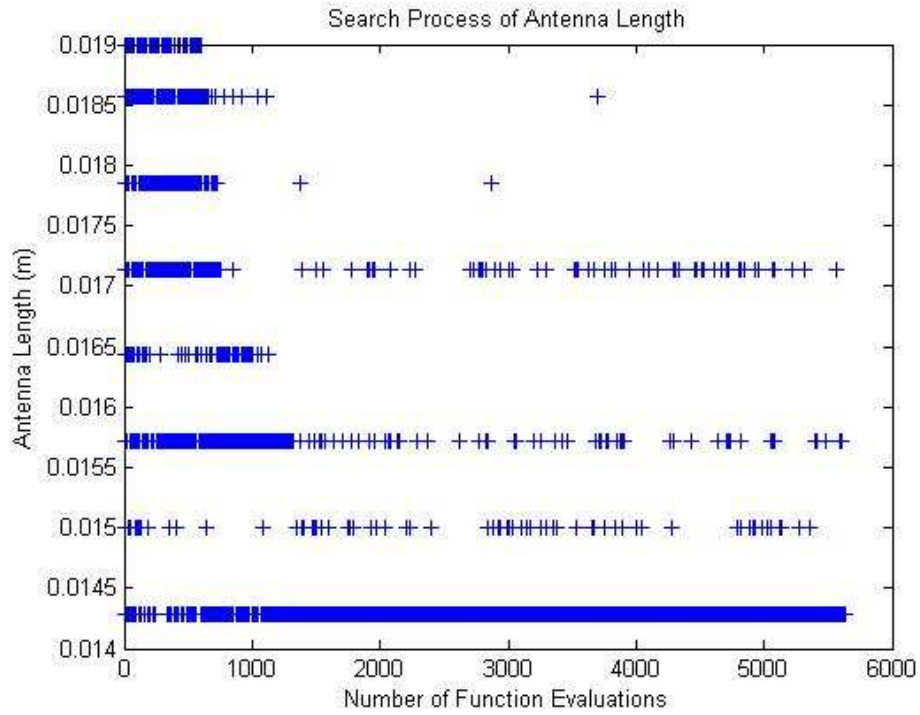
(a) Distribution of search points of antenna length and screen radius



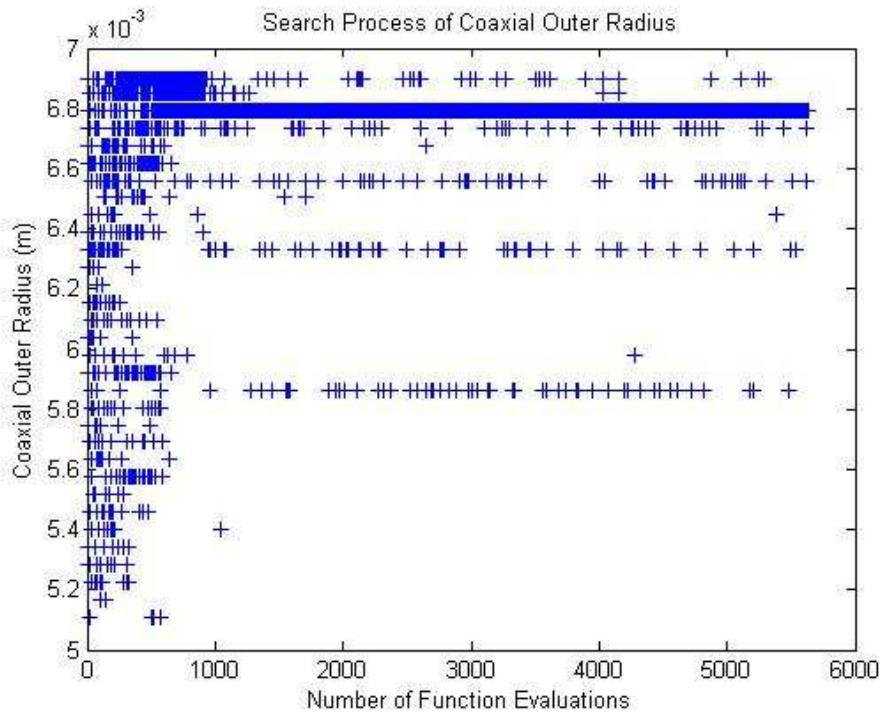
(b) Sensitivity of the resonant frequency

Figure 5-12 Relations between parameters from 2<sup>nd</sup> EA search

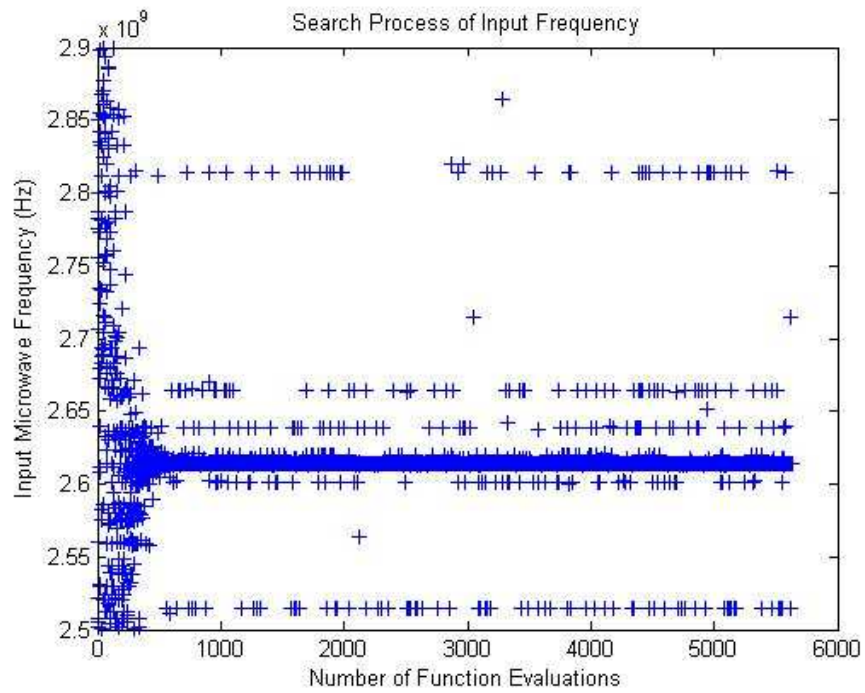
Figure 5-12 shows the relations between parameters and between the objective and parameters in 2<sup>nd</sup> EA search. Figure 5-12 (a) draws all search points of the screen of transmission line radius and antenna length in one figure to show the distribution of both parameters in the search range and the search trace of both parameters during the search. Figure 5-12 (b) draws the search objective, maximum electric field intensity against the search points of frequency to analyse the sensitivity of the frequency to screen of transmission line radius and antenna length and to compare with the results from exhaustive search.



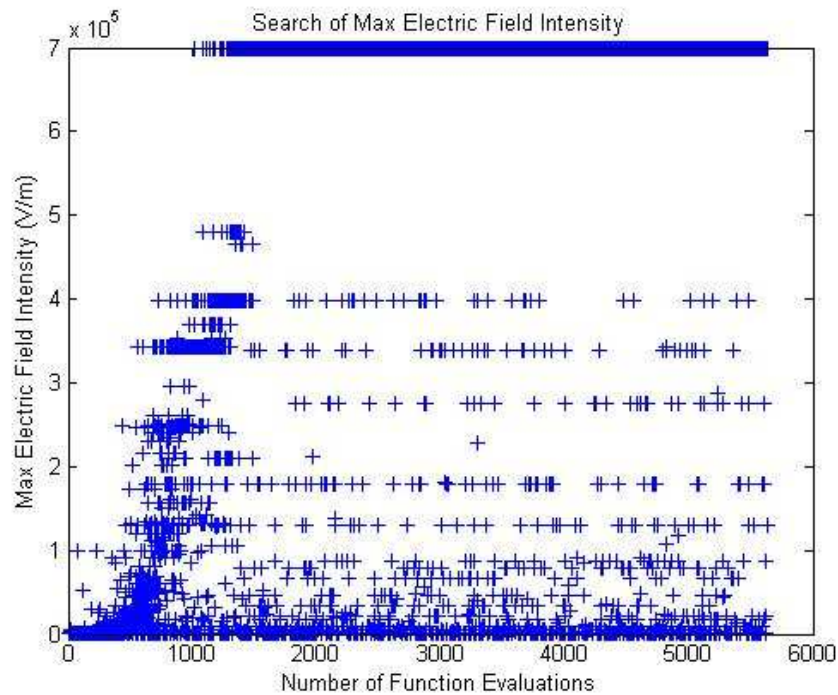
(a) Search trace of searching for antenna length with EA search method



(b) Search trace of searching for screen radius with EA search method



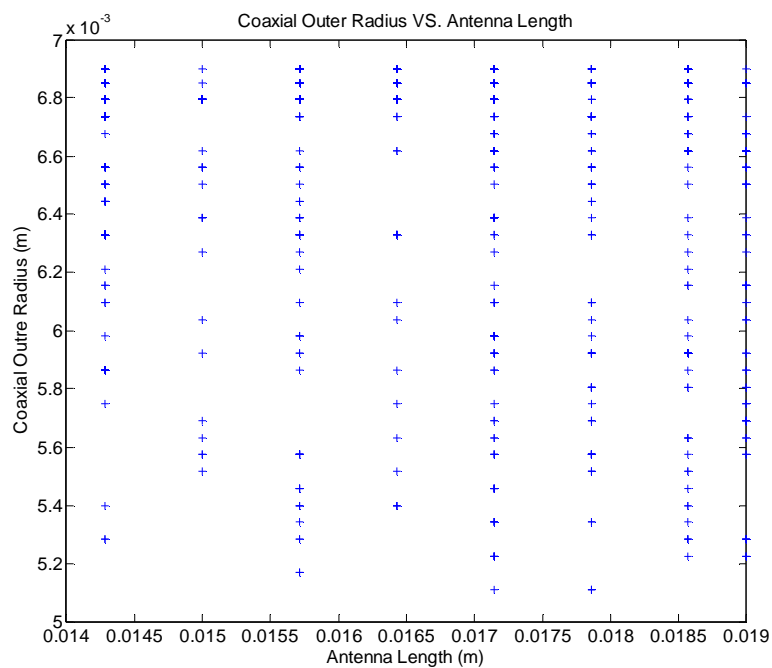
(c) Search trace of searching for resonant frequency with EA search method



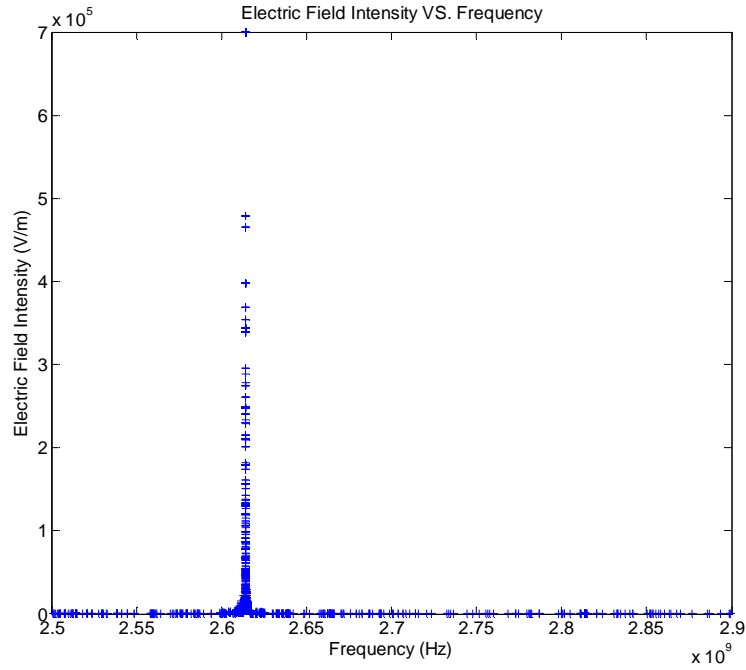
(d) Search trace of search objective: maximum electric field intensity

Figure 5-13 EA search for 3<sup>rd</sup> set of EA parameters in Table 5-3

Figure 5-13 shows the EA search process carried out with the 3<sup>rd</sup> set of EA parameters by showing all the points of each search step throughout the whole search process. Figure 5-13 (a) shows the values of the antenna length used to simulate resonance for each search step during the search process. Figure 5-13 (b) shows the values of the screen of transmission radius used to simulate resonance for each search step during the search process. Figure 5-13 (c) shows the values selected for the resonant frequency to simulate resonance for each search step during the search process. Figure 5-13 (d) shows the progress of the search objective at each step during the search process.



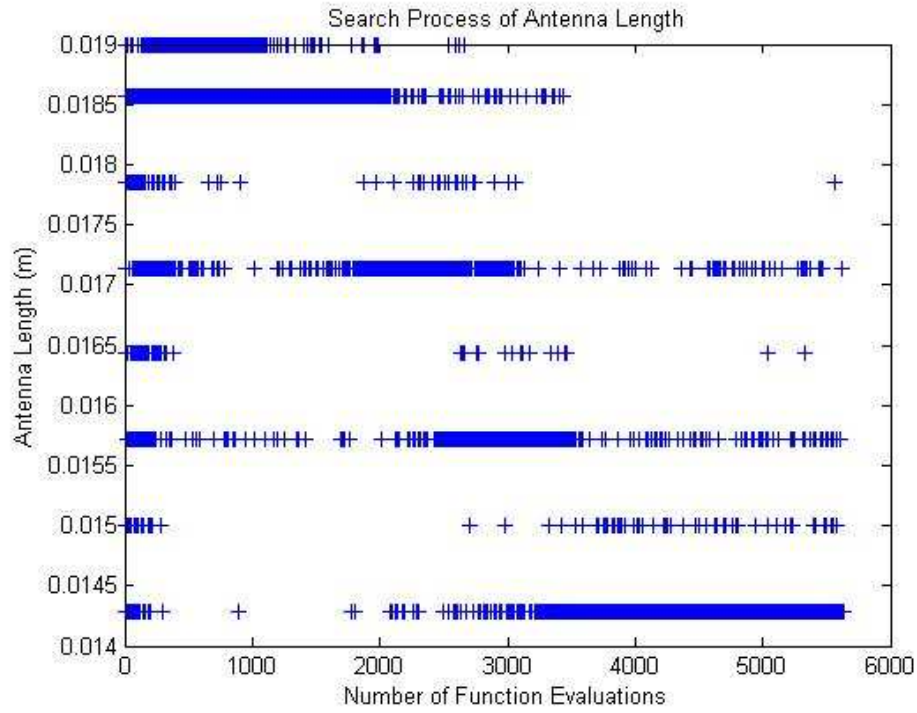
(a) Distribution of search points of antenna length and screen radius



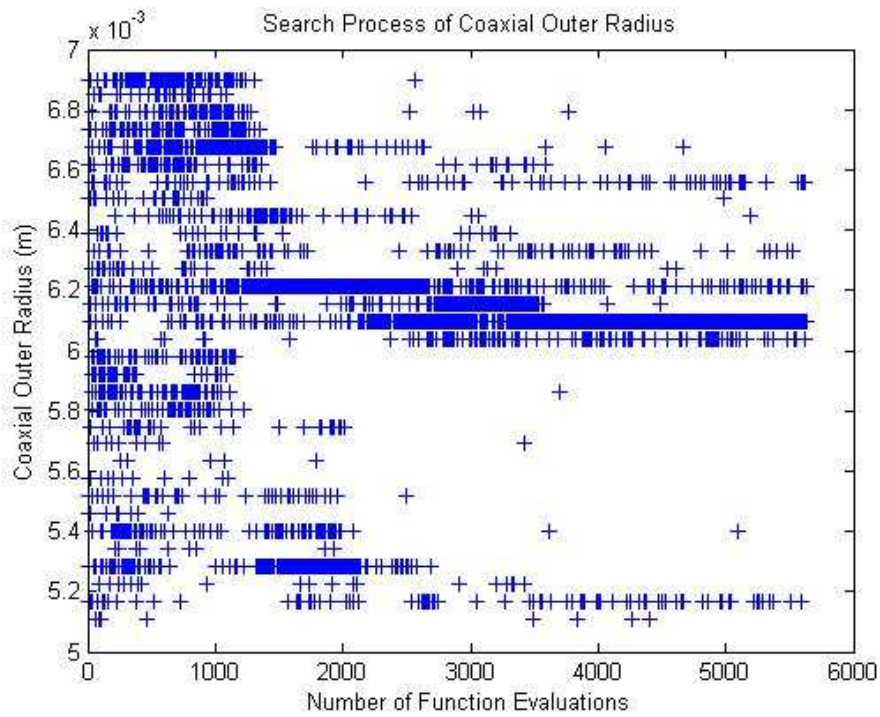
(b) Sensitivity of the resonant frequency

Figure 5-14 Relations between parameters from 3<sup>rd</sup> EA search

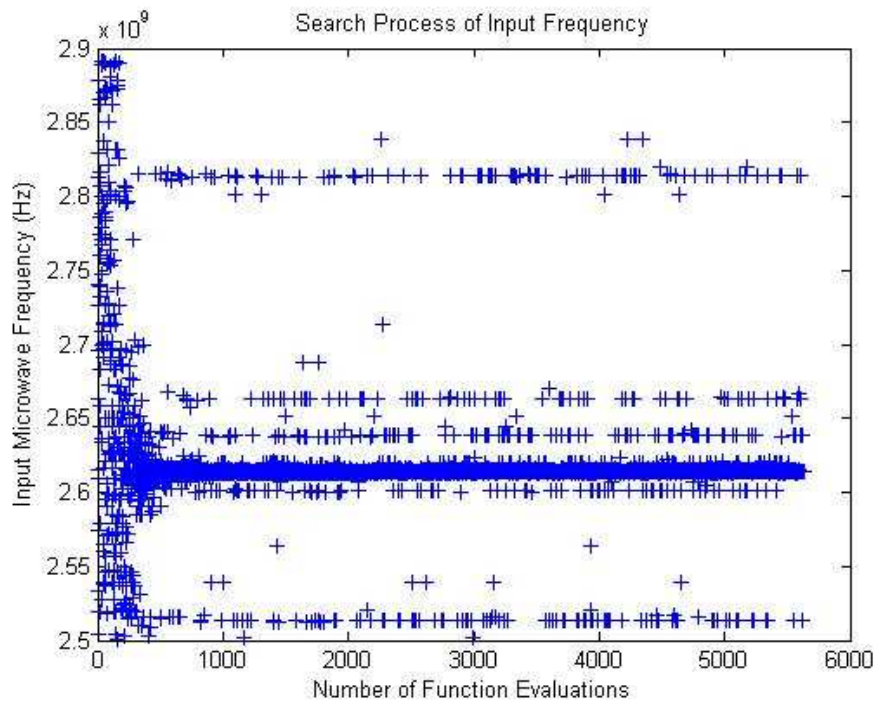
Figure 5-14 shows the relations between parameters and between the objective and parameters in 3<sup>rd</sup> EA search. Figure 5-14 (a) draws all search points of the screen of transmission line radius and antenna length in one figure to show the distribution of both parameters in the search range and the search trace of both parameters during the search. Figure 5-14 (b) draws the search objective, maximum electric field intensity against the search points of frequency to analyse the sensitivity of the frequency to screen of transmission line radius and antenna length and to compare with the results from exhaustive search.



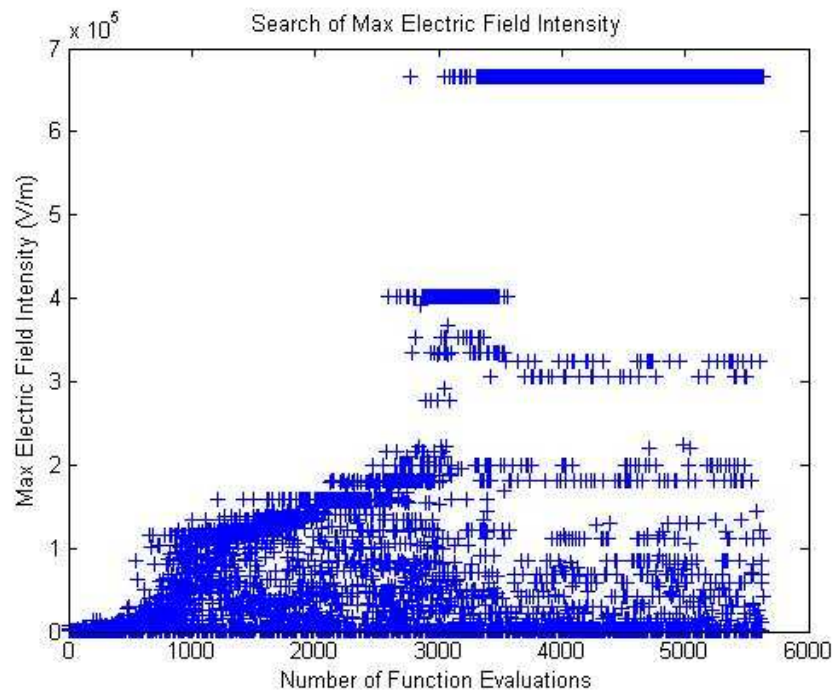
(a) Search trace of searching for antenna length with EA search method



(b) Search trace of searching for screen radius with EA search method



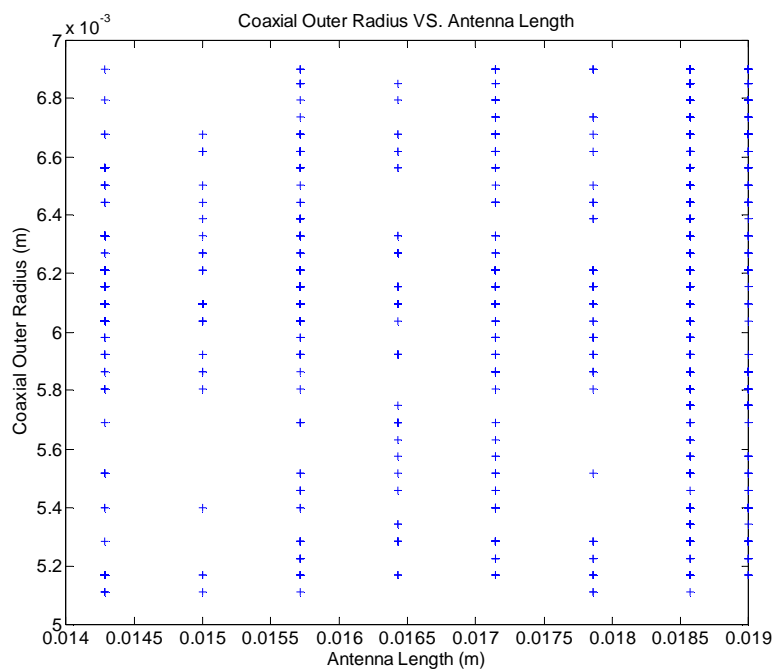
(c) Search trace of searching for resonant frequency with EA search method



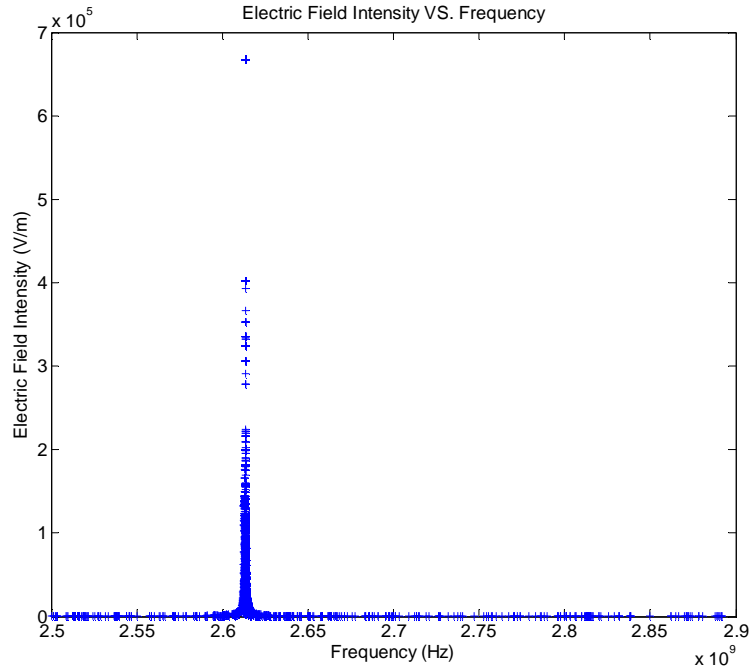
(d) Search objective: maximum electric field intensity

Figure 5-15 EA search for 4<sup>th</sup> set of EA parameters in Table 5-3

Figure 5-15 shows the EA search process carried out with the 4<sup>th</sup> set of EA parameters by showing all the points of each search step throughout the whole search process. Figure 5-15 (a) shows the values of the antenna length used to simulate resonance for each search step during the search process. Figure 5-15 (b) shows the values of the screen of transmission radius used to simulate resonance for each search step during the search process. Figure 5-15 (c) shows the values selected for the resonant frequency to simulate resonance for each search step during the search process. Figure 5-15 (d) shows the progress of the search objective at each step during the search process.



(a) Distribution of search points of antenna length and screen radius



(b) Sensitivity of the resonant frequency

Figure 5-16 Relations between parameters from 4<sup>th</sup> EA search

Figure 5-16 shows the relations between parameters and between the objective and parameters in 4<sup>th</sup> EA search. Figure 5-16 (a) draws all search points of the screen of transmission line radius and antenna length in one figure to show the distribution of both parameters in the search range and the search trace of both parameters during the search. Figure 5-16 (b) draws the search objective, maximum electric field intensity against the search points of frequency to analyse the sensitivity of the frequency to screen of transmission line radius and antenna length and to compare with the results from exhaustive search.

In these figures, the way of EA search method approaching the optimal results is presented. Unlike the NM simplex search method the EA search method keeps generating new search points for the population while the best values of each search parameters remains in the population. Therefore, in Figure (a, b, c, and d) of Figures 5-9, 5-11, 5-13, and 5-15, there is always more than one search point for each parameter at each search

step. However it can be seen through these figures the density of the points and the generation numbers indicate the location of the best value for each parameter found in the search processes.

From Figures (a, b, c, and d) in Figure 5-9, 5-11, 5-13, and 5-15, it can be seen that the best value of frequency is found in the early search stage, which is similar to the NM simplex search. This implies the frequency is sensitive to the rest parameters. From these figures it can be found that the best value of the coupling antenna length is always found at the same location, which is 0.0143 m. This implies the reliability of the EA search method. It also shows the possible best solution for the probe antenna length is 0.0143 m or around it. It also can be found from Figures (a and d) in Figure 5-9, 5-11, 5-13, and 5-15 that the coupling antenna length affects electric field the most amongst 3 parameters. The screen of transmission line radius does not affect electric field intensity as much as the coupling antenna length does. Therefore, the design of the proper coupling antenna length for the antenna could effectively increase the coupling efficiency and reduce the reflection. Figures (a) of Figure 5-10, 5-12, 5-14, and 5-16 show the distribution of the antenna length and the screen of transmission line radius in search range. In these figures, the search points of the antenna length and the screen of transmission line radius distribute all over the search range. This indicates that the EA search as a global search method searches different points through out the search range to find all possible peaks within search range while the NM search method only attempts limited amount of points within the search range. Figures (b) of Figure 5-10, 5-12, 5-14, and 5-16 show the sensitivity of the frequency. These figures indicate the frequency bandwidth of resonance is very narrow. Compare these figures with Figure 4-26, it can be seen that the EA search leads the similar results to the exhaustive search. This validates the reliability of the results from the EA search.

The search results of these four EA searches are summarised in Table 5-4.

Table 5-4 Search results of EA searches

	Antenna Length (m)	Screen Radius (m)	Resonant frequency (GHz)	Elec. Field Intensity (V/m)
1	0.0143	0.00586	2.62	$7.4 \times 10^5$
2	0.0143	0.00562	2.62	$7.1 \times 10^5$
3	0.0143	0.0068	2.63	$7 \times 10^5$
4	0.0143	0.0061	2.62	$6.8 \times 10^5$

Table 5-4 shows the search consistency of EA search method. It can be seen from Table 5-4 that all final magnitudes of maximum electric field intensity reach around  $7 \times 10^5$  V/m in those four EA searches. Obviously all results are stronger than the minimum requirement of the objective.

From this table it can also be seen that the resonant frequency varies from 2.62 GHz to 2.63 GHz, which agrees with the results of NM simplex search. The best values of the coupling antenna length found in four searches are all 0.0143 m, which implies that the EA search method is more reliable than NM simplex search method in this task. This also indicates the best solution for the coupling antenna length of this particular cylinder that is 14.3 mm, which agrees the results from the exhaustive search in chapter 4. The EA search found 4 different values for the screen transmission line radius, which varies from 0.0058 m to 0.0068 m. The electric field intensities from 4 searches are around  $7 \times 10^5$  V/m. This shows the screen of transmission line radius does not affect the electric field

intensity as much as the antenna length does, which implies that the screen transmission line radius does not affect the coupling efficiency significantly in its search range and it gives engineers more freedom to design the antenna while it can be adjusted to reduce the reflection.

## 5.2 Search of Relative Permittivity of the Air-Fuel Mixture

The AFR changes when an engine is running. It affects relative permittivity and consequently affects the  $Q$  factor and the natural frequency of a cylinder. In this section the relative permittivity as a search parameter is added. There are hence four parameters are searched at the same time, which is a 4d search.

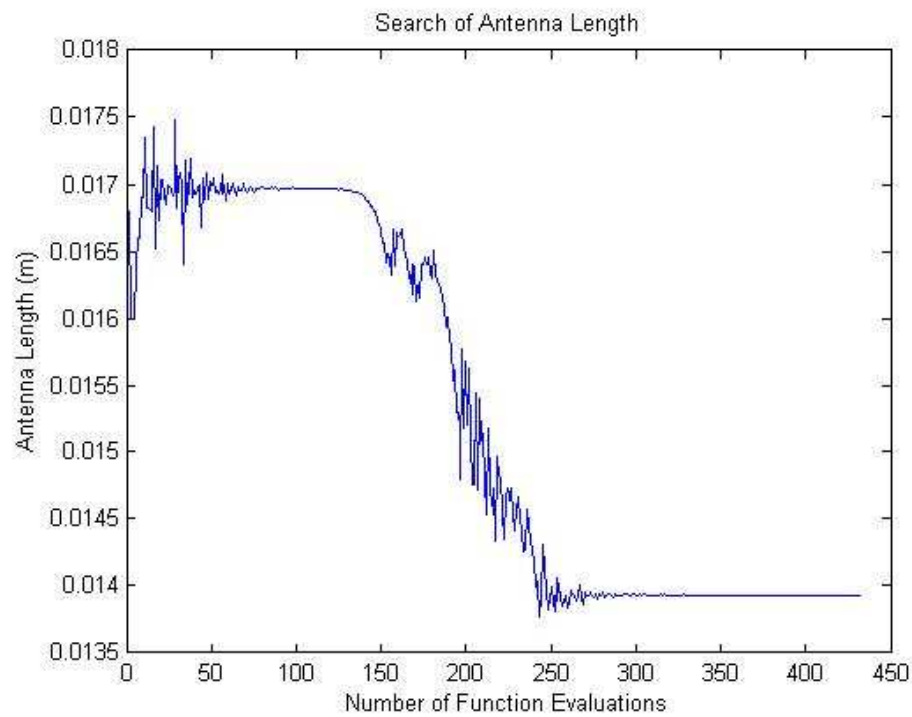
### 5.2.1 Search Using the NM Simplex method

Similar to the NM simplex search in 5.1, four sets of initial values of each parameter are preset in Table 5-5 with the consideration of practical constraints.

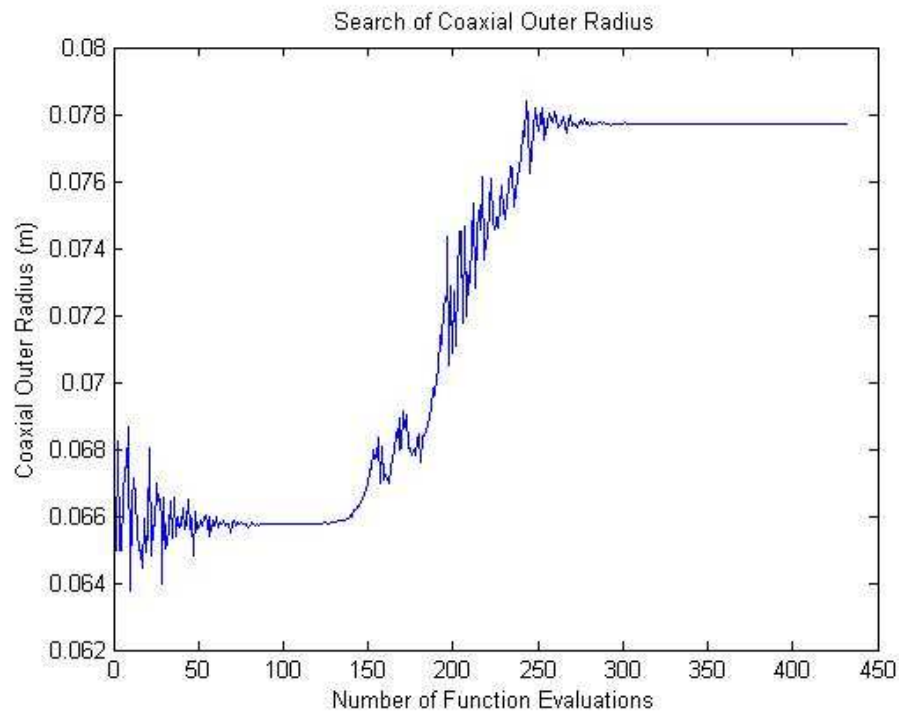
Table 5-5 Initial values of search parameters for NM search

	Antenna Length (mm)	Screen Radius (mm)	Resonant frequency (GHz)	Relative Permittivity
1	16	6.5	2.55	1.05
2	14.5	5.5	2.6	1.02
3	18	6	2.5	1.05
4	15	6.5	2.7	1.035

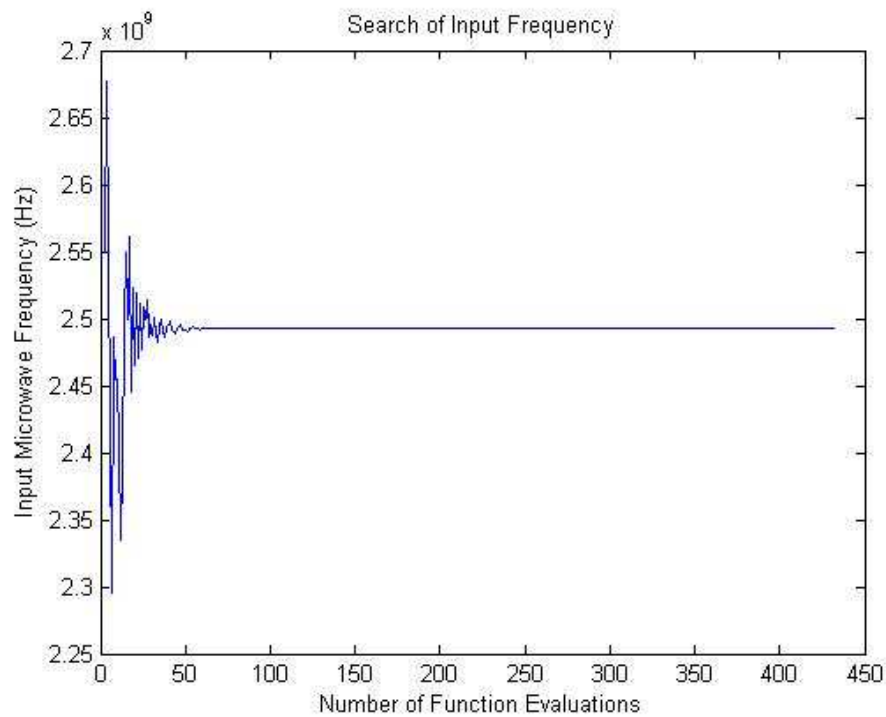
The search process and results of the NM search using initial values in Table 5-5 are shown in Figure 5-17 – 5-24.



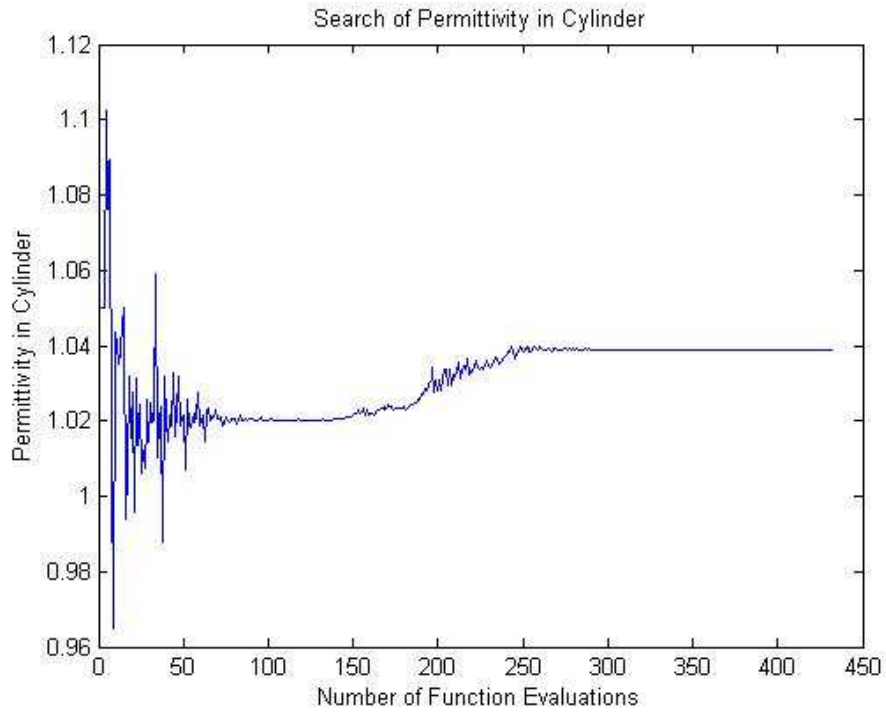
(a) Search trace of searching for antenna length with NM search method



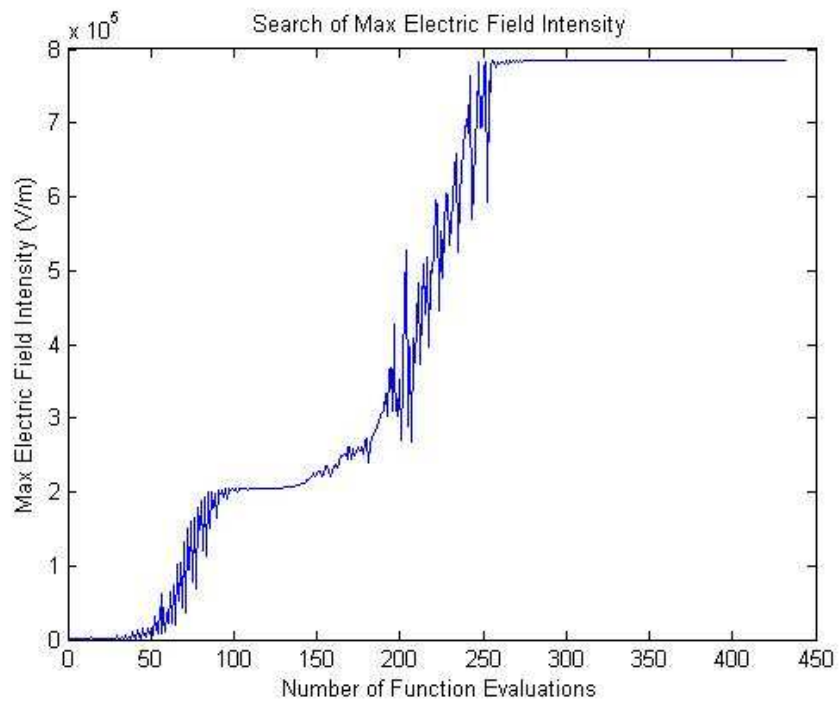
(b) Search trace of searching for screen radius with NM search method



(c) Search trace of searching for resonant frequency with NM search method



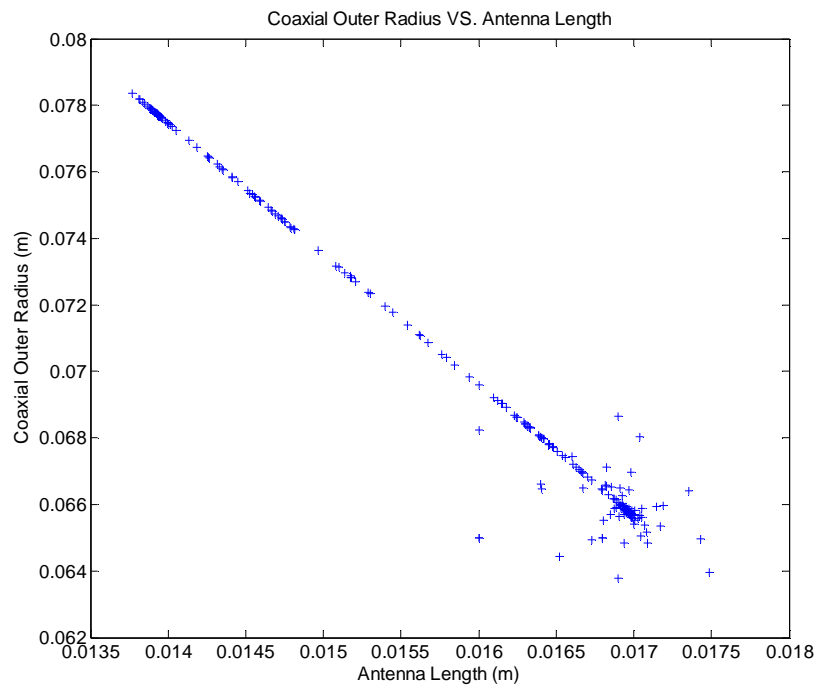
(d) Search trace of searching for permittivity with NM search method



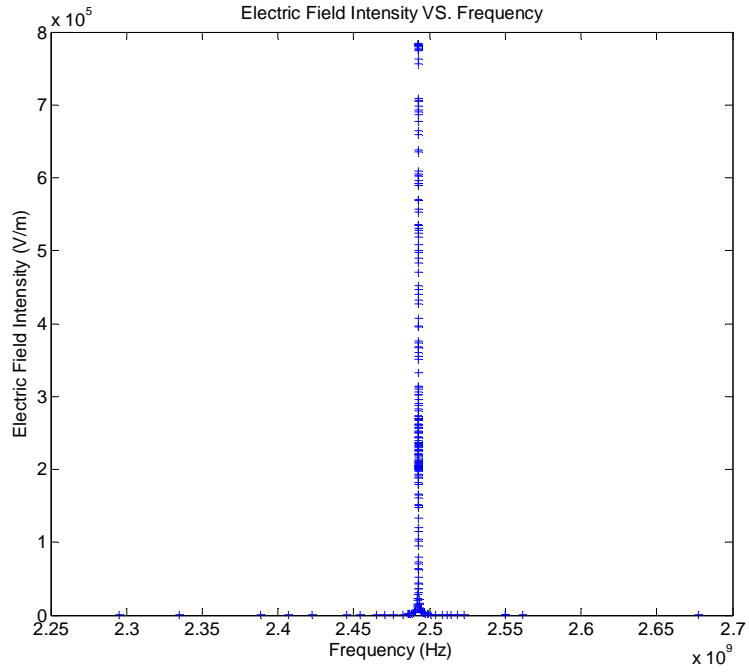
(e) Search trace of search objective: maximum electric field intensity

Figure 5-17 NM search for 1<sup>st</sup> set of initial values of parameters in Table 5-5

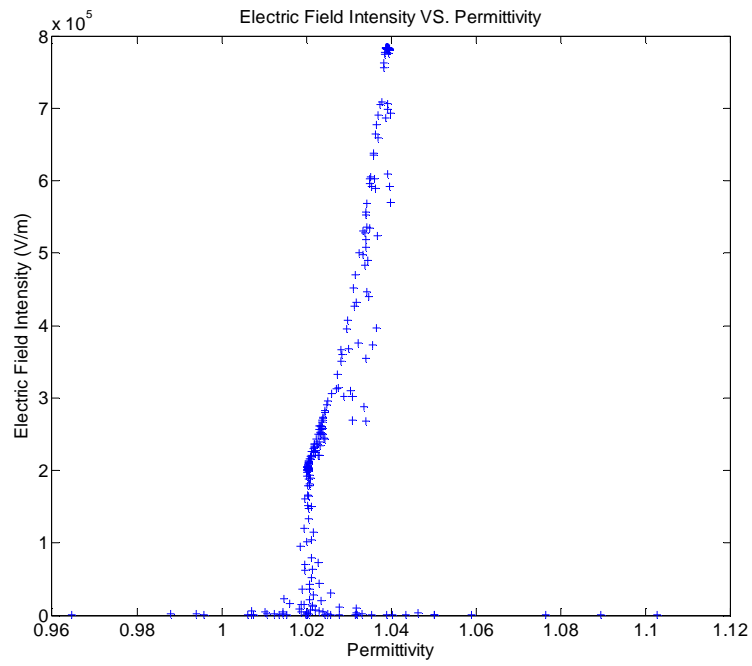
Figure 5-17 shows the NM simplex search process carried out with the 1<sup>st</sup> set of initial values by connecting each evaluation points. The figures show the parameters and the objective of each step in the search process. Figure 5-17 (a) shows the values of the antenna length used to simulate resonance for each search step during the search process. Figure 5-17 (b) shows the values of the screen of transmission radius used to simulate resonance for each search step during the search process. Figure 5-17 (c) shows the values selected for the resonant frequency to simulate resonance for each search step during the search process. Figure 5-17 (d) shows the values selected for the relative permittivity to simulate resonance fore each step during the process. Figure 5-17 (e) shows the progress of the search objective at each step during the search process.



(a) Distribution of search points of antenna length and screen radius



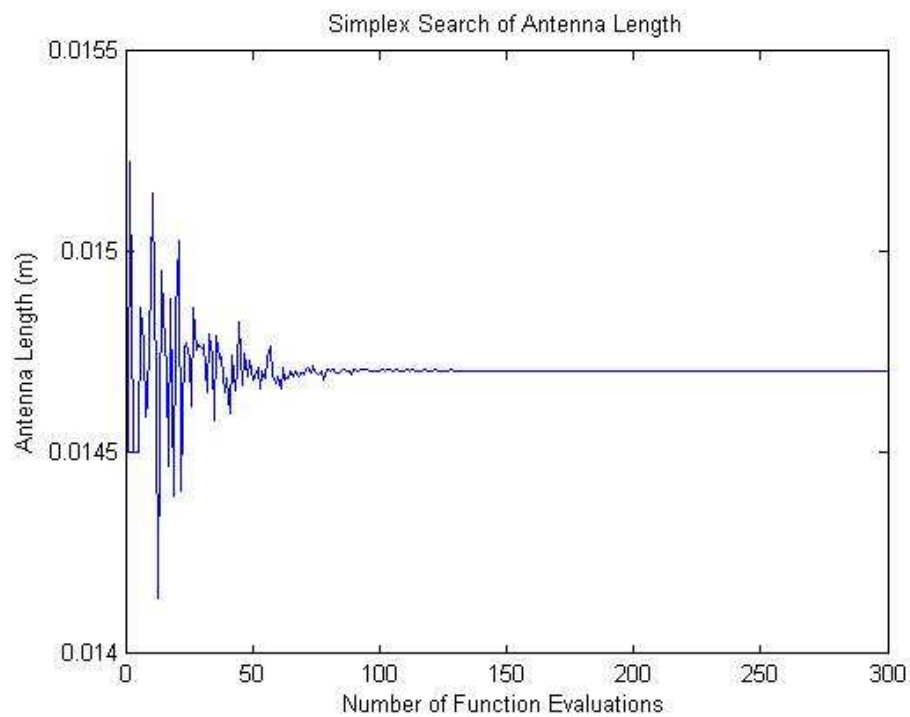
(b) Sensitivity of the resonant frequency



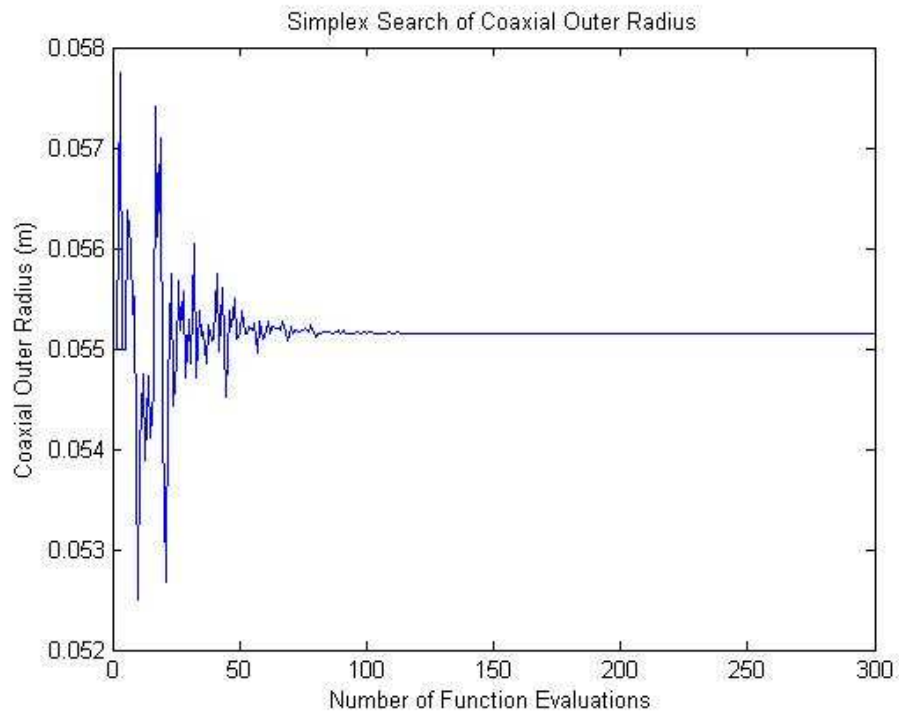
(c) Sensitivity of the relative permittivity

Figure 5-18 Relations between parameters from 1<sup>st</sup> NM search

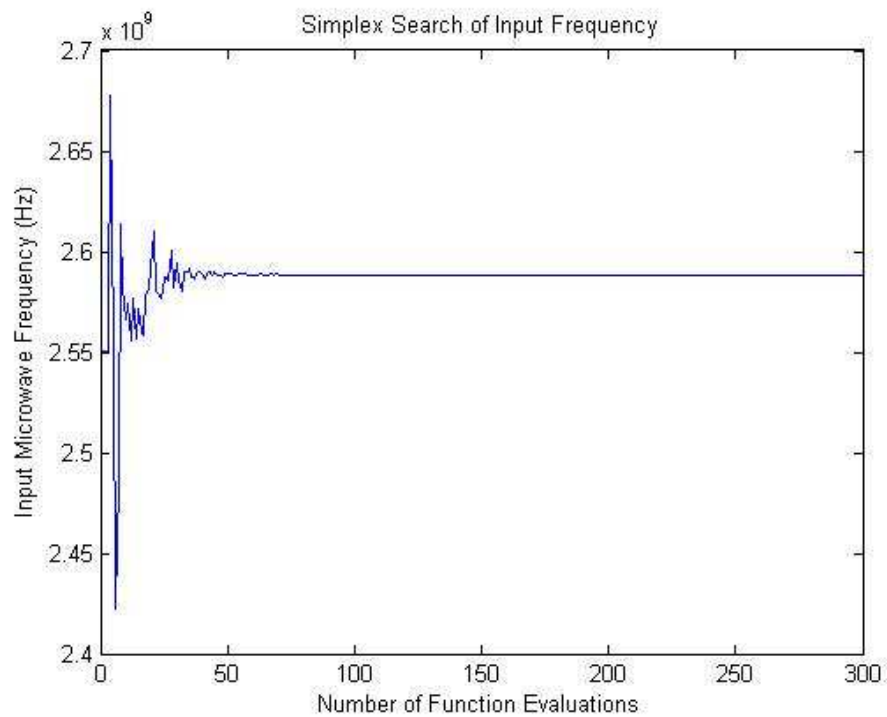
Figure 5-18 shows the relations between parameters and between the objective and parameters in 1<sup>st</sup> NM search. Figure 5-18 (a) draws all search points of the screen of transmission line radius and antenna length in one figure to show the distribution of both parameters in the search range and the search trace of both parameters during the search. Figure 5-18 (b) draws the search objective, maximum electric field intensity against the search points of frequency to analyse the sensitivity of the frequency to screen of transmission line radius and antenna length and to compare with the results from exhaustive search. Figure 5-18 (c) draws the electric field intensity against the permittivity to show the effects of the permittivity on electric field intensity in the search range.



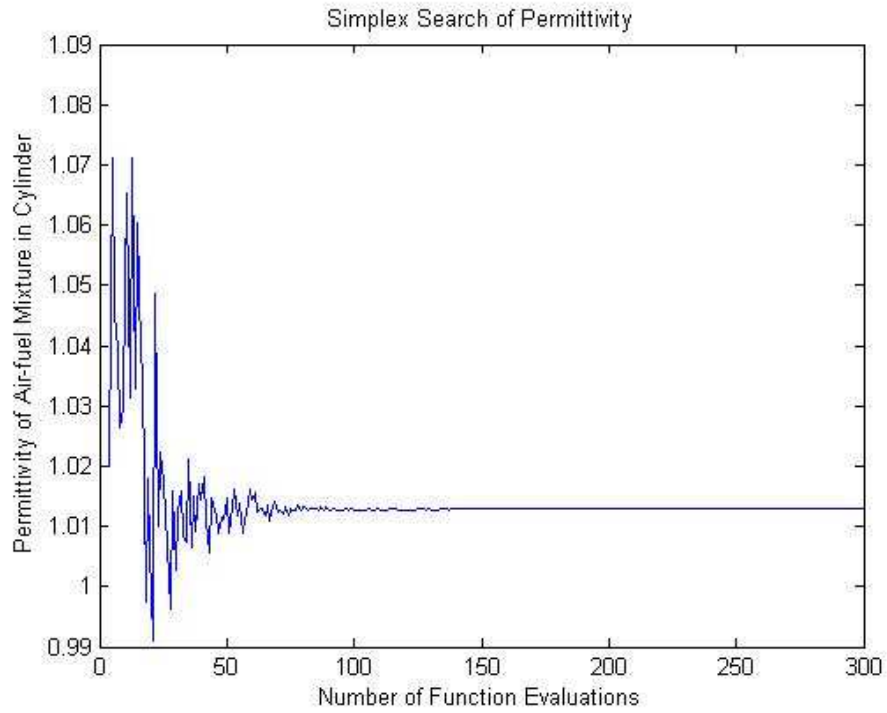
(a) Search trace of searching for antenna length with NM search method



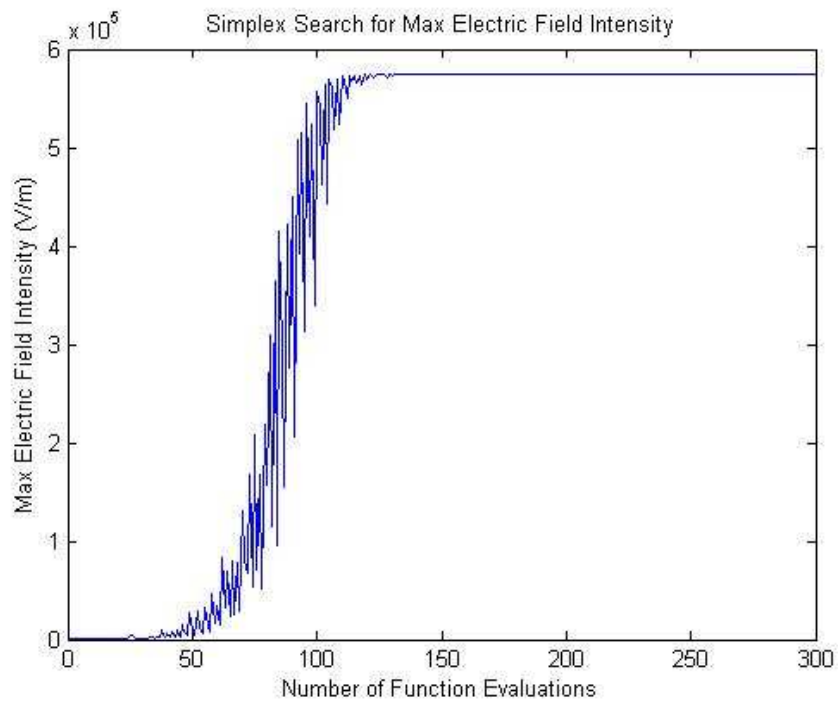
(b) Search trace of searching for screen radius with NM search method



(c) Search trace of searching for resonant frequency with NM search method



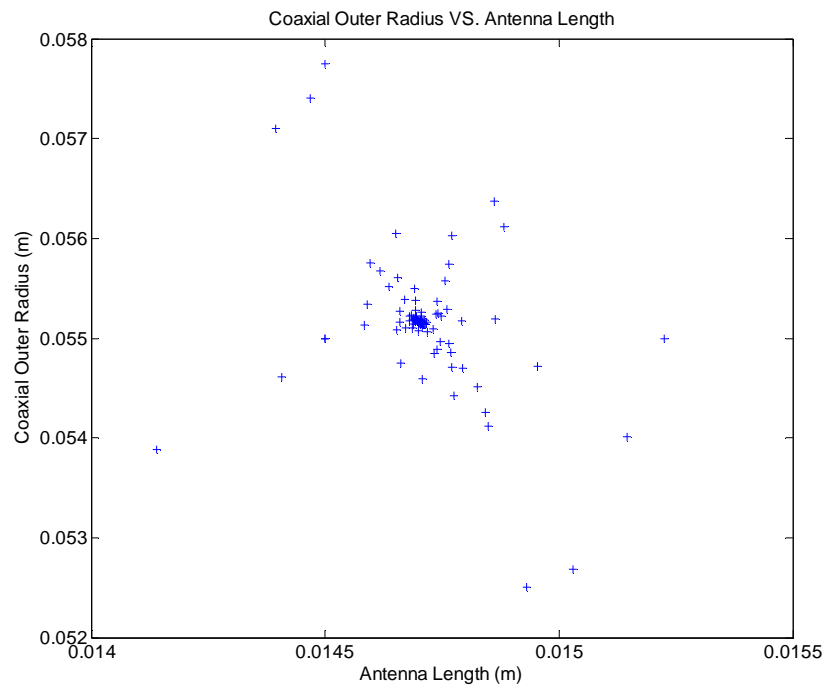
(d) Search trace of searching for permittivity with NM search method



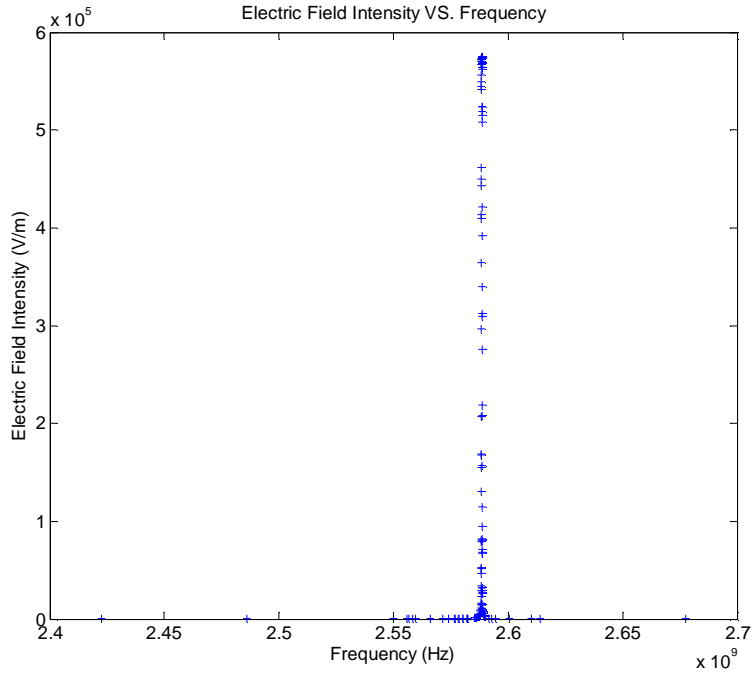
(e) Search trace of search objective: max electric field intensity

Figure 5-19 NM search for 2<sup>nd</sup> set of initial values of parameters in Table 5-5

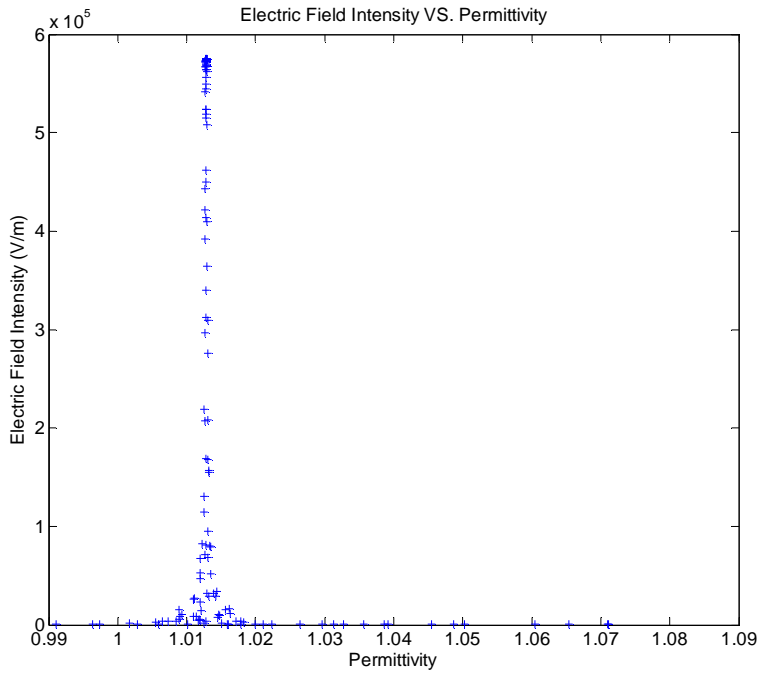
Figure 5-19 shows the NM simplex search process carried out with the 2<sup>nd</sup> set of initial values by connecting each evaluation points. The figures show the parameters and the objective of each step in the search process. Figure 5-19 (a) shows the values of the antenna length used to simulate resonance for each search step during the search process. Figure 5-19 (b) shows the values of the screen of transmission radius used to simulate resonance for each search step during the search process. Figure 5-19 (c) shows the values selected for the resonant frequency to simulate resonance for each search step during the search process. Figure 5-19 (d) shows the values selected for the relative permittivity to simulate resonance fore each step during the process. Figure 5-19 (e) shows the progress of the search objective at each step during the search process.



(a) Distribution of search points of antenna length and screen radius



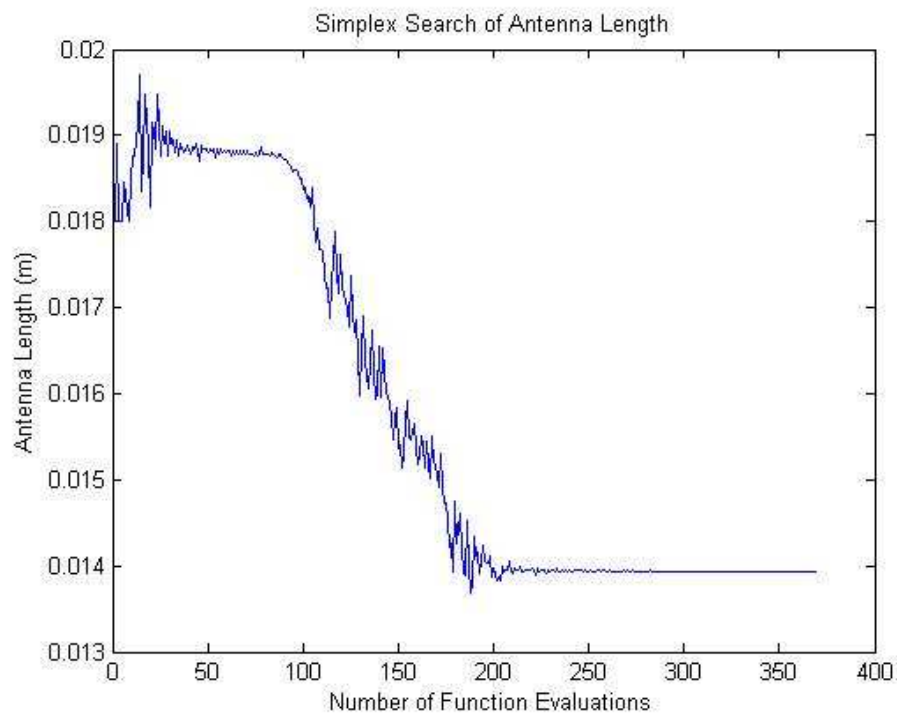
(b) Sensitivity of the resonant frequency



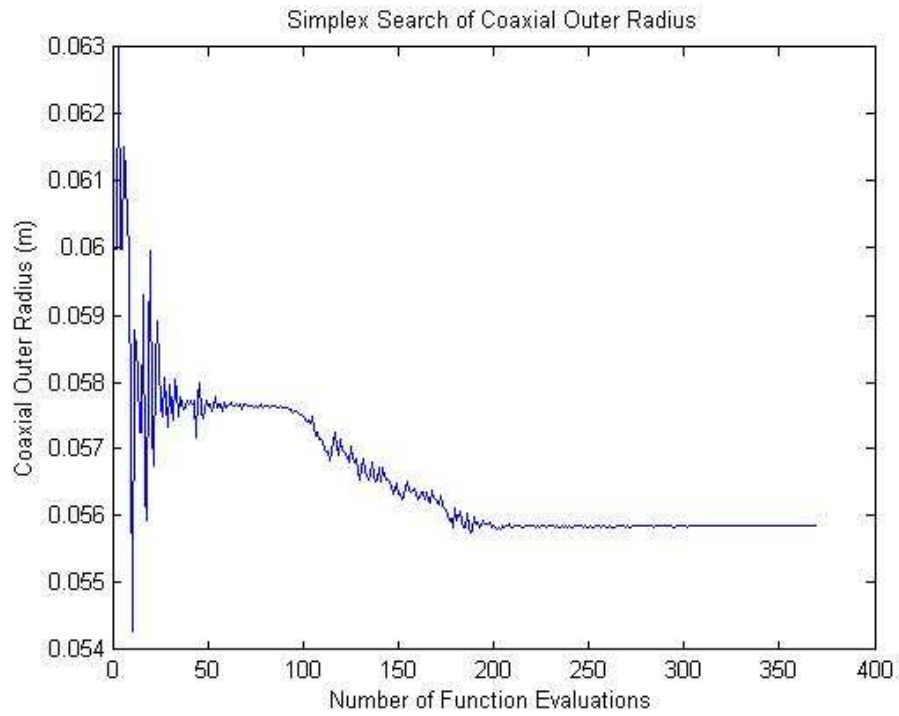
(c) Sensitivity of the relative permittivity

Figure 5-20 Relations between parameters from 2<sup>nd</sup> NM search

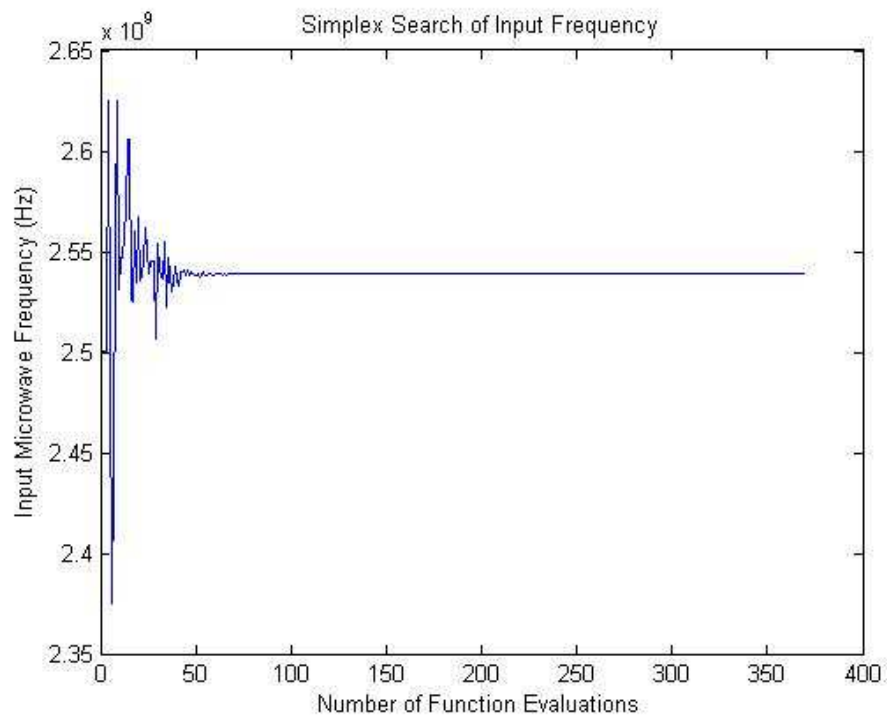
Figure 5-20 shows the relations between parameters and between the objective and parameters in 2<sup>nd</sup> NM search. Figure 5-20 (a) draws all search points of the screen of transmission line radius and antenna length in one figure to show the distribution of both parameters in the search range and the search trace of both parameters during the search. Figure 5-20 (b) draws the search objective, maximum electric field intensity against the search points of frequency to analyse the sensitivity of the frequency to screen of transmission line radius and antenna length and to compare with the results from exhaustive search. Figure 5-20 (c) draws the electric field intensity against the permittivity to show the effects of the permittivity on electric field intensity in the search range.



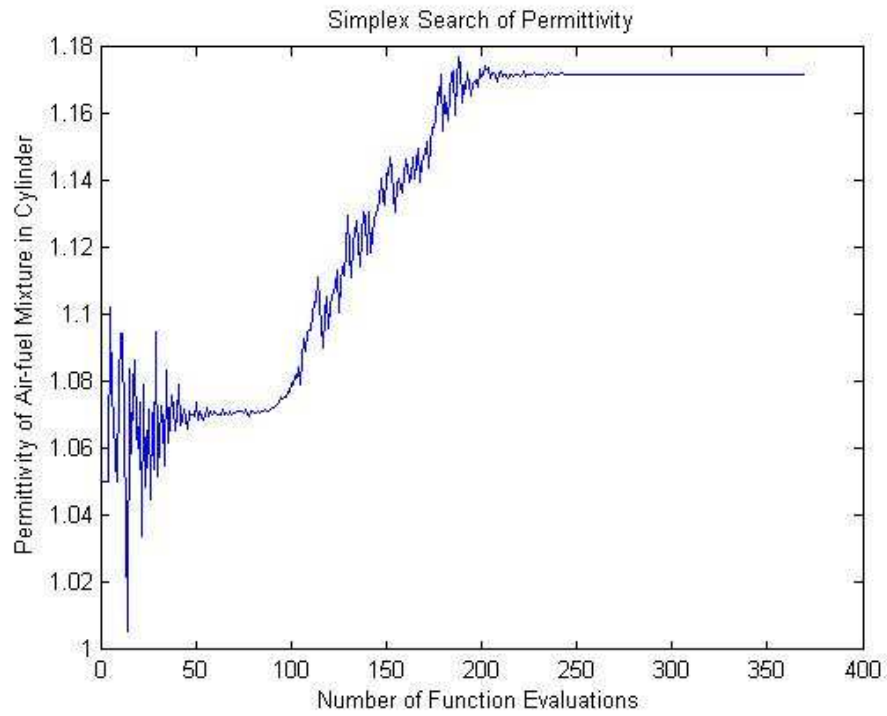
(a) Search trace of searching for antenna length with NM search method



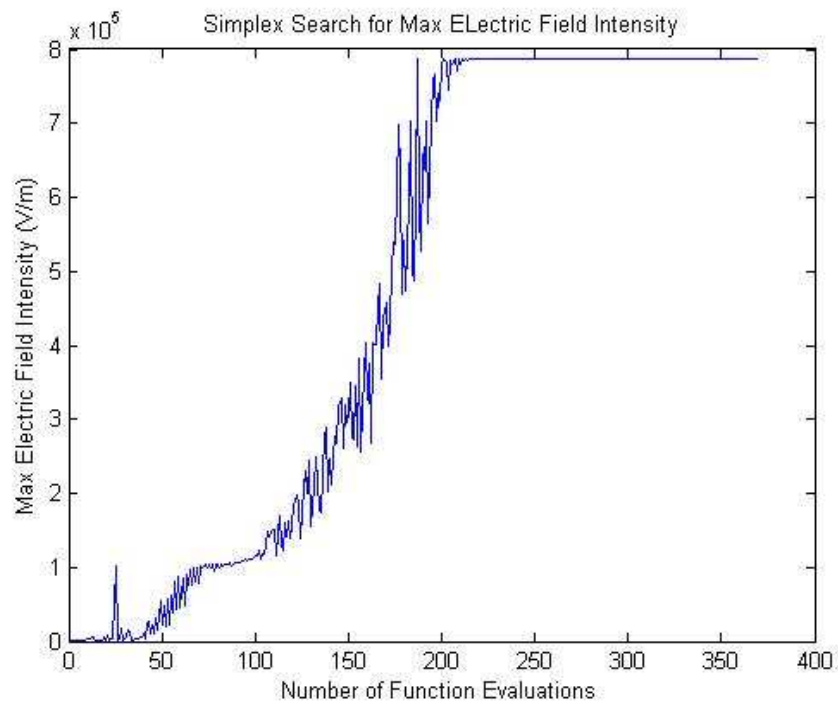
(b) Search trace of searching for screen radius with NM search method



(c) Search trace of searching for resonant frequency with NM search method



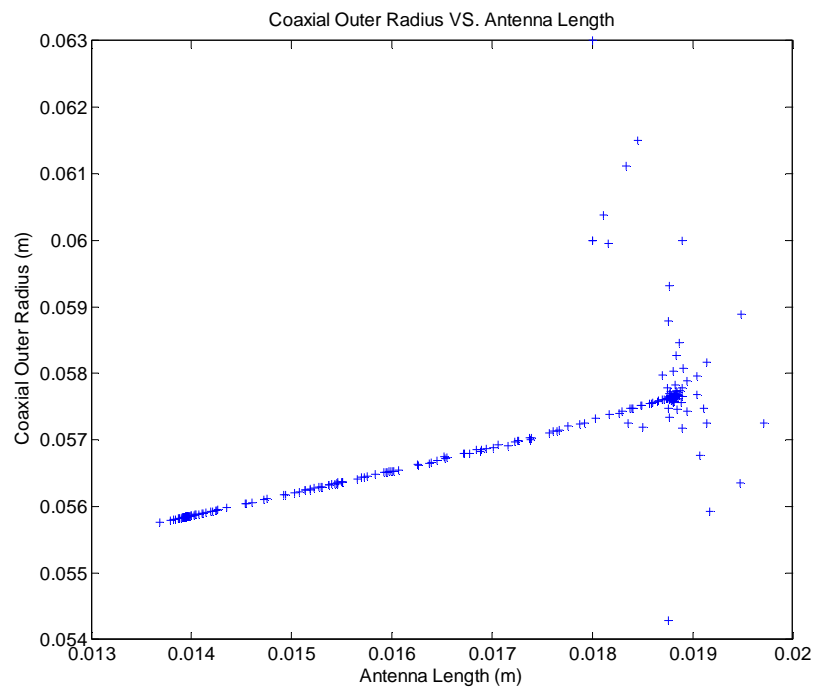
(d) Search trace of searching for permittivity with NM search method



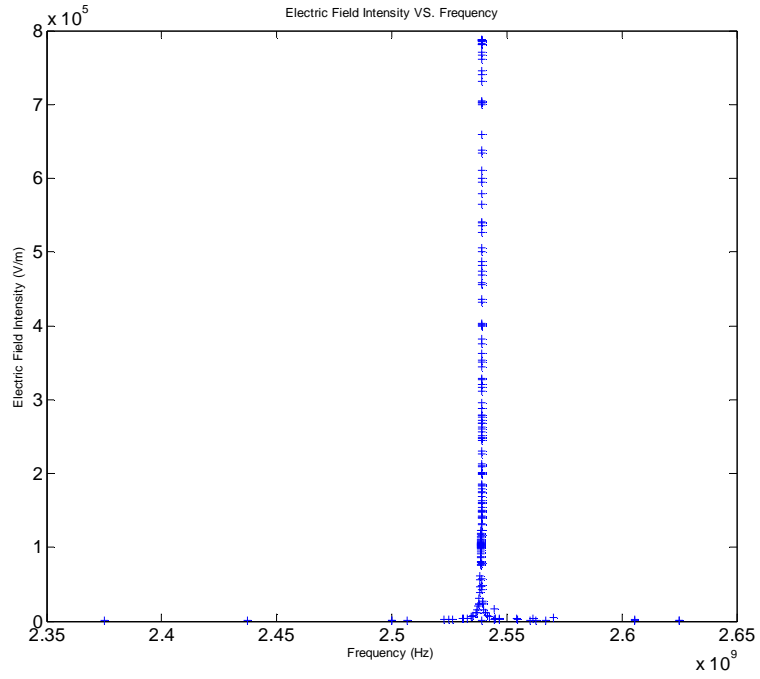
(e) Search trace of search objective: max electric field intensity

Figure 5-21 NM search for 3<sup>rd</sup> set of initial values of parameters in Table 5-5

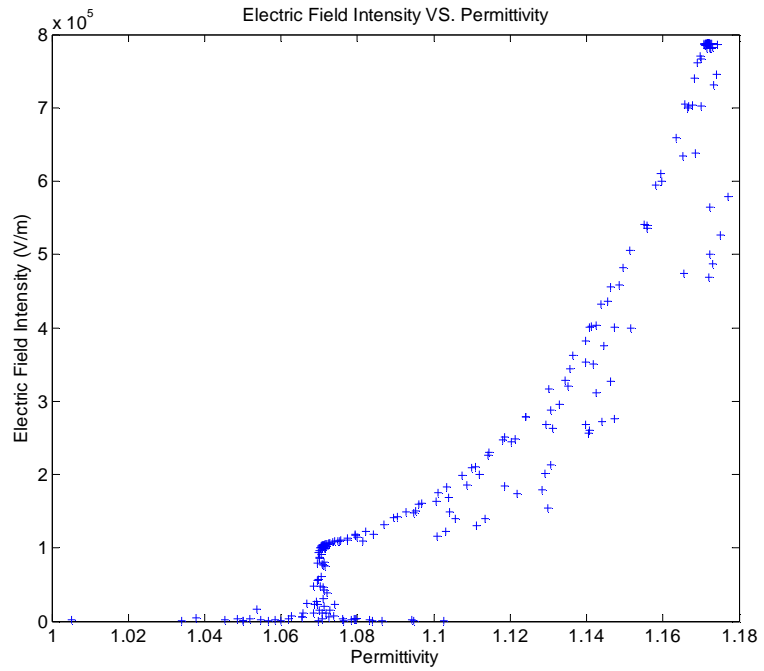
Figure 5-21 shows the NM simplex search process carried out with the 3<sup>rd</sup> set of initial values by connecting each evaluation points. The figures show the parameters and the objective of each step in the search process. Figure 5-21 (a) shows the values of the antenna length used to simulate resonance for each search step during the search process. Figure 5-21 (b) shows the values of the screen of transmission radius used to simulate resonance for each search step during the search process. Figure 5-21 (c) shows the values selected for the resonant frequency to simulate resonance for each search step during the search process. Figure 5-21 (d) shows the values selected for the relative permittivity to simulate resonance fore each step during the process. Figure 5-21 (e) shows the progress of the search objective at each step during the search process.



(a) Distribution of search points of antenna length and screen radius



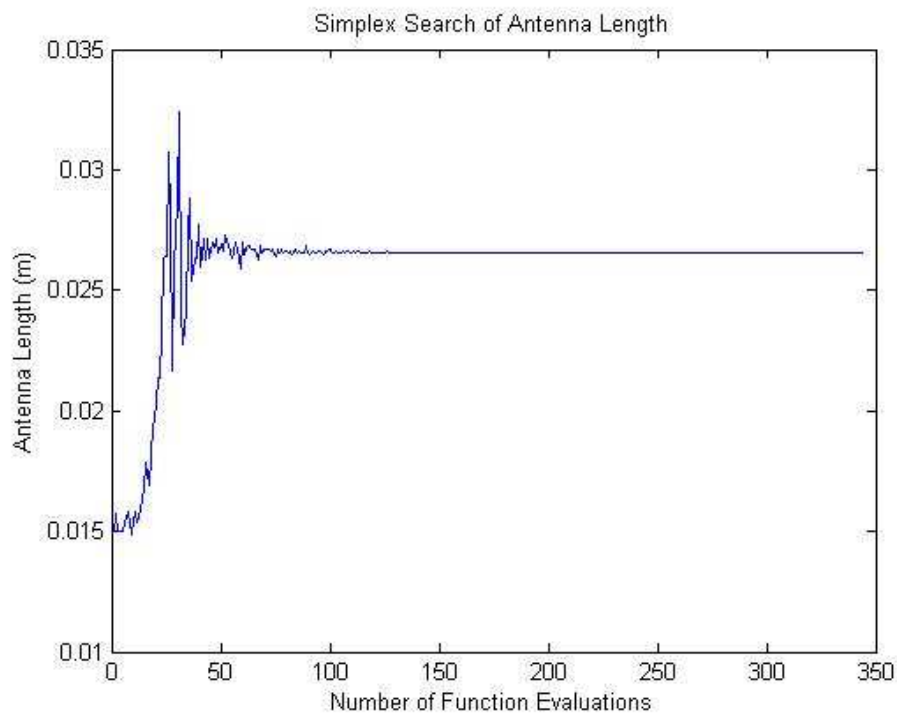
(b) Sensitivity of the resonant frequency



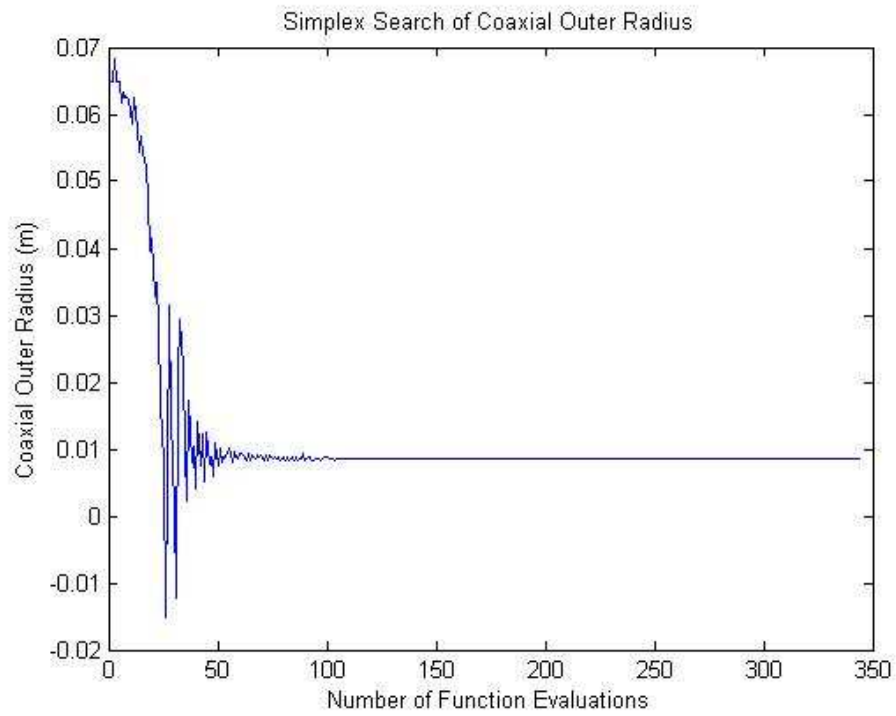
(c) Sensitivity of the relative permittivity

Figure 5-22 Relations between parameters from 3<sup>rd</sup> NM search

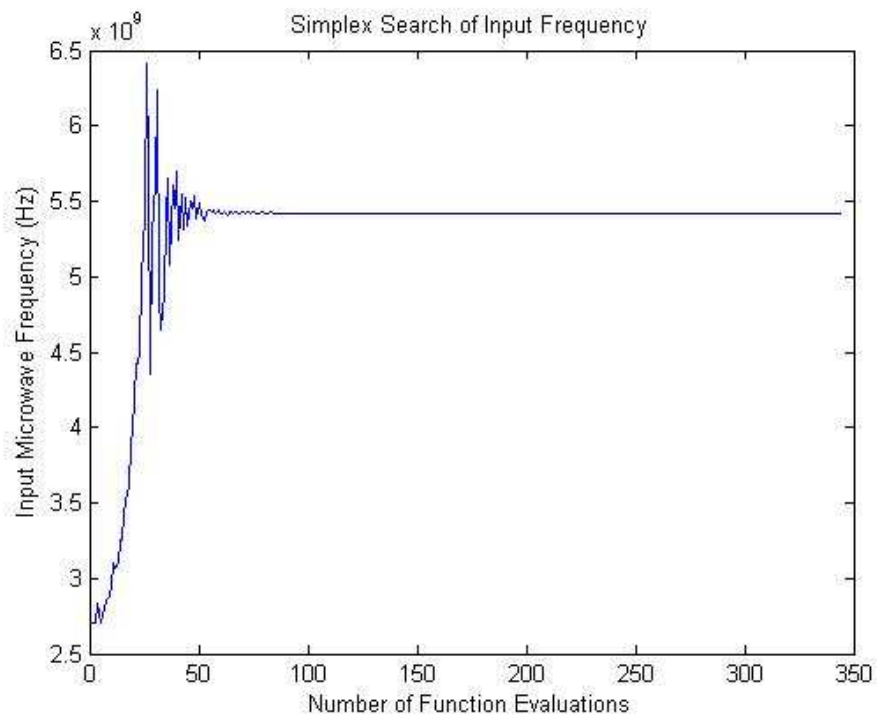
Figure 5-22 shows the relations between parameters and between the objective and parameters in 3<sup>rd</sup> NM search. Figure 5-22 (a) draws all search points of the screen of transmission line radius and antenna length in one figure to show the distribution of both parameters in the search range and the search trace of both parameters during the search. Figure 5-22 (b) draws the search objective, maximum electric field intensity against the search points of frequency to analyse the sensitivity of the frequency to screen of transmission line radius and antenna length and to compare with the results from exhaustive search. Figure 5-22 (c) draws the electric field intensity against the permittivity to show the effects of the permittivity on electric field intensity in the search range.



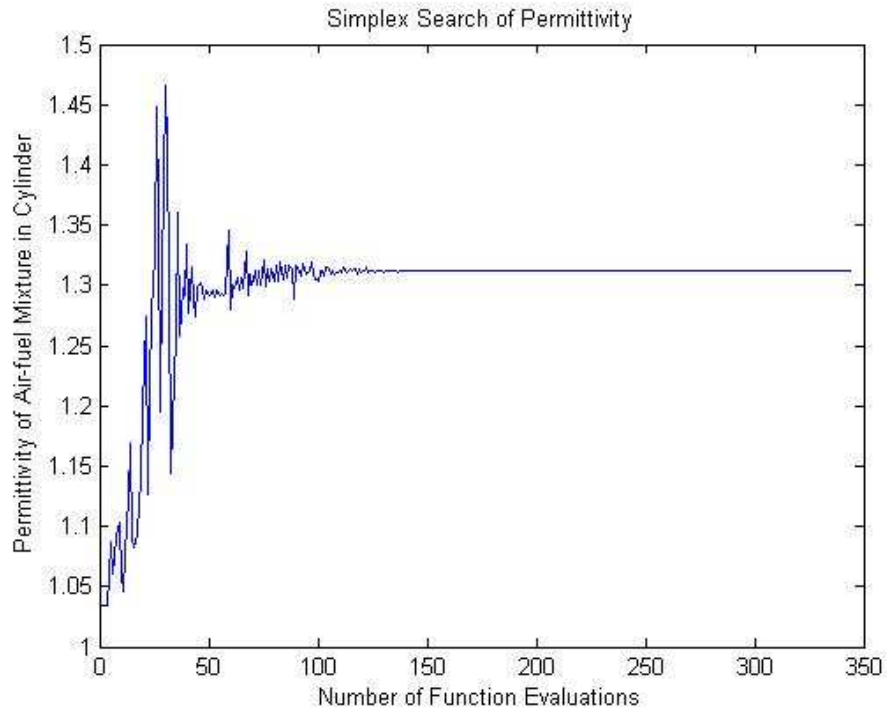
(a) Search trace of searching for antenna length with NM search method



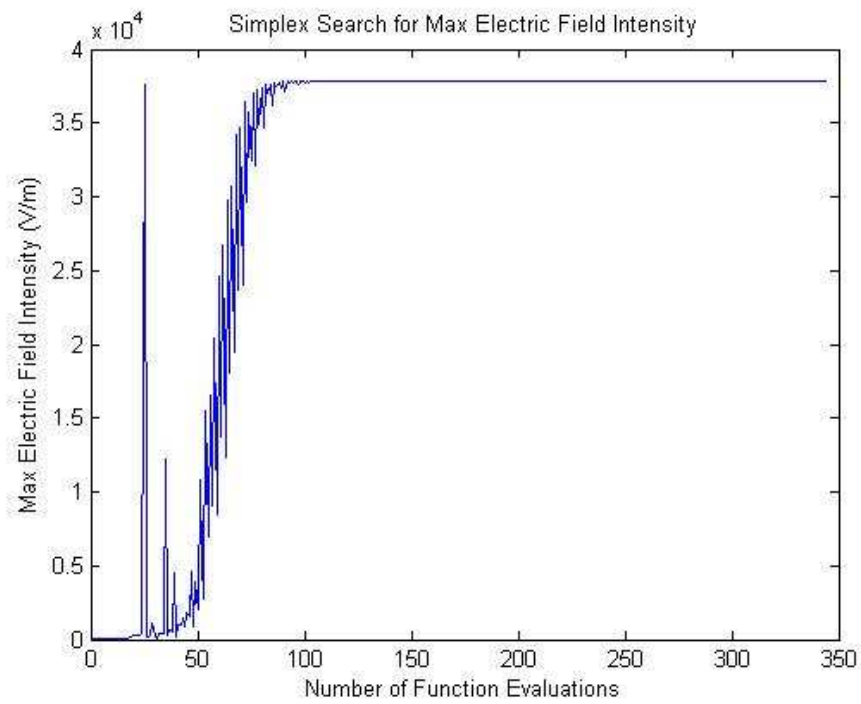
(b) Search trace of searching for screen radius with NM search method



(c) Search trace of searching for resonant frequency with NM search method



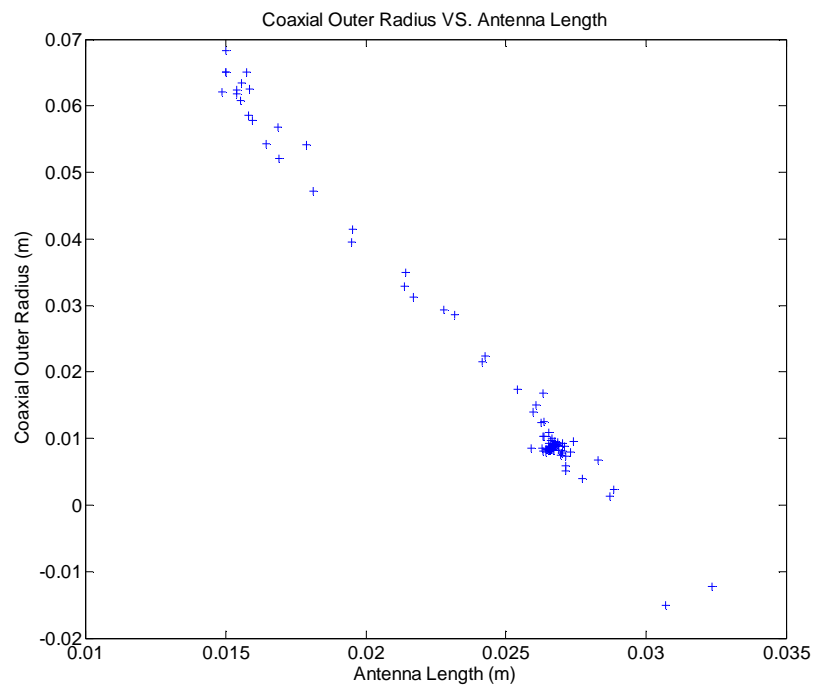
(d) Search trace of searching for permittivity with NM search method



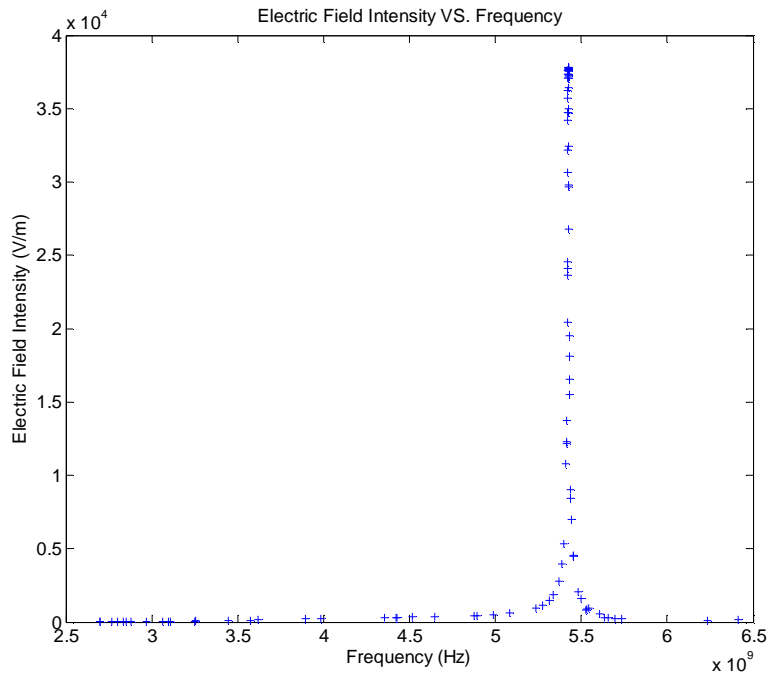
(e) Search trace of search objective: max electric field intensity

Figure 5-23 NM search for 4<sup>th</sup> set of initial values of parameters in Table 5-5

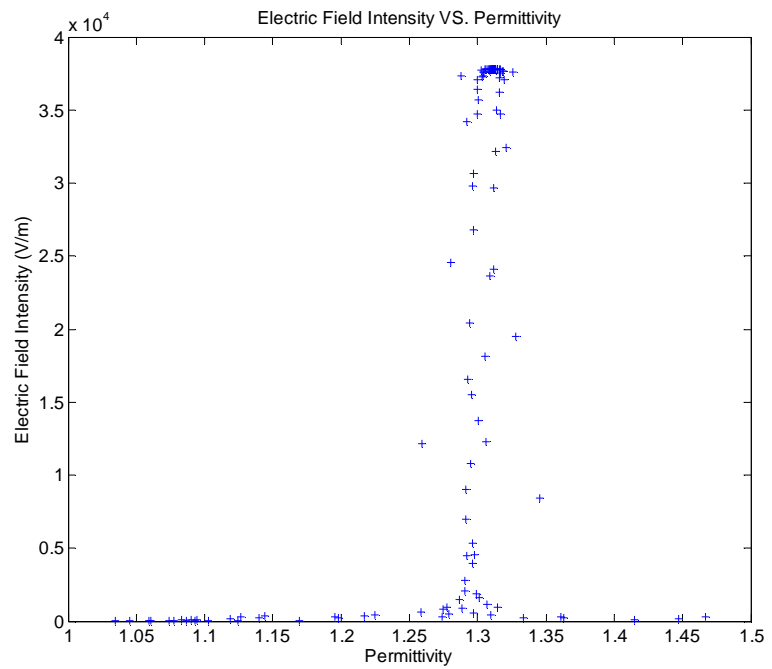
Figure 5-23 shows the NM simplex search process carried out with the 4<sup>th</sup> set of initial values by connecting each evaluation points. The figures show the parameters and the objective of each step in the search process. Figure 5-23 (a) shows the values of the antenna length used to simulate resonance for each search step during the search process. Figure 5-23 (b) shows the values of the screen of transmission radius used to simulate resonance for each search step during the search process. Figure 5-23 (c) shows the values selected for the resonant frequency to simulate resonance for each search step during the search process. Figure 5-23 (d) shows the values selected for the relative permittivity to simulate resonance fore each step during the process. Figure 5-23 (e) shows the progress of the search objective at each step during the search process.



(a) Distribution of search points of antenna length and screen radius



(b) Sensitivity of the resonant frequency



(c) Sensitivity of the relative permittivity

Figure 5-24 Relations between parameters from 4<sup>th</sup> NM search

Figure 5-24 shows the relations between parameters and between the objective and parameters in 4<sup>th</sup> NM search. Figure 5-24 (a) draws all search points of the screen of transmission line radius and antenna length in one figure to show the distribution of both parameters in the search range and the search trace of both parameters during the search. Figure 5-24 (b) draws the search objective, maximum electric field intensity against the search points of frequency to analyse the sensitivity of the frequency to screen of transmission line radius and antenna length and to compare with the results from exhaustive search. Figure 5-24 (c) draws the electric field intensity against the permittivity to show the effects of the permittivity on electric field intensity in the search range.

With one more parameters, the best value for the resonant frequency is still found in the early search stage. This confirms that the frequency is sensitive to the rest 3 parameter. From these figures it can be seen that the permittivity affects electric field more than the coupling antenna length and the screen of transmission line radius, which is already known from the exhaustive search in chapter 4.

From figures (c) of Figures 5-18, 5-20, 5-22 and 5-24, it can be seen that the increase of the permittivity causes the increase the electric field intensity. This does not agree with the results from exhaustive search or the electromagnetic theory. The reason that causes this trend is the NM simplex search tool searches 4 parameters at the same time. These four parameters affect each other during the search process. When the NM simplex search tries different permittivity values it also tries the different values of other parameters. Therefore, it can not be concluded that the greater permittivity results in stronger electric field. However it can be concluded that the permittivity does affect the electric field intensity, which means the change of the AFR will cause the change of the electric field intensity and possibly causes off resonance. From these figures it can be found when permittivity is added as a search parameter the resonant frequency varies from 2.495 GHz to 5.94 GHz. This also confirms that the permittivity affects the resonance and possibly causes off resonance.

Search results of each NM search are listed in Table 5-6.

Table 5-6 Search results of NM searches

	Antenna Length (m)	Screen Radius (m)	Resonant frequency (GHz)	Relative Permittivity of Mixture	Max Elec. Field Intensity (V/m)
1	0.014	0.078	2.495	1.039	$7.9 \times 10^5$
2	0.0147	0.055	2.57	1.01	$5.8 \times 10^5$
3	0.014	0.056	2.54	1.175	$7.9 \times 10^5$
4	0.027	0.01	5.49	1.3	$3.8 \times 10^4$

From Table 5-6 it can be found that the permittivity affects the resonant frequency and electric field strength much more than the coupling antenna length and the screen of transmission radius do. From the NM simplex searches with first 3 sets of initial values it can be seen while the coupling antenna length and screen of transmission line radius vary in the similar range in Table 5-4 from 0.014 m to 0.0147 m and 0.056 m to 0.078 m respectively, the frequency varies from 2.495GHz to 2.57 GHz, which is wider than the range of the frequency in Table 5-4. This is caused by the permittivity changed from 1.039 to 1.175. In Table 5-6 the frequency from the search with 4<sup>th</sup> set of initial values for each parameter is 5.49 GHz, which implies the NM simplex has failed to find a solution in expected range. The resonance at 5.49 GHz is not a TM<sub>010</sub> mode resonance. For the NM simplex search the search range is not preset so it is likely that the solution for the

parameters is found far away from the initial values of the parameters preset based on experience of previous research. However, this unexpected result can show researchers another possible local solution that researchers have not noticed and needs to be investigated.

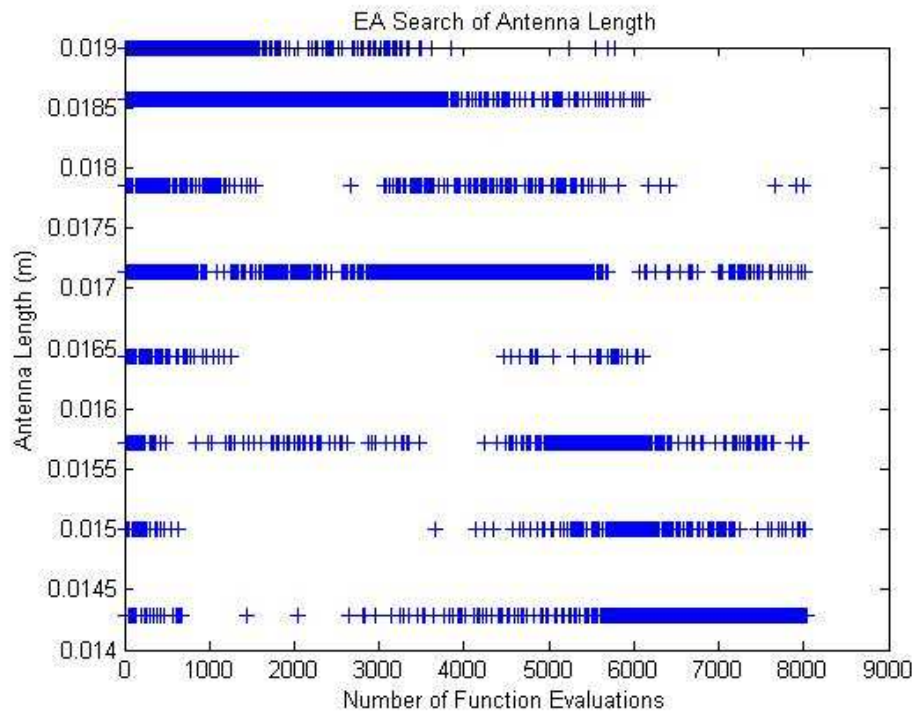
### 5.2.2 Search Using the EA Method

With one more design parameter the EA search parameters have to be adjusted. Table 5-7 shows 4 sets of EA parameters used for the searches in this section.

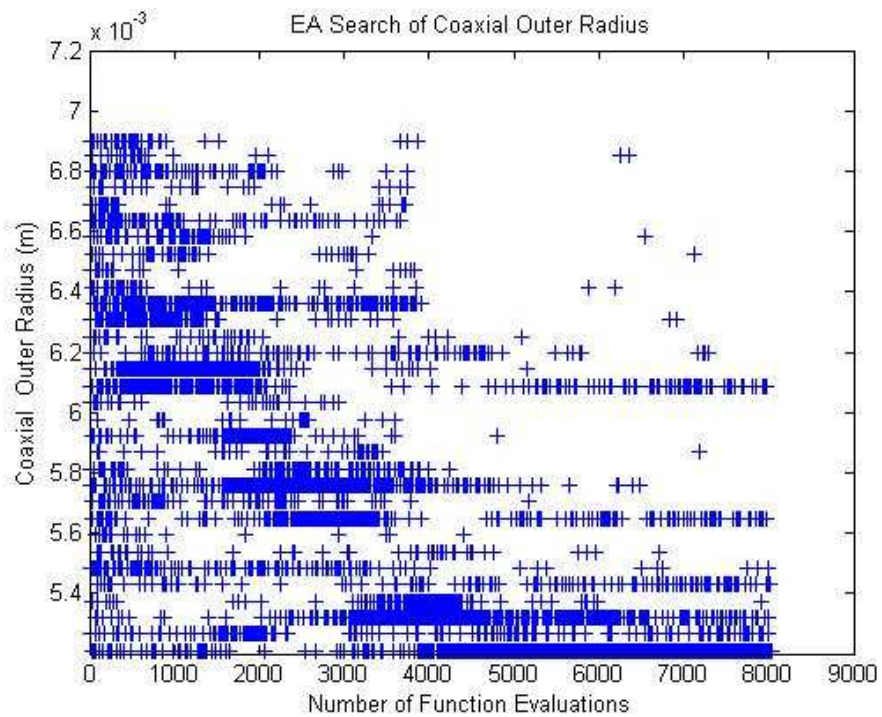
Table 5-7 EA parameter settings

	Population	Crossover Rate	Mutation Rate	Generations
1	131	70	0.02	80
2	131	70	0.01	70
3	131	50	0.01	60
4	131	50	0.02	60

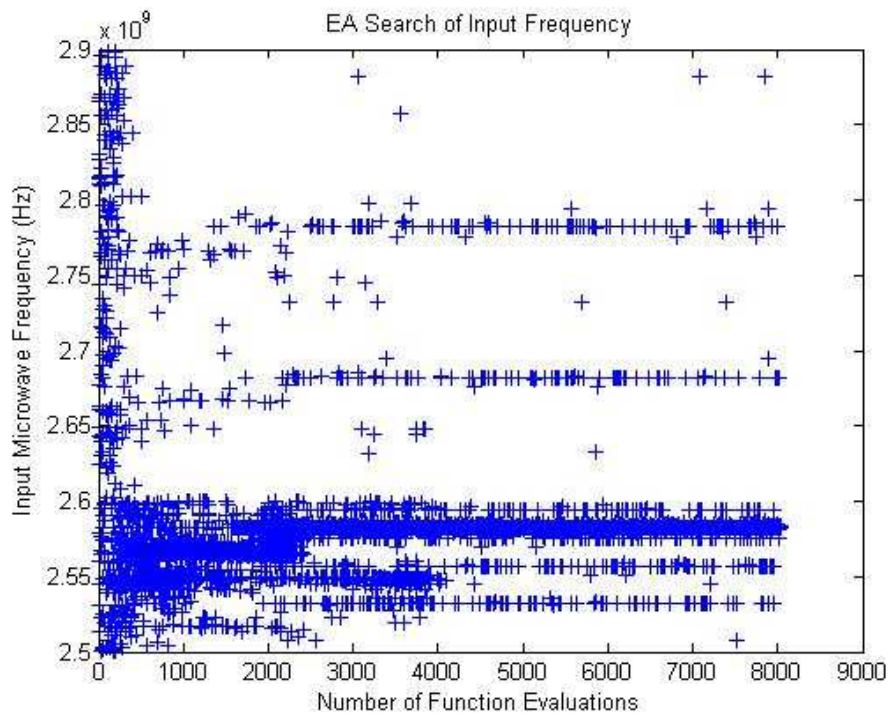
The search process and results of the EA search with the parameters in Table 5-7 are shown below in Figures 5-25 – 5-32.



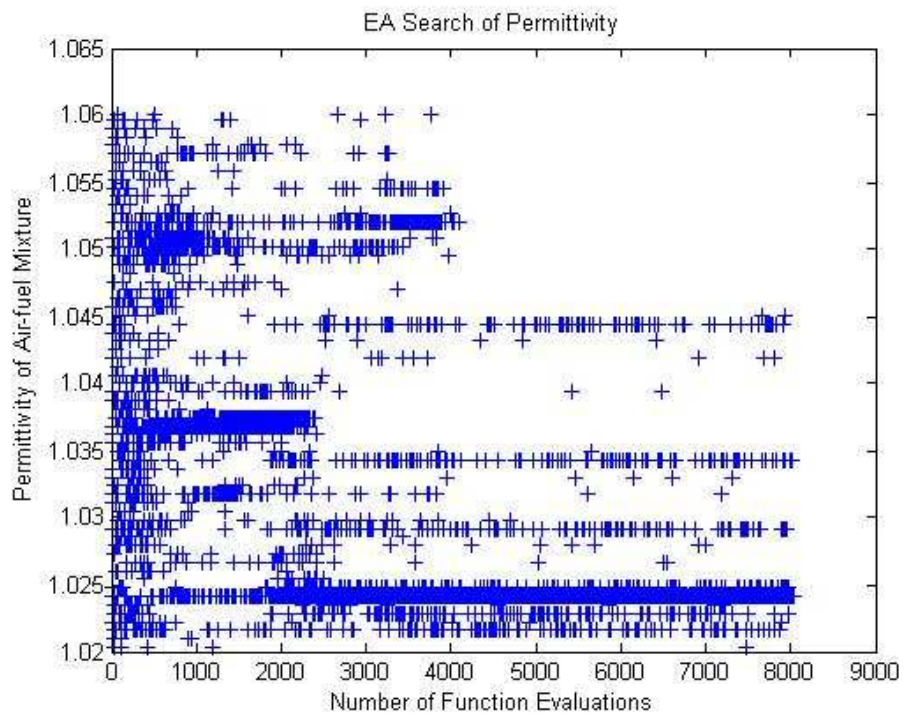
(a) Search trace of searching for antenna length with EA search method



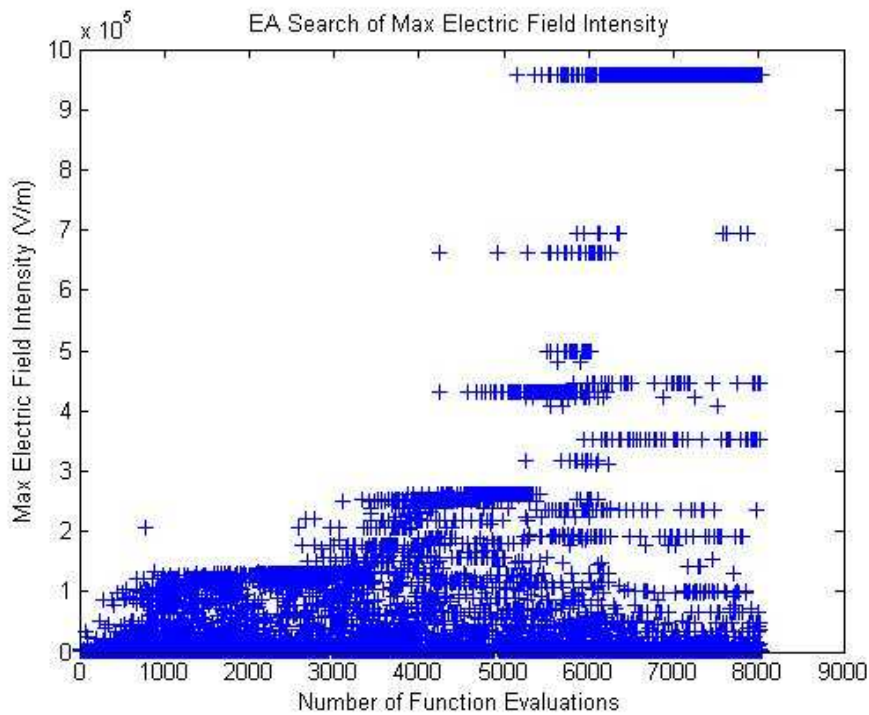
(b) Search trace of searching for screen radius with EA search method



(c) Search trace of searching for resonant frequency with EA search method



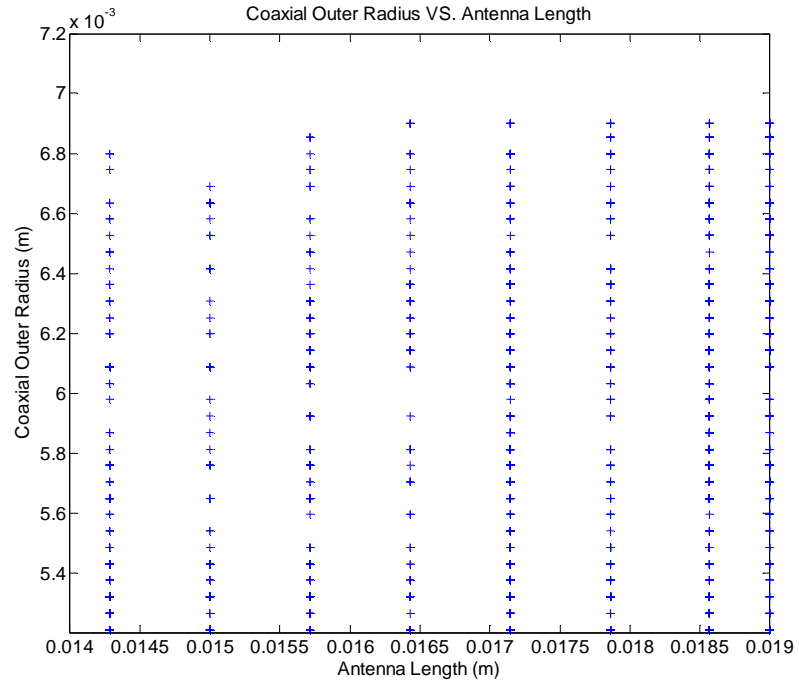
(d) Search trace of searching for permittivity with EA search method



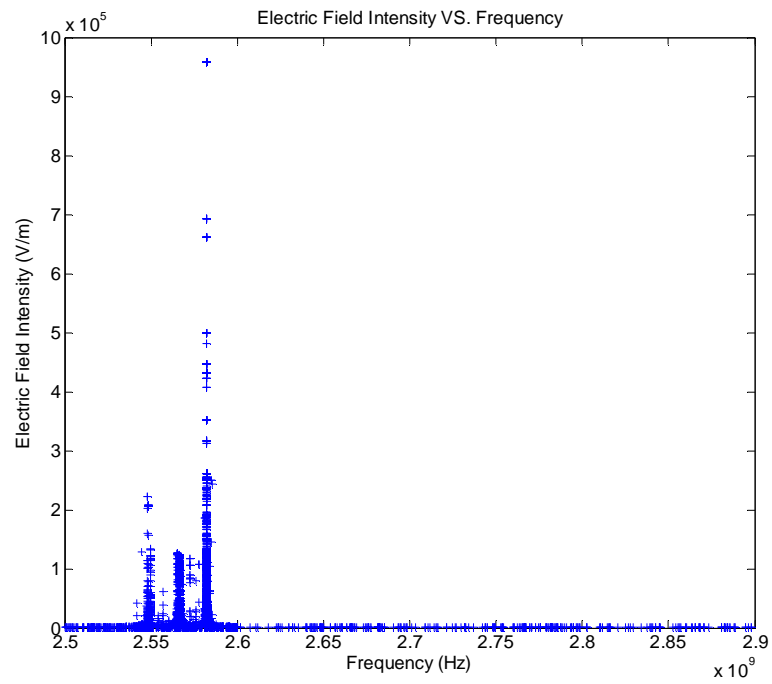
(e) Search trace of search objective: maximum electric field intensity

Figure 5-25 EA search for 1<sup>st</sup> set of EA parameters in Table 5-7

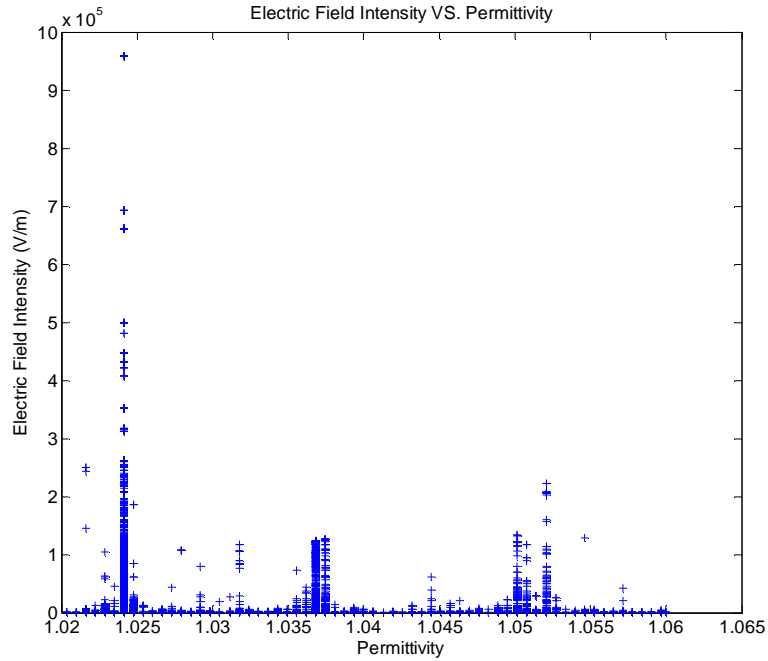
Figure 5-25 shows the EA search process carried out with the 1<sup>st</sup> set of EA parameters by showing all the points of each search step throughout the whole search process. Figure 5-25 (a) shows the values of the antenna length used to simulate resonance for each search step during the search process. Figure 5-25 (b) shows the values of the screen of transmission radius used to simulate resonance for each search step during the search process. Figure 5-25 (c) shows the values selected for the resonant frequency to simulate resonance for each search step during the search process. Figure 5-25 (d) shows the values selected for the relative permittivity to simulate resonance fore each step during the process. Figure 5-25 (e) shows the progress of the search objective at each step during the search process.



(a) Distribution of search points of antenna length and screen radius



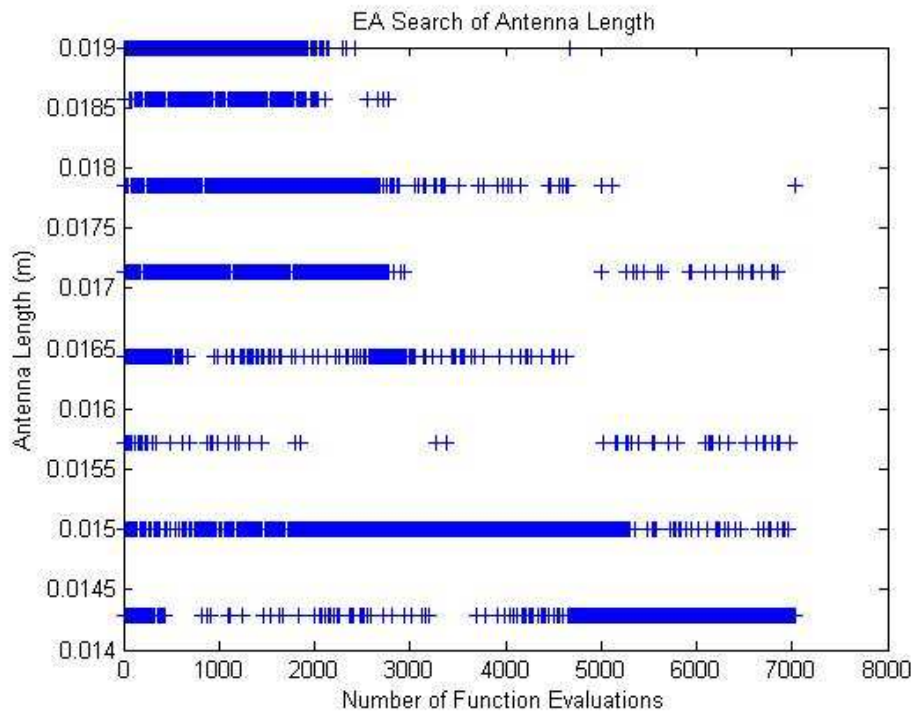
(b) Sensitivity of the resonant frequency



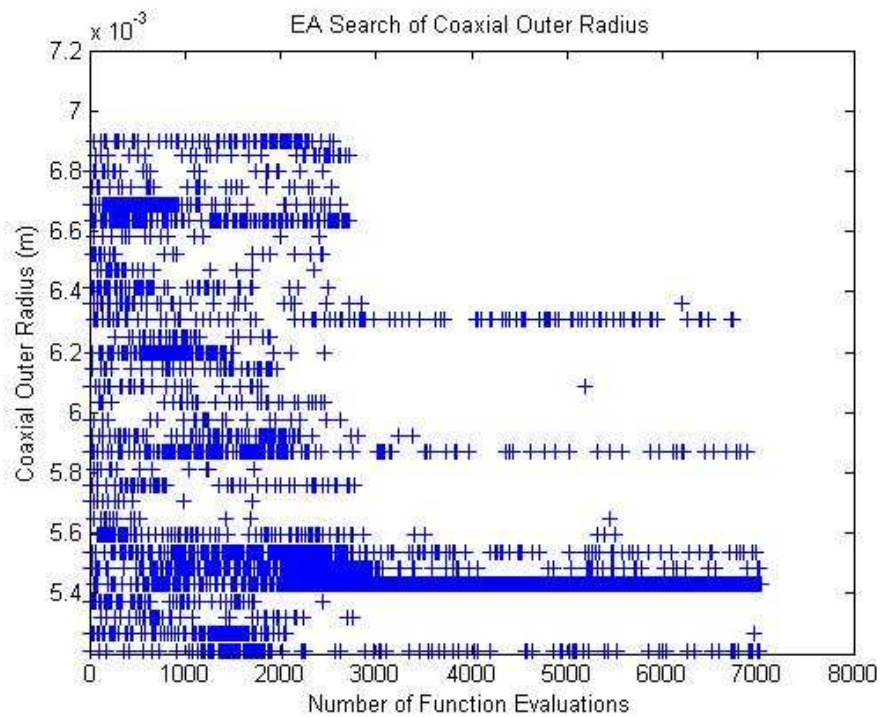
(c) Sensitivity of the relative permittivity

Figure 5-26 Relations between parameters from 1<sup>st</sup> EA search

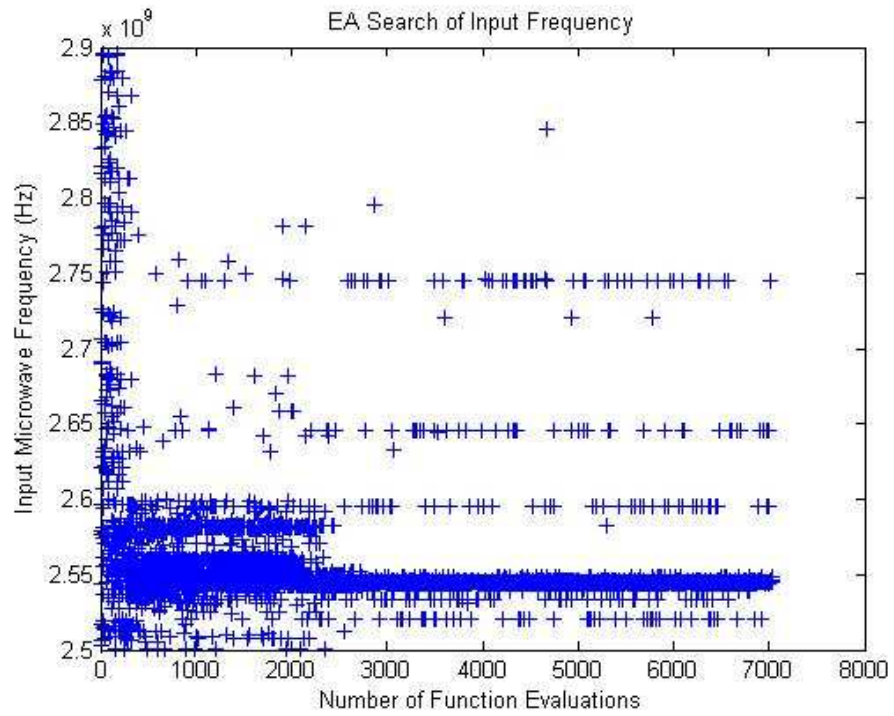
Figure 5-26 shows the relations between parameters and between the objective and parameters in 1<sup>st</sup> EA search. Figure 5-26 (a) draws all search points of the screen of transmission line radius and antenna length in one figure to show the distribution of both parameters in the search range and the search trace of both parameters during the search. Figure 5-26 (b) draws the search objective, maximum electric field intensity against the search points of frequency to analyse the sensitivity of the frequency to screen of transmission line radius and antenna length and to compare with the results from exhaustive search. Figure 5-26 (c) draws the electric field intensity against the permittivity to show the effects of the permittivity on electric field intensity in the search range.



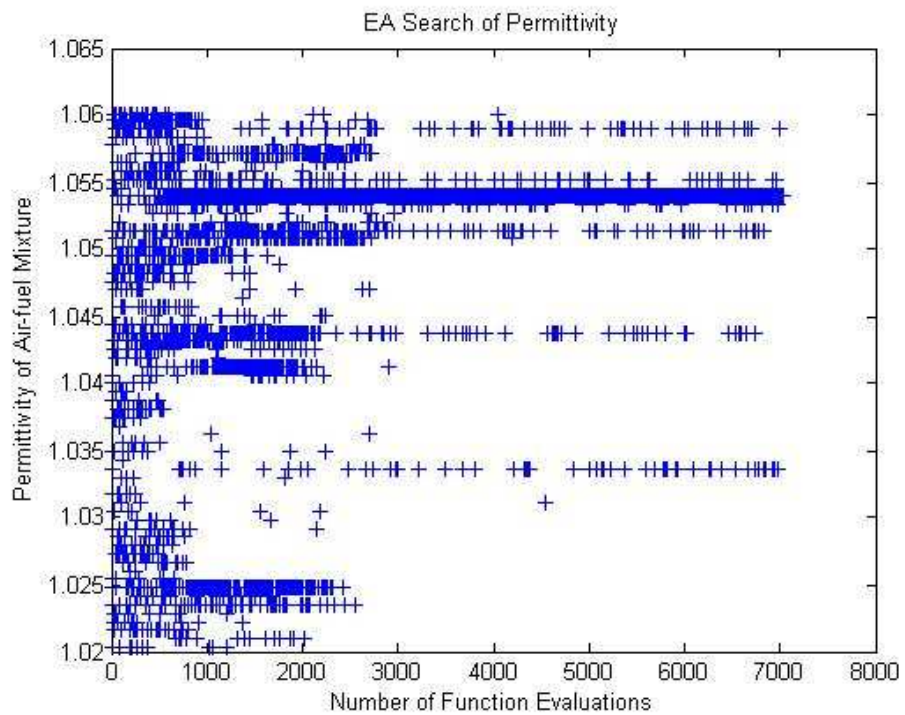
(a) Search trace of searching for antenna length with EA search method



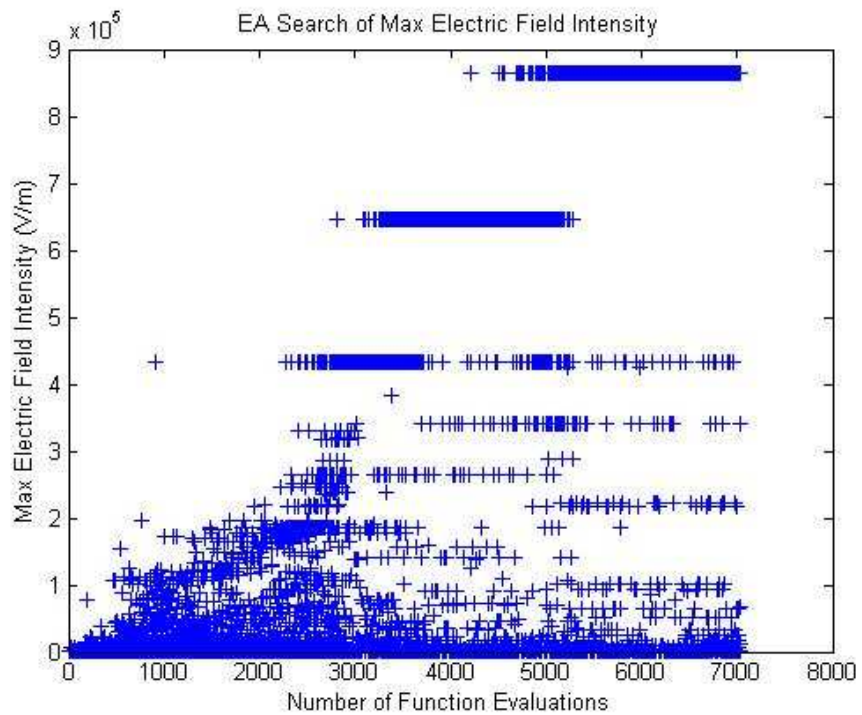
(b) Search trace of searching for screen radius with EA search method



(c) Search trace of searching for resonant frequency with EA search method



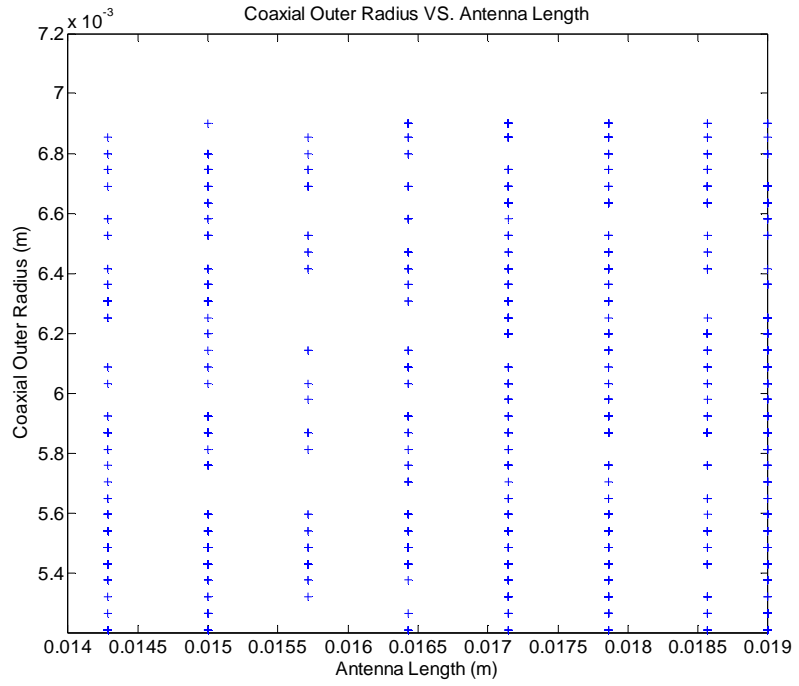
(d) Search trace of searching for permittivity with EA search method



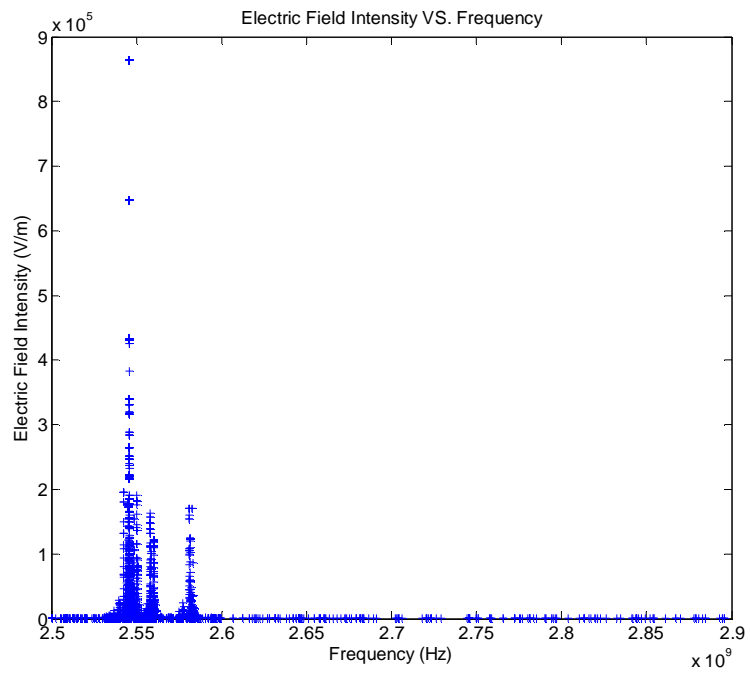
(e) Search trace of search objective: max electric field intensity

Figure 5-27 EA search for 2<sup>nd</sup> set of EA parameters in Table 5-7

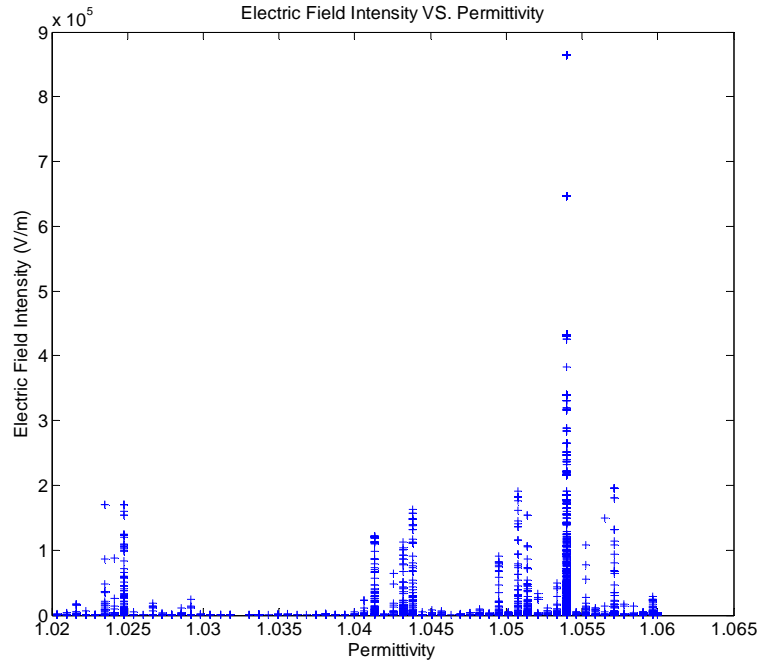
Figure 5-27 shows the EA search process carried out with the 2<sup>nd</sup> set of EA parameters by showing all the points of each search step throughout the whole search process. Figure 5-27 (a) shows the values of the antenna length used to simulate resonance for each search step during the search process. Figure 5-27 (b) shows the values of the screen of transmission radius used to simulate resonance for each search step during the search process. Figure 5-27 (c) shows the values selected for the resonant frequency to simulate resonance for each search step during the search process. Figure 5-27 (d) shows the values selected for the relative permittivity to simulate resonance fore each step during the process. Figure 5-27 (e) shows the progress of the search objective at each step during the search process.



(a) Distribution of search points of antenna length and screen radius



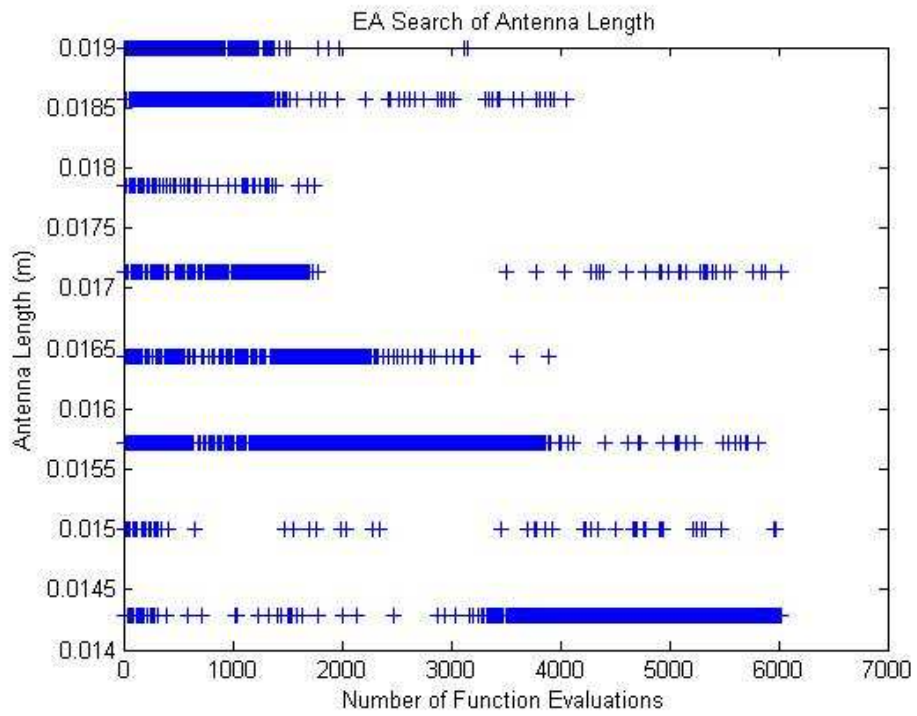
(b) Sensitivity of the resonant frequency



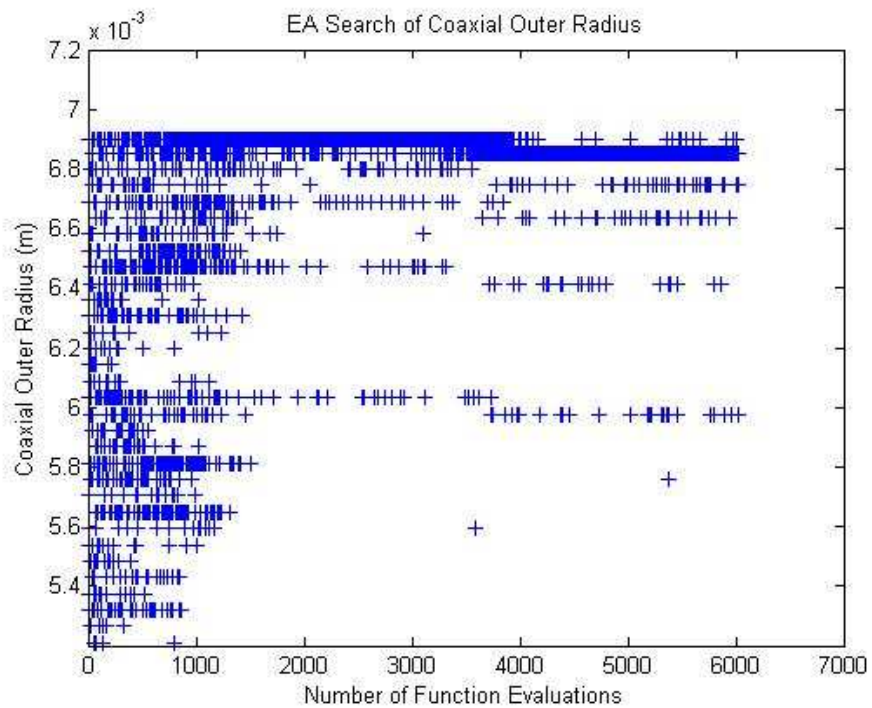
(c) Sensitivity of the relative permittivity

Figure 5-28 Relations between parameters from 2<sup>nd</sup> EA search

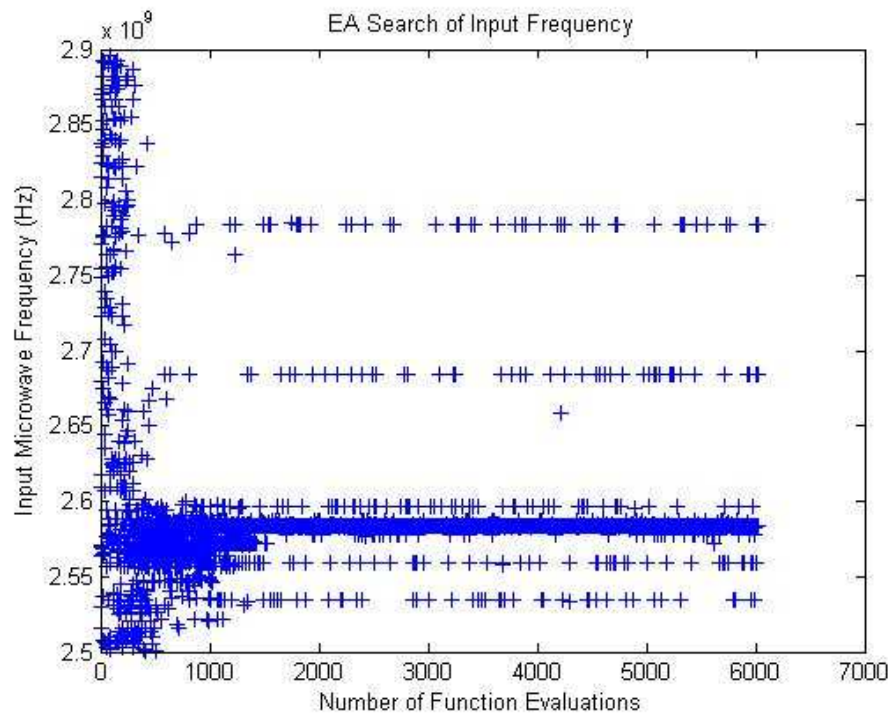
Figure 5-28 shows the relations between parameters and between the objective and parameters in 2<sup>nd</sup> EA search. Figure 5-28 (a) draws all search points of the screen of transmission line radius and antenna length in one figure to show the distribution of both parameters in the search range and the search trace of both parameters during the search. Figure 5-28 (b) draws the search objective, maximum electric field intensity against the search points of frequency to analyse the sensitivity of the frequency to screen of transmission line radius and antenna length and to compare with the results from exhaustive search. Figure 5-28 (c) draws the electric field intensity against the permittivity to show the effects of the permittivity on electric field intensity in the search range.



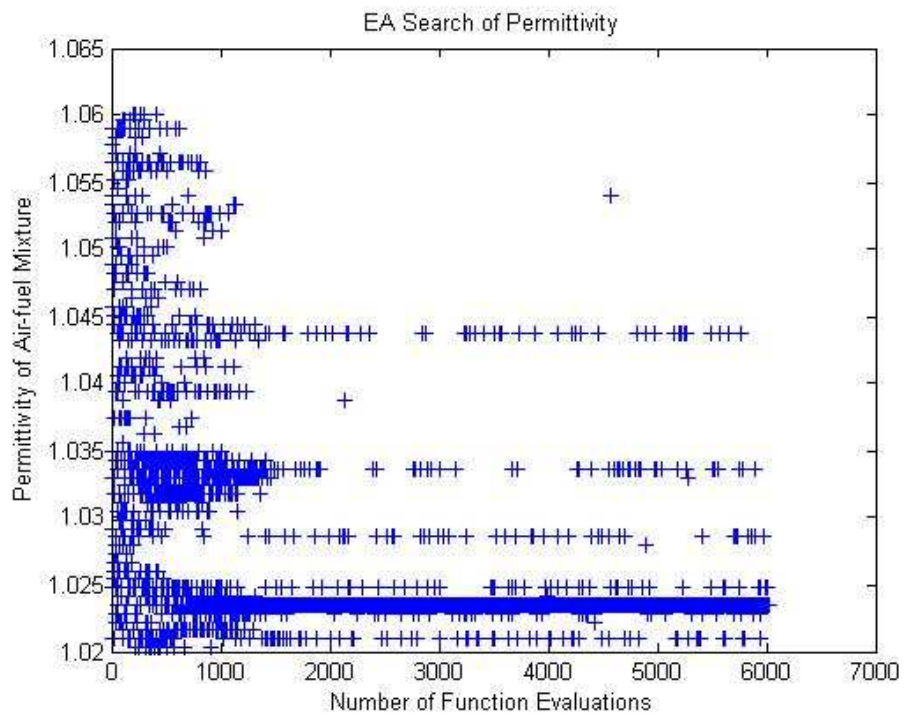
(a) Search trace of searching for antenna length with EA search method



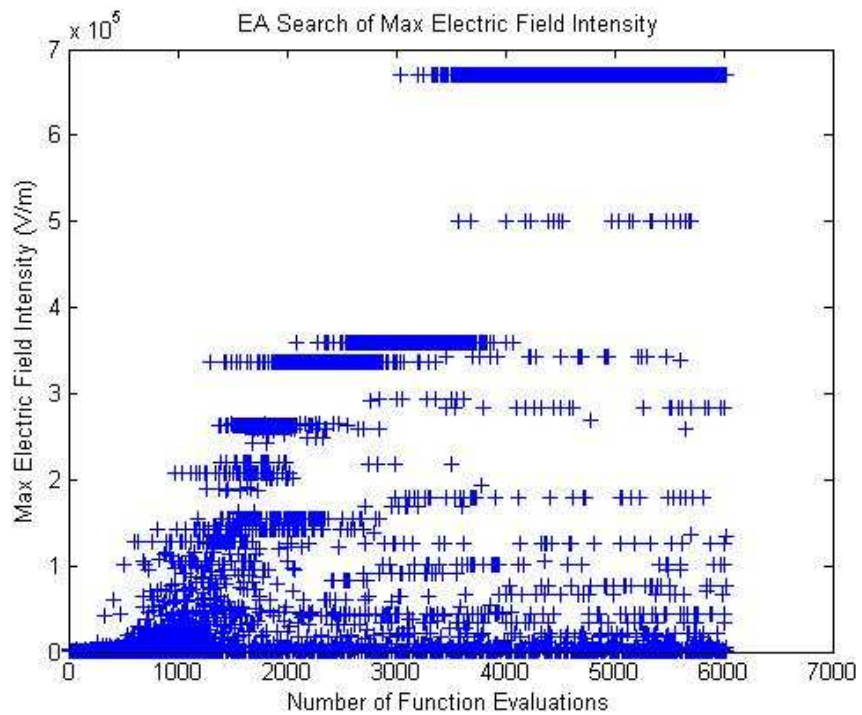
(b) Search trace of searching for screen radius with EA search method



(c) Search trace of searching for resonant frequency with EA search method



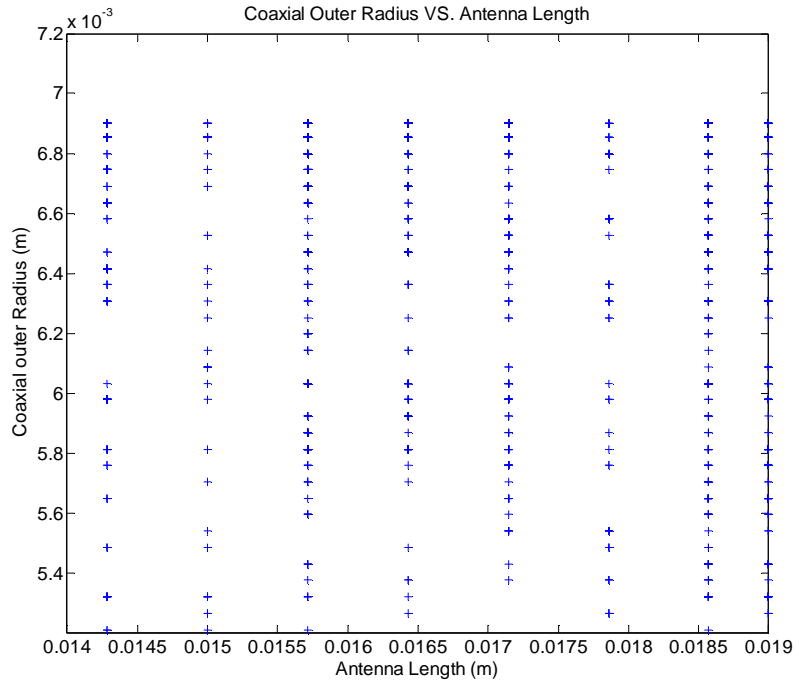
(d) Search trace of searching for permittivity with EA search method



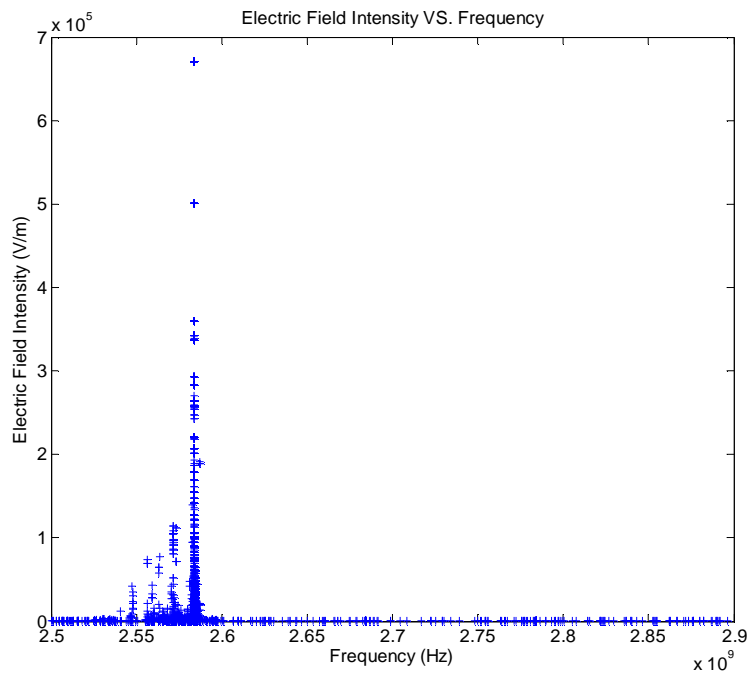
(e) Search trace of search objective: max electric field intensity

Figure 5-29 EA search for 3<sup>rd</sup> set of EA parameters in Table 5-7

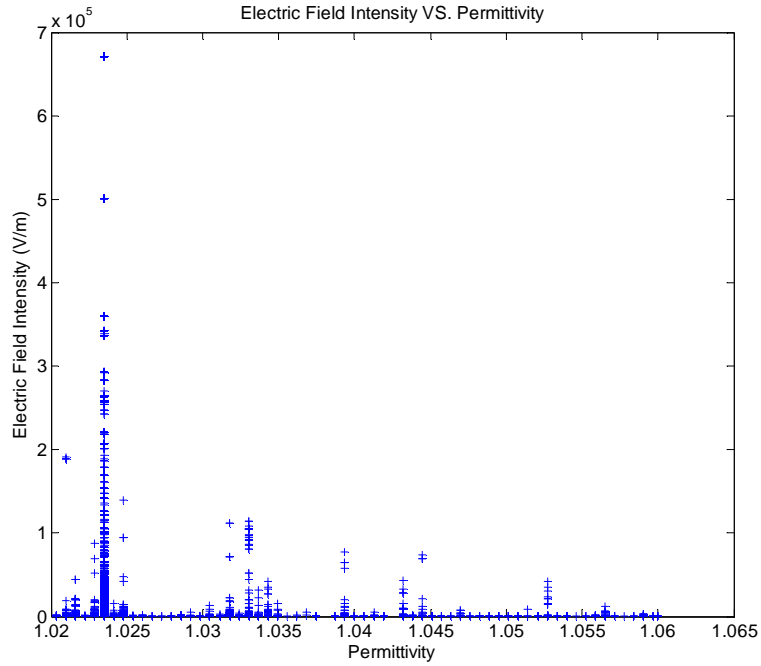
Figure 5-29 shows the EA search process carried out with the 3<sup>rd</sup> set of EA parameters by showing all the points of each search step throughout the whole search process. Figure 5-29 (a) shows the values of the antenna length used to simulate resonance for each search step during the search process. Figure 5-29 (b) shows the values of the screen of transmission radius used to simulate resonance for each search step during the search process. Figure 5-29 (c) shows the values selected for the resonant frequency to simulate resonance for each search step during the search process. Figure 5-29 (d) shows the values selected for the relative permittivity to simulate resonance fore each step during the process. Figure 5-29 (e) shows the progress of the search objective at each step during the search process.



(a) Distribution of search points of antenna length and screen radius



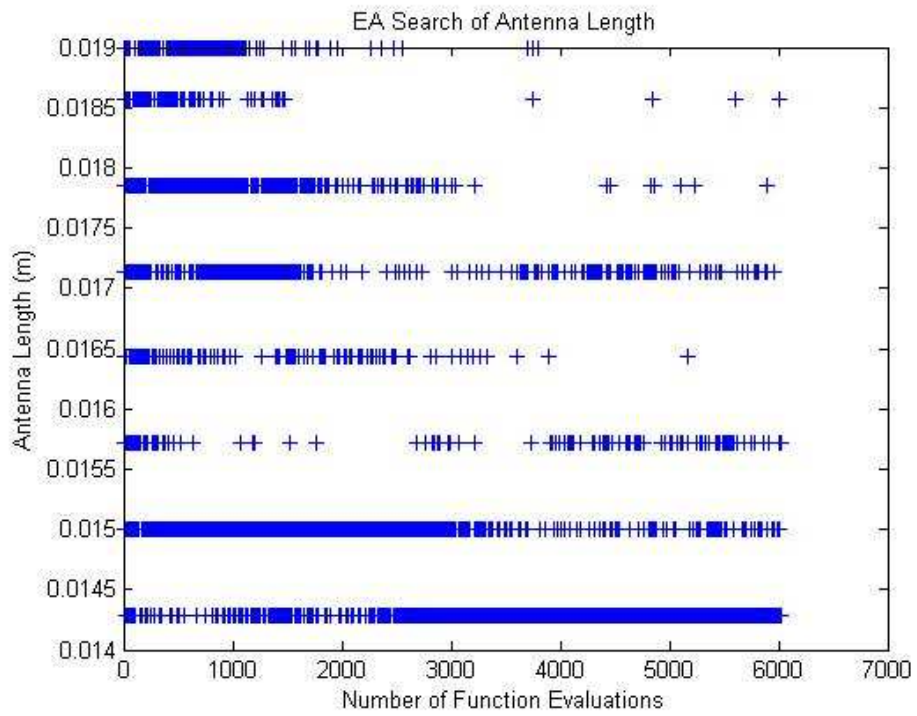
(b) Sensitivity of resonant frequency



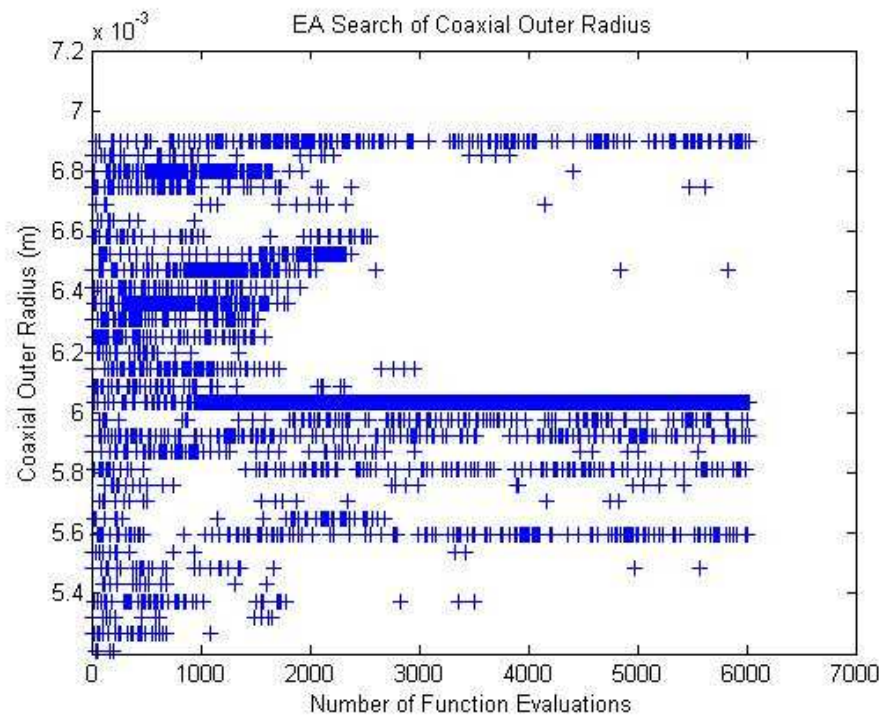
(c) Sensitivity of the relative permittivity

Figure 5-30 Relations between parameters from 3<sup>rd</sup> EA search

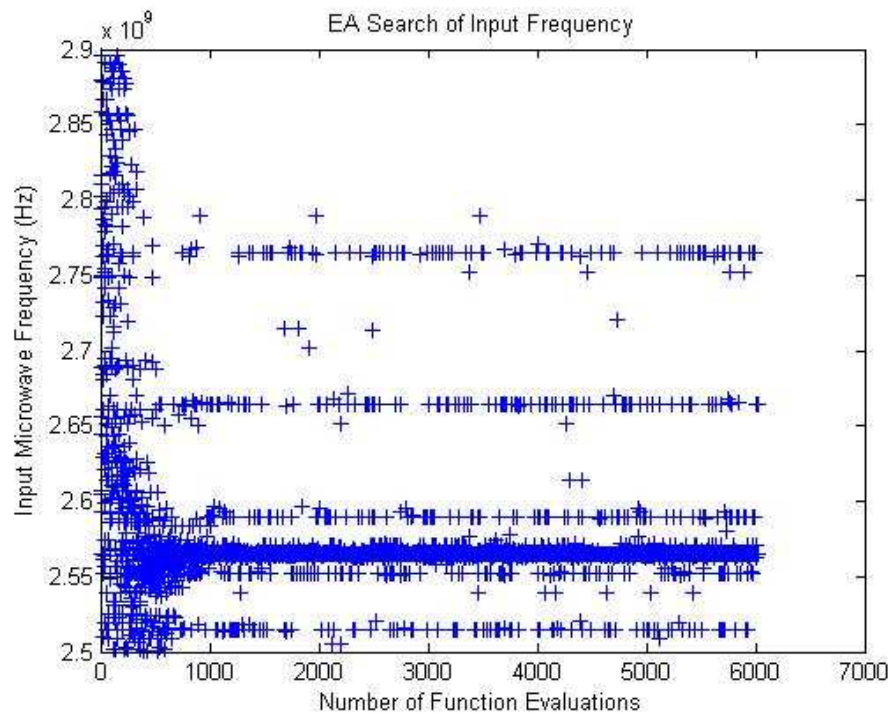
Figure 5-30 shows the relations between parameters and between the objective and parameters in 3<sup>rd</sup> EA search. Figure 5-30 (a) draws all search points of the screen of transmission line radius and antenna length in one figure to show the distribution of both parameters in the search range and the search trace of both parameters during the search. Figure 5-30 (c) draws the search objective, maximum electric field intensity against the search points of frequency to analyse the sensitivity of the frequency to screen of transmission line radius and antenna length and to compare with the results from exhaustive search. Figure 5-30 (c) draws the electric field intensity against the permittivity to show the effects of the permittivity on electric field intensity in the search range.



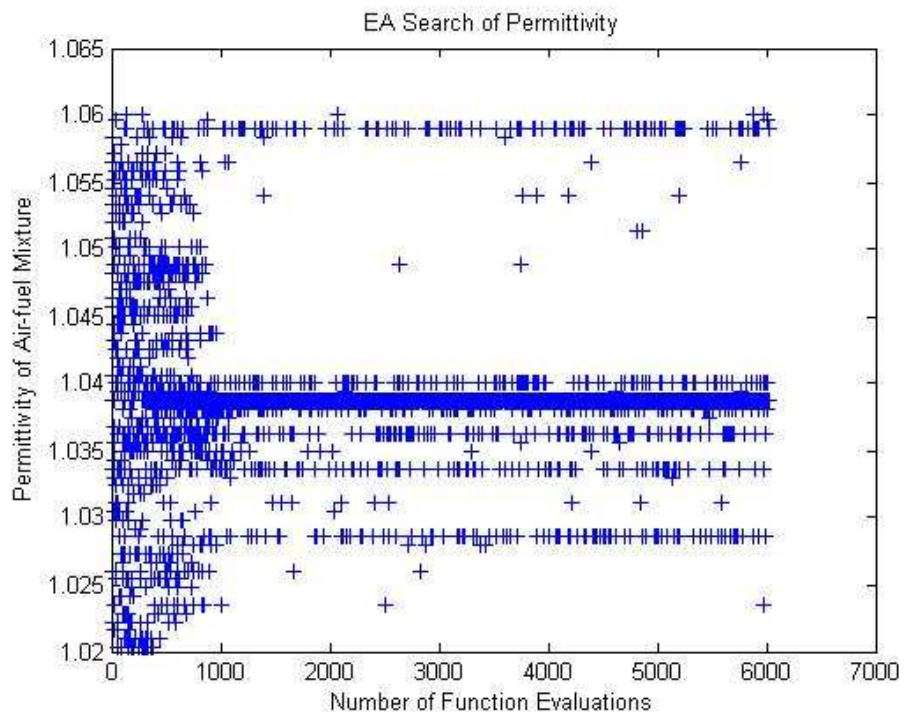
(a) Search trace of searching for antenna length with EA search method



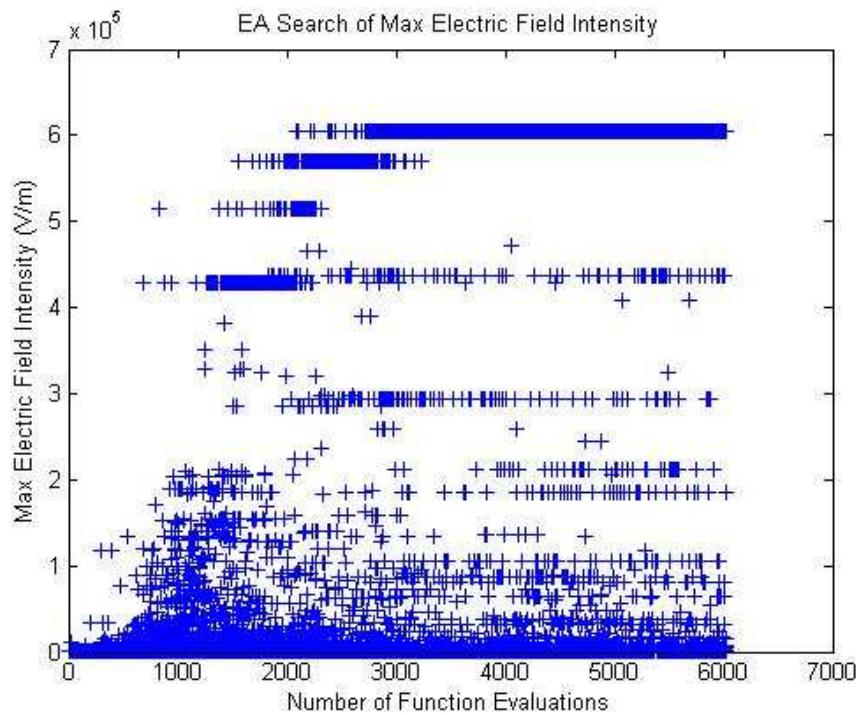
(b) Search trace of searching for screen radius with EA search method



(c) Search trace of searching for resonant frequency with EA search method



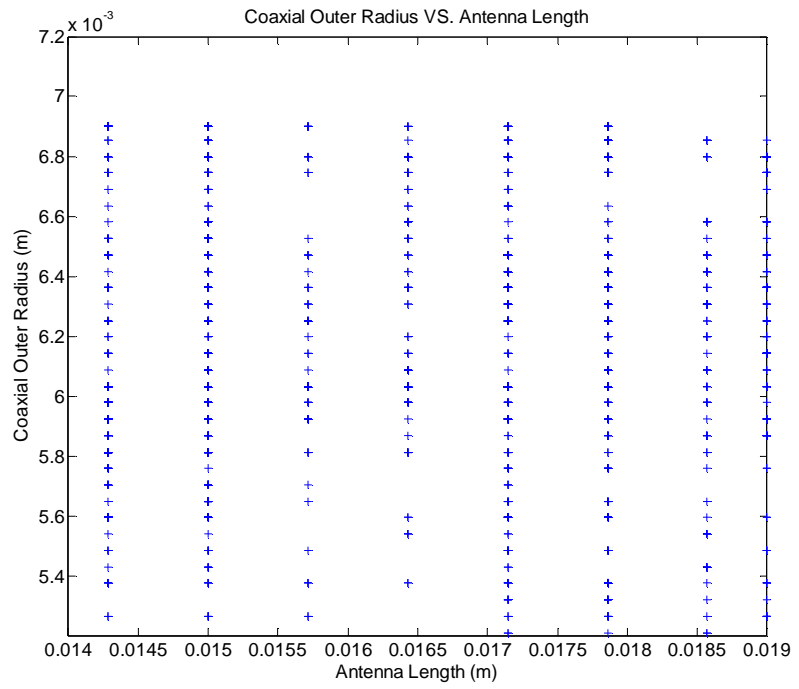
(d) Search trace of searching for permittivity with EA search method



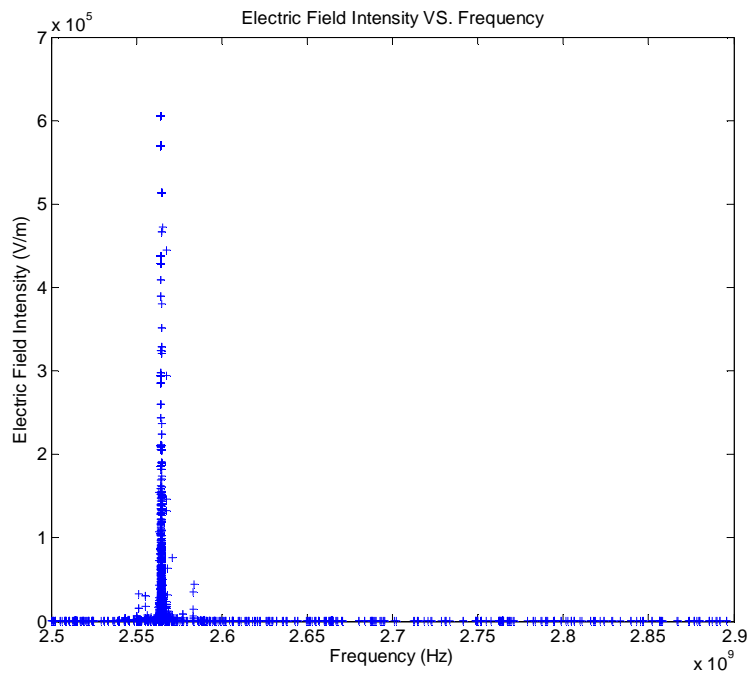
(e) Search trace of search objective: max electric field intensity

Figure 5-31 EA search for 4<sup>th</sup> set of EA parameters in Table 5-7

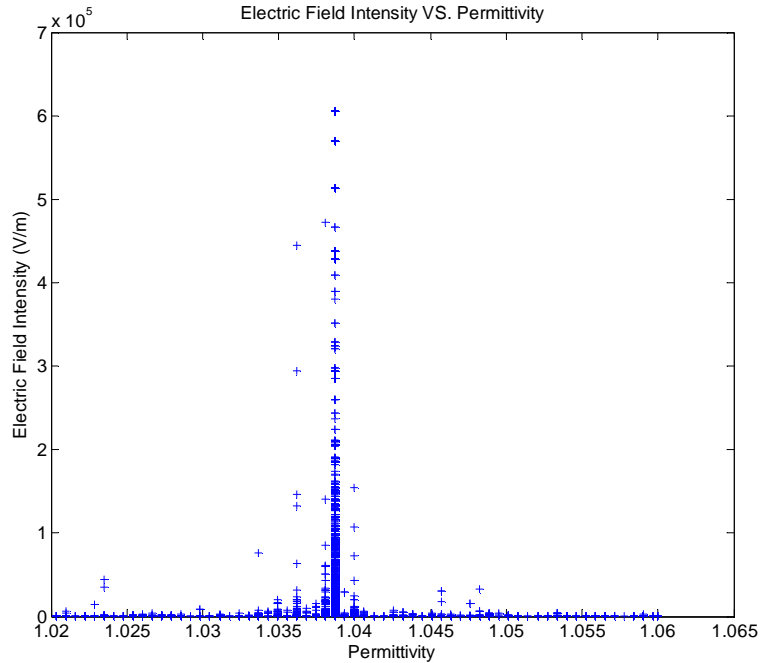
Figure 5-31 shows the EA search process carried out with the 4<sup>th</sup> set of EA parameters by showing all the points of each search step throughout the whole search process. Figure 5-31 (a) shows the values of the antenna length used to simulate resonance for each search step during the search process. Figure 5-31 (b) shows the values of the screen of transmission radius used to simulate resonance for each search step during the search process. Figure 5-31 (c) shows the values selected for the resonant frequency to simulate resonance for each search step during the search process. Figure 5-31 (d) shows the values selected for the relative permittivity to simulate resonance fore each step during the process. Figure 5-31 (e) shows the progress of the search objective at each step during the search process.



(a) Distribution of search points of antenna length and screen radius



(b) Sensitivity of the resonant frequency



(c) Sensitivity of the relative permittivity

Figure 5-32 Relations between parameters from 4<sup>th</sup> EA search

Figure 5-32 shows the relations between parameters and between the objective and parameters in 4<sup>th</sup> EA search. Figure 5-32 (a) draws all search points of the screen of transmission line radius and antenna length in one figure to show the distribution of both parameters in the search range and the search trace of both parameters during the search. Figure 5-32 (b) draws the search objective, maximum electric field intensity against the search points of frequency to analyse the sensitivity of the frequency to screen of transmission line radius and antenna length and to compare with the results from exhaustive search. Figure 5-32 (c) draws the electric field intensity against the permittivity to show the effects of the permittivity on electric field intensity in the search range.

Figures (a, b, c, d, and e) of Figures 5-25, 5-27, 5-29, and 5-31 show us the whole search process of each parameter. These figures show that due to permittivity is added as a search parameter the EA search needs more generations to find a global solution for

parameters from multiple local solutions. Figures (a and c) of Figure 5-26, 5-28, 5-30, and 5-32 show that the resonant frequency and permittivity have multiple peaks, which implies the EA search method has found a few local solutions for these parameters. These figures also confirm that the permittivity is more sensitive to frequency than the coupling antenna length and the screen of transmission line radius. This implies that the relative permittivity affects the resonance and the frequency and the change of permittivity can possibly cause off resonance. From Figures (a) of Figures 5-26, 5-28, 5-30, and 5-32 it can be seen that the points are distributed evenly in these figures. It implies the antenna length and the screen of transmission line radius do not affect electric field intensity as much as the permittivity does. The EA search does not focus on a specific range for these two parameters as they do not affect the electric field intensity significantly. It also implies that as a global search method the EA search method covers all area throughout the search range.

The search results are summarised in Table 5-8.

Table 5-8 Search results of the EA searches

	Antenna Length (m)	Screen Radius (m)	Resonant frequency (GHz)	Relative Permittivity of Mixture	Max Elec. Field Intensity (V/m)
1	0.0143	0.005	2.57	1.024	$9.8 \times 10^5$
2	0.0143	0.0054	2.54	1.054	$8.8 \times 10^5$
3	0.0143	0.0069	2.57	1.024	$6.9 \times 10^5$
4	0.0143	0.006	2.57	1.037	$6 \times 10^5$

Table 5-8 again shows the search consistency of EA search method. From Table 5-8 it can be seen that the best values for the antenna length found from 4 searches are all 0.014 m, which is exactly the same as in Table 5-4. This confirms that the most suitable coupling antenna length for the cylinder is found at 14.3 mm from the search in the previous section.

From this table it also can be seen that the search results for each parameter are close or the same. This shows that the EA search is more powerful and reliable than NM simplex search when search for several parameters. These search results from the EA search can guide the researchers to investigate the specific range for each parameter in depth without wasting time on searching for the solutions on wrong directions.

To assist verification of the search results and demonstrate the search for design, the first EA search result in Table 5-8 is simulated using COMSOL Multiphysics and drawn in Figure 5-33. The electric field intensity and distribution are shown in Figure 5-34.

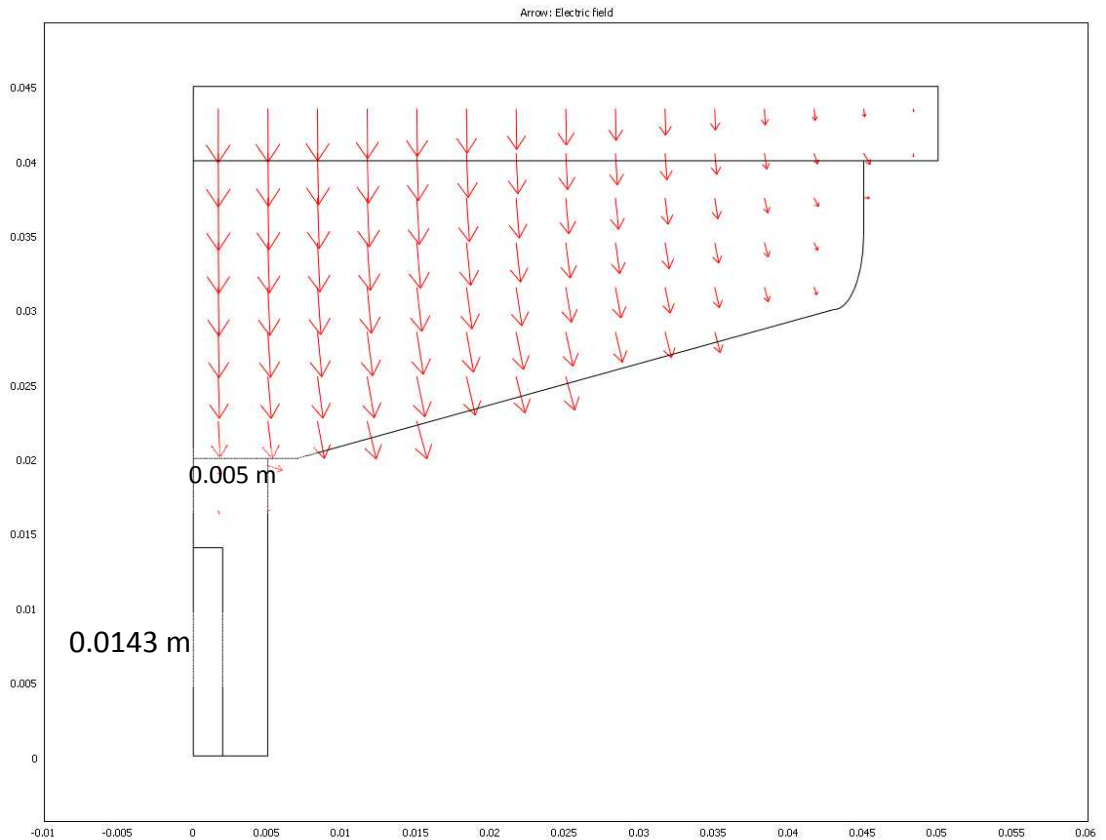


Figure 5-33 Distribution of the electric field of the first search result shown in Table 5-8

Figure 5-33 demonstrates the design of the coupling antenna length and transmission line radius with the best EA search results in Table 5-8 without applying exhaustive search on transmission line radius. The electric field intensity inside cylinder is drawn in Figure 5-34 to show the maximum electric field strength in the cylinder and the volume distribution of electric field in the cylinder.

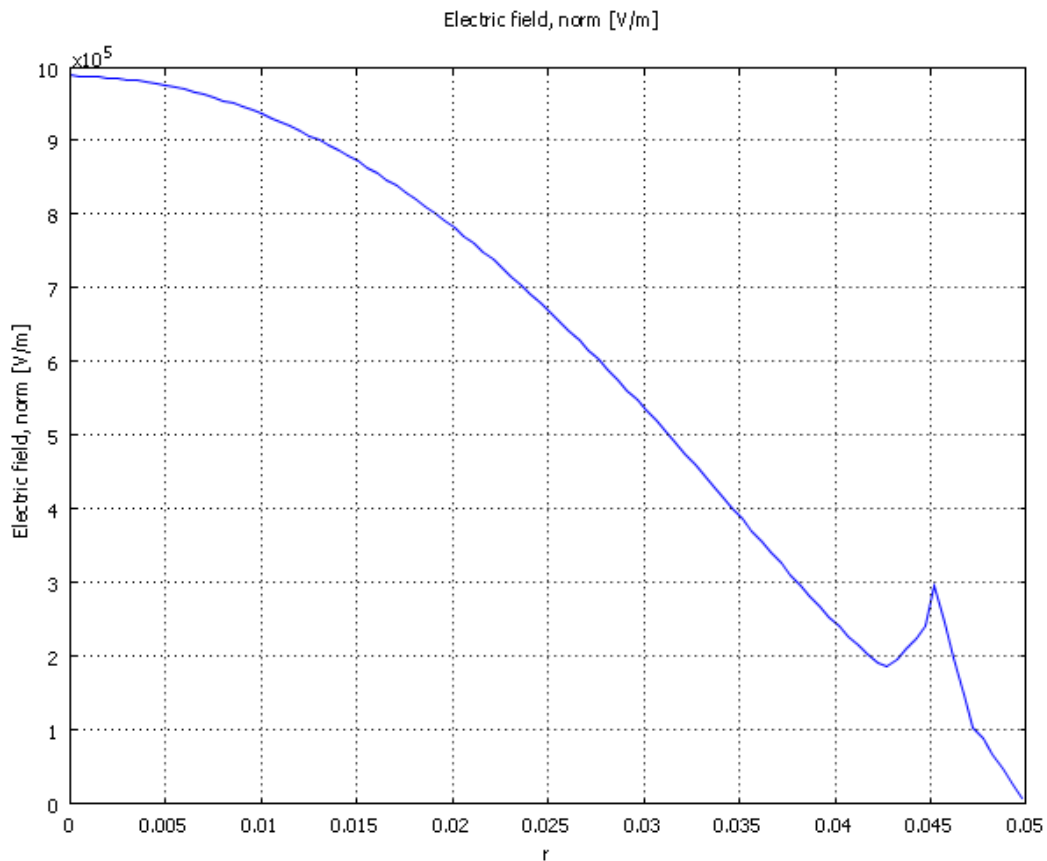


Figure 5-34 Electric field intensity and distribution of simulation in Figure 5-33

From Figure 5-34, it can be seen that the electric field intensity in most volume of the cylinder reach the minimum requirement for the ignition of the air-fuel mixture. It confirms that the automated search method is effective in finding the best design parameters for a certain problem under the given condition. It is also indicated that the EA search method are more efficient than exhaustive search with multiple parameters while it offers a reliable search performance. From Figure 5-25 it can be seen that the 1<sup>st</sup> EA search in Table 5-8 carried out 8000 times simulations. However, exhaustive search needs to carry out  $1.6 \times 10^7$  times simulations to search for 4 parameters within the same search range and with the same accuracy as of the EA search. If each simulation takes 1 second then the whole exhaustive search takes almost 6 months to finish. Therefore, the EA search method is much faster than exhaustive search on finding the optimal solutions especially for multiple parameters problems.

## 6. Conclusions and Future Work

### 6.1. Discussions and Conclusions

Through computer simulations this thesis has verified the feasibility of the microwave and radio frequency ICE ignition concept first proposed by Ward (1974). This simulation based research work is a world first. Further through simulations the thesis has attempted systematically to address problems encountered in the realisation of MI system reported by other researchers.

Following validation of the simulation, Chapter 4 has first investigated properties of microwave resonance in an ICE cylinder using finite element analysis and computerised 'design of experiments'. Investigation of effects of piston position confirms that the resonant frequency of the engine cylinder is very sensitive to the piston motion. This is the major factor that encumbers practical realisation of an MI system, because the motion of the piston can easily cause off-resonance and hence degraded field strength.

It is shown that the natural frequency changes 0.015 GHz per 0.5 mm in average when the piston moves from 5 mm to 0.5 mm to TDC and 0.0021 GHz per 0.05 mm when the piston moves from 0.5 mm to 0.05 mm to TDC. For the geometry of the given ICE cylinder, if the input microwave frequency is fixed, the resonance lasts for 7  $\mu$ s.

The investigation on various diameters of cylinders reveals the results of research on the effects of piston motion of a cylinder can be extended to other cylinders with different diameters. It also shows that different types of cylinders require different input microwave frequencies and hence the microwave source of the HCMI systems has to be designed for different types of cars.

For a single ignition, the air/fuel ratio is generally fixed. Therefore, the piston motion is the only factor that is likely to cause off-resonance if the ignition timing cannot be well

controlled. To improve the reliability of ignition in this case, the electric field intensity in the cylinder may be increased by increasing input power or improving coupling if possible.

The simulations have also revealed that a microwave based ignition takes 30 ns to 100 ns to break down the median of a permittivity and permeability that are the same as a 14.7:1 air-fuel mixture. This is much shorter than the duration of the microwave resonance and hence makes HCMI feasible in terms of duration.

For a running engine, the air/fuel ratio may vary. Therefore, the variations of the AFR can also cause off-resonance. For this, the effects of the relative permittivity on resonance have been studied. It is found that the AFR does not affect the resonant frequency as much as piston motion does. However, in practice, the AFR does not change significantly during operations, once it is preset at engine calibration. Through this investigation, it is revealed that the frequency only changes 38MHz when the AFR varies from 10:1 to 16:1. This result will help solve the problem of varying the input microwave frequency for ignition, where the power microwave source allows a very small range of adjustments of the frequency.

Following resonance simulations with graphical visualisation, properties and effects of microwave emitter and couples are studied. For an emitter in the form of a probe antenna, the resultant electric field intensity is dependant on the antenna length as anticipated. The field strength reaches the maximum when the probe antenna length is around 14 mm in the model studied in this thesis. This indicates that for the given geometry of the Chrysler-Dodge ICE, a probe antenna of a length around 30% of wavelength shorter than the end of transmission line offers the best coupling efficiency in an HCMI system.

To search for globally optimal designs, Chapter 5 has studied antennae and transmission lines using two a-posteriori search methods, i.e., the Nelder-Mead simplex method and the 'intelligent' evolutionary algorithm. The a-posteriori search results are verified by

comparing with exhaustive search results. The EA has shown excellent efficiency and reliability in dealing with multiple parameters.

Through the computerised global search interfaced with CAD simulations, the most promising and efficient ignition timing and AFR are found under the constraint conditions of a practical ICE as shown in this thesis. For a 100 W input, the electric field intensity in the cylinder can reach up to  $9.8 \times 10^6 \text{ V m}^{-1}$ , which almost doubles the minimum requirement of  $5.5 \times 10^6 \text{ V m}^{-1}$  for a plasma breakdown of the air-fuel mixture induced by an electromagnetic field.

In this work, six different geometric shapes of antennae have been studied. Through the EA based global search, it is confirmed that the antenna length and screen radius do not affect the resonant frequency significantly. For the given ICE geometry, an antenna length of 14.3 mm offers the best efficiency and the least reflection regardless of the screen radius. The best combination of the antenna length and the screen radius exists, providing the maximum electric field in the cylinder. However, the radius affects the resonance the least among all the parameters searched in Chapter 5, although it can contribute to enhancing electric field in the cylinder and reducing reflection of the coupling.

It has to be noticed that in this thesis the resolutions chosen for exhaustive search parameters affect the accuracy of search results. The search resolution of frequency for exhaustive search is chosen to compromise between accuracy and runtime of search. As calculated in Chapter 5, exhaustive search for multiple parameters takes much longer time than intelligent optimisation. For this reason, hiring optimisation methods is the essential and efficient way to investigate and solve this particular problem in the thesis. The model used in this thesis is a realistic simulation of a real situation. As an initial investigation in this thesis the accuracy of simulations is good enough to have an overall view of the influence of these facts that affect resonance. The exhaustive search results are then used for guiding optimisation.

## **6.2 Further Work**

Further work would involve simulations with more parameters, such as temperature, pressure and carbon deposits. Investigation of the effects of plasma formed before ignition occurs has been initiated as the starting point of further investigation of more parameters. Nevertheless, the intelligent search results contributed by this thesis would guide effective hardware prototyping. Tests and design refinements of the HCMI system can then be carried out based on hardware experiments.

## **Reference**

Allpar. The 2.4 Litre four-cylinder Chrysler-Dodge engine. 2004. [www.allpar.com](http://www.allpar.com) (accessed Aug. 2008).

Bellenoue, M., Labuda, S. A., and Engles, M., Corona discharge ignition and combustion promotion of methane/air mixtures. Proceedings of the European Combustion Meeting. 2005. Paper 207.

Bokulich, F., Aerospace engineering online: technology update. SAE International. 2001. <http://www.sae.org/aeromag/techupdate/05-2001/tech3.htm> (accessed Sep 2008).

Britannica. Typical piston-cylinder arrangement of a gasoline engine. 2007. <http://www.britannica.com/>.

Capuano, A., Simulation of microwave resonance in an internal combustion engine. University of Glasgow, 2006.

Cathey, C. D., Tang, T., Shiraishi, T., Kuthi, A., and Gundersen, M. A., Nanosecond plasma ignition for improved performance of an internal combustion engine. IEEE Transactions on Plasma Science, Vol. 35, No. 6. IEEE, 2007. 1664-1668.

Chan, C. C., The state of the art of electric and hybrid vehicles. Proceedings of the IEEE, Vol. 90, Feb. 2002: 247-275.

DanaCorporation. Dana Media Room. 2005. [http://dana.mediaroom.com/index.php/press\\_releases/2008](http://dana.mediaroom.com/index.php/press_releases/2008).

Davis, James A., Multipoint spark ignition system. US Patent 4805570. 1987.

Dawson, E.F., and Lederman, S., Pulsed microwave breakdown in gases with a low degree of preionization. (AIP) 44, no. 7 (1973): 3066-3073.

DeFreitas, Dennis M., Darling, Timothy W., Migliori, A., and Rees, Daniel E., Ignition methods and apparatus using microwave energy. Patent 5689949. 1995.

DeFreitas, Dennis Michael, and Migliori, A., Ignition methods and paratus using microwave energy. Patent 5673554. 1995.

Dorf, Richard C. The Engineering Handbook. CRC Press LLC, 1998.

Duniway. Paschen curve. 1998. <http://www.duniway.com/images/pdf/pg/paschen-curve.pdf> (accessed Aug 2008).

Esakov, I. I., Grachev, L. P., Khodataev, K. V., Vinogradov, V. A., and Van W., David M. Propane-air mixture combustion assisted by MW discharge in a speedy airflow. IEEE Transactions of Plasma Science, Dec. 2006: 2497-2506, Vol. 34, No. 6.

Eways, S. E., Booth, W. D., Carrera, R., Oakes, M. E., and Jaeger, E. F., Cavity resonance mode plasma breakdown for the IGNITEX experiment. Fusion Engineering, 1989. Proceedings., IEEE Thirteenth Symposium on. Knoxville, TN, USA, 1989. 838-841, vol2.

Frenken, K. Hekkert, M. and Godfroij, P., R&D portfolios in environmentally friendly automotive propulsion: Variety, competition and policy implications. Technological Forecasting and Social Change, Vol. 71, Jun. 2004: 485-507

Gilmour, A. S. Principles of traveling wave tubes. Artech House, Inc., 1994.

Gundersen, M., Energy efficient transient: plasma ignition: physics and technology. Los Angeles, Aug. 2007.

Gundersen, M., "Energy-efficient transient plasma ignition and combustion, Los Angeles, Apr. 2004.

Hagen, Jurgen V., Venot, Y., Zhang, Y., and Wiesbeck, W., Microwave-generated plasma in air under standard conditions. IEEE Transactions on Plasma Science. IEEE, 2001. 604-608.

Hartman, J. How to tune and modify engine system. 2004.

Haupt, R. L. , Haupt, S.E., Practical genetic algorithms. John Wiley & Sons, 1998, ISBN 0-471-1 8873-5

Heywood, J. B. Internal combustion engines fundamentals. McGraw-Hill Book Company, 1988.

Hoard, J. Wm. Plasma-catalysis for diesel exhaust treatment: current state of the art. SAE 2001 World Congress Session: Diesel Exhaust Emissions Control, 2001. 145-156.

Hu, Chengnan, Chen, W., and Tai, B., A compact multi-band antenna design. Asia-Pacific Microwave Conference 2005 Proceedings. Suzhou, 2005.

Jacobs, C. A., The doctor's step-by-step guide to optimizing your ignition. Jacobs Electronics, 1996.

Jonassen, Niel., "Ions" in Mr. Static. Compliance Engineering 16, No. 3, 1999: 24-28.

Karkkainen, Kimmo K., Sihvola, Ari H., and Nikoskinen, Keijo I., Effective permittivity of mixtures: numerical validation by the FDTD method. IEEE Transaction on Geoscience and Remote Sensing, Vol. 38, 2000: 1303-1308.

Katsuhiro K., Endo, A., and Takezaki, J. Ignition system for internal combustion engine. Patent 4446826. 1981.

Kutlar, Osman A., Arslan, H, and Calik Alper T., Methods to improve efficiency of four stroke, spark ignition engines at part load. Energy Conversion and Management, Mar. 2005: 3202-3220.

Kwon, Tae H., The determinants of the changes in car fuel efficiency in Great Britain (1978-2000). Energy Policy, Vol.34, 2006: 2405-2412.

Liu, J., Ronney, D. P., Want, F., Lee, L. C., and Gundersen, M. A., Transient plasma ignition for lean burn applications. 41st Aerospace Sciences Meeting and Exhibit. Reno, Nevada, 2003.

Maher, A.R., Sadiq A. B. , Effect of compression ratio, equivalence ratio and engine speed on the performance and emission characteristics of a spark ignition engine using hydrogen as a fuel. Renewable Energy, Vol. 29, Dec. 2004: 2245-2260

Maierl, W. B, Kadish, A., Buchenauer, C. J., and Robiscoe, R. T., Electrical discharge Initiation and a macroscopic model for formative time lags. IEEE Transaction on Plasma Science, 1993: 676-683.

Manning, M. P. Plasma ignition system reduces NOx emissions. Pipeline & Gas Journal (Pipeline & Gas Journal) v222, no. 10 (1995): 26-30.

Mao, J., Liu, Y., and Zhu, J., Fundamental of electromagnetic field and microwave engineering. Electric Industry Publishing Company, 2004.

Mitchell, M., An introduction to genetic algorithms. The MIT Press, 1996.

Morsy, M.H, Kob, Y. S., Chung, S. H., and Cho, P., Laser-induced two-point ignition of premixture with a single-shot laser. Combustion and Flame vol. 124 issue 4, 2001: 724-727.

Najt, P. M. and Foster, D. E., Compression-ignited homogeneous charge combustion. SAE paper 830264, 1983

Nelder, J. A. and Mead, R., A simplex method for function minimization. Computer Journal, 1965: 308-313, vol7.

Oldnall, N., Basic radiation. Physics. 2001. [www.e-radiography.net](http://www.e-radiography.net) (accessed Aug. 2008).

Pancheshnyi, S. V., Locoste, D. A., Bourdon, A, and Laux, C. O., Ignition of propane-air mixture by a repetitively pulsed nanosecond discharge. IEEE Transactions on Plasma Science, Dec. 2006: 2478-2487, Vol34, No. 6.

Paschen, F. Wied. Ann. 37, 1889: 69-96.

Pepper, D. W., and Heinrich, J. C., The finite element method: basic concepts and applications. Hemisphere Publishing Corporation, 1992

Pertl, F.A., and Smith, J. E., Electromagnetic design of an novel microwave internal combustion engine ignition source, the quarter wave coaxial cavity igniter. Proc. IMechE Vol.223 Part D: J. Automobile Engineering. Jun. 2009. 1405-1417.

Phuoc, T. X., Laser-induced spark ignition fundamental and applications. Optics and Lasers in Engineering vol. 44 issue 5, 2006: 351-397.

Porteanu, H. E. and Gesche, R., Ignition process of microplasmas. Proceedings of COMSOL conference, Hannover, 2008

Porteanu, H. E., Kuhn, S. and Gesche, R., Ignition delay for atmospheric pressure microplasmas, Contributions to Plasma Physics, Vol. 49, Issues 1-2, pp. 21-26, Mar, 2009

Porteanu, H. E., Kuhn, S. and Gesche, R., Low power microwave plasma conductivity, IEEE Transactions on Plasma Science, Vol. 37, Jan 2009

Qiao, J., The development of microwave systems to reduce diesel exhaust emissions. 16th International Conference on System Engineering, ICSE' 2003. Coventry, 2003.

Schaus, R. J., Spark plug with multi-point firing cap. Patent 6608430. 2001.

Schleupen, R., Ignition device for high frequency ignition. Patent 6357426. 2000.

Schmidt, E., and Ruoss, H. O., Device for igniting an air-fuel mixture in an internal combustion engine. Patent 6918366. 2003.

Schmidt, E., Thiel, M., Hasch, J., Ruoss, H. O., and Linkenheil, K., Induction driven ignition system. Patent 7204220. 2003.

Seely, S., and Doularikas, A. D., Electromagnetics - classical and modern theory and applications. New York: Marcel Dekker, 1979.

Smith, Dr. James E., Stile, R., and Thompson, G. Investigation of a radio frequency plasma ignitor for possible internal combustion engine use. International Congress & Exposition. Detroit, MI, USA: SAE-Paper 970071, 1997.

Spears, W. M. Evolutionary algorithms - the role of mutation and recombination. New York: Springer-Verlag Berlin Heidelberg, 2000.

Starikovskaia, S. M., Plasma assisted ignition and combustion. Journal of Physics D: Applied Physics, 2006: 265-299.

Taylor, C. F., Internal combustion engine in theory and practice, volume 2: combustion, fuels, materials, design. The Massachusetts Institute of Technology, ISBN 0-262-70027-1, US, 1985

Theiss, N., Levin, J., Liu, J., Zhao, J., Ronney, P, and Gundersen, M. A., Pulsed corona discharge ignition for internal combustion engines. Joint Meeting of the US Sections of the Combustion Institute. 2005.

Tran, N. Microwave ignition for car engines. Jan 02, 2004. <http://microwaveprocessing.com/ignition.html> (accessed Jan. 25, 2010).

Wang, X., and Cao, L., Evaluation algorithm: theory, application, and software realisation. Xian Jiaotong University Publishing Company, 2002.

Warnatz, J.; Maas, U. Dibble, R.W. , Combustion: physical and chemical fundamentals, modeling and simulation, experiments, pollutant formation. Springer, Berlin, Germany, 2006: 175-176.

Ward, and Michael A. V., Combustion in an internal combustion engine, Cambridge, US Patent 3934566. 1974.

Ward, Michael A. V., Reverse stratified, ignition controlled, emissions best timing lean burn. Patent 5211147. 1991.

Widmer, L. Honda H22 cylinder head. 2004. [www.theoldone.com](http://www.theoldone.com) (accessed Aug. 2008).

Wiki. Finite Element Method. Jan 2010. [http://en.wikipedia.org/wiki/Finite\\_element\\_method](http://en.wikipedia.org/wiki/Finite_element_method) (accessed Jan 2010).

Xu, A. Timing advance. 2004. [www.sdjtu.edu.cn/xdjyzx/engine/05/htm/d5z309.htm](http://www.sdjtu.edu.cn/xdjyzx/engine/05/htm/d5z309.htm) (accessed Aug. 2008).

Zhao, F , Asmus, T. N., and Assanis, D. N., Dec, James A. Eng, and Paul M. Najt. Homogeneous Charge Compression Ignition (HCCI) Engines. SAE International, Mar. 2003.

## Appendix A

```
% COMSOL Multiphysics Model M-file

fclear fem

% COMSOL version
clear vrsn
vrsn.name = 'COMSOL 3.2';
vrsn.ext = '';
vrsn.major = 0;
vrsn.build = 222;
vrsn.rcs = '$Name: $';
vrsn.date = '$Date: 2005/09/01 18:02:30 $';
fem.version = vrsn;

% Geometry
g7=rect2('0.0070','0.02','base','corner','pos',{0,'0'},'rot','0');
carr={curve2([0.045,0.045,0.043],[0.03,0.025,0.025],[1,0.707106781186548,1]), ...
      curve2([0.043,0.0070],[0.025,0.02],[1,0.707106781186548]), ...
      curve2([0.0070,0],[0.02,0.02],[1,1]), ...
      curve2([0,0],[0.02,0.03],[1,1]), ...
      curve2([0,0.045],[0.03,0.03],[1,1])};
g12=geomcoerce('solid',carr);
g14=rect2('0.05','0.0050','base','corner','pos',{0,'0.03'},'rot','0');
g15=rect2('0.00197',lenstr,'base','corner','pos',{0,'0'},'rot','0');
carr={curve2([0.0050,0.0050],[0.0175,0.02],[1,1]), ...
      curve2([0.0050,coaxial],[0.02,0.02],[1,1]), ...
      curve2([coaxial,0.0050],[0.02,0.0175],[1,1])};
g20=geomcoerce('solid',carr);
g21=rect2('0.0050','0.02','base','corner','pos',{0,'0'},'rot','0');
clear s
s.objs={g7,g12,g14,g15,g20,g21};
s.name={'R3','CO1','R1','R4','CO2','R5'};
s.tags={'g7','g12','g14','g15','g20','g21'};

fem.draw=struct('s',s);
fem.geom=geomcsg(fem);

% Initialize mesh
fem.mesh=meshinit(fem);

% (Default values are not included)

% Application mode 1
clear appl
appl.mode.class = 'AxisymmetricWaves';
appl.mode.type = 'axi';
appl.module = 'EM';
appl.gporder = 4;
appl.cporder = 2;
appl.assignsuffix = '_emweh';
clear prop
prop.field='TETM';
appl.prop = prop;
```

```

clear bnd
bnd.inport = {0,0,0,1};
bnd.modespec = {'userdef','userdef','userdef','coaxial'};
bnd.type = {'E0','cont','ax','port'};
bnd.ind = [3,1,3,2,3,2,3,2,1,2,4,2,1,2,2,2,1,1,1,1,1];
appl.bnd = bnd;
clear equ
equ.epsilonr = {'mat1_epsilonr',2.713,1.1};
equ.mur = {'mat1_mur',1,1};
equ.sigma = {'mat1_sigma',0,0};
equ.ind = [1,2,3,3,1,2];
appl.equ = equ;
appl.var = {'nu','frestr'};
fem.appl{1} = appl;
fem.sdim = {'r','z'};
fem.border = 1;
fem.units = 'SI';

% Library materials
clear lib
lib.mat{1}.name='Copper';
lib.mat{1}.varname='mat1';
lib.mat{1}.variables.sigma='5.998e7';
lib.mat{1}.variables.mur='1';
lib.mat{1}.variables.k='400';
lib.mat{1}.variables.epsilonr='1';
lib.mat{1}.variables.rho='8700';
lib.mat{1}.variables.C='385';
lib.mat{1}.variables.nu='0.35';
lib.mat{1}.variables.alpha='17e-6';
lib.mat{1}.variables.E='110e9';

fem.lib = lib;

```